Stratigraphic record of the glacio-eustatic cycles and the deformation during the Pleistocene along the central Ecuadorian margin : using the ATACAMES data campaign

Carlos Martillo Bustamante

THÈSE DE DOCTORAT DE L'UNIVERSITÉ DE NICE SOPHIA ANTIPOLIS

MENTION SCIENCES DE LA TERRE ET DE L'UNIVERS

*Carlos **MARTILLO** Bustamante*

ENREGISTREMENTS STRATIGRAPHIQUES DES CYCLES GLACIO-EUSTATIQUES ET DE LA DEFORMATION DURANT LE PLEISTOCENE LE LONG LA MARGE CENTRALE D'EQUATEUR (EXPLOITATION DES DONNEES DE LA CAMPAGNE ATACAMES)

2016

UNIVERSITE DE NICE-SOPHIA ANTIPOLIS – UFR Sciences
École Doctorale de Sciences Fondamentales et Appliquées

T H E S E

pour obtenir le titre de
Docteur en Sciences
de L'UNIVERSITE de Nice-Sophia Antipolis

Discipline **:** Sciences de la Planète et de l'Univers

présentée et soutenue par
Carlos MARTILLO Bustamante

ENREGISTREMENTS STRATIGRAPHIQUES DES CYCLES GLACIO-EUSTATIQUES ET DE LA DEFORMATION DURANT LE PLEISTOCENE LE LONG LA MARGE CENTRALE D'EQUATEUR (EXPLOITATION DES DONNEES DE LA CAMPAGNE ATACAMES)

STRATIGRAPHIC RECORD OF THE GLACIO-EUSTATIC CYCLES AND THE DEFORMATION DURING THE PLEISTOCENE ALONG THE CENTRAL ECUADORIAN MARGIN (USING THE ATACAMES DATA CAMPAIGN)

Thèse dirigée par : François MICHAUD et Jean-Noël PROUST

soutenue le 11 MAI 2016

Jury :

Marina Rabineau	CR CNRS (HDR)	Rapporteur
Etienne Jaillard	DR IRD	Rapporteur
Jean-Yves Collot	DR IRD	Examinateur
Marc Sosson	DR CNRS	Examinateur
Olivier Dauteuil	DR CNRS	Examinateur
François Michaud	MC UPMC (HDR)	Co-directeur de Thèse
Jean-Noël Proust	DR CNRS	Co-directeur de Thèse

A MI MAESTRO DE VIDA…

A MI AMADA ESPOSA LUPITA,
A MIS HIJAS KAREN ELIZABEHT Y MARÍA DANIELA.

A MIS PADRES
ARÍSTIDES Y FÁTIMA.

A MI PAÍS, ECUADOR.

REMERCIEMENTS

Personnels

La vida es sólo una, la que tengo, le doy gracias a Dios por habérmela regalado y por poner a mi lado personas tan valiosas que me han fortalecido durante esta experiencia de aprendizaje, sin ellos, Señor, no lo hubiera logrado…
Gracias a mi familia, mi amada esposa Lupita y mis entrañables hijas Karen y María Daniela!... Uds. han sido durante este tiempo mi fuente de motivación y alegría más grande. Gracias por haberse decidido atravesar conmigo el Atlántico y compartir esta aventura que nos ha fortalecido como familia… Las Amo!

Gracias a mis padres Arístides y Fátima, por su respaldo constante en todos mis proyectos, por creer en mí, por escucharme y por sus oraciones… Sé que me acompañan como ángeles a lo largo de mi vida… Que Dios les bendiga..! Gracias a mis hermanos por cuidar de mis padres mientras no he estado presente, gracias Jimmy, Danny y Fátima… Los quiero..!. Gracias a mis padres y hermanos político, por su cariño, detalles y oraciones durante este tiempo, han sido una gran fortaleza.

Merci mes encadrants François Michaud et Jean Noël Proust pour votre accompagnement et soutien pendant ce temps. Merci pour les discussions scientifiques, elles m´ont rapporté beaucoup de croissances et m´ont donné la guide nécessaire pour aller plus loin dans le monde de la recherche… Merci surtout pour vos amitiés, elle continue á travers le temps..!

Merci Jean-Yves Collot pour m´avoir motivé á faire ce doctorat, pour votre disponibilité à discuter avec moi sur les données de l´Équateur. Vous m´avez donné la possibilité de commencer le chemin de la recherche.

Un merci spécial pour mes amis Jean François et Essy Doumont ! On a reçu votre soutien tout le temps, dès discussion scientifique et livres jusqu´à conseilles pour la vie quotidienne… Vous êtes formidables..!

Un grand merci à vous Monique et Alain Vandroy pour m´avoir accueillir dans votre maison sans savoir rien de moi ...Je vous embrasse fortement..!

Je ne peux pas oublier à mes amis français á Rennes. Merci à la famille Chamié, à la famille Fauchille, à la famille Deroussen, à la famille Monloup, à la famille Génévriez, à l´ensemble des familles de l'Equipe de Notre Dame et du quartier Bourg l'évêque qui nous ouvraient les portes de leurs maisons. Vous êtes un véritable cadeau, on vous porte dans notre cœur !!!

Gracias a mis amigos que buscan desarrollar la ciencias geológicas en Ecuador, por la motivación y ayuda brindada en diferentes momentos del doctorado: Glendita, Miguel, María José, Mónica… Así como a mis amigos latinoamericanos que compartieron con mi familia hermosos momentos en Rennes: Juan Carlos y Helena con sus hijos, Javier y Andrea,

Alessandro y Neys, gracias por el tiempo compartido y su apoyo constante, Dios los ilumine siempre..! A Valeria Lucas, por su ayuda en las correcciones de último momento.

Gracias a todos y todas por haberme transmitido esa energía, esa fuerza, esa valentía, ese cariño, que el Señor les multiplique el 100 x 1!

Institutionnels

This work was carried out in the framework of the Joint French-Ecuador Laboratory LMI "Séismes et Volcans dans les Andes du Nord" with the financial support of the CNRS-INSU, IRD, Rennes 1 and Nice Universities and IFREMER.

Merci au Laboratoire Géosciences Rennes pour votre accueillement, au personnel scientifique Thierry Nalpas, Olivier Dauteuil et Yves Lagabrielle pour partager ses connaissances et ses expériences avec moi… Une grande merci à mon ami Guillaume Baby pour son soutien et amitié pendant tout ce temps… Gracias por todo, amigo… !

Merci l'équipage et les ingénieurs qui ont traité la sismique, et au personnel scientifique du GeoAzur spécialement à Laure Schenini pour toute le soutien donné pendant la thèse pour que je puisse voir le données sismiques en différents formats et logiciels…

Gracias a la Subsecretaría Nacional de Educación, Ciencia y Tecnología del Ecuador (SENESCYT) por haber confiado en mis capacidades y darme la oportunidad de aprender más para continuar con lo que me gusta hacer, aprender para enseñar y compartir.

Gracias a la Secretaría de Hidrocarburos del Ecuador (SHE), que a través del convenio con el IRD, ha permitido el acceso a los datos sísmicos en el margen del Ecuador de la campaña SCAN.

Gracias a la Escuela Politécnica del Litoral (ESPOL) por todo su respaldo, especialmente a mis maestros y colegas profesores por la motivación dada durante todo mi estancia de investigación en Francia, así como su personal administrativo por su gestión.

ABSTRACT

The aim of this study is to constrain recent deformation and stratigraphic evolution of an active margin, using sismo-stratigraphic analysis of Pleistocene sediment preserved on the margin shelf and upper slope. The Ecuadorian margin is characterized by the subduction of oceanic reliefs of the Nazca plate at local scale (seamounts) and regional scale (volcanic Carnegie ridge, 300 km-wide, 2km-high). The extensive geophysical and sedimentological investigations carried out along the Ecuadorian margin during the ATACAMES expedition (2012) complemented by the interpretation of some seismic profiles of the SHE, allow us to explore the expended sedimentary records preserved on this continental margin during the Pleistocene. The deepest sedimentary basin shows 26 Transgressive-Regressive (TR) sequences. Correlations of the TR sequences with the global eustatic-climatic curve and with coastal exposure, C14 age-dating of cores show that the sequence deposition occurred from the base of the Calabrian (1782-Ka) to the Present, i.e. MIS 63 to MIS 1. Several basins are identified along the slope and the shelf of the margin. A detailed analysis of the thickness, the lateral distribution and stacking patterns of the TR sequences in these basins show a complex distribution of sediments in time and space. At regional scale, we have identified a regional unconformity at the base (1782-Ka as minimum age), which can correspond to the signature of the beginning of the Carnegie ridge collision. The segmentation of the margin, with a progressive subsidence in the north and an uplift and erosion/bypassing in the south, mimics the gross shape of the subducting Carnegie ridge. At local scale, seamounts subduction disturbed and enhanced the regional deformation effect of the Carnegie ridge. In the Manta-Plata area, the palinspastic restoration of the deformation of the continental shelf support the collision of a topographic relief crested the Carnegie Ridge started c.500ka ago, together with the syntectonic sedimentation.

This work shows that the seismic-sequence stratigraphy analysis related to eustatic cycles of the Pleistocene is a very powerful tool to establish a morphostructural evolution of active margin. Calibrated by coring and correlations to global climate-eustatic curves and emerged sequences, this analysis enables to precise chrono-stratigraphy evolution of tectonic deformation of stratigraphic sequences in relationship with their deep structures.

RÉSUMÉ

L'objectif de cette étude est de contraindre les enregistrements climato-eustatiques et les déformations au cours du Pléistocène d'une marge active à partir de l'analyse sismo-stratigraphique des sédiments conservés sur la plate-forme et la pente supérieure. La plaque Nazca porte, le long de la marge d'Equateur, des reliefs océaniques d'échelle locale (seamounts) et d'échelle régionale (la Ride de Carnegie, 300 km de large à 2 km de haut). Les données de sismique haute résolution et de carottage collectées pendant l'expédition Atacames (2012), complétées par l'interprétation de quelques profils sismiques de la Secretaria de Hydrocarburos de Ecuador (SHE), nous ont permis d'explorer l'impact de la variabilité climatique et de la déformation sur l'organisation stratigraphique des sédiments, au cours du Pléistocène. Le bassin sédimentaire le plus profond, situé au Nord, montre 26 séquences sédimentaires (Régression-Transgression=T-R) préservées sous l'influence des cycles climato-eustatiques du Pléistocène. La corrélation des séquences T-R avec les affleurements côtiers, complétés par des datations C14 des carottes, et avec la courbe eustatique globale, indiquent que le dépôt des séquences débute à la base du Calabrien (MIS 63 - 1782-Ka) et s'étend jusqu'à aujourd'hui (MIS 1). Plusieurs bassins ont été identifiés le long de la pente et de la plate-forme. Une analyse détaillée de l'épaisseur, de la répartition latérale et de la succession des séquences T-R dans ces bassins montrent une distribution complexe des sédiments dans le temps et l'espace. A l'échelle régionale, nous avons identifié à la base une discordance régionale dont l'âge minimum est 1782-Ka et qui pourrait correspondre à la signature du début de l'entrée en subduction de la ride de Carnegie. La segmentation de la marge, avec de la subsidence croissante vers le nord et une érosion/« bypass » vers le sud, reproduit les grands traits de la forme du prolongement de la ride de Carnegie sous la marge. A l'échelle locale, la subduction de seamounts perturbe et renforce l'effet de déformation régionale de la ride de Carnegie. En particulier, dans la région de Manta-Plata, la reconstitution palinpastique de la déformation et de la sédimentation est cohérente avec la subduction, il y a c.500ka, d'un relief porté par la ride de Carnegie.

Ce travail montre que, le long des marges actives, l'analyse sismo-stratigraphique de l'enregistrement des séquences liées aux cycles eustatiques du Pléistocène est un outil très puissant pour analyser la déformation. Calibrée par des carottages et des corrélations aux courbes climato-eustatiques globales et aux séquences émergées, cette analyse permet d'établir une chrono-stratigraphie très précise qui peut servir de base à l'établissement d'une chronologie de la déformation tectonique et des corps sédimentaires permettant de reconstituer l'évolution morpho-structurale pléistocène d'une marge et ses relations avec les structures profondes.

RESUMEN

El objetivo del presente estudio es determinar el registro climato-eustático y la deformación durante el Pleistoceno de un margen activo, a partir del análisis sismo-estratigráfico de los sedimentos conservados en la plataforma y pendiente superior. La placa de Nazca porta, a lo largo del margen del Ecuador, relieves oceánicos de escala local (montes submarinos o "seamounts") y de escala regional (la Cordillera de Carnegie, 300 km de largo y 2 Km de altura). Los datos sísmicos de alta resolución con los datos batimétricos y núcleos sedimentarios, colectados durante la campaña científica Atacames (2012), completados con la interpretación de ciertos perfiles sísmicos de la Secretaría de Hidrocarburos del Ecuador (SHE), nos han permitido explorar el impacto de la variabilidad climática en el registro estratigráfico y la deformación ligada a la subducción durante el Pleistoceno. Las cuencas sedimentarias más profundas, situadas al Norte del margen central, muestran 26 secuencias sedimentarias (Transgresión-Regresión=T-R), conservadas bajo la influencia de ciclos glacio-eustáticos del Pleistoceno. La correlación de las secuencias T-R con los afloramientos costeros, complementados con datación de C14 de los núcleos sedimentarios y con la curva eustática global, sugieren que los depósitos comprenden las edades desde la base del Calabrian (MIS 63-1782-ka) hasta la actualidad (MIS 1). Algunos de cuencas se han identificado también en la pendiente y en el borde de la plataforma. El análisis detallado de los espesores, de la repartición lateral y de la sucesión de secuencias T-R dentro de estas cuencas, muestra una distribución compleja de sedimentos, en el espacio y en el tiempo. A la escala regional, la discordancia regional a la base de 1782 ka., podría corresponder a la marca del inicio de la subducción de la cordillera de Carnegie. La segmentación del margen, con una subsidencia creciente hacia el Norte y una erosión/bypass hacia el Sur reproduce, en rasgo general la forma de prolongación de la cordillera de Carnegie bajo el margen. A escala local, la subducción de montes submarinos perturba y refuerza el efecto de la subducción regional de Carnegie. En particular, en la región de Manta-Plata, la reconstrucción palinpástica de la deformación y de la sedimentación es coherente con la subducción, hace 500 Ka., de un relieve submarino portado por la Cordillera de Carnegie.

Este trabajo muestra que, a lo largo de los márgenes activo, el análisis sismo-estratigráfico del registro de secuencias depositadas durante la variación de los ciclos climato-eustáticos del Pleistoceno, es una herramienta muy importante para determinar la deformación. Con la calibración de edades a través los núcleos sedimentarios y la correlación con la curva eustática y secuencias emergidas, este análisis permite establecer una cronología de la deformación tectónica, y los cuerpos sedimentarios permiten reconstruir la evolución morfo-estructural de un margen y sus relaciones con las estructuras profundas.

TABLE OF CONTENTS

Abstract of Scientific Congress 1: Pleistocene stratigraphic signature of active deformation along the central Ecuadorian subduction margin. Martillo et al. 2013. 14eme Congrès Français de Sédimentologie, Paris-France.

Abstract of Scientific Congress 2: Margin sedimentary record of active deformation due to the subduction of topographic asperities (Carnegie Ridge, Manta Plata area, Central Ecuador. Proust et. al., 2015. 31st IAS Meeting of Sedimentology, Kraków-Poland.

TABLE OF FIGURES

Chapter 1

Chapter 2

Chapter 3

Chapter 4

Chapter 5

Chapter 6

LIST OF TABLES

Résumé étendu

Introduction

Les zones de subduction se caractérisent par une intense activité tectonique et sont en particulier le lieu de mouvements verticaux importants et rapides. Elles sont par ailleurs le lieu de création de reliefs importants et donc de flux sédimentaires conséquents. A l'échelle régionale, ces mouvements verticaux sont influencés par le régime de la subduction (subduction/érosion versus subduction/accrétion) et/ou à par l'arrivée de rides volcaniques et à l'échelle plus locale par la subduction de mont marins.

Comment suivre l'évolution et quantifier ces déformations le long des marges actives? La stratigraphie séquentielle est un outil particulièrement bien adapté à l'analyse des archives sédimentaires des marges actives. En effet le climat et la tectonique sont les deux principaux paramètres qui contrôlent le dépôt des séquences et la stratigraphie des bassins sédimentaires. C'est l'interaction de ces deux paramètres qui va contrôler l'espace disponible au niveau de la plateforme et du haut de pente pour l'accumulation des sédiments (=espace d'accommodation) au cours du temps. En raison de la forte amplitude des variations du niveau de la mer au cours du Pléistocène, le haut de pente (100-800m) situé à la charnière du plateau continental est le plus à même d'enregistrer le plus complètement, et avec le plus grand détail, les variations de flux sédimentaires liées aux changements climato-eustatiques. L'étude conjointe de l'influence relative du climat et de la tectonique dans les bassins avant arc sur l'évolution de l'espace accommodation au cours du temps permettra donc de reconstituer l'évolution de la déformation le long des marges actives et en particulier de la subduction de reliefs océaniques.

Les objectifs de notre étude sont 1) d'analyser l'enregistrement stratigraphique des cycles climato-eustatique et de la déformation tectonique au cours du Pléistocène d'une marge convergente, à partir de l'analyse sismo-stratigraphique des sédiments conservés sur la plateforme et sur la pente supérieure ; 2) de déterminer la dynamique des bassins avant-arc du Pléistocène de la marge active centrale de l'Equateur ; 3) de proposer une évolution géodynamique de la marge centrale de l'Equateur durant le Pléistocène en relation avec la subduction de la ride de Carnegie et des reliefs associés.

Cadre géologique

Le long de la marge d'Equateur, la plaque Nazca passe en subduction sous la plaque Sud-Américaine à une vitesse de 4.8 cm/an dans une direction générale W-E par rapport au Bloc Nord Andin (Nocquet al., 2014). La marge est fortement influencée par l'arrivée dans la subduction de reliefs portés par la plaque en subduction, dont le plus remarquable est la ride de Carnegie (300 km-de large et 2 km de haut) (Lonsdale, 1978). La ride de Carnegie est le résultat de l'interaction entre le point chaud des Galápagos et la dorsale Nazca/Cocos. Elle est caractérisée par une orientation W-E et une géométrie dissymétrique avec un flanc Nord plus abrupt que le flanc Sud. L'âge de l'arrivée en subduction de la ride de Carnegie est toujours très

discuté (entre 8Ma/1Ma) (Michaud et al., 2005) ainsi que la géométrie de son prolongement vers l'Est dans la subduction (Collot et al., 2009).

La déformation de la marge d'Equateur est aussi influencée par la subduction de monts sous-marins (Sage et al., 2006 ; Collot et al., 2009 ; San Clemente et al., 2015). En effet, de nombreux monts sous-marins sont entrés en subduction. Ils ont généré ponctuellement des déformations importantes sur la pente (Marcaillou et al., 2016).

Les dépôts quaternaires à terre le long de la marge ont été étudiés et la stratigraphie le long du littoral est localement bien connue (Cantalamessa et al., 2006 ; Di Celma et al., Pedoja et al., 2006). Ces dépôts sont principalement localisés sur les promontoires (cap, péninsule) le long de la côte. Leur âge s'étend du Calabrien (1.8 Ma) (formations Jama et Canoa inférieur) jusqu'au Pléistocène supérieur (MIS 5e) pour les terrasses marines soulevées. Ces dépôts quaternaires sont le résultat de l'enregistrement des variations climato-eustatique; leur présence à la côte a été associé au soulèvement de cette dernière par l'influence de la subduction de la ride de Carnegie.

La marge d'Equateur est donc un excellent laboratoire naturel pour discriminer dans les enregistrements sédimentaires les effets conjoints du climat (cycles eustatiques) et de la tectonique (processus de subduction et subduction de reliefs océaniques).

Données et Méthodes

Pour réaliser cette étude, nous avons utilisé principalement les données collectées Le long de la marge de l'Equateur durant la campagne océanographique ATACAMES (Archivage de la Tectonique Active et du Climat le long de la Marge d'Équateur en Subduction) qui s'est déroulée entre le 15 janvier et le 18 février 2012. Plusieurs outils ont été utilisés durant cette campagne: 1) La sismique, avec une chaîne d'acquisition sismique HR multitrace composée d'une source sismique (6 mini-GI canons à air 50-450 Hz) et d'une flûte sismique (récepteur de 72 traces) de 700 m de long; une chaîne d'acquisition THR monotrace (Sparker 100-1000 Hz) ; un sondeur de sédiment « Chirp »(1.8-5.3 kHz) 2) La bathymétrie, avec des sondeurs de bathymétrie multifaisceaux (Simrad EM710 73-97 kHz ; et Simrad EM112 11-13 Hz ; 3) un carottier Kullenberg. Les données sismiques ont été traitées à bord avec le logiciel Seismic Unix (Colorado School of Mines) et les données bathymétriques avec le logiciel « Caraibes » de L'IFREMER. Une grille bathymétrique d'un pas de 30 m a été homogénéisée à l'échelle de la marge. Pour l'analyse des données sismiques nous avons utilisé les logiciels Kingdom Suite (IHS) et Petrel (Schumberger) et reporté les résultats cartographiquement avec le logiciel Argis (ESRI).

L'interprétation des données sismiques a été réalisée en suivant les critères de la stratigraphie sismique. Nous avons successivement identifié.les faciès sismiques (configuration, amplitude, continuité et fréquence), 2) les terminaisons des réflecteurs (onlap, toplap, downlap, truncation, offlap) pour pointer les surfaces stratigraphiques (MFS, MRS, BSFR, C.C.) qui limitent les différents cortèges sédimentaires (« systems tracks «), et identifié les variations du niveau marin relatif par l'analyse de la trajectoire des offlap breaks (transgressive, régressive, forcée).

Ces élements nous ont permis de distinguer les cortèges de dépôts de transgression (Transgressive Systems Tract – TSF) et de régression (Highstand Systems Tract-HST, Falling Stage systems Tract et Lowstand Systems Tract). Enfin, les cortèges de transgression et de transgression ont été regroupés en séquences T-R qui ont pu être corrélées avec les variations du niveau de la mer associées aux différents stades isotopiques (Marine Isopotic Stages –MIS).

L'analyse des données sismiques HR de la campagne ATACAMES a été complétée par l'analyse de données pétrolières SCAN qui fournissent une imagerie basse résolution et qui est continue et homogène sur l'ensemble de la marge. Ceci nous a permis d'effectuer un suivi à l'échelle de la marge des dépôts pléistocènes, reconnus en détail par l'imagerie haute résolution de la campagne ATACAMES

Les carottes sédimentaires ont été coupées en section de 1m de long, photographiées et décrites visuellement. La description des facies et environnements de dépôts, l'identification des surfaces de discontinuité et l'interprétation en séquences de dépôts ont été réalisés dans le but de valider l'interprétation sismique. Après l'analyse stratigraphique nous avons prélevé des échantillons de coquilles pour les dater au C14 et ainsi dater les séquences sédimentaires T-R identifiées à partir des données sismiques. Une fois datées les séquences les plus jeunes, et considérant que la succession des séquences T-R est continue nous avons estimé l'âge des séquences plus anciennes par la corrélation des séquences T-R avec la courbe climato-eustatique mondiale et, quand cela était possible, avec les affleurements des formations du Pléistocène à terre.

Résultats

Nous présentons les résultats en deux parties. D'abord une analyse détaillée qui a été réalisée dans le secteur de Manta-La Plata, et qui servira de référence en particulier pour la datation et l'identification des séquences T-R. Puis nous généralisons la démarche à l'ensemble des bassins de la marge.

1) Secteur de péninsule de Manta Ile de La Plata,

Les résultats de ce secteur correspondent à ceux exposés dans un article publié à Marine Geology "*Subduction of seafloor asperities revealed by a detailed stratigraphic analysis of the active margin shelf sediments of Central Ecuador*, Proust, Martillo, et al., (Marine Geology, 2016)"

Facies sismique et cortèges sédimentaires

Nous avons identifié sur les profils sismiques 9 faciès. Les faciès sismiques du cortège régressif comprennent des faciès de plaine d'inondation, de front deltaïque soumis aux vagues, de barres littorales sub-tidales,,d'avant-plage inférieure et de prodelta jusqu'aux dépôts de transport en masse ou turbidites. Les faciès du cortège transgressif comprennent des dépôts fins de front deltaïque et des dépôts reliques de ravinement. La distribution des faciès et des environnements de dépôt entre les différentes surfaces stratigraphiques, permet de définir les

cortèges sédimentaires régressifs (« R »)(HST, FSST, FST) et transgressifs (« T ») (TST) et donc de définir 10 séquences T-R dans ce secteur (numérotées I à X depuis la base vers le sommet).

Datation des séquences T-R

Nous avons daté au C14 trois coquilles provenant d'échantillons prélevés dans les carottes en face de la péninsule de Manta. Ces âges vont de 40 ka à 30 ka. En cohérence avec la limite des séquences déterminée à partir de l'interprétation sismique, ces âges nous permettent de dater la séquence IX qui correspond donc à la séquence TR comprise entre le stade isotopique MIS 3 et MIS2. A partir de ce repère chronologique et en faisant l'hypothèse que l'enregistrement des séquences est continu, nous attribuons un âge à l'ensemble des 10 séquences par corrélation avec la courbe climato-eustatique mondiale (depuis le stade MIS 19 =780 ka pour la séquence I). Enfin certaines des séquences ont été géométriquement corrélées aux affleurements du Pléistocène que constituent, dans ce secteur, les terrasses marines soulevées de la péninsule de Manta et de l'île de La Plata ; ce qui donne des âges cohérents avec l'âge supposé des terrasses.

Modèle d'évolution des basins

Deux bassins caractérisent ce secteur. Un en face de la péninsule de Manta (bassin de San Lorenzo et un au sud de l'île de La Plata (bassin de La Plata). A partir de l'interprétation des milieux de dépôt, des séquences T-R et de leurs âges nous avons réalisé une analyse spatiale de l'évolution de la subsidence sur l'ensemble de ce secteur. Nous avons considéré 120 puits fictifs le long des profils sismiques. Le long de ces puits fictifs nous avons reporté pour chaque séquence TR : la lithologie correspondant aux facies sismiques, la profondeur actuelle, la paléo-bathymétrie et les âges des séquences. A partir de ces paramètres nous avons réalisé une analyse de dénudation (back-stripping) pour chacun des puits. Ceci nous a permis en interpolant entre chaque puits de générer des cartes de subsidence pour chaque séquence et d'établir un suivi de la subsidence au cours du temps.

En conclusion, l'analyse sismo-stratigraphique des 10 séquences préservées dans la partie supérieure de la plateforme et le haut de pente (méga-séquence UTR, voir plus loin) a permis d'établir une charte chrono-stratigraphique de la marge. L'établissement d'une chronologie de la déformation tectonique (subsidence) et du dépôt des corps sédimentaires a permis de reconstituer l'évolution morpho-structurale pléistocène de ce secteur de la marge et ses relations avec les structures profondes. Dans la région de Manta-La Plata, la reconstitution palinspatique de la déformation et de la sédimentation est cohérente avec la subduction depuis 500 ka, d'un relief porté par la ride de Carnegie (Proust et al., 2016).

2) Généralisation de la démarche à l'ensemble de la marge

En utilisant les mêmes critères d'interprétation utilisés dans la zone de référence Manta-Isla de La Plata, nous avons réalisé l'analyse sismo-stratigraphique le long la marge centrale d'Equateur (entre la péninsule de Salinas et la péninsule de Galera).

Identification des bassins

En combinant l'analyse des profils ATACAMES et SCAN nous avons pu élaborer une carte isopaque du Pléistocène à l'échelle de la marge centrale d'Equateur qui nous a permis d'identifier et de caractériser plusieurs bassins sédimentaires. Nous avons considéré trois zones. Une zone nord, où nous avons identifié sur la plateforme trois bassins Cojimies, Jama et Cabo Pasado. Une zone centrale (secteur Manta-La Plata) avec le bassin de La Plata sur la plateforme et le bassin de Manta-La Plata sur le haut de pente. Une zone sud avec des bassins de pente (le bassin de Ayampe, le bassin de Montanita, Salinas et Santa Elena).

Identification de 26 séquences T-R

Les 10 séquences supérieures T-R (= UTR) définies dans la zone La Plata-Manta ont été reconnues dans les autres bassins. L'âge des séquences les plus récentes (IX et X) a été confirmé par la datation C14 d'échantillons de carottes aussi bien dans les bassins de la zone nord (bassins de Jama et Cabo Pasado) que dans les bassins de la zone sud (Bassin d'Ayampe).

Dans le bassin de Jama nous avons identifié 16 séquences T-R plus anciennes que les 10 séquences supérieures. Ces 16 séquences ont été regroupées en deux ensembles limités par des discontinuités d'extension régionale. Le groupe de séquences de la partie inférieure (LTR) repose sur le substratum acoustique et comprend 11 séquences TR. Le groupe de séquences de la partie médiane de la pile sédimentaire (MTR) repose sur une importante discontinuité et comprend 5 séquences TR. La reconnaissance des deux groupes de séquences LTR, MTR dans les autres bassins, repose plus sur la corrélation des discontinuités qui les limitent que sur la reconnaissance de chacune des séquences TR élémentaires qui les composent.

Estimation de l'âge des groupes de séquences LTR- MTR- UTR

Si l'âge du groupe des 10 séquences élémentaires superficielles (UTR) est relativement bien contraint, il n'en va pas de même pour les groupes plus anciens MTR et LTR. La corrélation avec les courbes eustatiques (Lisieky & Raymo, 2005) nous donne un âge minimum de 1 Ma (MIS 29) pour la base de MTR, et de 1,5 Ma pour la base de LTR (MIS 50-51). Nous ne pouvons totalement exclure que certaines des séquences TR élémentaires aient été érodées ou ne se soient pas déposées. Dans cette hypothèse l'âge maximum de la séquence TR la plus ancienne pourrait être de 2.6 Ma, âge du cycle climatique le plus ancien du Pléistocène. Néanmoins, les âges proposés pour le groupe des séquences LTR peuvent être corrélés avec l'âge du membre Punta Ballena de la Formation Jama. L'âge suggéré par Cantalamessa et al. (2006) est le stade MIS 49 pour la base et le stade MIS 34 pour le sommet. Les séquences du groupe MTR, pourraient être corrélées avec les âges du membre El Matal, daté, à la base, à 1,16 Ma par Ar/Ar par Cantalamessa et al. (2006).

En conclusion, sans exclure la possibilité d'un âge plus important (c.2.5 Ma), la corrélation des séquences LTR- MTR- UTR avec la courbe eustatique et avec le Pléistocène onshore suggère plutôt que l'âge pourrait être compris entre 1.8 Ma (= âge des séquences TR les plus anciennes connues à terre) et l'actuel. En conséquence nous proposons que pour LTR un âge compris

entre 1000 ka-1800 ka, pour MTR un âge compris entre 700 ka-1000 ka et pour UTR un âge compris entre 14 ka-700 ka.

Distribution des groupes de séquences LTR, MTR et UTR

Dans la partie nord de la marge, les méga-séquences LTR, MTR et UTR sont bien représentées sur la plateforme, dans les bassins de Cojimies, Jama et Cabo Pasado. L'épaisseur des dépôts diminue du Nord vers le Sud d'un bassin à l'autre. Toujours sur la plate-forme plus au sud, dans le bassin de San Vicente, seule la méga-séquence UTR est présente.

Dans la partie centrale, sur la plateforme, les méga-séquences LTR et MTR sont quasi absentes et la méga-séquence UTR est faiblement représentée alors que sur le haut de la pente les méga-séquences LTR, MTR et UTR sont bien représentées

La répartition des groupes de séquences à l'échelle de la marge montre que, sur toute une partie de la plate-forme les méga-séquences LTR et MTR sont absentes ou peu représentées alors que régionalement les méga-séquences LTR, MTR et UTR sont présentes sur la pente.

Déformation des séquences

Le long des profils sismiques E-W, depuis le bassin de Jama jusqu'au Sud du bassin de Cabo Pasado la comparaison de la position des dépôts centres correspondants respectivement aux méga-séquences LTR, MTR et UTR suggère une migration vers la côte. Nous interprétons ces géométries comme étant associées au soulèvement de la bordure de la plateforme depuis la base de LTR.

Le long des profils N-S, dans ce même secteur, la position des dépôts centres montre une migration progressive du sud vers le nord, ce qui suggère une déformation de la plateforme dans la direction N-S.

Discussion

Influences respectives du climat et tectonique sur la sédimentation

Dans tous les bassins nous avons identifié l'enregistrement des changements climato-eustatiques à travers l'interprétation des séquences T-R. Cependant, d'un bassin à l'autre l'évolution de la succession verticale des séquences est parfois très différente. Par exemple dans le bassin Cojimies on peut observer une succession complexe comprenant un épisode de progradation, puis de rétrogradation, une nouvelle progradation et enfin une rétrogradation. Alors que dans le bassin de San Lorenzo, un premier épisode d'aggradation est suivi d'une régression constante des séquences, en dépit des changements eustatiques enregistrés dans chaque séquence. Cette différence de géométrie et d'évolution dans l'empilement vertical des séquences TR traduit un contrôle tectonique différentiel le long de la marge.

Déformation : échelle régionale

La géométrie des terminaisons des séquences, la trajectoire des « offlap break » et la migration des dépôts centres à l'échelle des trois méga-séquences LTR, MTR et UTR, suggèrent que de

nombreux secteurs de la bordure de la plateforme sont soulevés depuis LTR. De plus, face à la ride de Carnegie (là où, sur la plaque plongeante, elle est bien exprimée dans la bathymétrie) les bassins sont répartis plutôt sur la pente alors que, de part et d'autre de la ride (là où commencent les bords de la ride de Carnegie) ils sont plus plutôt développés sur la plateforme. Nous interprétons les géométries et la répartition des bassins à l'échelle de la marge comme étant le résultat du soulèvement de la plateforme qui pourrait marquer la signature de la subduction de la ride de Carnegie. Face à la ride de Carnegie un processus d'érosion/bypass accompagnerait le soulèvement de la bordure de la plate-forme. La chronologie de cette déformation montre qu'elle aurait débutée avant LTR c'est à dire avant 1800 ka. Elle nous permet de proposer cet âge comme un âge minimum pour le début d'entrée en subduction de la ride de Carnegie.

Déformation : échelle locale :

A l'échelle locale la déformation peut être contrôlée par la subduction d'un mont sous marin comme par exemple le montre le segment nord de la marge. Suivant une direction NS, parallèle à la marge, les deux bassins du Nord (Cojimes et Jama) montrent une augmentation de la profondeur de leur dépôts centres respectifs du Sud vers le Nord, accompagné d'une géométrie en divergence des réflecteurs du Sud vers le Nord. On peut par ailleurs observer une continuité latérale entre les bassins de Jama et Cojimies beaucoup plus marquée vers la côte que vers la bordure de la plateforme, là où précisément les effets de la subduction d'un mont sous marin sont connus (Marcaillou et al., 2016 ; Collot et al., 2009). Ceci suggère que les deux bassins du Nord pourraient s'être formés comme un bassin unique et qu'ils ont ensuite été séparés au niveau de la pente par la subduction d'un mont sous marin. Le segment central (Proust et al., 2016) montre également que localement les monts sous marins portés par la ride déforment les bassins. Cette déformation locale se surimpose à la déformation régionale de la subduction de la ride. De même, le long du segment Sud, le bassin de pente d'Ayampe révèle des évènements gravitaires qui correspondent à l'enregistrement successif de la subduction de monts sous-marins.

A l'échelle locale, la déformation peut être aussi contrôlée par des failles de la plaque supérieure. Le bassin de San Vicente bassin est localisé dans le domaine de la pente. Le développement de San Vicente Bassin semble être associé au prolongement du système de failles de Jama vers le large (Collot et al., 2004). Ceci se traduit par la formation de faille décrochantes (système de fleur négative contrôlant le basin) suivi de la formation d'un système de fleur positive déformant la bordure orientale du bassin.

Conclusion

La stratigraphie du Pléistocène en mer de la marge d'Equateur a été précisée par l'identification de 26 séquences T-R, regroupées à l'échelle de la marge en 3 méga-séquences avec de la base au sommet LTR (11 séquences TR), MTR (5 séquences TR), UTR (10 séquences TR). La datation directe par échantillonnage de carottes sédimentaires a été réalisée sur les deux séquences les plus récentes. La datation a ensuite été étendue aux séquences TR plus anciennes par la corrélation avec les affleurements côtiers et la courbe climato-eustatique. Dans l'hypothèse ou

la succession des séquences est continue, ceci permet de proposer un âge minimum MIS 63-MIS 1 = 1800 ka pour la séquence élémentaire la plus ancienne Cela implique pour la discordance régionale à la base de LTR un âge minimum du même ordre.

La distribution des bassins pléistocènes sur la marge montre que le long du segment Nord les bassins sont localisés sur la plate-forme comblés par les trois méga-séquences LTR-MTR et UTR. Le long du segment Sud les bassins sont plutôt localisés sur la pente et comprennent aussi les méga-séquences LTR-MTR et UTR.

La répartition des méga-séquences et des bassins sur le marge reproduirait les grands traits de la forme de la ride de Carnegie en subduction ; avec en particulier : 1) la présence d'une zone d'érosion/bypass sur la plateforme face à la ride de Carnegie 2) la présence de bassins en subsidence sur la plateforme de part et d'autre de l'impact de la ride.

A cette déformation régionale se surimpose localement la déformation associée à la subduction des reliefs sous-marins. Le long du segment nord, la subduction d'un mont sous marin contribue à la séparation des bassins Cojimíes et Jama. Le long du segment central, les différentes étapes de la subduction d'un relief ont été reconstituées et datées par l'enregistrement de la déformation des bassins de part et d'autre de l'île de Plata (les bassins San Lorenzo et La Plata) de 700ka à aujourd'hui.

Resumen Extendido

Introducción

Los márgenes activos en subducción son sectores de movimientos verticales importantes y rápidos. Estos movimientos verticales están influenciados, a parte del proceso mismo de subducción, a escala regional por la erosión tectónica y el barrido de cordilleras oceánicas, y a escala local por la subducción de montes submarinos.

Los márgenes activos en subducción son zonas que están sometidas a procesos de deformación en cortos periodos de tiempo. Las cuencas de ante-arco de estos márgenes en subducción han estado al mismo tiempo influencias por las variaciones eustáticas de gran amplitud registradas durante el Pleistoceno.

Una herramienta particularmente adaptada para estudiar la deformación en estos márgenes activos, influenciados por la fuerte variación climato-eustática en el Pleistoceno, es la Estratigrafía Secuencial. Uno de los conceptos más importantes en la estratigrafía secuencial es el de "Acomodación". La Acomodación es el espacio disponible para la depositación de sedimentos, su aumento o disminución está directamente controlada por la relación entre la eustacia y la tectónica. La variación en la acomodación más la el cambio en el flujo sedimentario registran un cambio en las secuencias depositacionales mediante una progradación, agradación o transgresión.

El objetivo principal del presente estudio es el de analizar el registro sísmico-estratigráfico de los ciclos glacio-eustáticos del Pleistoceno en la Plataforma y Pendiente de un margen convergente para: a) proponer un calendario crono-estratigráfico del margen, b) analizar la evolución tecto-sedimentaria de cuencas, c) establecer un marco geo-dinámico de deformación en relación a la subuducción de relieves oceánicos (cordilleras y montes submarinos).

Marco geológico

El margen continental del Ecuador se encuentra localizado al Nor-Oeste de la plata tectónica Sudamericana, y se encuentra influenciado por la subducción de la placa de Nazca a una velocidad de promedio 5.8 cm/año . Frente al margen central del Ecuador se localiza la cordillera submarina Carnegie, cuyo espesor alcanza los 2 km y cuyo origen está ligado a la relación geológica entre el punto caliente de Galápagos y el centro de divergencia Cocos-Nazca. La edad de colisión de la cordillera de Carnegie con el margen Ecuatoriano está en discusión, y las edades propuestas varían desde 8 Ma. hasta 1 Ma. La cordillera de Carnegie presenta una morfología muy irregular y su orientación general es Este-Oeste, sin embargo existen algunos modelos propuestos sobre su forma de subducción y de cómo ésta ha influenciado en la evolución geo-dinámica del margen del Ecuador evidenciados con levantamientos y subsidencias en la zona costera del Ecuador.

Sin embargo el margen ecuatoriano está influenciado, además de la subducción de la Cordillera de Carnegie, por la subducción de montes submarinos, localizados al Norte y al Sur de la Cordillera de Carnegie. La subducción de estas asperidades "puntuales" han generado una fuerte deformación evidenciada por las irregularidades morfológicas en la zona de pendiente y borde de plataforma, así como por la interpretación de datos de sísmica multicanal.

El registro estratigráfico de la deformación generada por de la subducción de estas asperidades (cordillera de Carnegie y montes submarinos,) durante el Pleistoceno, en el margen continental del Ecuador no han sido estudiadas hasta el momento. Sin embargo, en la zona costera los depósitos Cuaternarios han sido bien estudiados. Estos depósitos se localizan principalmente en las zonas prominentes de la costa (puntas, cabos, penínsulas). Las edades propuestas para estos depósitos abarcan desde la base del Pleistoceno Calabrian (1.8 Ma.), formaciones Jama y Canoa Inferior, hasta el Pleistoceno superior límite del Pleistoceno Medio y Superior (MIS 5e), Tablazos. Estos depósitos Cuaternarios han sido relacionados con el registro de la variación glacio-eustática del Pleistoceno, y su emersión en la zona costera ha sido explicada con la subducción de la cordillera de Carnegie.

Datos y métodos

Para este estudio se han utilizado, principalmente, los datos de la campaña ATACAMES, colectados a bordo del buque de investigación francés L'Atalante en el año 2012. El conjunto de datos colectados y utilizados abarca: 1) datos de sísmica de alta resolución, i.e. sísmica multicanal (72 canales, 50-450 Hz), sísmica monocanal sparker (100-1500 Hz) y perfilador de sedimentos (chirp 1.8 – 5.3 KHz); 2) batimetría de alta resolución (Kongsberg-Simrad 73-97 KHz y 11-13 kHz); 3) núcleos de sedimentos de pistón (3-5 m).

Los datos sísmicos fueron procesados a bordo con el software Seismic Unix (Colorado School of Mines) y los datos batimétricos con el software Caraibes (Ifremer). Para el análisis de datos se utilizaron los softwares Kingdom Suite (IHS) y Petrel (Schlumberger) y ArcGIS (ESRI).

Los datos sísmicos fueron interpretados mediante: a) los criterios de la estratigrafía sísmica, i.e. configuración, amplitud, continuidad y frecuencia para la identificación de facies sísmicas; b) la identificación de terminaciones de reflectores (onlap, toplap, downlap, truncation y offlap), para discriminar las superficies que limitan los diferentes cortejos sísmicos (systems tracts). La sucesión genética de cortejos sísmicos fueron analizados a través del análisis de la migración del offlap break (transgresiva, normal y forzada), distinguiendo los cortejos sísmicos de transgresión (Transgressive Systems Tract – TST), y de regresión (Highstand Systems Tract- HST, Falling Stage Systems Tract – FSST, y Lowstand Systems Tract). Finalmente los cortejos sedimentarios fueron agrupados en Transgresivos y Regresivos, formando las secuencias T-R, que permitió realizar la correlación entre estos y los diferentes periodos isotópicos marinos (Marine Isotopic Stages- MIS).

Los núcleos de sedimentos fueron cortados en secciones de 1m de largo para la toma de fotografía, descripción visual y análisis estratigráfico. Luego del análisis estratigráfico se

extrajeron muestras de conchas para la datación de C14, las mismas que sirvieron para datar las secuencias sedimentarias T-R interpretadas a partir de los datos de sísmica multicanal.

Una vez datados las secuencias T-R del tope, y asumiendo que las secuencias T-R corresponden al registro continuo de las transgresiones y regresiones causadas con las variaciones de los ciclos eustáticos del Pleistoceno, se procedió a datar cada una de las secuencias en correlación con la las curva de los MIS. Con la datación de las secuencias y la interpretación de las facies sísmicas se realizó un análisis de back-stripping mediante la definición de 120 pozos virtuales alrededor de la zona de Manta-Plata. Este análisis permitió generar mapas de subsidencia a las diferentes edades de los depósitos de las secuencias T-R.

Resultados

Los resultados son presentados en dos partes: 1) El análisis detallado de un sector de referencia o clave, i.e. la zona de Manta-La Plata, con el cual se realizó una publicación en la revista Marine Geology (Subduction of seafloor asperitiies revelead by a detailed stratigraphy analysis of the active margin shelf sediments of Central Ecuador, Proust et al., 2016); 2) Una extensión regional, a todo el margen central, de los resultados de la interpretación de datos sísmicos obtenidos en el sector clave.

Facies sísmicas y cortejos sedimentarios

En la zona de Manta-La Plata se identificaron nueve facies sísmicas (Fs), las mismas que fueron interpretadas con diferentes ambientes de sedimentación que van desde la parte continental, hasta la parte marino profunda. Estas fueron agrupadas como facies características de cortejos sedimentarios (systems tracts) regresivos y transgresivos.

Las facies sísmcias relacionadas con los cortejos regresivos fueron: Fs1 fueron relacionadas con un ambiente fluviátil meándrico o de llanura de inundación; Fs2 con el frente deltaico influenciado por olas; Fs3 con un ambiente de barras litorales subtidales; Fs4 con depósitos de la zona submarina de transición del shoreface; Fs5 con depósitos submarinos del prodelta; y, Fs6 con depósitos de transporte de masa o turbiditas.

Las facies sísmicas interpretadas como características de los cortejos sedimentarios transgresivos son: Fs7 con depósitos marinos de limos y arcillas del frente deltaico, y Fs8 depósitos transgresivos sobre la llanura aluvial (lag deposits). La facies del basamento acústico fue denominada como Fs9.

Con la identificación de las facies sísmicas, el análisis de la migración del offlap break y las terminaciones de los reflectores, se interpretaron los cortejos sedimentarios transgresivos (TST) y regresivos (HST, FSST, LST). A partir de ellos se identificaros 10 secuencias T-R en el sector de Manta-Plata, denominados desde I hasta X, desde la más antigua a la más actual.

Datación de secuencias T-R

Se dataron tres muestras de conchas con C14, extraídas de dos núcleos de pistón localizados frente a la península de Manta. De acuerdo a la interpretación estratigráfica de los núcleos y su correlación con los datos de sísmica de 3.5 Khz (chirp), estas muestras corresponde al tope de la secuencia IX. Las edades obtenidas abarcan desde 40 a 30 Kyrs, lo cual nos da una relación que la secuencia IX está relacionada con el periodo Transgresión-Regresión entre los MIS 3 y MIS 2. A partir de esta referencia, mediante la correlación continua con la curva eustática (asumiendo un registro continuo de los periodos isotópicos marinos), se dataron las 10 secuencias T-R. Sus edades abarcan desde el MIS 19 (780 Kyrs.), i.e. desde el Pleistoceno Medio.

Estas secuencias fueron correlacionadas geométricamente con los afloramientos cuaternarios localizados en la zona costera, y sus edades son concordantes con las edades propuestas para los tablazos en la Península de Manta y en la Isla de la Plata.

Modelo de evolución geológica local

Con la interpretación de los ambientes sedimentarios de las secuencias T-R, y de sus edades, se realizó un análisis de subsidencia espacial de la zona, para lo cual se definieron 120 pozos virtuales. En cada pozo virtual se definió para cada grupo de secuencia T-R: la litología inferida a partir de las facies sísmicas, la profundidad actual, la paleo-batimetría y las edades de las secuencias. Con estos datos se aplicó el análisis de denudación (back-stripping) de cada pozo. Con estos datos, y mediante interpolación, se generaron 10 cartas de subsidencia en la zona de estudio, una carta para cada edad de la secuencia. Estas cartas, correlacionadas con el proceso de subducción de un monte submarino propuesto por la literatura en la zona de estudio, permitieron plantear un modelo de evolución del margen continental de la zona de Manta-Plata, desde el Pleistoceno Medio.

Análisis extendido al margen central

A partir de los criterios de interpretación planteados en el área de referencia (Manta-La Plata), se analizaron los depósitos sedimentarios a lo largo del margen central del Ecuador. Se identificaron tres zonas con cuencas distribuidas entre la plataforma y la pendiente del margen continental. En la zona Norte se localizaron las cuencas Cojimíes, Jama y Cabo Pasado, las mismas que están situadas principalmente en la plataforma. La zona Central corresponde a las cuencas de San Lorenzo y La Plata (zona Manta-Plata), las mismas que se localizan en la de pendiente y en la plataforma respectivamente. La zona Sur se caracteriza por tener cuencas de pendiente, i.e. Ayampe, con las cuencas Ayampe, Montañita, Salinas y Santa Elena.

Identificación de cuencas y datación de secuencias T-R

En todas estas cuencas se identificaron las 10 secuencias T-R interpretadas en la zona de referencia. Las edades de las secuencias superiores IX y X fueron corroboradas mediante la datación con C14, en las cuencas Jama, Cabo Pasado y Ayampe. Sin embargo, en la cuenca

Jama se interpretaron 16 secuencias T-R más profundas y antiguas que las 10 definidas a partir de la zona de Manta-La Plata, obteniendo un total de 26 secuencias T-R en esta cuenca.

A partir del arreglo vertical de las 26 secuencias T-R, mostradas en la cuenca Jama, estas fueron reagrupadas en tres mega-secuencias: secuencias inferiores T-R (Low T-R), secuencias intermedias (Middle T-R) y secuencias superiores (Upper T-R). La mega-secuencia LTR abarca 11 secuencias, la MTR 5 secuencias y la UTR las 10 secuencias definidas a partir de Manta-La Plata. Las 16 secuencias T-R correspondientes a LTR y UTR fueron también datadas en correlación con las edades de los MIS, asumiendo un registro continuo de las transgresiones y regresiones causadas por los cambios glacio-eustáticos. De esta manera se obtuvo una edad para el contacto entre MTR y LTR de 1 Ma. (MIS 29), y para la base de LTR de 1.5 Ma. (MIS 51).

Sin embargo, considerando que es posible que algunas de las secuencias T-R hayan sido erosionadas, o que su registro no haya sido evidenciado o interpretado en las líneas sísmicas, se ha propuesto que la edad de la base de LTR corresponde a la base del Pleistoceno. La base del Pleistoceno estuvo definida hasta el 2009 en 1.8 Ma., en la actualidad está definida en 2.6 Ma. Como las edades de las formaciones Cuaternarias que afloran en la costa Ecuatoriana están definidas desde 1.8 Ma. En el presente trabajo se propone que la base de LTR corresponde a la edad de 1.8 Ma.

Interpretación de mega-secuencias

La interpretación de los contactos entre las mega-secuencias LTR, MTR y UTR fueron extendidos a lo largo de todo el margen. La interpretación de estos contactos entre las cuencas del Norte se lo realizó mediante la correlación entre las cuencas. La interpretación en las zonas Central y Sur, al tener cuencas aisladas, se lo realizó mediante la identificación de discordancias principales. Sus interpretaciones estuvieron validadas mediante correlación en edades con los afloramientos Cuaternarios más cercanos de la costa.

La identificación de las mega-secuencias a lo largo del margen continental, permitió distinguir que existe un registro diferencial de la presencia de las tres mega-secuencias entre la zona de pendiente y la plataforma. Mientras en la pendiente, de manera general, están depositadas las tres mega-secuencias; en la plataforma se evidencia una depositación importante de las tres mega-secuencias en la zona Norte, pero una erosión o no depositación (by pass) marcada en la zona central de las mega-secuencias LTR y MTR, con depósitos localizados de las secuencias UTR.

En las líneas sísmicas con sentido E-W de la zona Norte, las mega-secuencias muestran un levantamiento del offlap break y una migración permanente del depocentro hacia la zona costera, desde la cuenca de Jama hasta el sur de la cuenca de Cabo Pasado. Esta deformación se muestra desde las primeras secuencias de LTR. En sentido N-S, las líneas sísmicas se la zona Norte, muestran una migración del depocentro en dirección Sur-Norte, desde la cuenca de Cabo Pasado hasta la cuenca de Cojimíes.

En las zonas Central y Sur, las mega-secuencias, han sido interpretadas en las cuencas, las mismas que se presentan aisladas unas de otras, por lo cual la interpretación de la deformación registrada en las mega-secuencias son particulares y no generales. Así se puede observar que en la cuenca Ayampe, LTR está compuesto por depósitos con facies sísmicas caóticas, interpretadas como depósitos de masa, cubiertas por MTR y UTR las cuales presentan facies sub-paralelas pero con migración del depocentro desde Oeste al Este.

Discusión de resultados

Influencia del clima y la tectónica en la sedimentación

Las secuencias T-R han sido interpretadas, a lo largo del margen central del Ecuador, como el registro continuo de las transgresiones y regresiones causadas por las variaciones climato-eustáticas de los ciclos de Milankovitch. De acuerdo a las edades propuestas para las secuencias T-R, el margen del Ecuador consta de cuencas submarinas que conservan el registro climático,la menos, desde el Pleistoceno Calabrian (1.8 Ma.), los cuales se relacionan con las edades de los registros estratigráficos en la zona costera, reportados por la literatura.

A pesar de que en estos registros estratigráficos, fueron interpretados los cortejos depositacionales regresivos y transgresivos, ellos presentan un apilamiento vertical y un comportamiento diferencial de la migración en el offlap break en las diferentes cuencas del margen. Este comportamiento diferencial en la geometría del apilamiento de las secuencias, ha sido interpretado como influencia de la tectónica.

La tectónica ha causado el levantamiento del borde de plataforma, registrado con la migración del offlap break y la migración del depocentro hacia la costa, desde la cuenca de Jama hacia el Sur. Este levantamiento ha sido interpretado como evidencia del proceso de subducción. Sin embargo, los hechos que: 1) la cuenca de Cojimíes no presente un levantamiento del borde de la plataforma; 2) la zona Norte del margen central presente cuencas con la presencia de las mega-secuencias LTR, MTR y UTR, mientras en las zonas Sur y Central las secuencias LTR y MTR hayan sido erosionadas de la plataforma; y 3) la migración de los depocentros de Sur a Norte, mostrados en las cuencas de la zona Norte, sugieren un proceso tectónico diferente desde la zona Sur de la cuenca de Jama, alrededor de la latitud de 0 grados.

La influencia de la Cordillera de Carnegie

El límite sur de la cuenca de Jama coincide con el actual límite norte de la subducción de la Cordillera de Carnegie. Por lo cual es probable, que la diferenciación tectónica mostrada a lo largo del margen esté influenciada por la subducción de esta asperidad elongada. La literatura indica, que entre las consecuencias de la subducción de una asperidad elongada se encuentran: a) el levantamiento constante de la placa superior frente a la zona de subducción de la asperidad, b) la subsidencia de la placa superior en las partes circundantes de la subducción de la asperidad, c) la erosión de la zona en levantamiento por la subducción de la asperidad.

Estas consecuencias, se evidencian en el comportamiento estratigráfico a lo largo del margen del Ecuador, por lo cual se propone que la subducción de la Cordillera de Carnegie generó,

desde de la cuenca de Jama hacia el Sur: el levantamiento del margen del Ecuador y la erosión de las mega-secuencias LTR y MTR.

La deformación de las secuencias T-R se comienzan a evidenciar desde la base de LTR, por lo cual se propone que es a partir de este tiempo que la Cordillera de Carnegie inició su subducción, al menos con una morfología parecida a la que posee actualmente. La migración del depocentro de las cuencas de la zona Norte (Cojimíes, Jama y Cabo Pasado), en sentido Sur-Norte sugiere que esta subducción ha sido, al menos desde el Pleistoceno Calabrian, en una dirección preferencial de W-E. Sin embargo, esto no descarta que la subducción de la cordillera de Carnegie haya presentado un barrido hacia el Sur por el movimiento relativo con respecto al Bloque Nor-Andino. Las cuencas localizadas en la zona Sur del margen continental, habrían sido formadas o influenciadas por la subducción de asperidades locales como montes submarinos o macizos oceánicos.

INTRODUCTION

The influence of climate and tectonics as control parameters on basin stratigraphy and depositional sequence development are largely accepted. The interaction of these two parameters controls the accommodation space of the sedimentary basins through time.
Climatically driven eustasy is usually considered as the dominant mechanism of sedimentary sequence generation during Pleistocene times. The effect of climate is also reflected in the amount of sediment supply, by modifying the efficiency of weathering, erosion and sediment transport processes.

Tectonics controls the vertical movements of the basins (subsidence uplift). Along convergent margins the high rates of tectonic deformation are expected to strongly influence the fore arc basin-shape evolution as well as its basin-fill architecture. Although active margins represent open systems in which part of the terrestrial sediment flux reaches the trench a significant part of the sediment load is captured in the fore-arc basins. Furthermore, in the convergent margins, the roughness of the subducting oceanic plate influences the shape of the overriding plate and of the forearc basins. The subduction of oceanic asperities accelerate locally the tectonic erosion, and disrupt the morphology of the margin with subsidence and uplift areas that may, in turn, influence the distribution of sediments and the architecture of depositional sequences.
Investigating this record offers an access to the relative influences of climate and tectonics on the morphogenesis of active margins, particularly during the Pleistocene, when large amplitude variations of sea level fostered thick sediment preservation on subsiding margins. The study of the relationship between climate and tectonics in forearc basins by a detailed analysis of the changes in accommodation space thought time, could foster our knowledge of the evolution of convergent margins and the influences of subduction of oceanic asperities on their deformation and earthquake generation.

The Ecuadorian margin is setting where the Nazca Plate subducts beneath the South American Plate. The subduction process is strongly influenced by the subduction of various oceanic asperities at different scales. The most significant asperity is the Carnegie Ridge, an elongated oceanic plateau (300 km-wide, 2 km-high), responsible for the coastal uplift of the central Ecuadorian margin during the Quaternary. Thus, the Ecuador convergent margin is an excellent target to tentatively discriminate the effects of eustatic changes and tectonic evolution on the sedimentary record.

The ATACAMES geophysical cruise conducted onboard the research vessel L'Atalante (Ifremer) in January–February 2012 acquired high-resolution multichannel seismic-reflection and 3.5 kHz mud penetrator (Chirp) data in 100–1,000 m water depths, together with multibeam bathymetry and piston cores along the entire Ecuador margin. The analysis of seismic and core data by using the principles of seismic and sequence stratigraphy, allowed us to describe the evolution of the Quaternary marine forearc basins, which complement the onshore studies of

the Ecuadorian margin. The present work aims to: 1) identify and discriminate the record of climate and tectonics controls into marine forearc basins during Pleistocene; 2) estimate the time and spatial relationship of their respective record, and; 3) discuss the influence of the subduction asperities, with different sizes and morphology, on the geological evolution of these basins.

This manuscript is organized in six chapters. The first chapter proposes a state-of-the-art on oceanic asperity subduction process and principles of seismic and sequence stratigraphy. The second chapter presents the main geological aspects of the central subduction margin of Ecuador. The third chapter describes the scientific data and methods used in this study. The fourth and the fifth chapters correspond to the presentation of the results. The fourth chapter describes in details, in an article format, the sedimentary record in the Manta-Plata area, which will be used as a reference frame for the stratigraphy of the entire margin; this sedimentary record is used to reconstruct its geodynamic evolution in relation with the subduction of an asperity. The fifth chapter focuses on the description and interpretation of: a) seafloor morphology along of the central margin (bathymetry data); b) the stacking pattern of depositional sequences into each of the ten basins identified in the margin (multichannel seismic data); c) the sedimentary record and dating of sequences (piston core data), and; d) the onshore correlation of sequences. The last part includes the discussion and proposed an evolution of the margin at local scale (for each basin) and at regional scale for the entire central margin.

INTRODUCTION

Le climat et la tectonique sont les deux principaux paramètres qui contrôlent le dépôt des séquences et la stratigraphie des bassins sédimentaires. En particulier c'est l'interaction de ces deux paramètres qui va contrôler l'espace disponible pour l'accumulation des sédiments (espace d'accommodation) au cours du temps.

Durant le Pléistocène, les cycles climatiques sont très contrastés et sont associés à d'importantes variations eustatiques qui affectent l'enregistrement sédimentaire et contrôlent la distribution et la géométrie des séquences sédimentaires. La variabilité du climat du Pléistocène contribue également à la modulation de l'érosion et de la quantité d'apport sédimentaire.

Les mouvements verticaux dus à la tectonique sont aussi un facteur de contrôle très importants des bassins sédimentaires. En particulier les marges actives, qui sont des zones majeures de création et de destruction des reliefs à la surface de la Terre et en conséquence des zones importantes de transferts de sédiments. En effet les marges actives sont considérées comme des systèmes ouverts dans lesquels une partie des flux sédimentaires terrestres transite vers la fosse où ils sont recyclés par la subduction. Mais une partie non négligeable est cependant préservée dans les bassins avant-arc et les bassins de pentes. Ces bassins sont aussi sensibles à la subduction de reliefs portés par la plaque océanique qui modifie les équilibres et induit des mouvements verticaux importants qui influencent la distribution et l'architecture des séquences de dépôts.

L'analyse des flux sédimentaires le long des marges actives offre donc la possibilité de décrypter les influences relatives du climat et de la tectonique sur la morphogenèse des marges en particulier durant le Pléistocène. En raison de la forte amplitude des variations du niveau de la mer du Pléistocène, le haut de pente (100-800m) situé à la charnière du plateau continental est le plus à même d'enregistrer le plus complètement, et avec le plus grand détail, les variations de flux sédimentaires liées aux changements climato-eustatiques. L'étude conjointe de l'influence relative du climat et de la tectonique dans les bassins avant arc sur l'évolution de l'espace accommodation au cours du temps permet de reconstituer l'évolution de la déformation le long des marges actives et en particulier de la subduction de reliefs océaniques.

Le long de la marge d'Equateur, la plaque Nazca passe en subduction sous la plaque Sud-Américaine. La marge est fortement influencée par l'arrivée dans la subduction de reliefs portés par la plaque en subduction, dont le plus remarquable est la ride de Carnegie (300 km-de large et 2 km de haut). C'est donc un excellent laboratoire naturel pour discriminer dans les enregistrements sédimentaires les effets conjoints du climat (cycles eustatiques) et de la tectonique (subduction de reliefs océaniques).

Le long de la marge de l'Equateur la campagne océanographique ATACAMES (Archivage de la Tectonique Active et du Climat le long de la Marge d'Équateur en Subduction) s'est déroulée entre le 15 janvier et le 18 février 2012 en Équateur. Plusieurs outils ont été utilisés durant cette campagne: une chaîne d'acquisition sismique HR composée d'une source sismique (6

canons à air) et d'une flûte sismique (récepteur de 72 traces) de 700 m de long; des sondeurs de bathymétrie multifaisceaux pour cartographier le fond marin, un sondeur de sédiment « Chirp » pour imager les premières dizaines de mètres sous le fond, et un carottier pour prélever des échantillons de sédiments du fond marin. Au total plus de 5000 kms de profils de sismique haute résolution ont été réalisés ainsi que plus de 30 carottages sur le plateau continental et les bassins du haut de pente (entre 50 et 1000 m de profondeur).

L'analyse des archives tectono-climatiques du Pléistocène par stratigraphie séquentielle (sismique marine) complétée par l'étude de carottes et par des corrélations avec le Pléistocène connu « onshore », nous a permis de reconstituer l'évolution morpho-structurale pléistocène de la marge. Notre travail a permis 1) d'identifier et de discriminer l'effet du climat et de la tectonique dans l'enregistrement sédimentaire ; 2) d'établir une chronologie de dépôts des séquences et de la déformation tectonique des corps sédimentaires ; 3) de discuter l'influence sur la déformation/sédimentation de la marge de la subduction des reliefs portés par la plaque océanique à différentes échelles de temps et d'espace.

Ce manuscrit est organisé en 6 chapitres. Le premier chapitre est une revue sur l'effet de l'entrée en subduction d'un relief océanique et sur les principes de la stratigraphie sismique. Le deuxième chapitre montre le cadre géologique et géodynamique de la marge d'Equateur. Le troisième chapitre décrit les données géophysiques et les méthodes que nous avons utilisées. Les chapitres 4 et le chapitre 5 correspondent à la présentation des résultats. Le chapitre 4 se présente sous la forme d'un article scientifique et décrit dans le détail les séquences de dépôt et la chronologie de la déformation de la zone de Manta-Ile de la Plata. Le chapitre 5 débute par une description et une interprétation de la bathymétrie et des séquences de dépôts dans les bassins identifiés le long de la marge. Ce chapitre se poursuit par une description des faciès sédimentaires des carottes et l'apport de leur datation. Il se termine par l'établissement de corrélations entre séquences sismiques et séquences identifiées dans les affleurements connus à terre. La dernière partie comprend une discussion et propose une évolution de la marge à l'échelle locale (chaque basin) et régionale pour l'ensemble de la marge.

CHAPTER 1: The stratigraphic record of the deformation on subduction margins

"Savoir s'étonner à propos est
le premier pas fait sur la route
de la découverte"

Louis Pasteur (1822-1895)

1. The active subduction margins

Active margins refer to plate margins along which two lithospheric plates are moving to or along each other. Plates include both oceanic crust and continental crust. When one of the two adjacent tectonic plates moves under another, generally due to the difference of density between them, it is called subduction. This process allows to recycle the oceanic lithosphere and to accrete a part of the mantle to the continental lithosphere (Lallemand, 1999).

Mostly of the subducted lithosphere is oceanic, but not exclusive, while the over-riding lithosphere may or may not be oceanic. Therefore there are some types of subduction depending of the nature of plates involved as well as the context where is given the process.

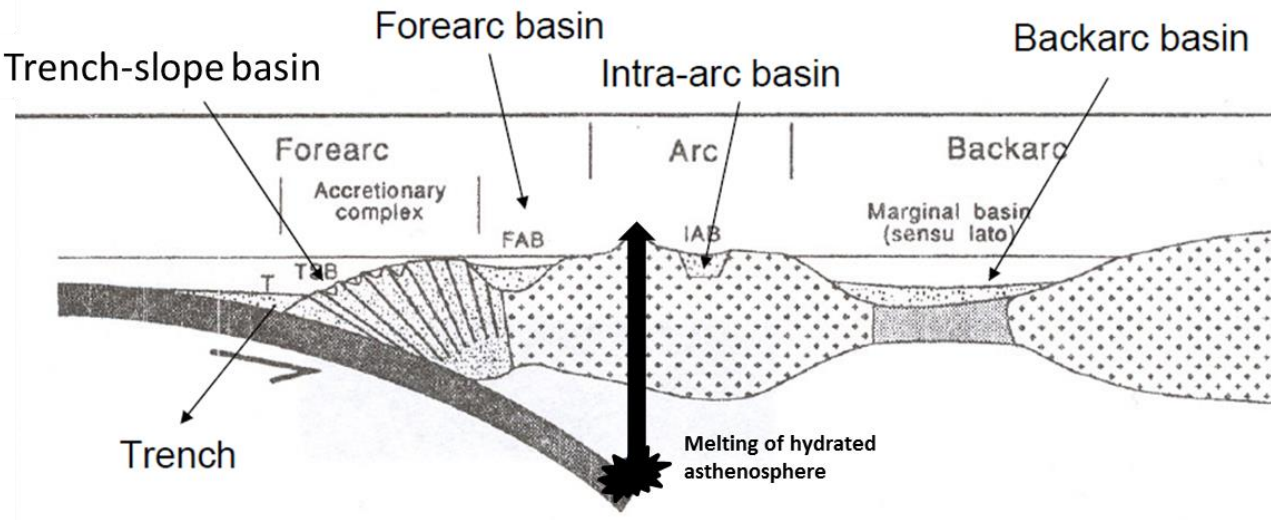

Figure 1.1: The morpho-structure elements in an oceanic-continental subduction zone.

The oceanic-continental subduction generally consists of some characteristic structural elements, which are developed according to the context, so their presence may not be systematic. As a principal topographic expression, the subduction boundary shows, an oceanic trench on the ocean side and mountain ranges on the continental side. These mountain arcs, generally parallel to the ocean trench, are characterized by the presence of volcanoes which tend to be explosives due to partial melting of asthenospheric mantle for the presence of water derived from subducted slab. It creates in these cases the continental volcanic arcs (e.g. Andes, Cascades). When this process is an oceanic-oceanic subduction it produces the volcanic islands arcs (e.g. Aleutians, Mariannas). These arcs contain the intra-arc basins, behind the arcs are located the back-arc basins, and between the trench and the volcanic arc is set the forearc region (Figure 1.1).

The morpho-structure of the forearc area is influenced: by the thickness of sediments in the trench, by the geological structures of the upper plate and by the structural complexities or

segmentation of the subducting plate (Cloos, 1993). This region is usually composed for: the accretionary prism, the slope basins and the fore-arc basins (Figure 1.1).

The accretionary prism is made up of the sediments that are accreted onto the over-riding plate. According to the volume of accreted sediments, these margins are classified into two categories: (1) accretionary margins and (2) erosive margins (Clift and Vannucchi, 2004; von Huene and Scholl, 1991) (Figure 1.2).

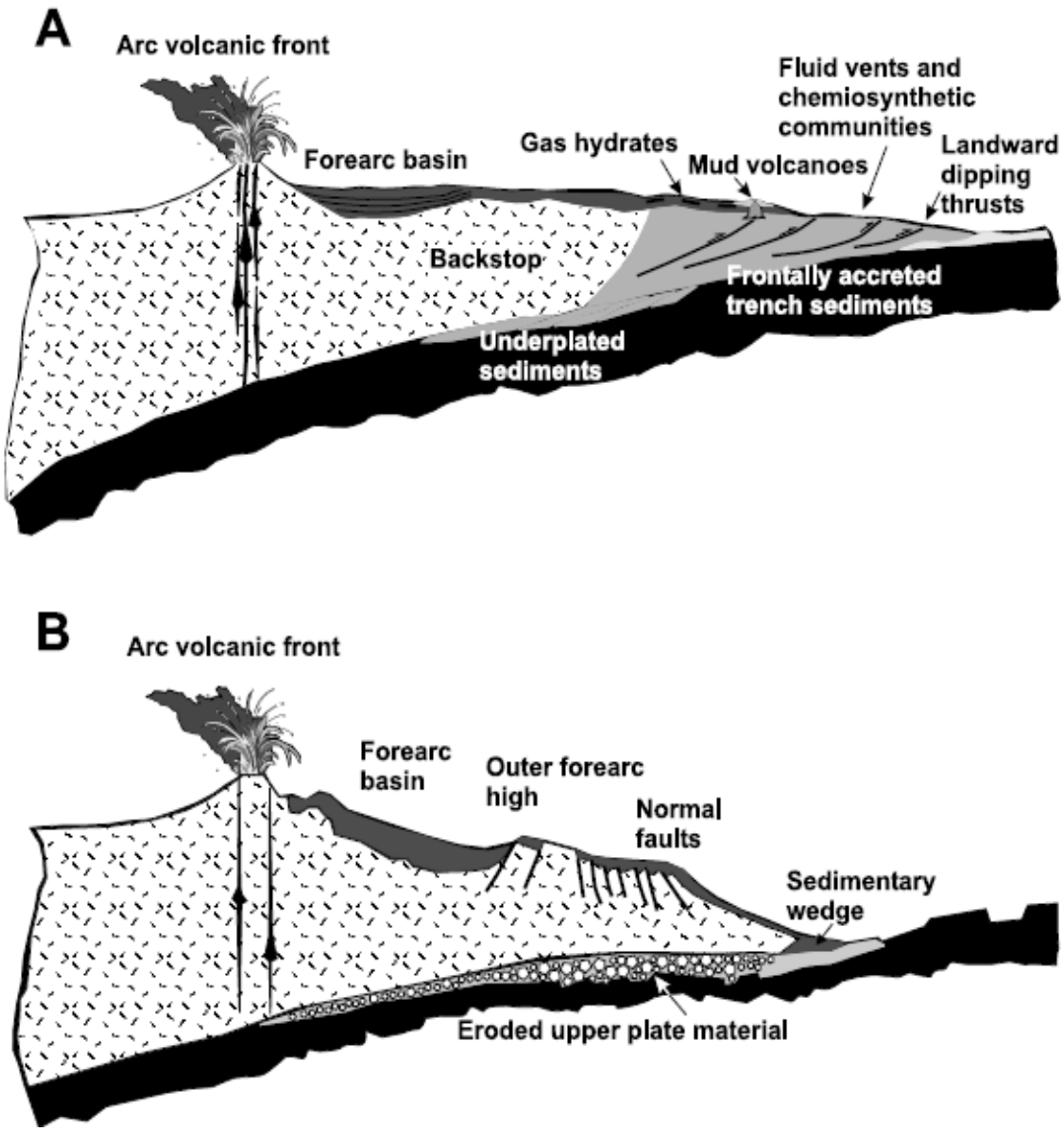

Figure 1.2 Basic types of active margin: a) accretionary and b) erosive. Schematic diagrams showing their common features. From Clift and Vannucchi (2004).

A margin is accretionary if a fixed point on the forearc migrates upward and landward over long periods of geological time due to net sediment accumulation in the trench because of the transfer of material from the subducting plate into the overriding plate, either by frontal off scraping at the trench axis or by underplating of the forearc wedge at greater depths (Clift and Vannucchi, 2004). They are characterized by an external wedge or accretionary prism formed by thrusted and deformed slices of trench and oceanic sediments (Clift et al., 2009). Such

margins, like Barbados or Nankai, exhibit low angle continental slopes (2-4 °) with soft anticlines and thrust faults structures (Collot et al., 2009).

A margin is erosive if is in a state of long-term (>10 m.y.) trench retreat due to the removal of material from the underside of the forearc wedge (Clift and Vannucchi, 2004).
The limited amount of sediment preserved in the trench and at the toe of slope (no or very small accretionary wedge) results from a partial or total removal of sedimentary material by the subduction erosion. The subduction erosion produces a progressive mass transfer from upper to lower plate, probably by physical abrasion involving high stress and fluid-assisted abrasion involving low stress (Von Huene and Lallemand, 1990; von Huene et al., 2004).

The tectonic or subduction erosion occurs both by frontal and basal erosion. The frontal erosion results from a combination of erosion and structural collapse of the forearc wedge into the trench; whereas the basal erosion is produced by abrasion and hydrofracturing of the base of the overriding plate above the subduction channel (Figure 1.3).

The subduction erosion causes in the margins (1) long-term subsidence and tilting of the continental slope, (2) regional tectonic extension of the slope apron, and (3) disrupted topography across the lower slope and in the wake of subducted ocean-floor reliefs (Vannucchi et al., 2004, 2001; Von Huene and Lallemand, 1990; Von Huene et al., 2000).

These erosive margins show steep continental slopes (> 7-8°) with seaward dipping normal faults, causing superficial erosion of the continental slope with abundant landslides and debris flows, which accumulate in a small sediment wedge at the toe of the slope (Collot et al., 2009; Ranero and von Huene, 2000). Consequently, these types of margins as in Guatemala (Aubouin et al., 1984, 1982; Vannucchi et al., 2004) , Mexico (Mercier de Lépinay et al., 1997), Nicaragua (Ranero et al., 2000), Costa Rica (Ranero and von Huene, 2000), Peru (Sosson et al., 1994; Hampel et al., 2004) and Tonga (Clift and MacLeod, 1999) exhibit abundant seafloor irregularities along the slope.

Along a lot of margins, long term quasi-stable tectonic erosion is reported (Mercier de Lépinay et al., 1997; Sosson et al., 1994; Vannucchi et al., 2004). However, subduction-erosion could be enhanced locally by the subduction of seamounts or ridges of the in-coming plate. Indeed, there are some triggering mechanisms which accelerate the tectonic erosion (Table 8, Lallemand, 1999), but the presence of asperities (seamounts, ridges, grabens, horsts, etc.) on the subducting plate appear critical (Lallemand et al., 1994).

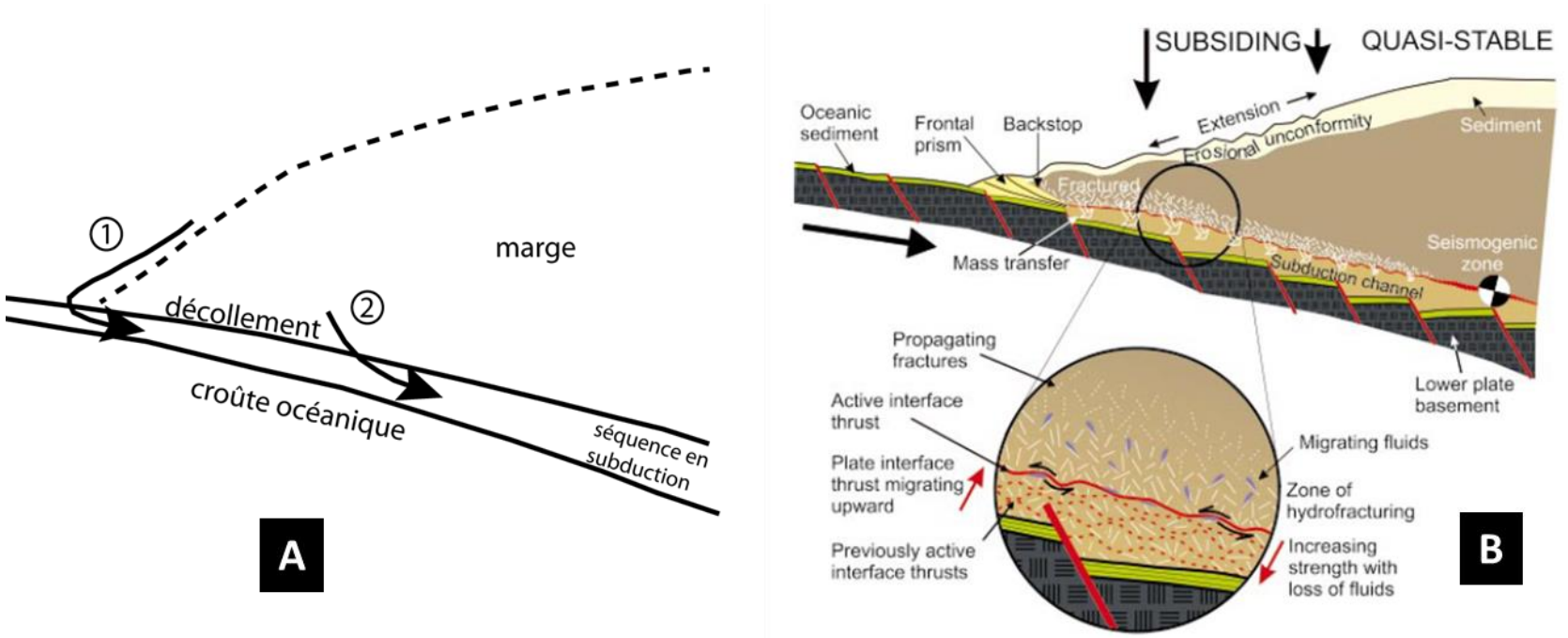

Figure 1.3: The subduction erosion process. Diagrams A from Lallemand (1992) and B from von Huene et. al (2004) show the two types of tectonic erosion of a subduction margin. A) Frontal erosion is caused by surface collapse over the slope's base, transporting the eroded material to the subduction interplate zone (arrow 1). The basal erosion drags the material from the prism to the subduction channel (arrow 2). B) Basal erosion is caused by hydro-fracturing in the interplate zone and fractures propagation at the base of the overriding plate.

1.1. The oceanic asperities subduction

The term asperities refer to all the reliefs on the subducting oceanic plate, i.e.: horst and grabens, submarine volcanoes, isolated or multi-peaks seamounts built by mid-ocean ridges or volcanic arcs, plateaus and micro-continents (Lallemand, 1999). These reliefs are generically called “asperities” when they are subducted beneath the margin. It has been demonstrated experimentally, and verified on many margins, that seamounts and oceanic ridges strongly increase tectonic erosion (Lallemand, 1999). The different shapes and the orientations of the reliefs with respect to the margin generate a multitude of possible deformations on the overriding plate.

According to Lallemand (1999), one of the most important indicators of the subduction of an asperity, is the succession in time and space of vertical movements. The strong subsidence of the margin caused by tectonic erosion can last a few million years, triggering at the same time local uplifts due the subduction of positive features, like seamounts (Figure 1.4).

1.2. Margin deformation associated to the subduction of an oceanic relief

Subducting plate asperities, by considering their length/width ratios, are: “local”, “punctual” or “isolated” like seamounts, and “elongated” or “continuous” like ridges. Some models have been proposed to show the deformation of the upper plate due to the impact of seamounts and ridges. For the deformation caused by isolated asperities is regularly referred the analogic model from Dominguez et al. (1998a) and Lallemand (1999). Some natural models have been also discussed by Ballance et al. (1989); von Huene (1990); Ranero and von Huene (2000) and Laursen et al. (2002).
The subduction of elongated asperities have been modeled in laboratory by Hampel et al. (2004b), Martinod et al. (2010), Espurt et al. (2008) and Dominguez et al. (1998b). The natural effect of the subducting elongated asperities has been discussed by Clift (2003), Von Huene et al. (2000), Hampel et al, (2004a), and Gardner et al. (1992).

The model for isolated asperities performed by Dominguez et al. (1998a) was in reference to accretionary margins, whereas Hampel et al. (2004b) carried out their elongated asperities models with respect to erosive margins. The main features observed in these models are described below.

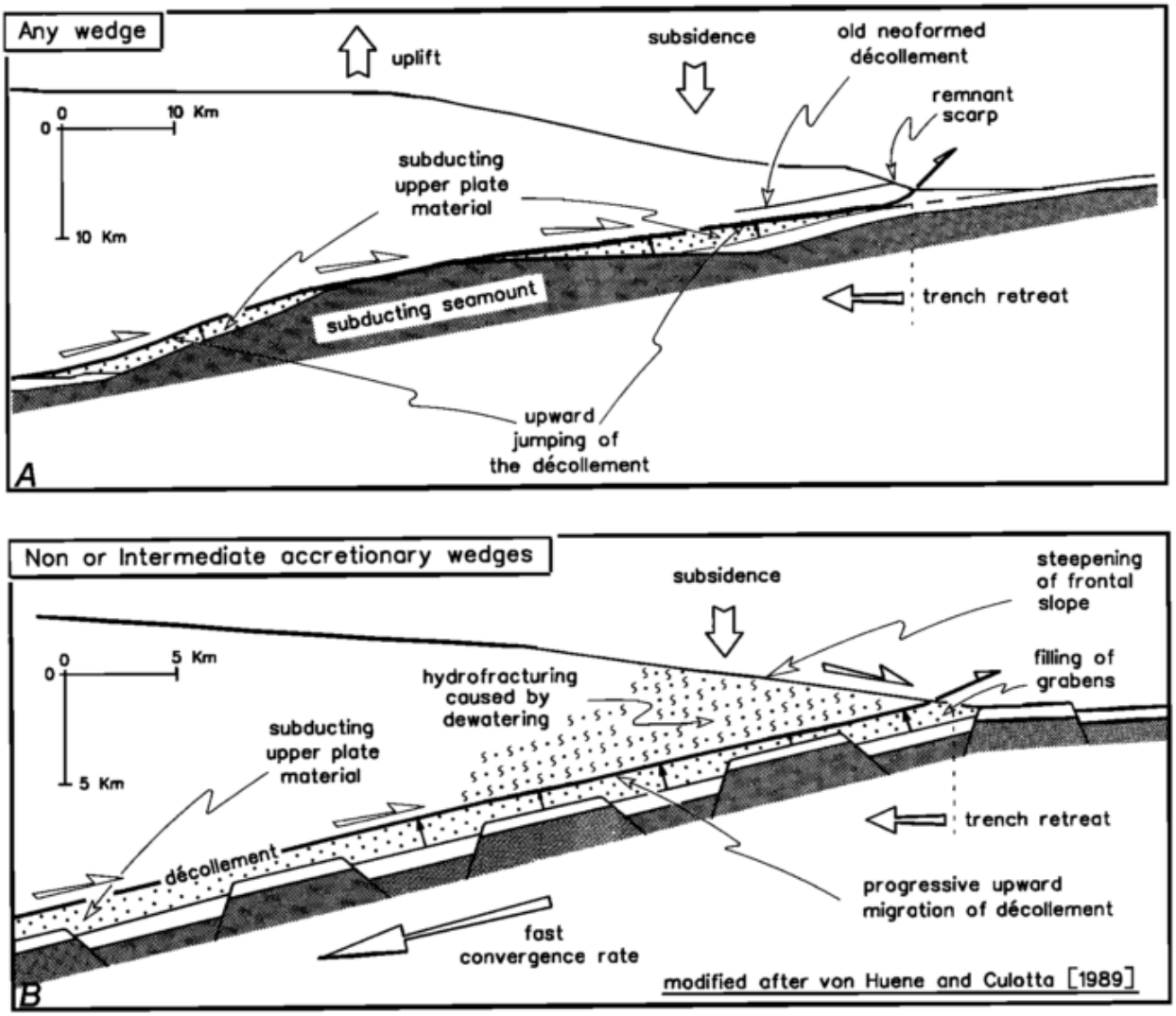

Figure 1.4: Mechanism of the tectonic erosion along the convergent margins (from Lallemand et al., 1994). It shows the different processes and types of deformation caused by the diverse shapes of asperities when they get in subduction. In the first case (A) an isolate asperity produces locally vertical movements; In the second case (B) the roughness of the subducting plate produces long term subsidence.

1.2.1. The subduction of seamounts

The analogic / physical modeling of the subduction of seamounts of different shapes and sizes beneath an accretionary margin shows the range of deformations that can appear on the overriding plate (Dominguez et al., 1998a). The main morphostructural deformations are the followings (Figure 1.5):

- A morphological re-entrant at the base of the slope. This re-entrant is filled by landslides and hemi-pelagic sedimentation. On accretionary margins this filling is faster than on erosive margins.
- A sub- vertical scarp on the middle slope. The height of the scarp is proportional to the height of the seamount. Sediments progressively cover the scarp during the subduction of the seamount, but the top of the scarp is an important morphological element that can stand even when the seamount is behind it.
- A set of (back) thrust faults deep in a seaward direction. The push of the asperity against the margin produces a local uplift and a set of reverse fault which propagates in a landward direction. It forms a circular knoll whose geometry and volume are controlled by the shape and size of the asperity. (Figure 1.5B and C)
- A set of normal and strike-slip faults. Normal faults are present principally around the scarp provoking landslides. The strike-slip faults occur on the right and left sides of the re-entrant in the wake of the subducting seamount, accommodating the deflection of the margin caused by the asperity (Figure 1.5C).

The accretion in the wake of the seamount depends on the sediment supply, so the rate of the filling of the re-entrant caused by a seamount is different between the accretionary and erosive margins. In erosive margins the slope indentations remains for a long time after the seamount subduction (Dominguez et al., 1998; Laursen et al., 2002; Hampel, etal., 2004), while in the accretionary margin the re-entrant are swiftly filled by sediments (Figures 1.5A and 1.6).

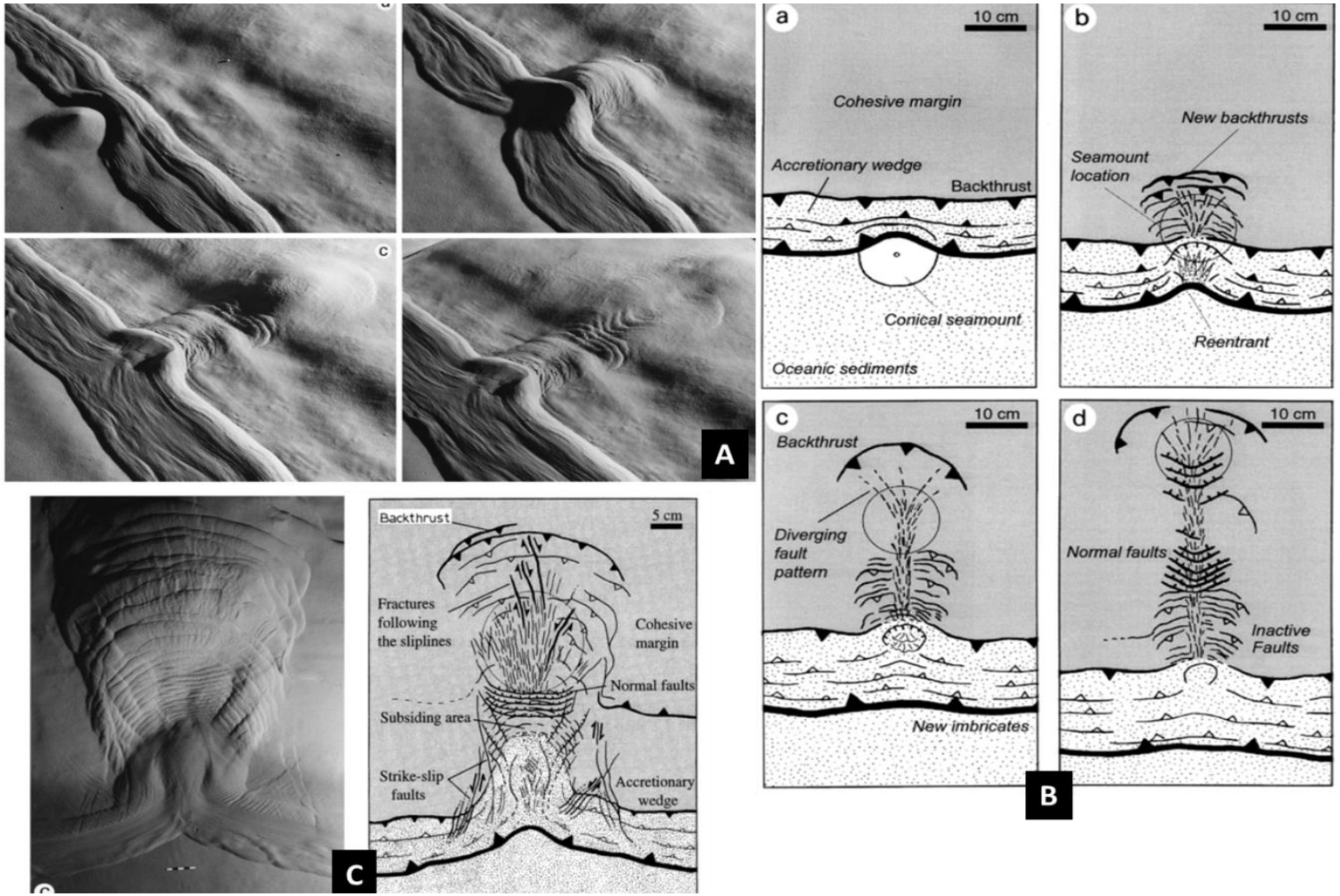

Figure 1.5: Subduction seamount into an accretionary margin, (from Dominguez et al., 1998). A) The figures show the different stages of the subduction of a conical seamount. B) The figures display the interpreted deformation in the overriding plate caused by continous stages of the seamount subduction. C) Resume of the principal deformation elments caused by a subduction seamount (in this case by a a flat-topped seamount or guyot). We can note in general that the models display: reentrant, sub-vertical scarp, backthrust, normal and strike-slip faults. We can observe in this figure the deformation caused just beside of the zone of the onset of the subducting seamount.

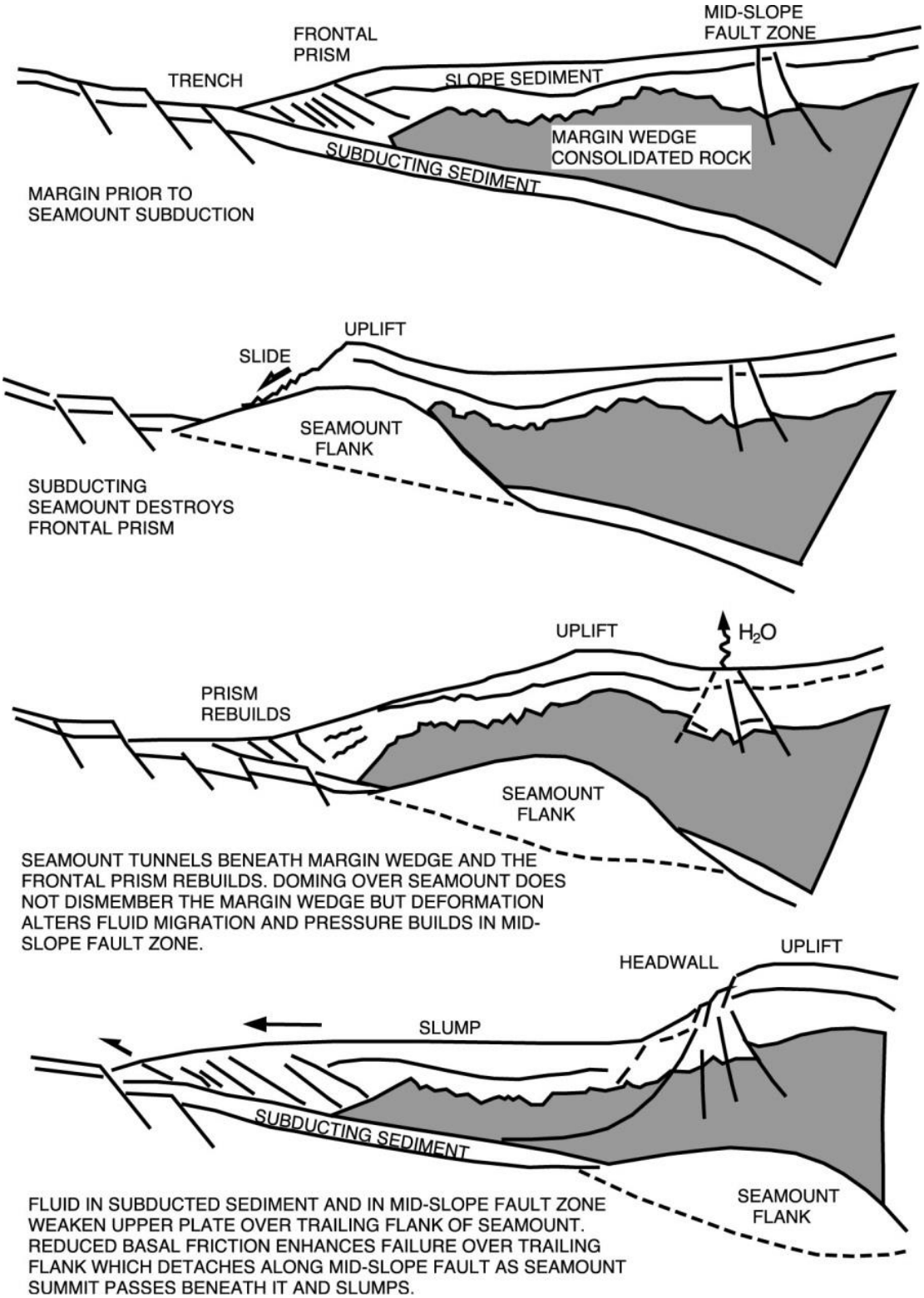

Figure 1.6: Effects of the seamount subduction along a margin (von Huene et al., 2004). First the frontal sedimentary wedge is destroyed following by the uplift of the slope seafloor, and then rebuild of the frontal prisms (von Huene et al., 2004).

1.2.2. The subduction of ridges

The first physical models of the subduction of ridges were inspired by the Nazca ridge subduction, which is obliquely subducting below the erosive Peruvian margin (Hampel et al., 2004b). These models focus on the subduction of elongated bathymetric highs that are oriented obliquely to the convergence direction and migrating along the plate boundary. The most important features shown in these models are the followings (Figure 1.7):

- A prominent change on the overriding plate morphology, caused by surface erosion and oblique normal faulting. The oblique normal faults are induced by the oblique convergence of the ridge, causing extension at the trailing flank with slumping and the perturbation at the leading flank.
- An uplift of the margin in front of the leading flank of the ridge. On the Peruvian margin, the uplift is characterized by uplifted marine terraces (Pisco marine terraces, Macharé and Ortlieb, 1992) and the active subsidence is highlighted by gullies and submarine canyons on the upper slope (Hampel, et al., 2004a).
- In erosive margin under ridge subduction are generally characterized by a minor reentrant than the accretive margin, resulting from a mechanically strong frontal wedge.

Espurt et al. (2008) shows, using analogic models of perpendicular plateau subduction that the topography of the overriding plate uplifts suddenly as soon as a plateau (ridge) enters in subduction (Figure 1.8a). After the onset of the subduction of the ridge, the uplift will continue slowly in a long-term during the subduction of the asperity. These authors interpreted the rapid uplift at the beginning of the plateau subduction as an isostatic adjustment re-accommodating the asperity subduction, whereas the long-term slow uplift has been explained as a thickening of the overriding plate (Figure 1.8b).

Although physical models explain some of the deformation features observed when asperities subduct, natural examples appear far more complex. Examples of the deformation produced by the combination of different types of subduction asperities can be seen along of the Costa Rica (Von Huene et al., 2000) and Chile (Laursen et al., 2002) margins (Figures 1.9 and 1.10).

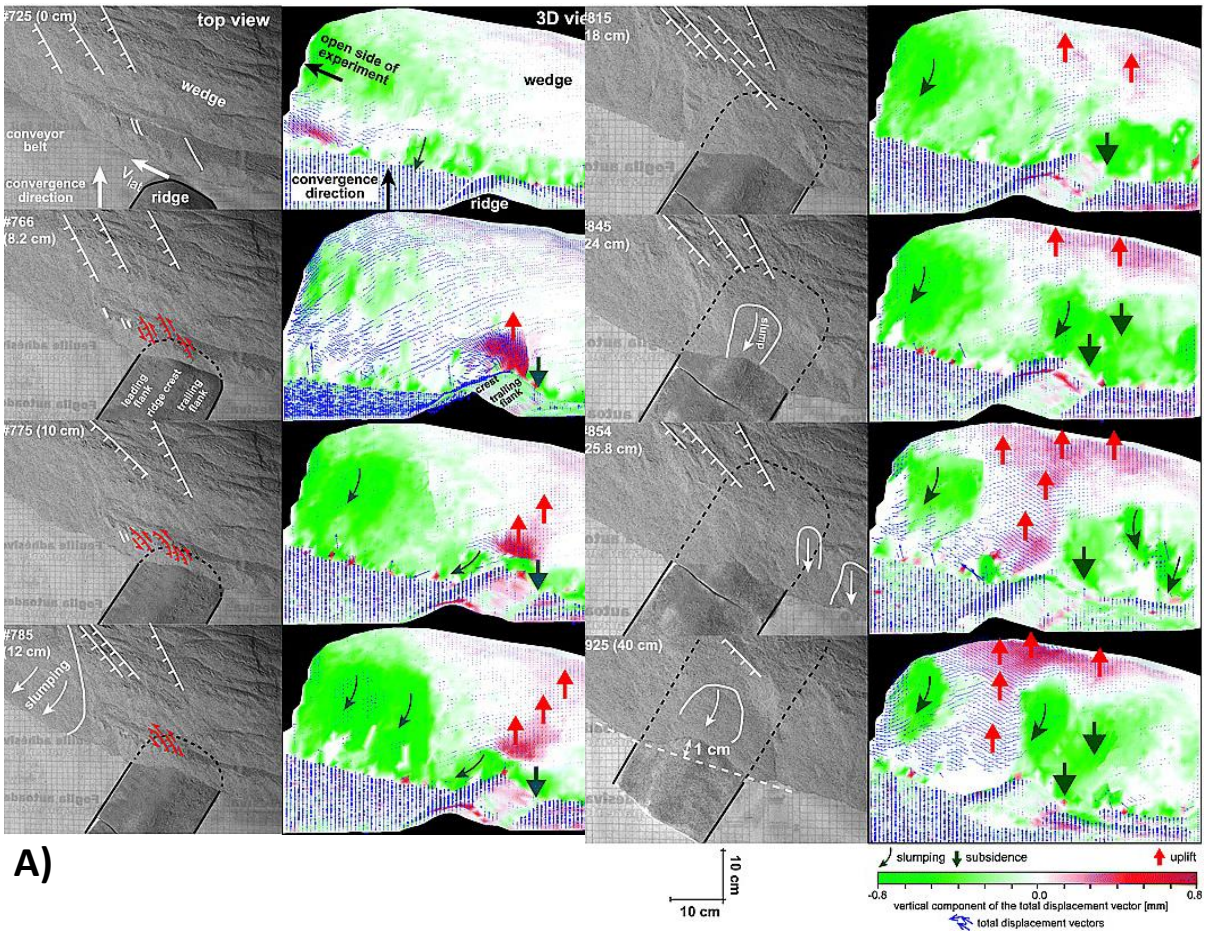
top view
3D view
wedge
conveyor belt
convergence direction
ridge
open side of experiment
#725 (0 cm)
#766 (8.2 cm)
#775 (10 cm)
#785 (12 cm)
leading flank
ridge crest
trailing flank
slumping
815 (18 cm)
845 (24 cm)
854 (25.8 cm)
925 (40 cm)
slump
21 cm
10 cm
10 cm
slumping
subsidence
uplift
-0.8
0.0
0.8
vertical component of the total displacement vector [mm]
total displacement vectors

A)

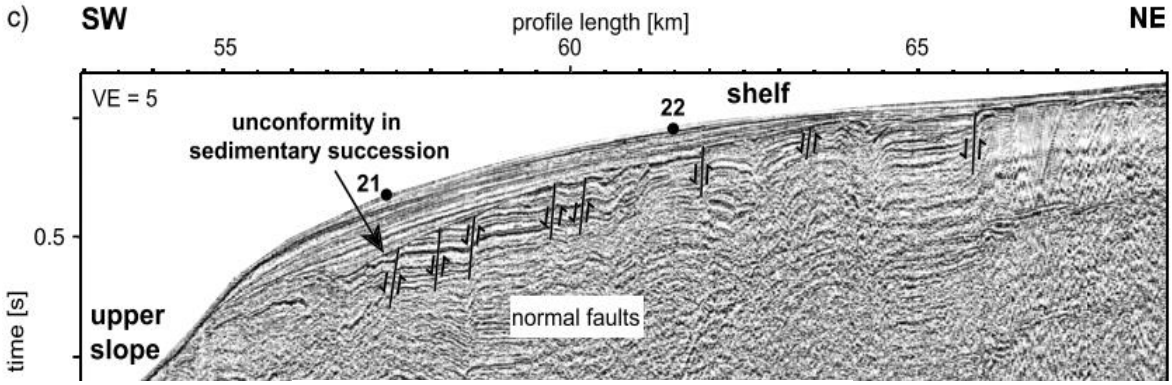
c)
SW
NE
profile length [km]
55
60
65
VE = 5
unconformity in sedimentary succession
21
22
shelf
upper slope
normal faults
time [s]
0.5

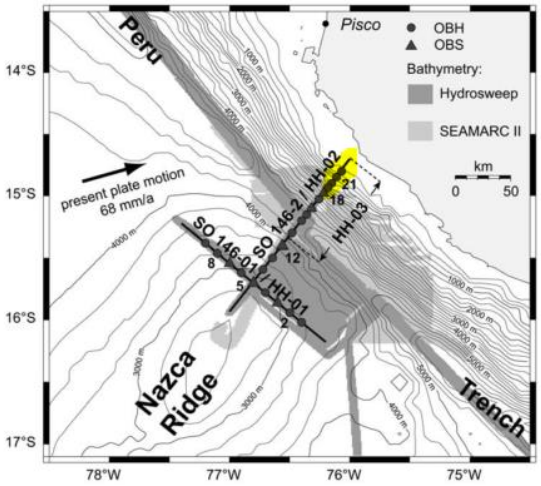
Peru
Pisco
OBH
OBS
Bathymetry:
Hydrosweep
SEAMARC II
km
0
50
present plate motion
68 mm/a
SO 146-2 / HH-02
SO 146-01 / HH-01
HH-03
Nazca Ridge
Trench
14°S
15°S
16°S
17°S
78°W
77°W
76°W
75°W

B)

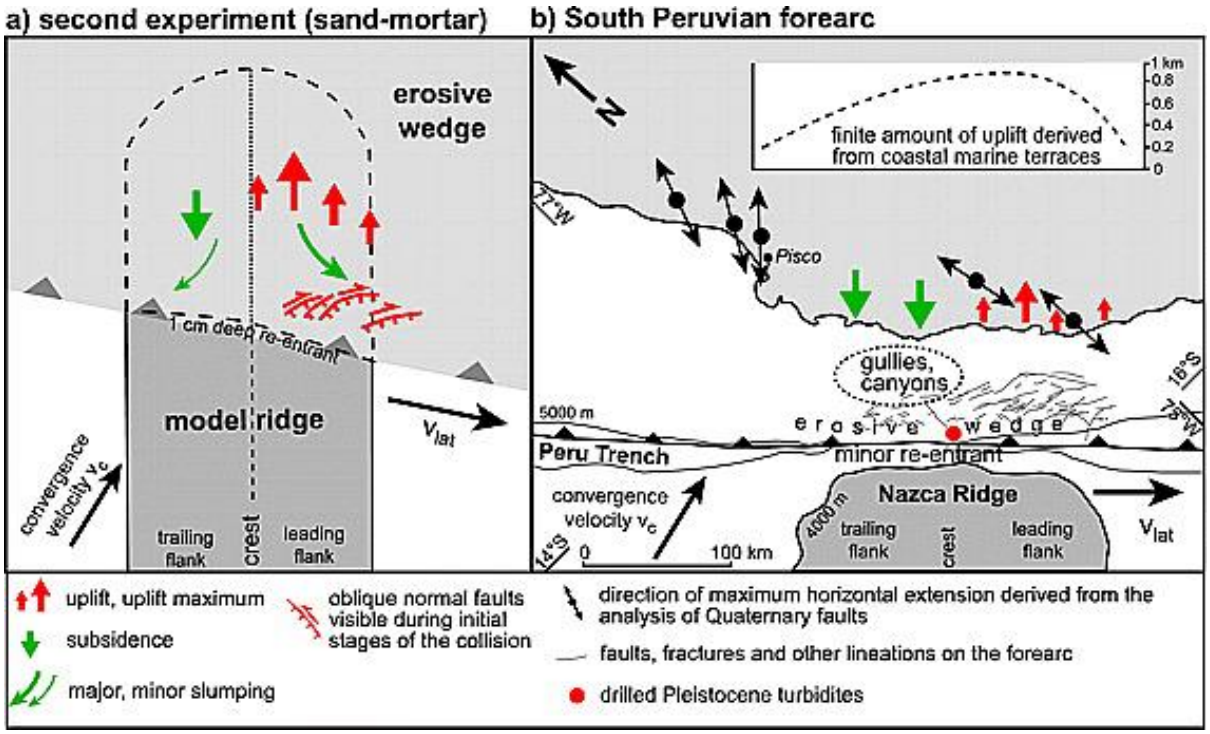

C)

Figure 1.7: Deformation caused by an obliquely subducting ridge in a erosive margin, according the analogic model carried out by Hampel et al. (2004b). A) The upper images show the different stages of their model, standing out the uplift of the margin toward the motion direction (in front of the leading flank), and the subsidence at the trailing flank of the ridge. B) The central images show a multichannel seismic profile located at platform of the overriding plate, just in front of the Nazca ridge, where is possible to observe a subsidence of the shelf break. This image shows that although there is a general uplift of the margin, due to the subduction of the Nazca ridge, there is also a tectonic subsidence caused by the tectonic erosion (Hampel et al., 2004a). C) The lower image presents the relationship, present by Hampel et al. (2004b) between the analogic model and the natural situation around the Pisco coastal zone, where it is subducting the Nazca ridge.

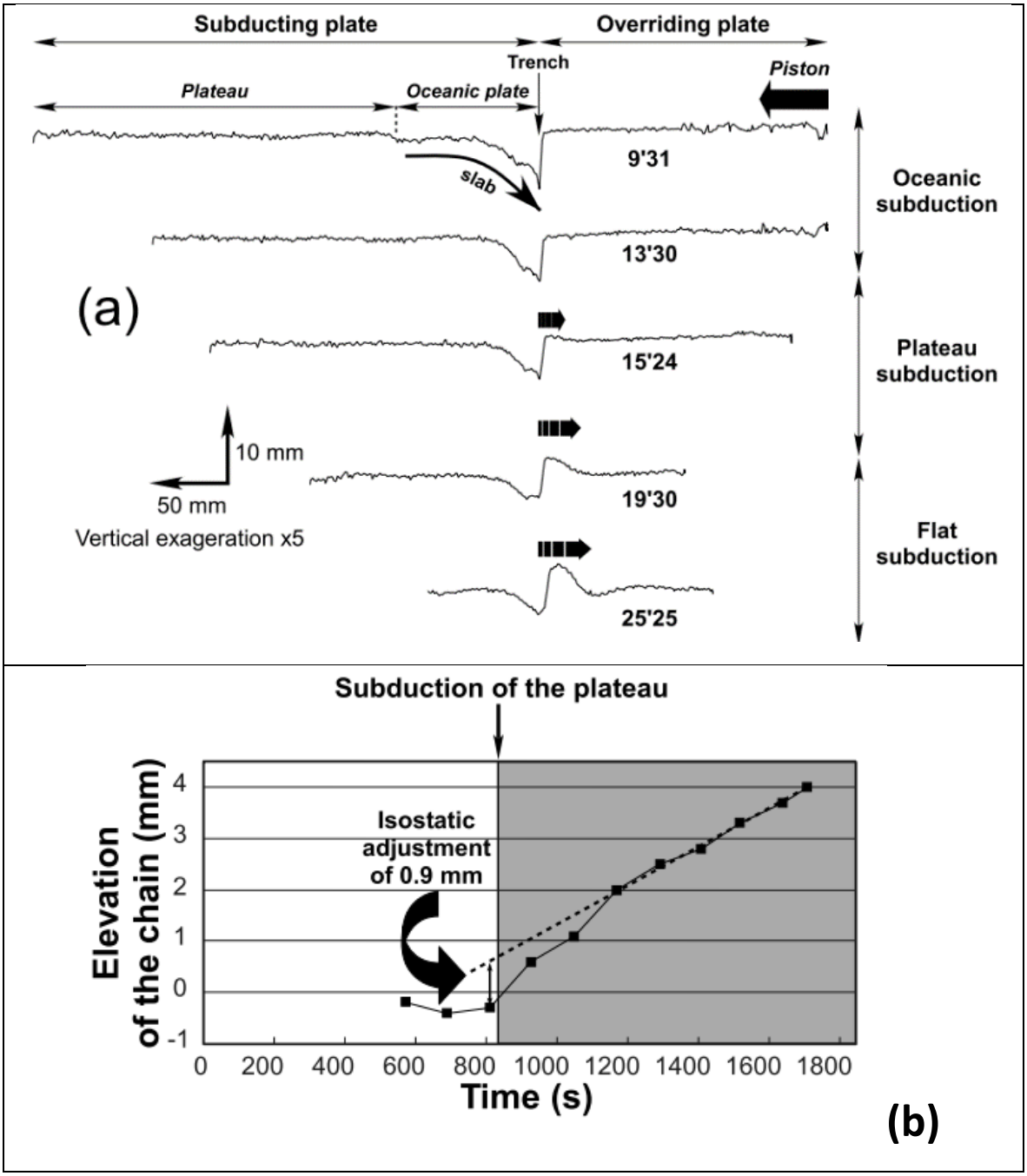

Figure 1.8: Results displayed by the analogic model from Espurt et al. (2008). A) This model, which simulates a perpendicular plateau subduction, shows a suddenly uplift of the margin as soon as the plateau enters in subduction. B) This diagram displays the rapid uplift at the beginning of the plateau subduction and the long-term slow uplift during the time of subduction asperity.

Along the Costa Rica margin, above the segment where the Cocos ridge is subducting, long-term erosion of shelf sediment strata shapes the top of the margin wedge (Figure 1.9C). For Von Huene et al. (2000) this outer shelf uplift corresponds to the signature of the subduction of the Cocos ridge, the "sister" ridge of the Carnegie ridge.

Along the Chile margin, above the segment where the Juan Fernandez Ridge is subducting, the margin deformation records successively the oceanic ridge subduction at the regional scale, enhanced localy by seamounts, which crests the ridge (Fig. 1.10). The local effect of seamount subduction is added to the effect of the Juan Fernandez ridge; the effect of the Juan Fernandez ridge is enhanced when it is crested by seamounts (Laursen et al., 2002).

In these examples we can note that active margins show significant vertical movements that are illustrated by the slope subsidence and failure, (Collot et al., 2009; Mercier de Lépinay et al., 1997; Sage et al., 2006; Sosson et al., 1994) and in some places by onshore marine terraces (Cantalamessa and Di Celma, 2004; Macharé and Ortlieb, 1992; K. Pedoja et al., 2006). Regionally, tectonic erosion process is associated to long-term subsidence along the slope (Vannucchi et al., 2004). More locally the subduction of oceanic roughness, as oceanic ridge or seamounts, produce/enhance a deformation of the slope associated with vertical movements (Dominguez et al., 1998a; Espurt et al., 2008; Hampel et al., 2004a; Lallemand, 1999; Von Huene et al., 2000). They are much less documented on the platform itself.

However, the platform records with precision any tectonic or eustatic-sea level changes. The platform is also an area where you can date the sediments with details measuring the impact of climate and eustatic change at least for the Pleistocene (see examples in Paquet et al., 2009; 2011) (Figure 1.11).

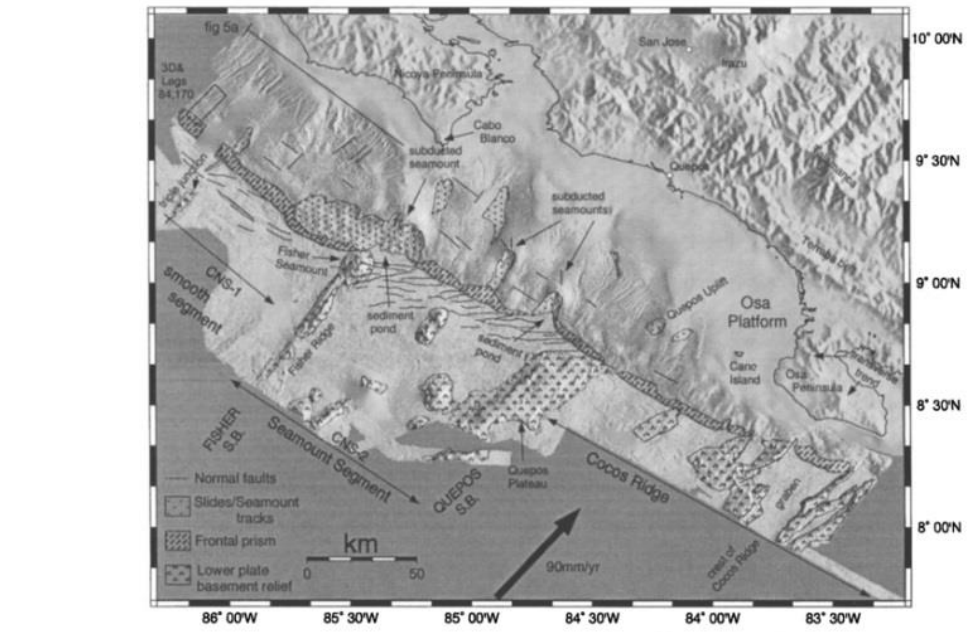

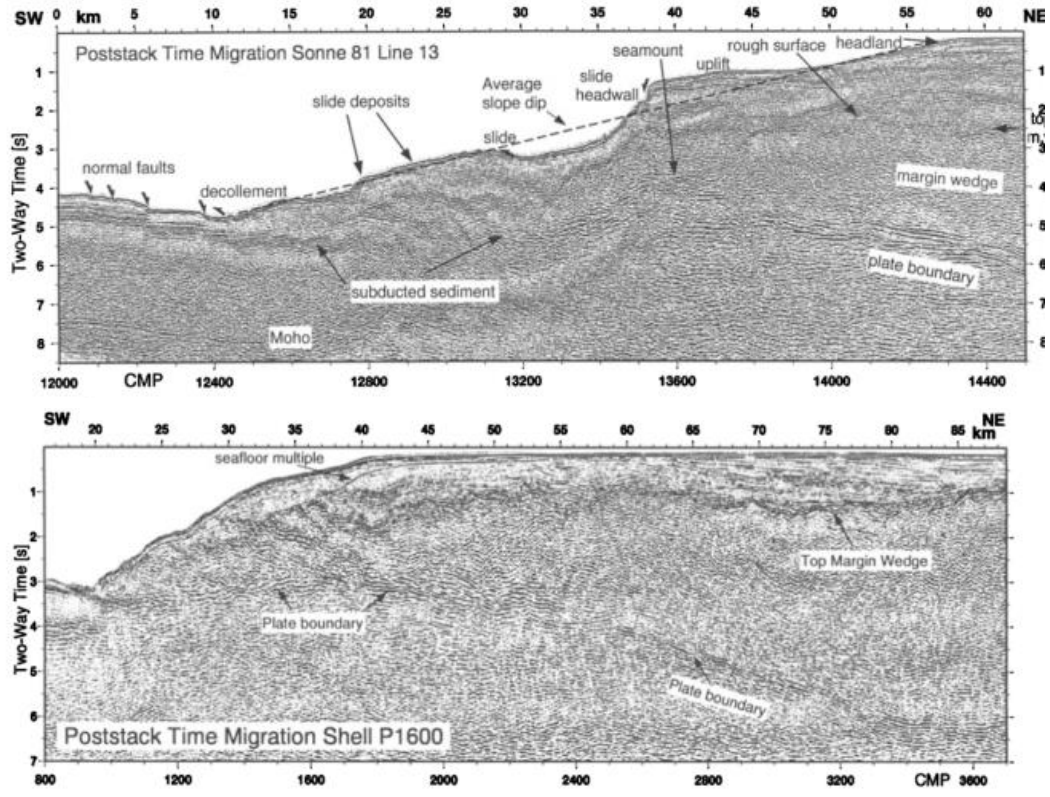

Figure 8. Migrated time section of Shell Internationale Petroleum Mij.B.V. Line 1600 across the Osa platform. See Plate 1 for location. Erosion of shelf sediment strata occurs between km 50 and 70.

Figure 1.9: Deformation caused by different shapes of aspertities at Costa Rica margin, as it is showed by von Huene et al. (2002). Figure (A) shows that some "punctual"asperities are subducting at the northern zone (seamount segment), while toward the southern zone an elongated asperity (Cocos Ridge) is subudcting. Figure (B) shows the morphological characterics left by a subducted seamount like is the one showed by Dominguez et al. (1998). Figure (C) presents the margin uplift caused by an elongated asperity as it has been suggested by Hampel et al. (2004) and Espurt et al. (2008). The outer shelf is uplifted and controls the formation of a "top margin wedge"on the inner shelf.

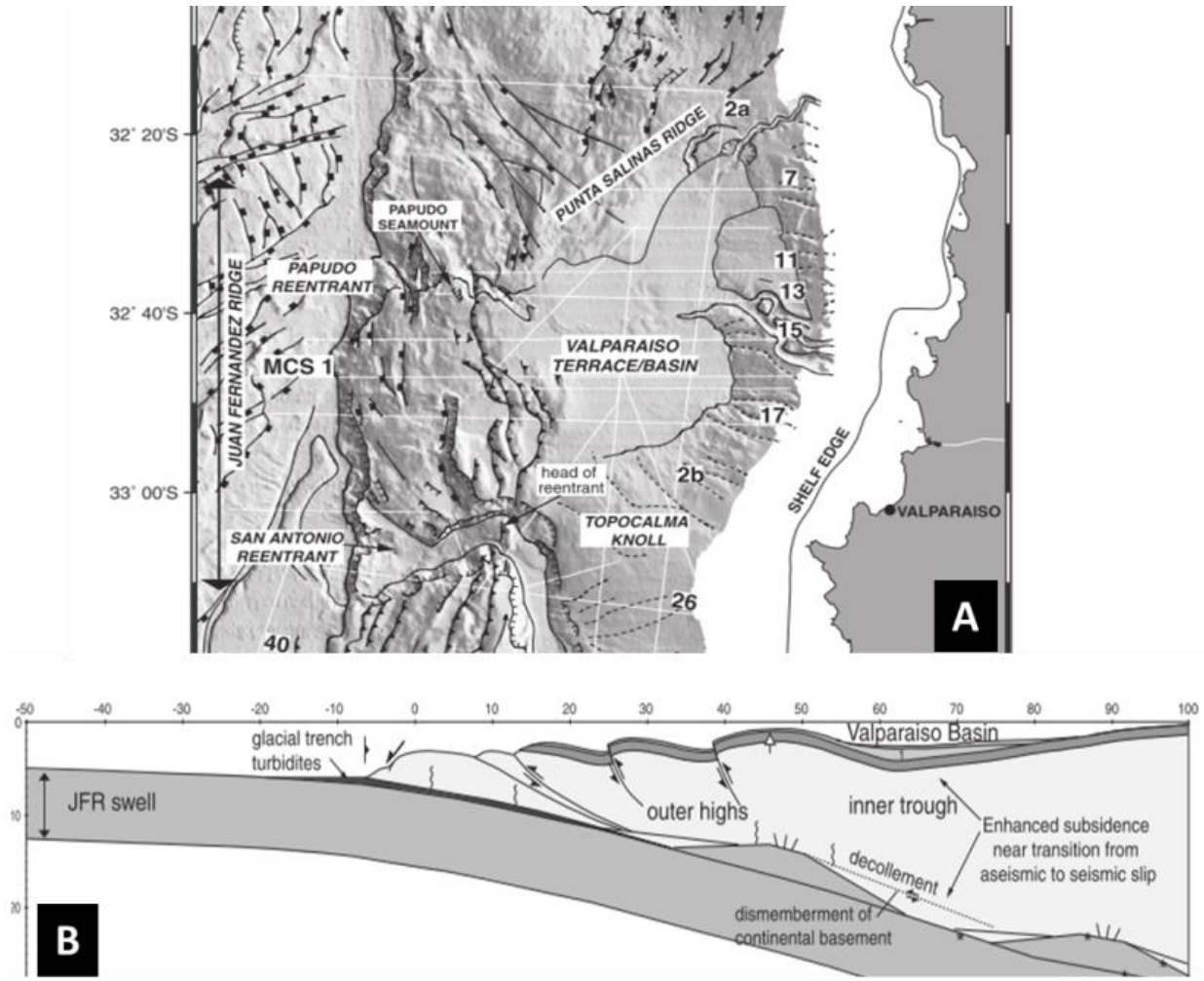

Figure 1.10: Structural interpretation made by Laursen et al., (2002) of seafloor around of the Valparaiso forearc basin. (A)The Valparaiso basin is located at the margin of the over-riding plate subducted by Juan Fernandez Ridge (JFR swell). (B)This image displays one of the evolution stages of this basin interpreted by the same authors, which suggests a continuous subduction of JFR (elongated asperity) and the eventual subduction of the seamounts ("punctual"asperities).

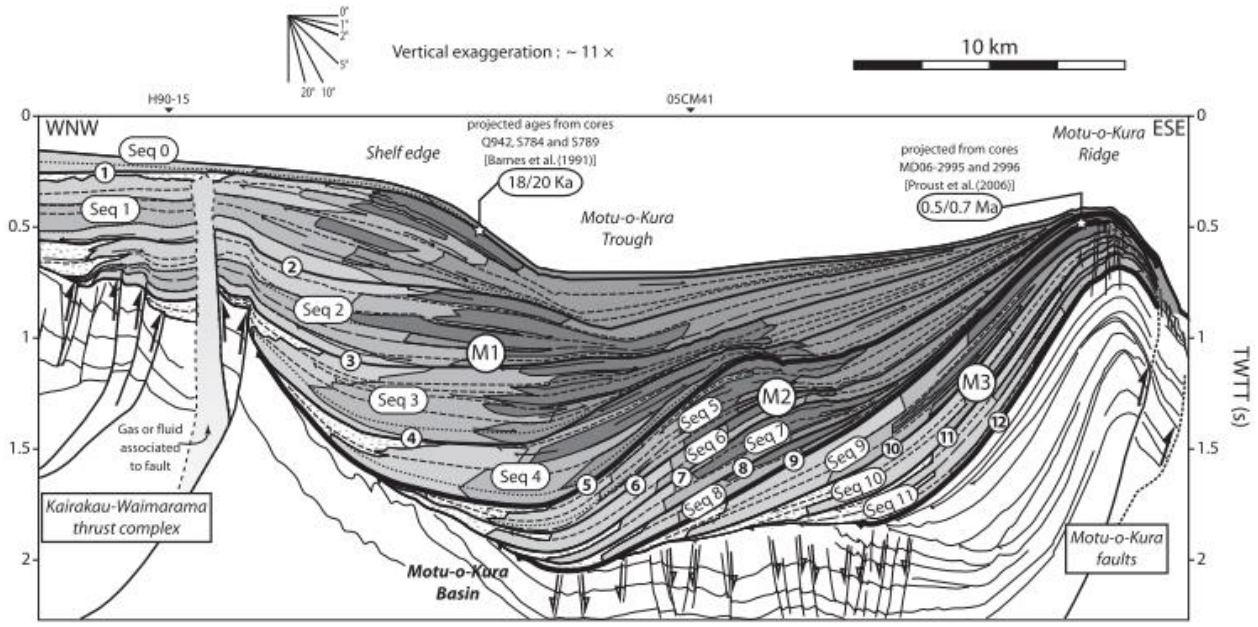

Figure 1.11: The stacking pattern of the depositional sequences interpreted by Paquet et al., (2011) showing the stratigraphic evolution record of the deformation in the Motu-o-Kura forearc basin located at New Zealand active margin.

The Ecuadorian active margin is affected by the subduction of asperities (Lonsdale, 1978; Marcaillou, 2015; Sage et al., 2006; Sanclemente, 2014). The offshore forearc basins register the history of Pleistocene geodynamic deformation of the margin (Deniaud, 2000; Michaud et al., 2015; Ratzov et al., 2008).

Therefore the Ecuador convergent margin is an excellent target to tentatively discriminate the details of the effects of eustatic changes and from its tectonic evolution. First, subduction erosion and related subsidence of the outer- margin wedge is the geodynamic process that dominates the recent evolution of the 700-km-long margin of Ecuador (Collot et al., 2009, 2002; Gutscher et al., 1999); this regional subsidence facilitates the record of sedimentary accumulation. Second, in response to the Carnegie Ridge subduction, the submarine forearc records a Plio- Pleistocene segmentation of the margin (Dumont et al., 2014; Gailler et al., 2007; Gutscher et al., 1999).

2. The stratigraphic record of the Quaternary deformation

The deformation over the erosive margin is recorded in the sedimentary deposits of the forearc and slope basins, which are preserved in the space made available by tectonic deformation and eustatic changes (i.e. accommodation). Due to the high rates of deformation of active margins it is expected that tectonic processes have a stronger influence on basin-fill architecture than sea-level changes (Paquet et al., 2009). However, during the Quaternary period eustasy had an important influence in the development of depositional sequences due to the high-amplitude in climate variations (Lobo and Ridente, 2013; Siddall et al., 2007) which can encompass tectonic deformation even in active margin settings (Proust and Chanier, 2004). Therefore, in order to run an analysis of the Quaternary deposits of the marine Ecuadorian forearc it is necessary to untangle the interplay between tectonic and eustasy. For this reason, we review below some important concepts that allow the study of the evolution of sedimentary basins.

2.1. Factors controlling the sedimentary record

The two processes that control the geometry of the stratigraphic record (stacking pattern) and the type of sediments in a basin are: a) the internal or autogenic processes, and b) the external or allogenic processes. The autogenic controls are related with the hydrodynamic of the sedimentary system (e.g. currents velocity, sediment transport capacity, erosion, etc.). The allogenic controls are external to the sedimentary system. They control the architecture of the accommodation spaces for sediment accumulation, saving its record at any given time in all environments of the basin (Catuneanu, 2006, pag. 73).

2.2. The allogenic processes

The allogenic processes which control sediment preservation in sequences are: tectonic, eustasy and climate (Catuneanu et al., 2011; Schwarzacher, 2000). All of them are interrelated, but they worked in different scales of time and space. From the largest to the smallest scales of sedimentary sequences, we distinguish the First order sequences, with the formation and breakup of supercontinents (200-400 My) to Fourth and Fifth orders related to changes in insolation driven by orbital forces (0.01-1 My) (Catuneanu, 2006. pag. 74).

The tectonic is in function of time and space. It controls the basin shape and thus its rate of subsidence or uplift. The tectonic controls can encompass from creation and fragmentation of continent until regional or local plate kinematics with 1-10 Ma (Robin, 1997). Other factors that can modify the shape of the basin, which is expressed in its total subsidence, are the crustal cooling, crustal loading and sediment compaction (Catuneanu, 2006).

Eustasy, or absolute sea level, is the fluctuation of global sea level independently of local factors. It is the position of the sea surface referenced to a fixed point like the center of the Earth or a satellite in stationary orbit around the earth. The relative sea level is the depth between a fix point in the layer of the basin and the absolute sea level. The distance between

the sea level and specific points of the seafloor is known as bathymetry (water depth) (Allen and Allen, 2013; Emery and Myers, 1996; Kendall and Schlager, 1981) (Figure 1.12).

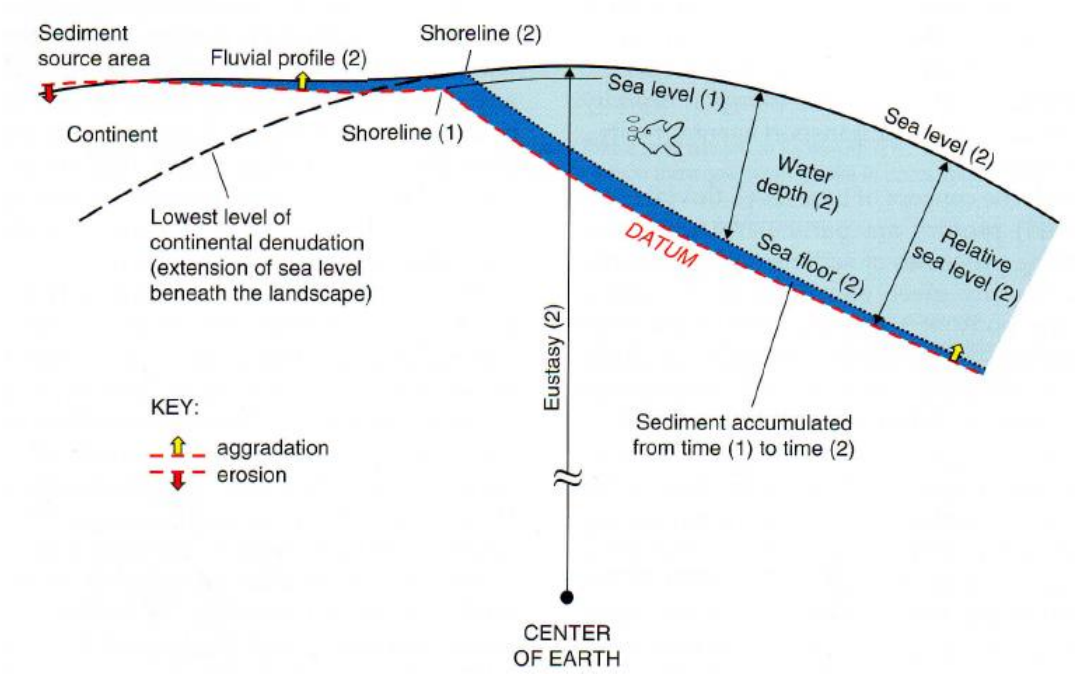

Figure 1.12: Eustatic sea-level, relative sea level and water depth as a fuction of sea level, seafloor, and datum reference surfaces. (From Catuneanu, 2006. Modified from Posamentier et al., 1988).

The eustatic variation over time is measured according to the current position of absolute sea level. This variation can be influenced by processes that modify the bathymetry of seafloor related to internal geodynamic controls of the Earth (thermal subsidence, rate of oceanic ridges production, etc), but also by process that modifies the amount of water in the oceans. The quantity of ocean water can change by internal process like volcanic degassing and climate change due to orbital forces (e.g., Milankovitch cycles) causing casting or icing in icecaps and mountain ranges (Allen and Allen, 2013; Paquet, 2008).

The climate change has an important role in the basin filling by affecting the filling space (accommodation space) during the glacio-eustatic falls and rises of sea level. It also has an important role changing the energy levels from continental to marine environments (e.g. seasonal fluvial discharge; wind regime in eolian environment, fair-weather vs. storm waves and currents in marine or lacustrine settings). The effect of climate is also reflected in the amount of sediment supply, by modifying the efficiency of weathering, erosion and sediment transport processes (Catuneanu, 2006. pag. 74)

2.3. Accommodation

The term accommodation refers to the space available for the sediments accumulation (Jervey, 1988). Thus the accommodation is directly influenced by allogenic process such as tectonic and eustasy (Figure 1.13). The inter-action between tectonic and eustasy can create or eliminate the accommodation, hence it is important to consider the sediment supply which occupy those spaces, and the compaction of these sediments that increases the accommodation. Allen and

Allen (2013), propose to express the accommodation with the next equation ΔA= ΔE+ΔS+ΔC, where A = accommodation, E = eustasy, S = subsidence, and C = Compaction.

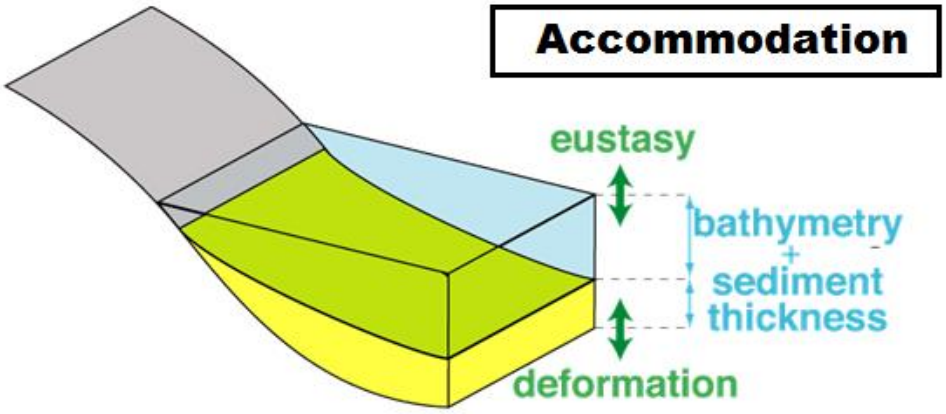

Figure 1.13: Parameters involved in the creation or elimination of accommodation. (Diagram from Robin, courses presentation 2013. Modified from Lafont, 1994).

2.4. Sediment Supply

The *sediment supply* or sedimentation is the quantity and type of sediments that is transported from a source area to the basin by different types of agents (i.e. water, wind or gravity). The origin of the sediment supply is directly related to climate variations through weathering, erosion and transport of the sediments. However the sediment supply is also very influenced by the tectonic with the rejuvenation of the area through its uplift and increasing the slope gradients by tectonic tilt (Catuneanu, 2006. pag. 77).

The amount of the sediments preserved in a basin depends on the aggradation-erosion balance, which is a consequence of the energy flux from each particular environment. Aggradation occurs only where sediment supply outpaces energy flux, and erosion occurs only where energy outpaces sediment (load) (Catuneanu, 2006. Pag. 78).

2.5. Shoreline Trajectories

The inter-action between accommodation and sedimentation is the key for the shoreline (or offlap break) migration. When the accommodation is created faster than it is consumed by sedimentation, it produces a shoreline transgression. While the sediment supply exceeds the accommodation, it generates a shoreline regression (forced regression). When the time of variation of the accommodation and the sedimentation are almost similar, occurs an aggradation, producing a normal regression (Figure 1.14) (Allen and Allen, 2013; Catuneanu et al., 2009a).

The transgression (landward migration of the shoreline) produces retrogradational stacking patterns, and cause marine facies shifting towards and overlaying non-marine facies (Figure 1.15B). The forced regression (seaward migration of the shoreline), generates progradational stacking patterns, producing non-marine facies shifting towards and overlaying marine facies

(Catuneanu, 2006. Pag. 90) (Figure 1.15C). In normal regressions the shoreline will migrate vertically upward, having an agradational stacking patterns.

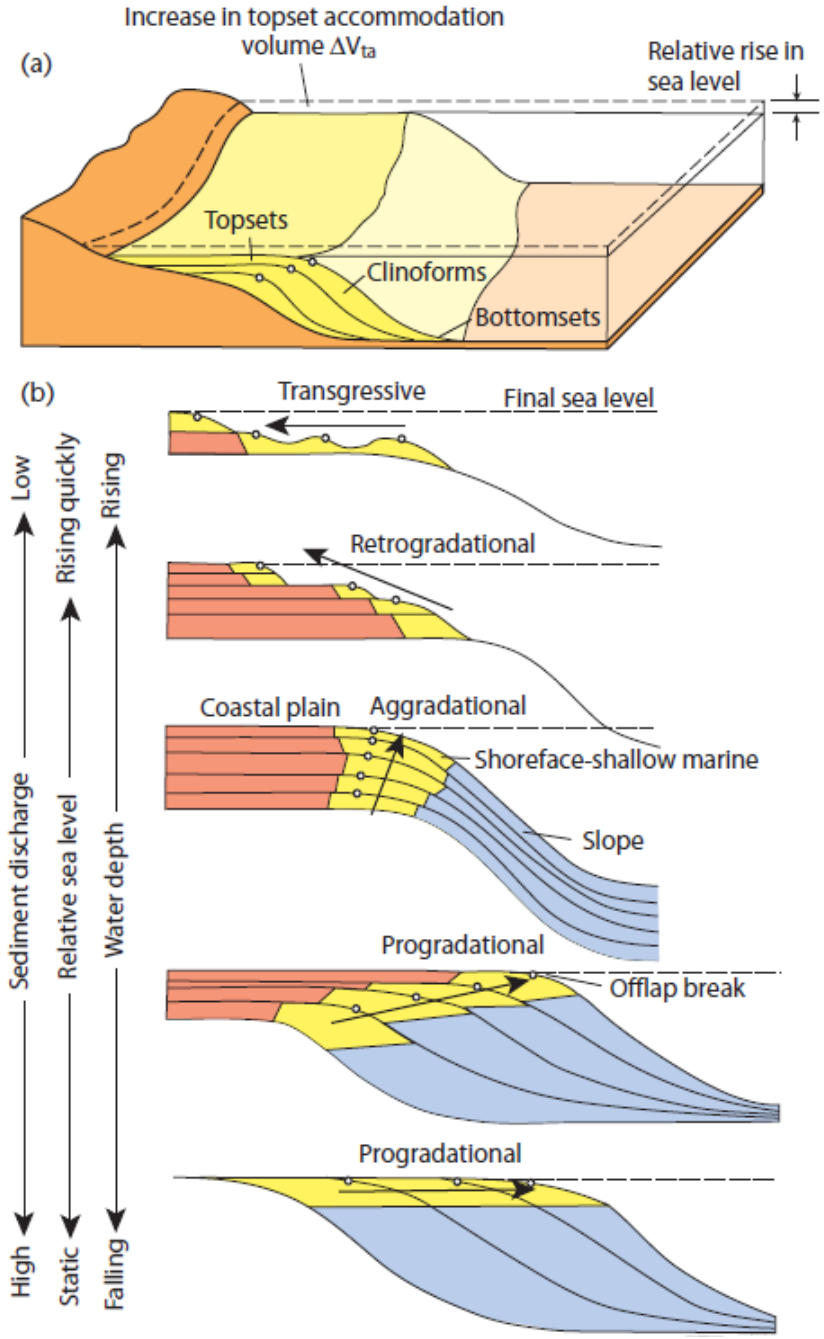

Figure 1.14: A) The shoreline trajectories (or offlap break migration) and the architecture of depositional units in relation to accomodation and sediment supply (From Allen and Allen, 2013. Modified after Galloway, 1989).

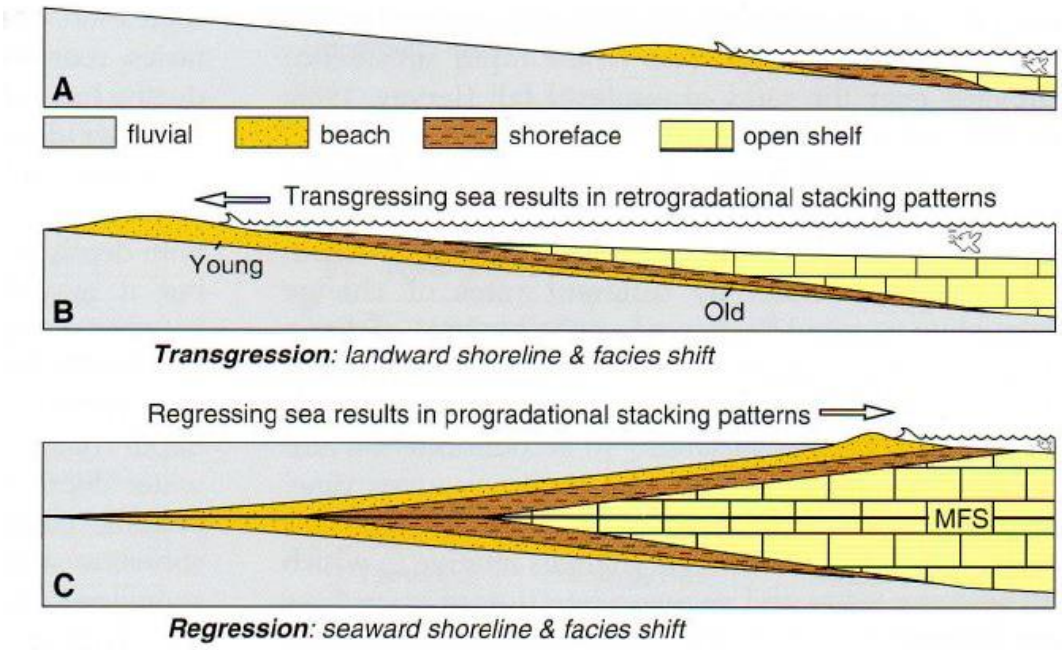

Figure 1.15: The shifting facies caused by the transgression and regression (From Catuneanu, 2006).

2.6. The sequence stratigraphy

The sequence stratigraphy is a geological discipline that tries to explain how stratigraphic units, facies tracts, and depositional elements are interrelated in time and space in sedimentary basins. The base of the sequence stratigraphy is to study the cycle of the base-level changes, which determines the formation of strata packages associated with particular depositional trends characterized by specific stacking patterns, known as systems tracts. (Catuneanu et al., 2009a).

The stratigraphic sequence attempts to integrate scientific disciplines (e.g. sedimentology, stratigraphy, geophysics, basin analysis, etc.), data (e.g. seismic data, core, outcrops, etc.), and natural process (climate, sea level change, tectonic, etc.) to improves the knowledge of Earth's geological record from local to global changes, and for the research of the natural resources (e.g. coal, placer deposits, petroleum, etc.) (Catuneanu, 2006).

2.6.1. The Systems Tracts

A systems tract is "a linkage of contemporaneous depositional systems, forming the subdivision of a sequence" (Brown Jr and Fisher, 1977). It consists of a relative conformable succession of genetically related strata bounded by conformable or unconformable sequence stratigraphic surfaces (Catuneanu et al., 2011). Systems tracts are interpreted based on stratal stacking patterns, position within the sequence, and types of bounding surface, and are assigned particular positions along an inferred curve of base-level changes at the shoreline (Catuneanu, 2006) (Figure 1.16). The nomenclature of systems tracts currently in uses is:

- The transgressive systems tract (TST) comprises the deposits that accumulated from the onset of coastal *transgression* until the time of maximum transgression of the coast, because the accommodation has been created faster than it is consumed by sedimentation;
- The highstand systems tract (HST), comprises the progradational deposits that form when sediment accumulation rates exceed the rate of increase in accommodation space. This is the normal regression produced between the end of the transgression and the onset of the forced regression;
- The falling stage systems tract (FSST) includes all the regressional deposits that accumulated after the onset of a relative sea-level fall and before the start of the next relative sea-level rise. It is deposited during the forced regression, caused because the sedimentation has outpaced the accommodation; and
- The lowstand systems tract (LST) includes deposits that accumulate after the onset of a relative sea-level rise, which is the normal regression after the finish of the forced regression and at the beginning of the transgression (Catuneanu et al., 2009).

Systems tracts may be either shoreline-related, where their origin can be linked to particular types of shoreline trajectory, or shoreline-independent, where a genetic link to coeval shorelines cannot be determined. Shoreline-related systems tracts consist of correlatable depositional systems that are genetically related to specific types of shoreline trajectory (i.e. forced regression, normal regression, transgression) (Catuneanu et al., 2011. Pag. 13), which give a practical way to identify the different systems tracts for the seismic data interpretation (Figures 1.16 and 1.7).

2.6.2. The Sequence Stratigraphic Surfaces (SSS)

The sequence stratigraphic surfaces (SSS) are the unconformities with their correlative conformities that mark the shoreline shift and the changes in depositional trends, being the boundaries of the system tracts (Figures 1.16 and 1.17). They may correspond to “conceptual” horizons (i.e., without a lithological contrast) or physical surfaces, depending on their outcrop expression (Catuneanu et al., 2011).

Although the base-level shifts is recorded along the basin, this record could not be similar within all the basin, actually above the base-level there is a tendency to erosion and below it a tendency to deposition (Catuneanu, 2006; Sloss, 1962). Thus these surfaces are not equally easy to identify in outcrops or subsurfaces, nor equally useful as time markers in a chronostratigraphic framework. But each surface may be defined as a distinct stratigraphic contact that marks a specific event or stage of the base-level cycle (Catuneanu, 2006. Pg. 112).

The principal surfaces, currently relating to shoreline migrations, that bound systems tract (Catuneanu et al., 2009b) (Figure 1.16 and 1.17) are:

- the Maximum Flooding Surface (MFS), at the end of the transgression, at the top of the TST;
- the Basal Surface of the Forced Regression (BSFR), at the onset of the forced regression, at the top of the HST;
- the Correlative Conformity Surface (c.c.) (sensu Hunt and Tucker, 1992) at the end of the forced regression, at the top of the FSST; and
- the Maximun Regressive Surface (MRS) at the end of the regression, at the top of the LST.

It may be important to note that the MRS and the BSFR surfaces are located at the top of a normal regression, at the beginning and at the finish of the transgression respectively (Figure 1.16).

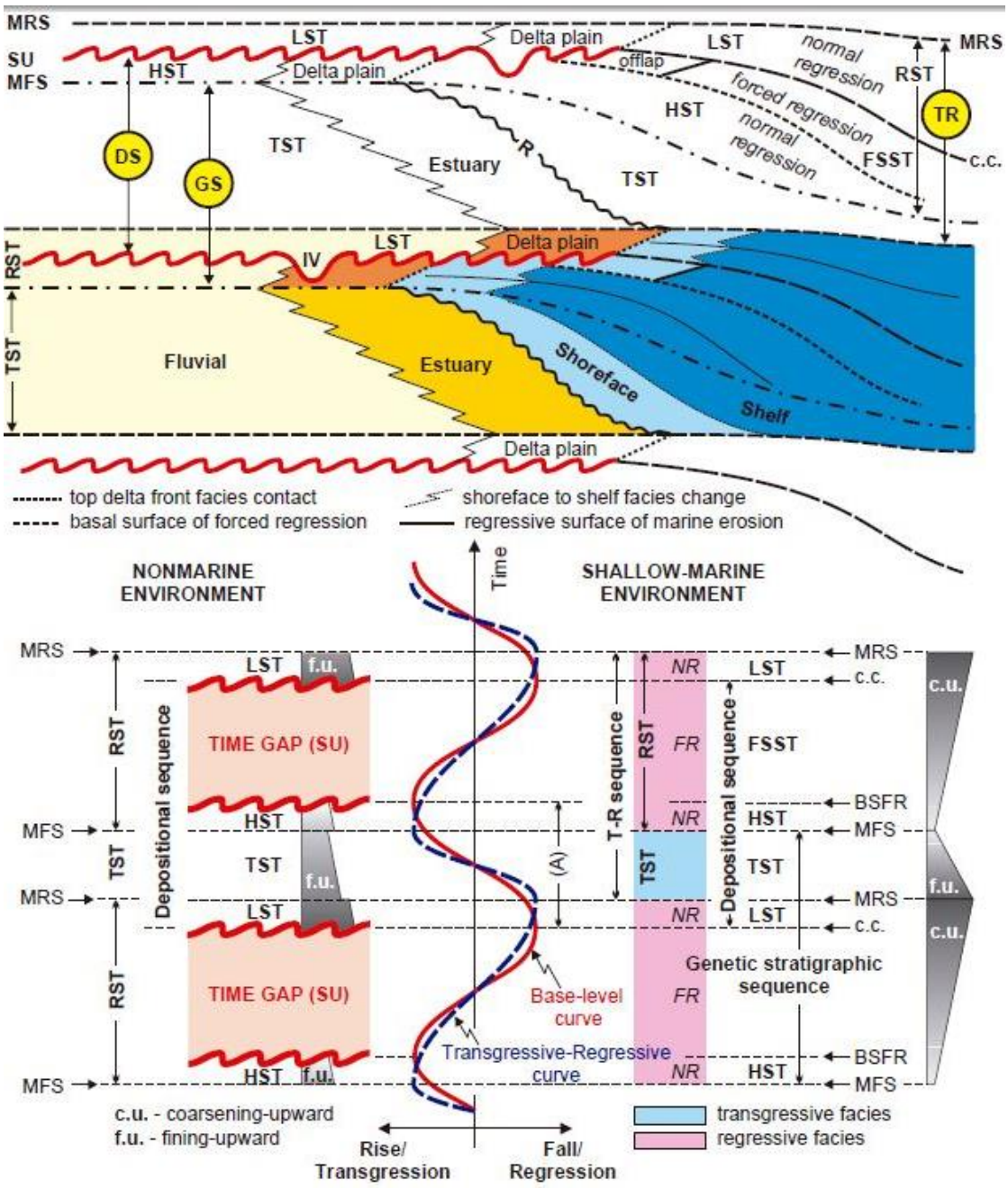

Figure 1.16: Sequences, systems tracts, and stratigraphic surfaces defined in relation to the base-level and the transgressive-regressive curves (Catuneanu, 2006. Modified from Catuneanu et al., 1998b).

There are other three surfaces presented by Catuneanu et al., (2009a), formed during the shift of the base-level, which may be important to identify, depending in what zone of the basin we are working and what type of data we have. They are:

- The subaerial unconformity (SU), "is a surface of erosion or non deposition created generally during base-level fall by subaerial processes, such as fluvial incision, wind degradation, sediment bypass, or pathogenesis,… it corresponds to the largest stratigraphic hiatuses in the sedimentary rock" (Catuneanu, 2006).

- The Regressive Surface of Marine Erosion (RSME), " a subaqueous erosional surface that forms by means of wave scouring in regressive, wave-dominated lower shoreface to inner shelf settings" (Catuneanu, et al., 2009)
- Transgressive Ravinement surfaces: "are scours cut by tides and or waves during the landward shift of the shoreline… they are superimposed and onlapped by the transgressive shoreface (i.e. coastal onlap)" (Catuneanu, 2006).

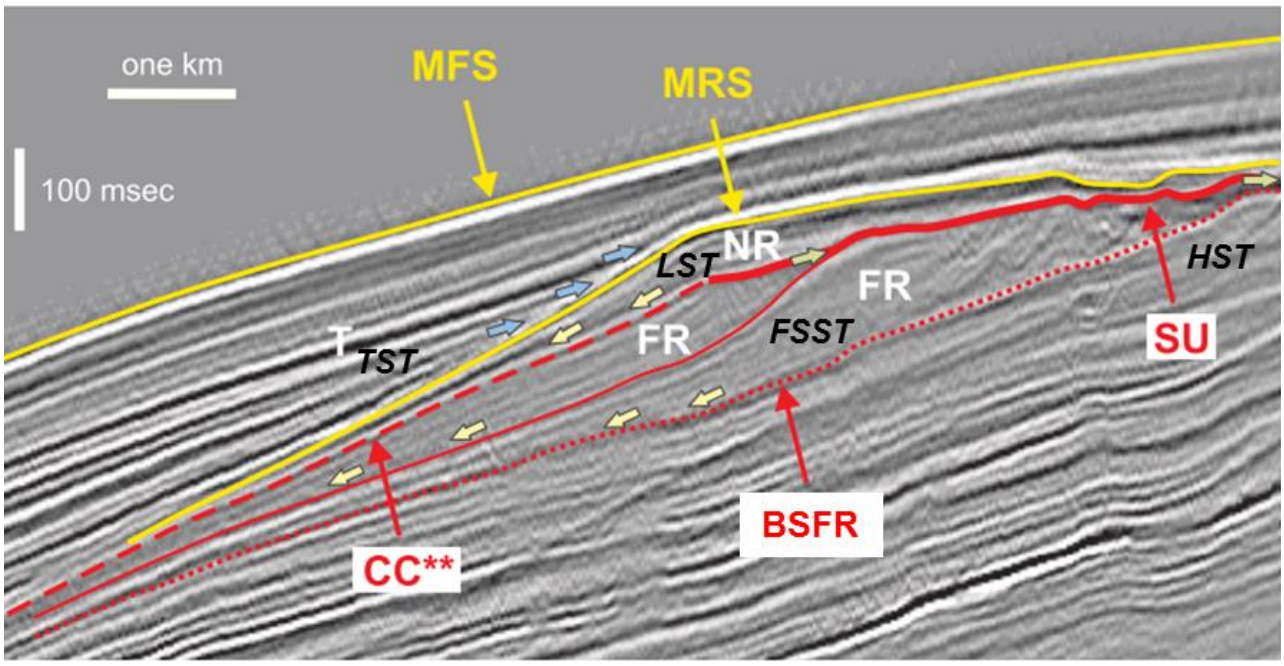

*Figure 1.17: Seismic line showing the interpretation of the shoreline trajectories (forced regression, normal regression and transgression), and the systems tracts bounded by some of the sequences stratigraphic surfaces. (Modified from Catuneanu et al., 2011). Stratal terminations: green arrows - offlap; yellow arrows - downlap; blue arrows - onlap. Abbreviations: FR - forced regression; NR - normal regression; T - transgression; SU - subaerial unconformity; BSFR - basal surface of forced regression); CC** - correlative conformity in the sense of Hunt and Tucker (1992); MRS - maximum regressive surface; MFS - maximum flooding surface; HST – high stand systems tract; FSST – falling stage systems tract; LST – lowstand systems tract; TST – transgressive systems tract.*

The sequences stratigraphic surfaces could be identified in the seismic line, in the same way as the systems tracts (Figure 1.17), from the combination of some of the next criteria (Catuneanu, 2006):

- ✓ Stratal terminations (e.g. onlap, donwlap, offlap, etc.) which refer to the geometric relationships between strata and the stratigraphic surfaces against which they terminate, allowing identifying the unconformities between the depositional systems.
- ✓ Shoreline shifts, especially when the seismic data show the offlap break migration.
- ✓ Vertical variation of seismic facies, applying the criteria of configuration, amplitude, continuity and frequency of seismic reflectors (Sangree and Widmier, 1977).

2.6.3. The Stratigraphic Surfaces as chrono-stratigraphic framework

Since the sequence stratigraphic surfaces are event-significant, and indicate changes in depositional trends, they can give a chronostratigraphic framework for the sedimentary succession under analysis (Catuneanu, 2006. Pg. 69). However because the stratigraphic surfaces are unconformities, they can present some limitations as time surfaces.

Some of these limitations are explained by Miall (2010) as follow: a) because a stratigraphic surface is an unconformity, it may have a complex genesis, representing amalgamation of more than one event; b) it may be markedly diachronous from one place to another, i.e. the sequences boundary unconformities could differ in ages between the center and around of margin of the basin (Jordan et al., 1988; Susan M. Kidwell, 1988); c) an unconformity puts in contact a truncated older strata with younger strata, which may vary in age considerably, therefore in spite of we can know the ages of the two strata, it is too difficult to provide an accurate estimate of age to the stratigraphic surface (Figure 1.18).

Consequently, it is necessary to take into account that the stratigraphic surfaces are not true time lines and they have some degree of diachroneity. However, depending on the mode of formation and variation of the parameters along dip and strike of the basin (e.g. tectonism and sedimentation), they can be used as proxies for time lines (Catuneanu, 2006 p. 11, 291). Thus, considering these reasons sequence stratigraphy gives an important chronological context, but it is essential to correlate the stratigraphic sequences with additional time data to have an accurate time framework.

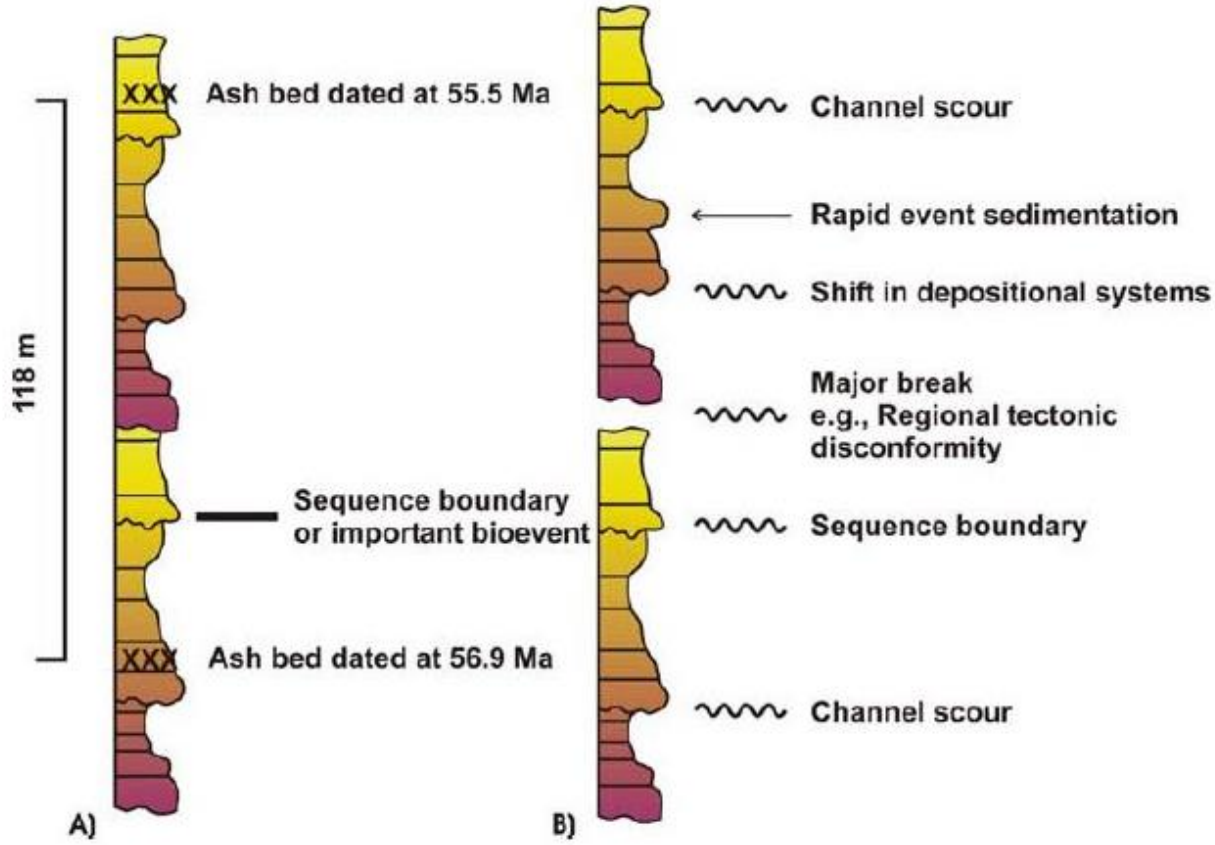

Figure 1.18: Logs showing some of the limitations that could present the sequence stratigraphy used as chronostratigraphic reference, according to Miall (2010).

2.7. Transgressive-Regressive (T-R) Sequence Model

The sequences are the stratigraphic record that shows the change of a complete cycle of depositional trends. They are composed by the systems tracts, and the upper boundary of a sequence can be located depending on the sequence model chosen to do the interpretation (Catuneanu, 2006).

Different models are proposed by various authors during sequence stratigraphy history (Catuneanu et al., 2009b; Embry, 1995, 1993; Galloway, 1989; Hunt and Tucker, 1992; Posamentier, 1988; Van Wagoner, 1988); but they can be grouped into two broad families, genetic stratigraphic model and transgressive-regressive sequence model (Catuneanu, 2009a).

The transgressive-regressive sequence model (T-R) proposed by Embry and Johannessen (1993), comprises only two large systems tracts: the transgressive systems tract and the regressive systems tracts. The regressive systems tract groups the Highstand, Falling-Stage and Lowstand systems tracts. In this way this model attempts to avoid some of the drawbacks observed in the depositional sequence and the genetic stratigraphic sequence (Catuneanu, 2006). One additional advantage of this model is that it would allow to correlate the boundaries of the T-R sequences with the glacio-eustatic changes, expressed in the Marine Isotopic Stages (MIS) (Martillo et al., 2013) (Figure 1.19).

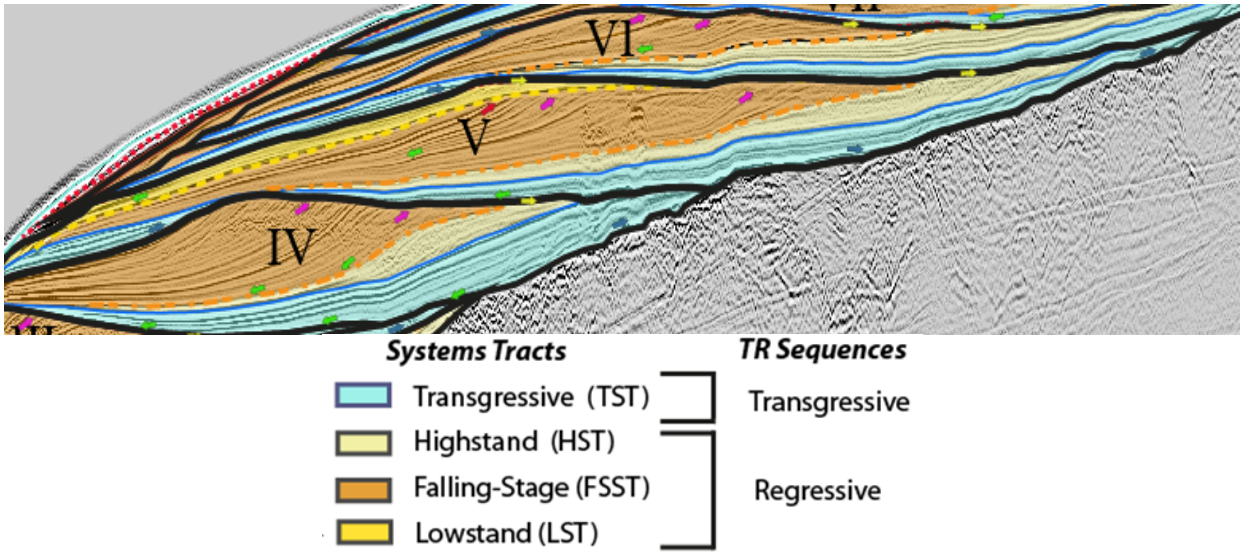

Figure 1.19: Interpretation of the four genetic systems tracts in a multichannel seismic line. The three regressive system tracts (HST, FSST and LST) have been grouped in Regressive sequences (yellow and orange color tones), which with the TST (light blue color), as Transgressive sequences, form the TR sequences. The TR sequences are limited by the black lines. (Martillo et al., 2013).

2.8. The stratigraphic record of the deformation

The sequence stratigraphy analysis and sedimentation give an important knowledge of the behavior of the deformation during the time. As shown above, the tectonics creates or eliminates the accommodation space for sedimentation. It controls: the geometry of the basin, the layer thickness, the change of the sediment facies (sources area and depositional profile) and shoreline migration (progradation and retrogradation) (Figure 1.20). Nevertheless in an active margin the tectonic have an important control over the geometry of the basin, and thus in the form and/or thickness variation of the stratigraphic sequences. So for the analysis of the basin deformation it could be important to observe the depocenter migration through time, i.e. by comparison of isopach maps of the sequences or group of sequences.

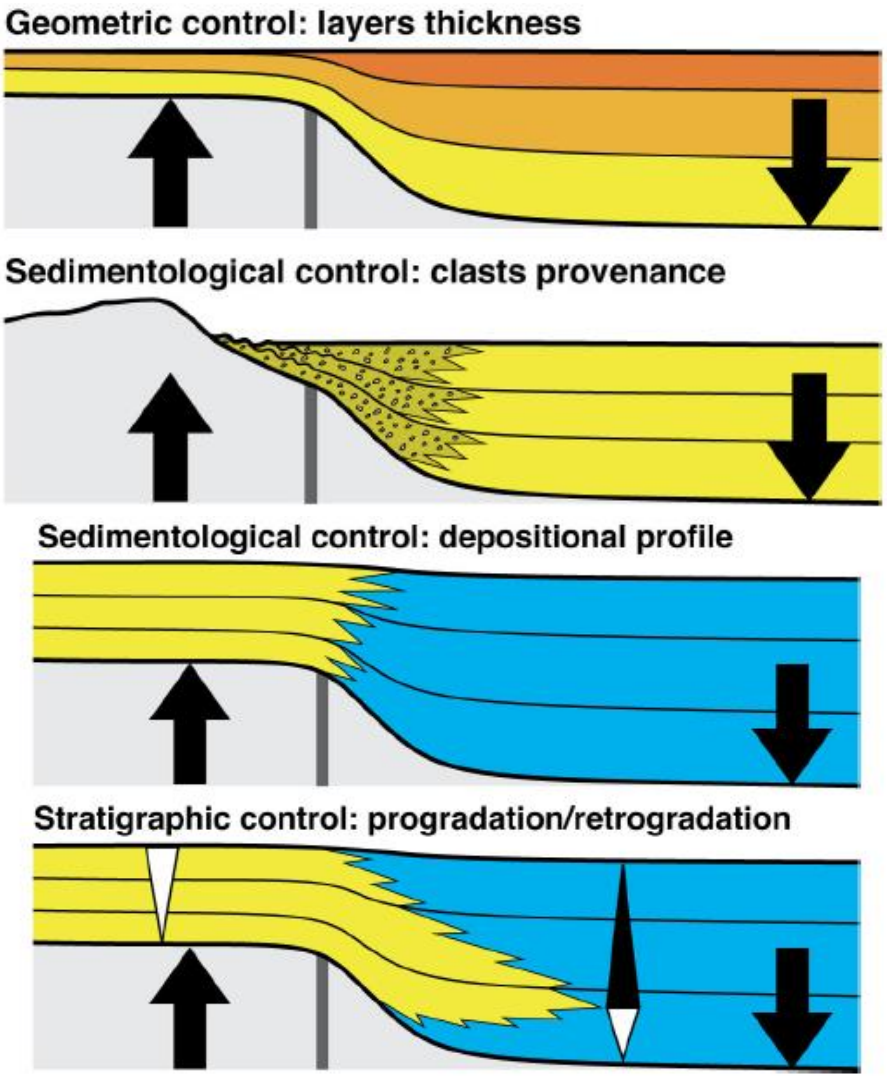

Figure 1.20: The relationship between the deformation and the differents stratigraphy and sedimentation record in a basin. The tectonic controls the variation of accommodation space during the time, like the eustatism. But the tectonic have an influence over the geometry of the basin that is displayed in the variation of the depot center spatial location during the time, which could show in a sequence of isopach maps of the basin. (From Nalpas, courses presentation 2013).

3. The Glacio-Eustatic variations in the Quaternary

The Quaternary is the current Period of the Cenozoic Era; it includes de Pleistocene and the Holocene Epochs (Figure 1.21). It is characterized by rapid and abrupt climate and environmental changes that have caused cycles of sea-level variations of different durations and amplitudes. The Quaternary global eustatic variations (the Milankovitch cycles) are controlled principally by the earth's orbital geometry, i.e. precession, obliquity and eccentricity that modulate changes in solar radiation with periodicities of 20, 40 and 100 ka. (Schwarzacher, 2000). The Holocene corresponds to the current interglacial time.

Traditionally the base of Quaternary was fixed at 1.8 Ma before the present (BP), but since year 2009 the International Commission on Stratigraphy (ICS) and the International Union of Geological Sciences (IUGS) changed this time boundary and put it down to 2.588 Ma BP,

including now the Gelasian Stage into the Pleistocene, formerly considered at top of the Pliocene (Gibbard et al., 2010).
Thus the current International Chronostratigraphic Chart (v.2015/01) divides the Pleistocene in the Stages: Gelasian (2.588-1.8 Ma), Calabrian (1.8-0.781 Ma), Middle Pleistocene or Ionian (0.781-0.126 Ma), and Upper Pleistocene or Tarantian (0.126-0.0117 Ma.). The Holocene is dated, as it was before 2009, from 0.0117 Ma (boundary Pleistocene-Holocene) to the present days (http://www.stratigraphy.org/index.php/ics-chart-timescale) (Figure 1.21A).

The Quaternary cold periods are called "glacial", separated by warmer periods called "interglacial". At the beginning the glacial periods were defined in different regions (i.e. Alps, North Europe, British Isles, Midwest U.S.) which have their own glacial history, being difficult to correlate between them (Gibbard and van Kolfschoten, 2004).

The sea-level changes related with the temperature shifts between the glacial and interglacial periods of the Quaternary are studied from the measure of the oxygen isotope ratio between oxygen-18 and oxygen-16 present in the calcite of the oceanic core samples (Lisiecki and Raymo, 2005; Siddall et al., 2003) and in glacial ice cores. High levels of oxygen-18 represent the cold glacial periods, while lower levels of oxygen-18 represent interglacial intervals (Shackleton et al., 2003; Waelbroeck et al., 2002). The curves derived from this changes in the oxygen isotopic composition of the global ocean are referred as Marine Isotopic Stages (MIS), which is currently used as a global crhonostratigraphic framework for marine and coastal sediments (Jordá, 1995; Pedoja et al., 2014).

The MIS time scale takes the current stage as MIS 1, working backwards to the ancient stages with even numbers for cold glacial periods, and odd numbers for warm interglacial intervals. However due to the poor initial dating of these stages, they correspond not only to glacial and interglacial phases but also to intermediate episodes, called interstadials; in this way, for example, the last glacial period (named Würm in Europe) roughly corresponds to isotopic stages 2, 3, 4, with its maximum at stage 2, while stage 5 is the penultimate interglacial period (Eemian in Europe) which have five interstadials, from 5.5 (or 5e) to 5.1 (or 5a). The interstadials have been numbering with the same logic that the stages, i.e. odd numbers for warm periods 5.5 (e), and even numbers the cooler / temperate periods.

The base of the Gelasian stage (the actual base of the Pleistocene) corresponds to the MIS 103; the beginning of the Calabrian stage is located at MIS 64, the start of the Ionian stage (Middle Pleistocene) is correlated with the MIS 19; and the Tarantian stage (Upper Pleistocene) corresponds to MIS 5. The Holocene is addressed as the current interglacial period (MIS 1) and it began 11700 years BP (http://www.stratigraphy.org/upload/QuaternaryChart1.JPG) (Figure 1.21B).

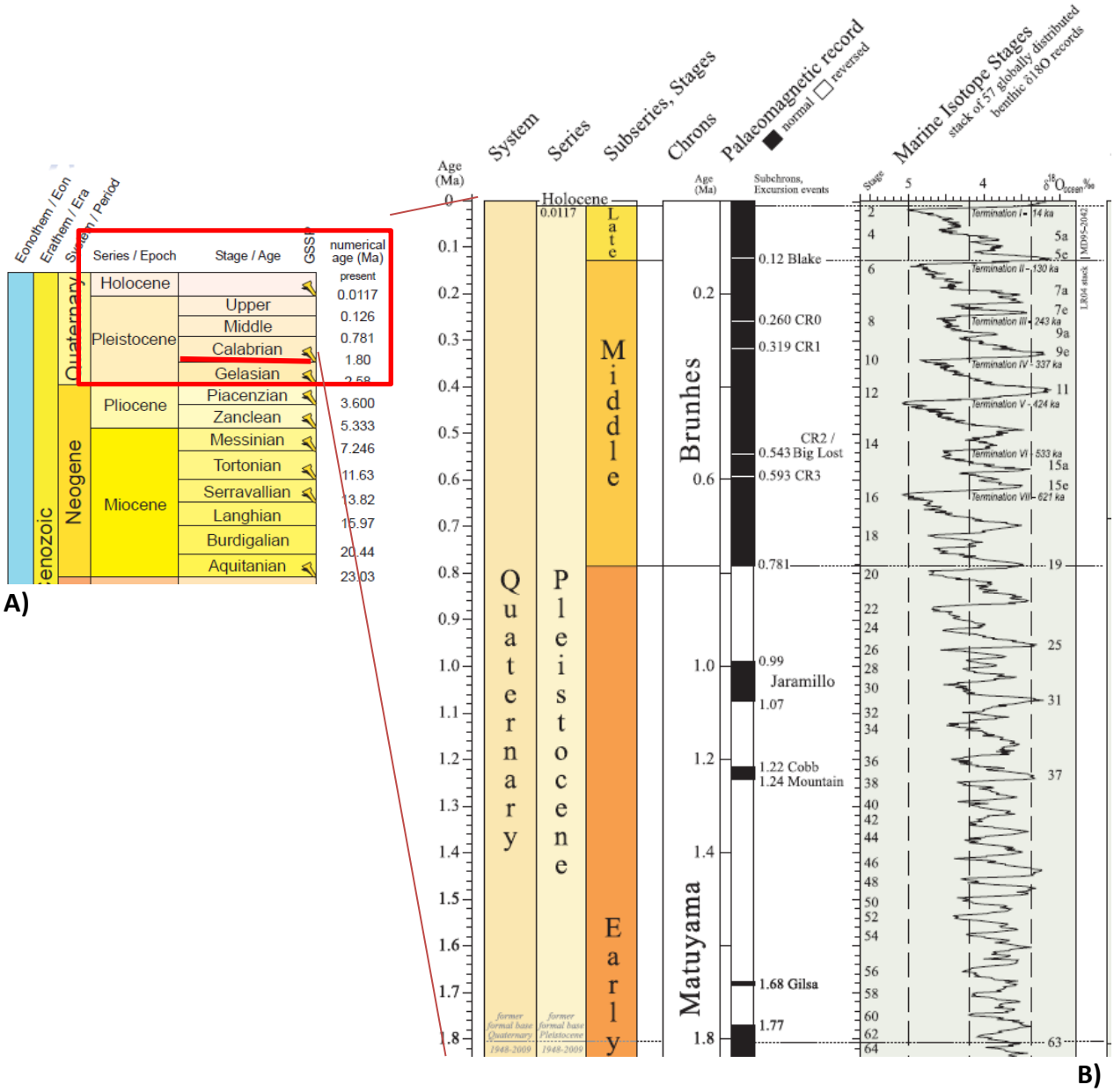

Figure 1.21: A) The chronostratigraphic chart of the Pleistocene (v2015/01), showing the actual lower limit, with the Pliocene, at 2.58 Ma. Before 2009 the Pleistocene-Pliocene boundary was established at 1.8 Ma. The literature before 2009 referenced the current Calabrian stage as Early Pleistocene. B) The Marine Isotopic Stages (MIS) curve from the Calabrian stage to Holocene according to Lisiecki and Raymo (2005).

CHAPTER 2: The Ecuadorian subduction margin

"Learning never exhausts the mind"

Leonardo da Vinci (1452 – 1519)

1. Introduction

The Ecuadorian margin is located at the boundary of two convergent tectonic plates. The Nazca oceanic plate subducts beneath the continental South American plate with a N80°E trend (Pedoja et al., 2006b) and at a rate of 58 mm/yr^{-1} (Trenkamp et al., 2002) (Figure 2.1A). The basement of the coastal area of Ecuador consists of accreted oceanic terranes (Jaillard et al., 1996). The subduction of the Carnegie Ridge (Collot et al., 2009; Gutscher et al., 1999; Michaud et al., 2009) and the northward escape of the North Andean block (NAB) relative to the South American plate (Trenkamp et al., 2002; Witt et al., 2006; Nocquet et al., 2009) at a 0.95 cm.yr^{-1} rate (Nocquet et al., 2014) both control the geologic evolution of the margin. The Ecuador subduction zone has experienced five large megathrust earthquakes (Mw > 7) during the 20th century from central Ecuador to northern Colombia (Chlieh et al., 2014), meanwhile no large earthquake is known southward along the margin.

The seafloor morphology of the Nazca plate was influenced, since at least Miocene times, by the interaction between the Galapagos Hot Spot and Galapagos Spreading Center (Galapagos Rift) (Lonsdale and Klitgord, 1978; Lonsdale, 2005; Sallarès and Charvis, 2003), which are at the origin of numerous and significant seafloor reliefs. Some of them are in subduction today (Lonsdale, 1978) (Figure 2.1B). The geological evolution of the Ecuadorian margin is strongly influenced by the subduction of these asperities which could have caused the uplift of the Coastal Cordillera (Pedoja, et al., 2006; Reyes, 2013), the uplift and subsidence of the forearc zone (Deniaud et al., 1999; Hernández, 2014; Witt et al., 2006), the emersion of islands (Pedoja et al., 2006a; Cantalamessa et al., 2007), and the formation of escarpments and reentrants on the slope of the margin (Sage et al., 2006; Collot et al., 2009; Ratzov et al., 2010; Marcaillou, 2015).

This chapter recalls some important aspects of the geological processes of the Ecuadorian margin, which will be useful in the following part of the manuscript, i.e. the subduction of the ridges and asperities and their role in the segmentation of the margin and formation of the Quaternary basins.

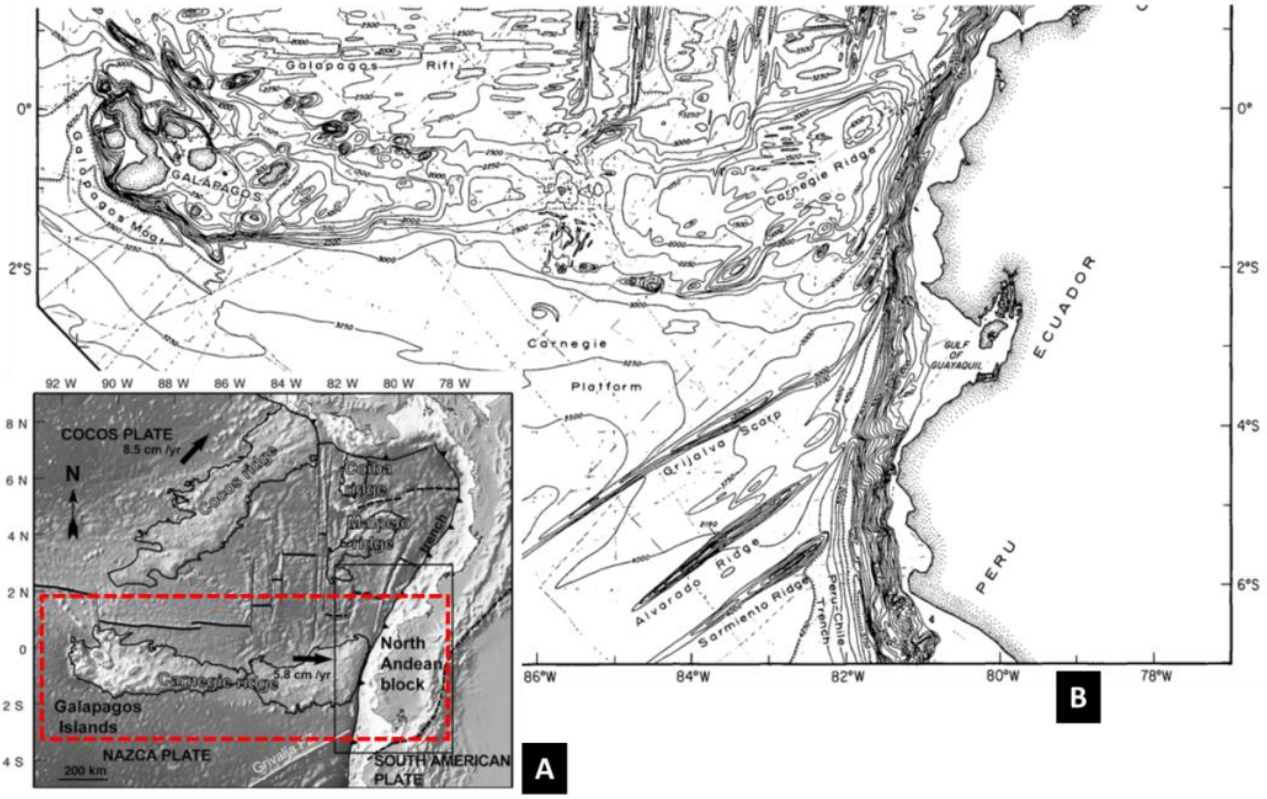

Figure 2.1: Regional geodynamic framework. A) Regional location of the Ecuadorian subduction margin (from Michaud et al., 2015). B) Seafloor morphology of the Nazca tectonic plate, which is strongly influenced by the relationship between the Galapagos Hot Spot and Galapagos Spreading Center (from Lonsdale and Klitgord, 1978).

2. The subduction of asperities

2.1. The subduction of the Carnegie Ridge

The most remarkable of the subduction asperities is the Carnegie Ridge. This oceanic plateau, c. 200 km wide and 1 km high, which abuts the Ecuadorian trench, presents a crustal thickness ranging from 14 km (Graindorge et al., 2004) to 19 km (Sallarès and Charvis, 2003). The crust of the Carnegie Ridge is thus ~10 km thicker than the crust of the surrounding oceanic basins (Michaud et al., 2009).

As has been discussed by Michaud et al. (2009), many geological features of Ecuador are commonly ascribed to the Carnegie Ridge subduction (Hall and Wood, 1985), not only in the forearc area, but also as far as the backarc area (Figure 2.2C). Some of these features include: (1) subduction-erosion (Calahorrano, 2005; Sage et al., 2006) and current coastal uplift (Cantalamessa and Di Celma, 2004; Pedoja et al., 2006a, 2006b); (2) the northward drift of the North Andean block and opening of the Gulf of Guayaquil (Lonsdale, 1978; Witt et al., 2006); (3) high exhumation rates for the volcanic materials in the Andes (Steinmann et al., 1999; Spikings, et al., 2001); (4) the presence of a flat slab corresponding to a landward prolongation of the Carnegie Ridge beneath the overriding plate (Gutscher et al., 1999); and (5) changes in the chemistry of the active volcanic arc related to the flat-slab geometry (Gutscher et al., 2000; Bourdon et al., 2002; Samaniego et al., 2002) (Figure 2.2D). Thus, the CR subduction plays an important role in the evolution of the Ecuadorian geology.

The ages for the Carnegie Ridge–trench collision is still a matter of debate. The proposed age for this collision varies between 1 to 3 Ma old (Cantalamessa and Di Celma, 2004; Contreras-Reyes and Carrizo, 2011; Graindorge et al., 2004; Lonsdale, 1978; Witt et al., 2006) to 8 Ma old (Collot et al., 2009; Gutscher et al., 1999) to up to 15 Ma old (Pilger, 1984; Spikings et al., 2005, 2001).

The subduction of the CR and the obliquity of the subduction – from orthogonal to approximately 40° (Pedoja et al., 2006) – influence the motion towards the north of the terrain of the North Andean block (NAB) (Dumont et al., 2005; Ego et al., 1996; Nocquet et al., 2009).

According to recent GPS work by Nocquet et al. (2014), the relative convergence velocity between the CR and NAB is 4.7 cm/yr in a 83° eastward direction. Taking this kinematic plate pattern into account and assuming that the actual trends of the CR flanks prolong in the subduction below the upper plate, Collot et al. (2009) proposed a reconstruction of the location of the CR since 4-5 Ma ago. This reconstruction, using bathymetric data, is based on the identification of the perturbed slope of the margin on the northern side of Galera Cape to the actual position of the northern flank of the CR (Figure 2.2B).

This model also suggests a migration of the CR from north to south, as it was suggested to the subduction of the Nazca Ridge by Cande et al. (1985). In the CR model, the shape of the subducted ridge is assumed to follow the current morphology of the plateau. For the Nazca Ridge, the subduction geometry is supposed to mimic the shape of the Tuamotu Ridge (Figure 2.2D). Therefore, although the form of the asperity is one of the most important parameters influencing the subduction process (Dominguez et al., 1998a; Hampel et al., 2004a; Lallemand, 1999), this geometry is almost impossible to know precisely for the subducted zone of the ridges.

The CR is a long continuous asperity with peaks, platforms, step faults and/or scarps, with a roughness that persists at least from the trench axis to 75 km in a seaward direction (Lonsdale, 1978) (Figure 2.3A). This external roughness of the seafloor is actively subducting at the present (see the seismic single-channel profiles of Figure 2.3B and their location in Figure 2.3D). The influence of the positive relief of the CR is assumed to persist until 110 km east of the trench (profile Y-Y'), reaching the onshore area, with approximately the same width as the exposed part of the ridge (profiles X-X' and Y-Y' in Figures 2.3C and D) (Gutscher et al., 1999). Therefore, the subducted zone of the CR might show a general shape that conforms to the current shape that has influenced the deformation of the overriding plate, possibly in an analogous way as in the physical model used by Hampel et al. (2004) (See Chapter 1).

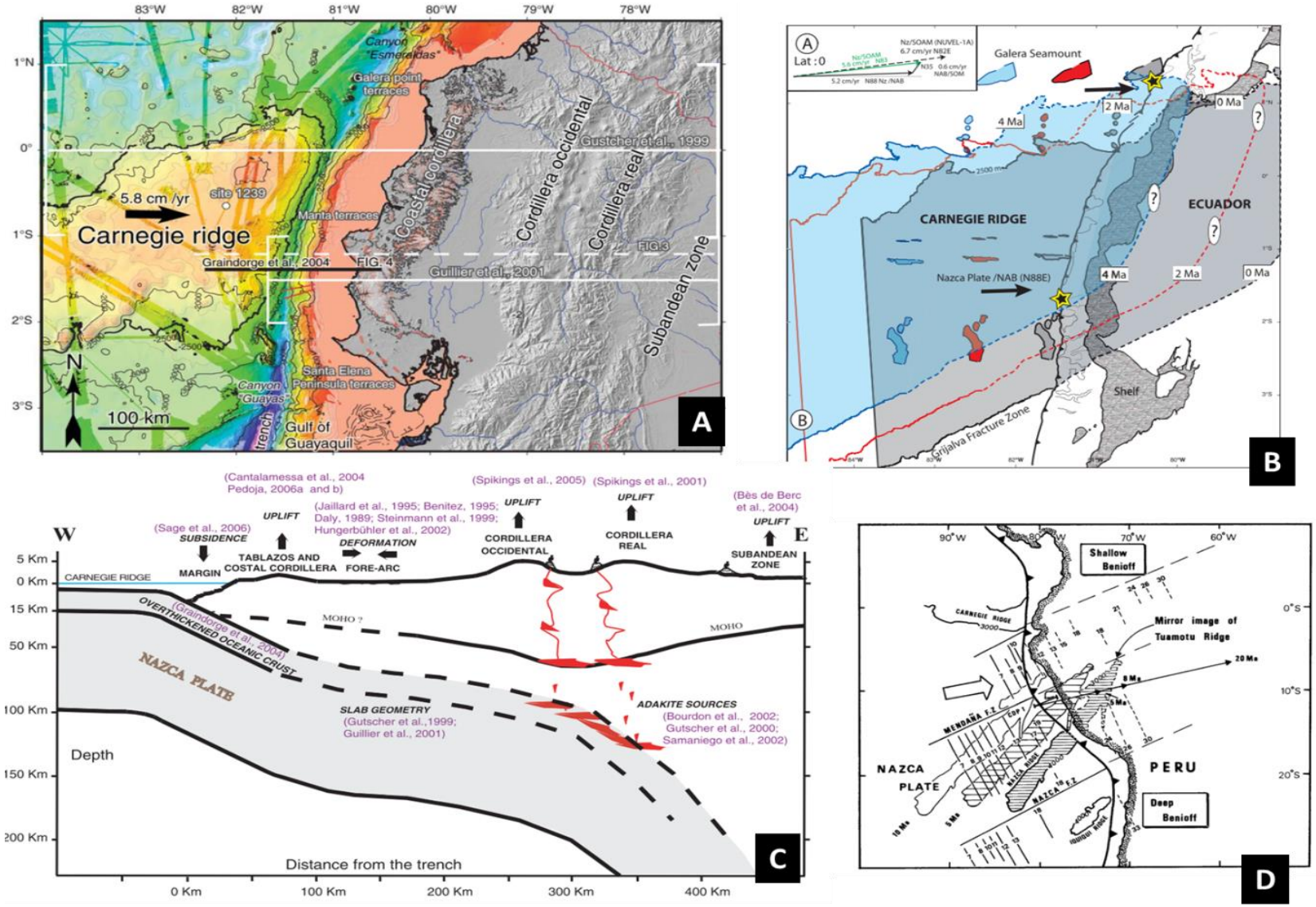

Figure 2.2: The effects of the Carnegie Ridge subduction. A) Location of the Carnegie Ridge (CR) in front of the Ecuadorian margin (from Michaud et al., 2009). B) Model of the evolution of the CR location related to the upper plate, assuming a southward migration of the CR ridge flanks from 4-5 Ma (from Collot et al., 2009). C) Cross-section showing the geological effects attributed in the literature to the CR subduction (location in A) (from Michaud et al., 2009). D) The subduction model for Nazca Ridge, proposing a subducted morphology from a mirror image of the Tuamotu Ridge (from Cande et al., 1985).

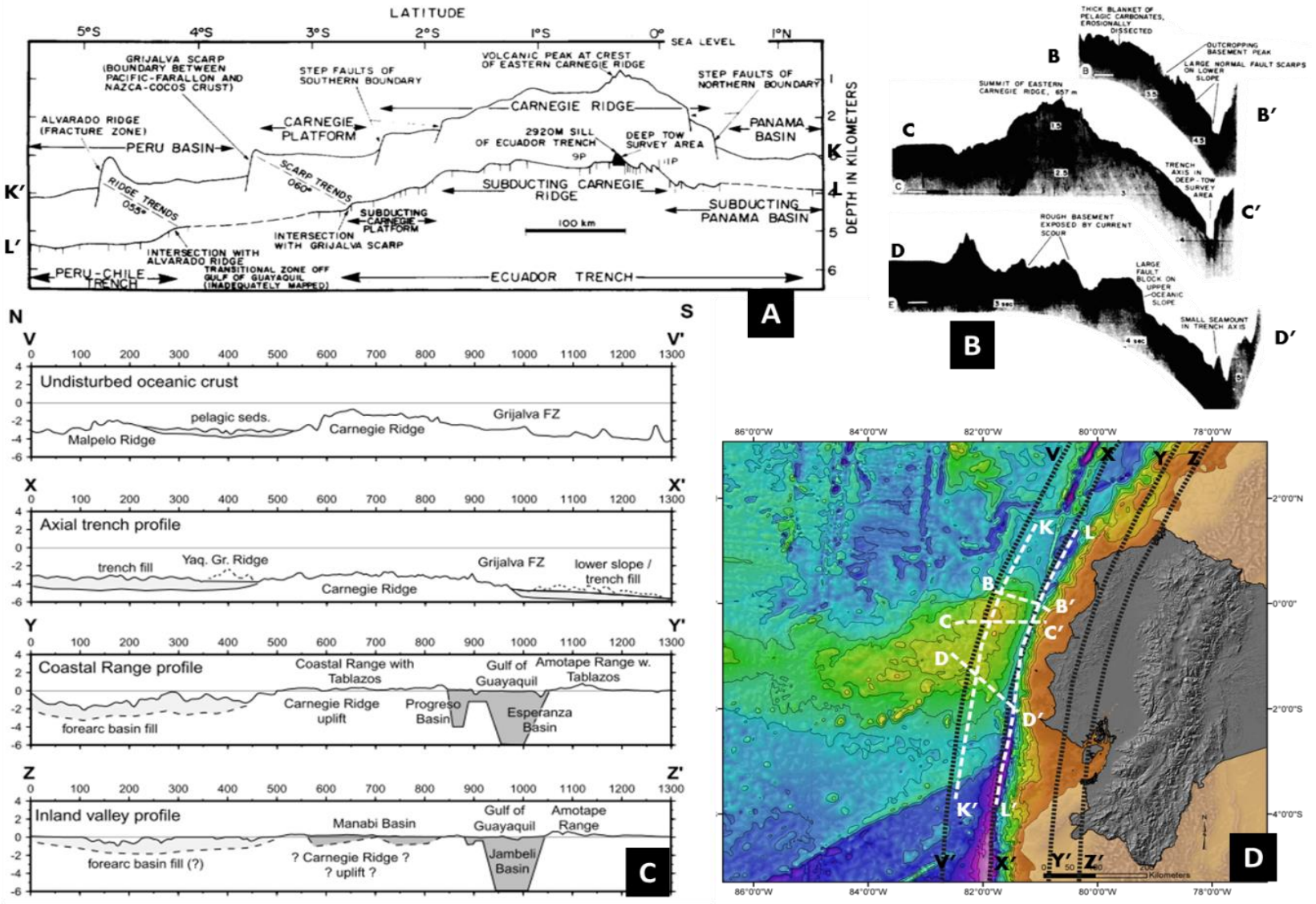

Figure 2.3: Morphological profiles around the Ecuadorian margin. A) N-S bathymetry profile along the trench (profile D-D'); and bathymetry profile 75 km seaward of the trench axis (profile K-K') (modified from Lonsdale, 1978) B) Seismic single-channel profiles oriented W-E, where it is possible to observe the external roughness of the CR (modified from Lonsdale, 1978). C) Four N-S bathymetry profiles: one on the CR, another on the trench, and two onshore (110 and 180 km east of the trench). They try to display the morphological influence of the CR into the coast (from Gutscher et al., 1999). D) Location of the A, B and C profiles.

2.2. The subduction of seamounts

In addition to the Carnegie Ridge, smaller asperities like seamounts subduct beneath the central Ecuadorian margin. They are reported from multibeam data along the slope and from deep penetration multichannel seismic reflection (MCS) data. They are located in front of the Galera-Cojimíes coastal zone (Marcaillou et al., 2016), the Manta-La Plata coastline (Sanclemente, 2014) and the Salango-Salinas coastal sector (Sage et al., 2006; Sanclemente, 2014; Villamar, 2001) (Figure 2.4).

In front of the Galera-Cojimíes coastal zone, the bathymetry data exhibit seamounts aligned in a N-S direction near the trench (Collot et al., 2009); these seamounts form the so-called Atacames seamount chain. In this zone, using the seismic data profiled from the scientific campaign SISTEUR (Figure 2.5B), Marcaillou et al. (2016) proposed the subduction of the double peak seamount (Figure 2.5C). These asperities could be part of the current N-S chain of seamounts exposed on the seafloor (Figure 2.5A), which affect the local geodynamic evolution of the area.

In the Manta-Plata zone (black dotted frame in Figure 2.6A), an oceanic massif (=large, very smooth seamount) with some peaks subducts below the shelf (red dots with white stars in Figure 2.6B). The subduction of this asperity could start at c. 1.4 Ma and might be at the origin of the emersion of La Plata Island (Figure 2.6C) (Sanclemente,2014).

To the south of La Plata Island, between Salango and Salinas (brown dashed-line frame in Figure 2.6A), the literature reports the subduction of a seamount (Sage et al., 2006; Villamar, 2001) (Figure 2.6D). The overriding plate shows morphological characteristics similar to the model proposed by Dominguez et al. (1998) (Figure 1.5). However, based on the reprocessing of the deep penetration MCS data, it more likely corresponds to the subduction of a multi-peak seamount (Sanclemente, 2014) (Figure 2.6E, red dots with white stars in the seismic line) or several little seamounts, which control the morphology of the slope and platform in this area.

These asperities appear to be quite a common feature of subduction in the Ecuadorian margin, especially north and south of the Carnegie Ridge (Fig. 2.7A) where they perturbed the slope morphology. Like in other subduction margins, they play an important role in the subduction process affecting the subsidence, uplift, erosion, basin construction, seafloor and coastal morphology (see Chapter 1).

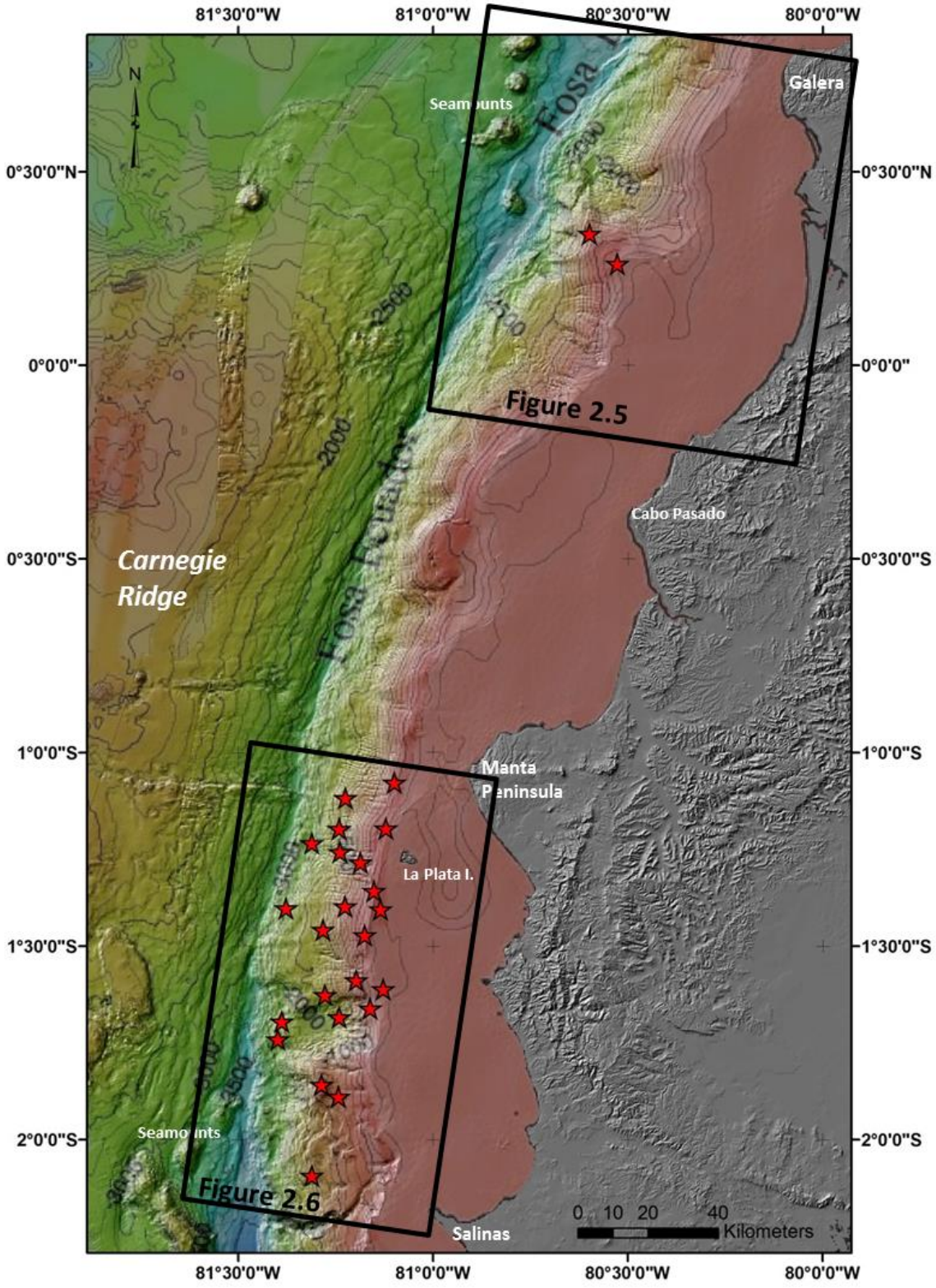

Figure 2.4: Subducted seamounts and peaks. The map shows, using red stars, the interpreted seamounts and peaks along the Ecuadorian margin, shown in the literature (Marcaillou et al., 2016; Sage et al., 2006; Sanclemente, 2014; Villamar, 2001)*. The details of each zone are shown in Figures 2.5 and 2.6.*

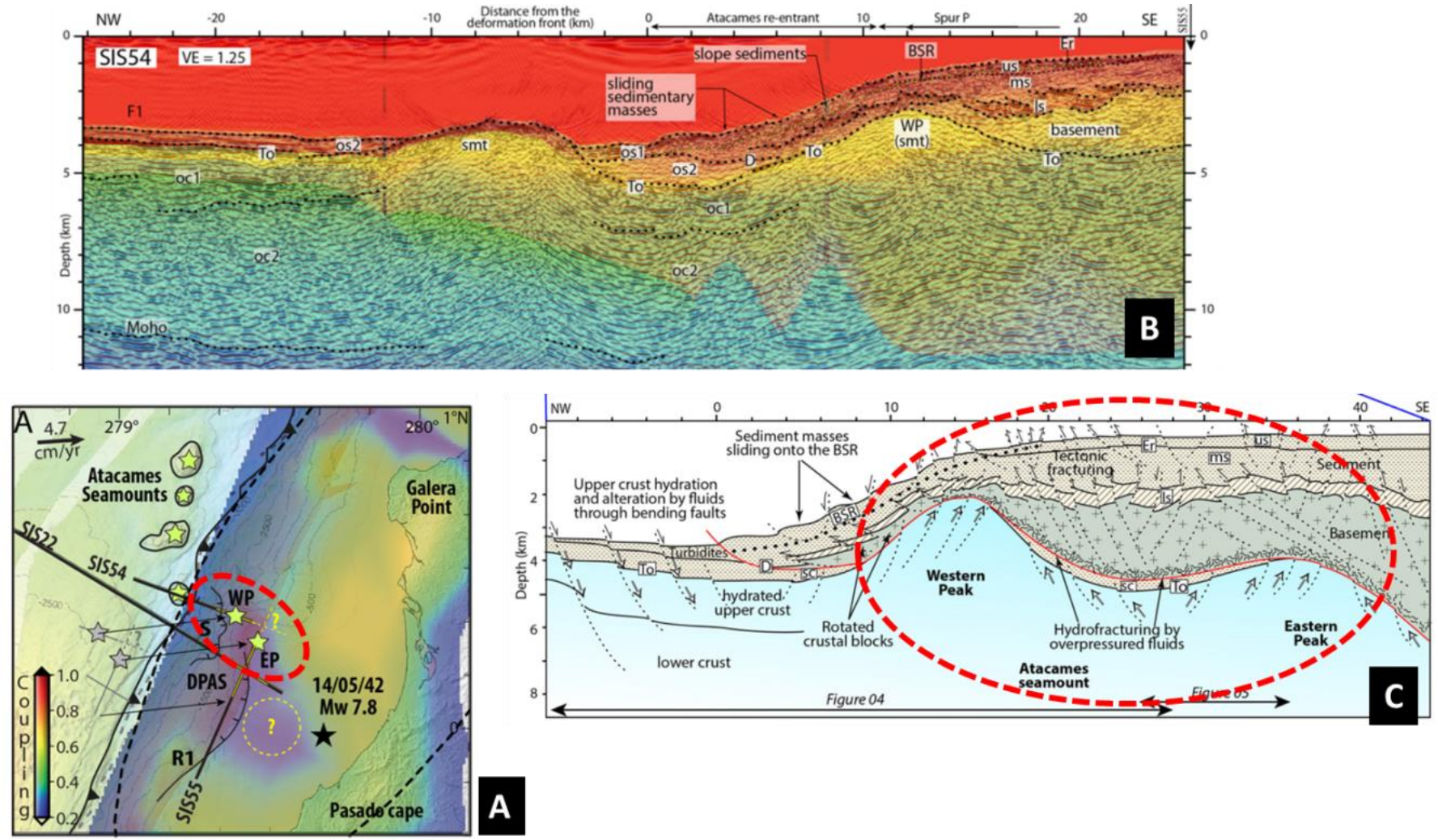

Figure 2.5: Location of the Atacames double-peak subducted seamount in front of the Galera-Cojimíes coastal zone, from Marcaillou et al. (2016). A) Location map of the two peaks displaying the spatial relationship with the Atacames seamount chain and some morphological elements from the margin. The authors use the color palette to represent the interseismic coupling along the interplate contact. B) The interpreted pre-stack depth multichannel seismic SIS54, showing the location of the western peak. C) Interpretative cross-section of the margin showing the location of the two peaks of the subducted seamount on the margin.

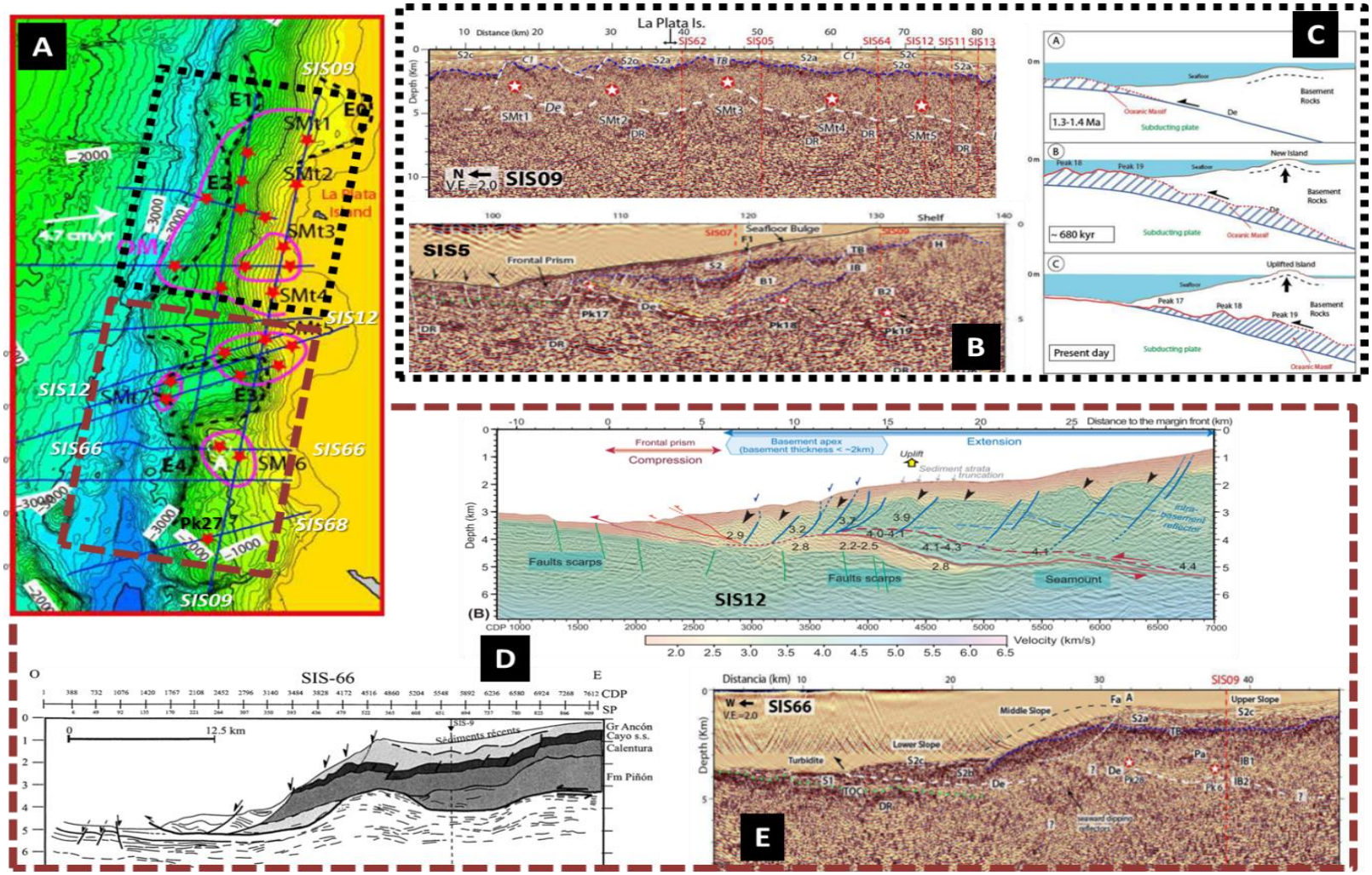

Figure 2.6: A) The location of the numerous peaks interpreted by Sanclemente (2014) in the Manta-Salango zone (black dotted frame) and in the area between Salango-Salinas (brown dashed line frame) (figure modified from Sanclemente, 2014). B) Some of the interpretations of the seismic lines in the zone between Manta-Salango, carried out by Sanclemente (2014), where we can note the peaks of the inferred subducted oceanic massif (the peaks are shown as red dots with white stars). C) The subduction massif model, which explains the suggested relationship between the oceanic massif subduction and the emersion of La Plata Island (from Sanclemente, 2014). D) The interpretation of the seismic lines from Sage et al. (2006) (SIS12) and Villamar (2001) (SIS 66) in the Salango-Salinas area which shows the seamount subduction. E) The re-interpretation of the seismic line SIS-66 carried out by Sanclemente (2014); we can note in this case that the interpretation of the subduction of the two peaks is different *from Villamar's (2001) interpretation.*

3. *The segmentation of the margin*

By considering the general structure of the continental margin and the trend of the coastline, the Ecuadorian margin has been segmented into three zones: Northern, Central and Southern (Collot et al., 2009). The Central segment (from approximately 1ºN to roughly 2ºS in latitude) is characterized by a smooth and regular slope, while the Northern zone and Southern zone have a perturbed margin with slope-failure scarps and a rough morphology (Figure 2.7A). This continental margin segmentation, according to Collot et al. (2009), is related to the CR subduction, for which the northern and southern flanks may extend in subduction below the margin, from Galera Cape to Salinas Cape.

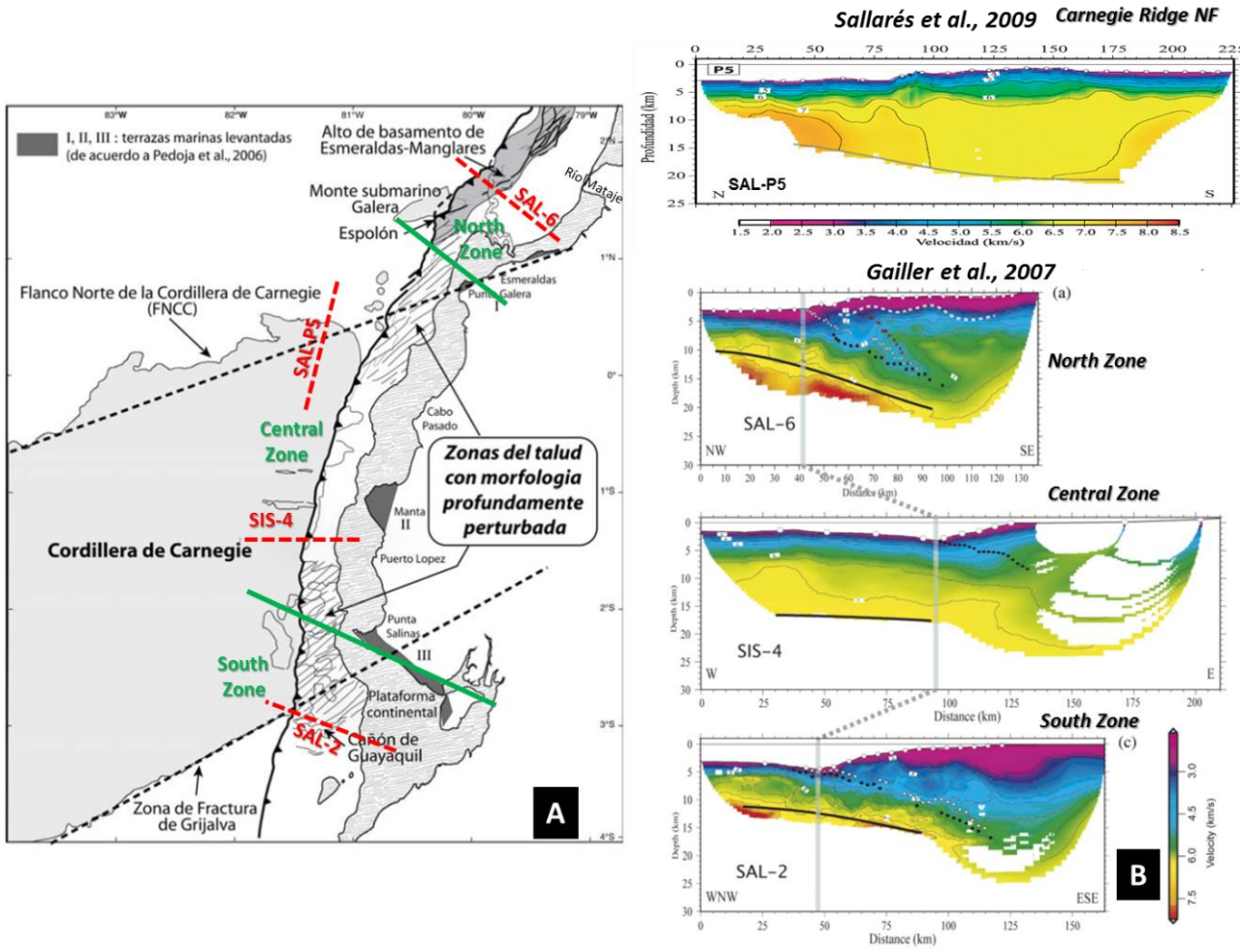

Figure 2.7: Ecuadorian margin segmentation. A) Map showing the influence of the northern and southern border of the CR subduction to the slope morphology of the margin, modified from Collot et al. (2014). On this map,we located the wide-angle model velocity profiles from the northern flank of the CR (from Sallarés et al., 2009) and from the different zones (Northern, Central and Southern) along the Ecuadorian margin (from Gailler et al., 2007). The red dashed line shows the profile locations, while the green line indicates the limits between the Northern, Central and Southern zones of the margin. B) Velocity profiles on the CR (from Sallarés et al., 2009) and on the margin (from Gailler et al., 2007).

The velocity profiles from the wide-angle seismic data at the trench allowed Gailler et al. (2007) to propose a segmentation where each segment (Figure 2.7B) is defined from the related over-thickened oceanic crust of the Carnegie Ridge. The CR over-thickened central segment

increased the buoyancy of the Nazca plate (Gailler et al., 2007), as shown by the velocity profiles on the northern flank of the CR (Sallarés et al., 2009). The segmentation of the margin extends to the onshore area, which is reflected in the coast morphology; these segments encompass, from north to south: 1) Mataje River estuary to Galera Cape, 2) Galera Cape to Santa Elena Cape, and 3) the Gulf of Guayaquil (Blanco-Chao et al., 2014; Dumont et al., 2014).

4. The Quaternary deposits along the central margin

4.1. The onshore outcrops

Pliocene to Pleistocene marine sedimentary rocks are mainly preserved in offshore depocenters (Deniaud et al., 1999), but there is not a detailed description of these basins in the central segment of the margin. However, while sedimentation still continues beneath the modern-day sea level, some borders of these basins have undergone gentle Pleistocene uplift along the coastal line (Cantalamessa and Di Celma, 2004; Pedoja et al., 2006). The main Quaternary outcrops are on the coastal cliffs and marine terraces, which show excellent coastal exposures of the Plio-Pleistocene siliciclastic successions in the central Ecuadorian margin (Benitez, 1995; Cantalamessa and Di Celma, 2004; Pedoja et al., 2006; Reyes, 2013). The Pleistocene formations outcrop at two principal locations along the central margin (J and C in Figure 2.8), meanwhile the marine terraces show a broader distribution along the coast and are not specific at the same place as the Pleistocene formations (I, II and III in Figure 2.8).

4.2. The Pleistocene formations

4.2.1. The Jama Formation

The Jama Formation is Early Pleistocene in age (currently called the Calabrian Pleistocene). It is well exposed along the uplifted eastern margin of the Esmeraldas-Caraquez basin (***J*** in the map shown in Figure 2.8), mainly on the coastal cliff west of the city of Jama (Cantalamessa et al., 2005).

The Jama formation is a variable assemblage of marine to continental strata, which have been subdivided into three formal units and described by Cantalamessa et al. (2005), as follows: “(1) the ~20-m-thick, marine, Punta Pasa Borracho Member exposed between Punta Pasa Borracho and Punta Cabuya; (2) the ~100-m-thick, mixed fluvial-marine Punta Ballena Member, exposed extensively from Punta Cabuya to Punta Alcatraz; (3) the ~60-m-thick, fluvial El Matal Member, exposed between Punta Alcatraz and the village of El Matal. The fluvial strata of the El Matal Member are intercalated with several tephra horizons up to 50-cm-thick.”

The Punta Ballena Member (PBM), according to these authors, consists of eight superposed unconformity-bounded depositional sequences or cyclothems, which were numbered successively from PB1 to PB8 (J in Figure 2.9). An ideal sequence ranges for the PBM is ~5 to 25 m, and is composed of a transgressive systems tract (TST) at the base, followed by a highstand systems tract (HST). From an radiometric Ar/Ar age obtained from volcanic ash above the

contact between the Punta Ballena and El Matal Members (1.16 ± 0.06 Ma), and by correlation between the eight cyclotems with the oxygen isotope sea-level index of the Pleistocene, Cantalamessa et al. (2005) propose that the PBM started to accumulate close to 1.5 Ma BP, during interglacial oxygen stage 49.

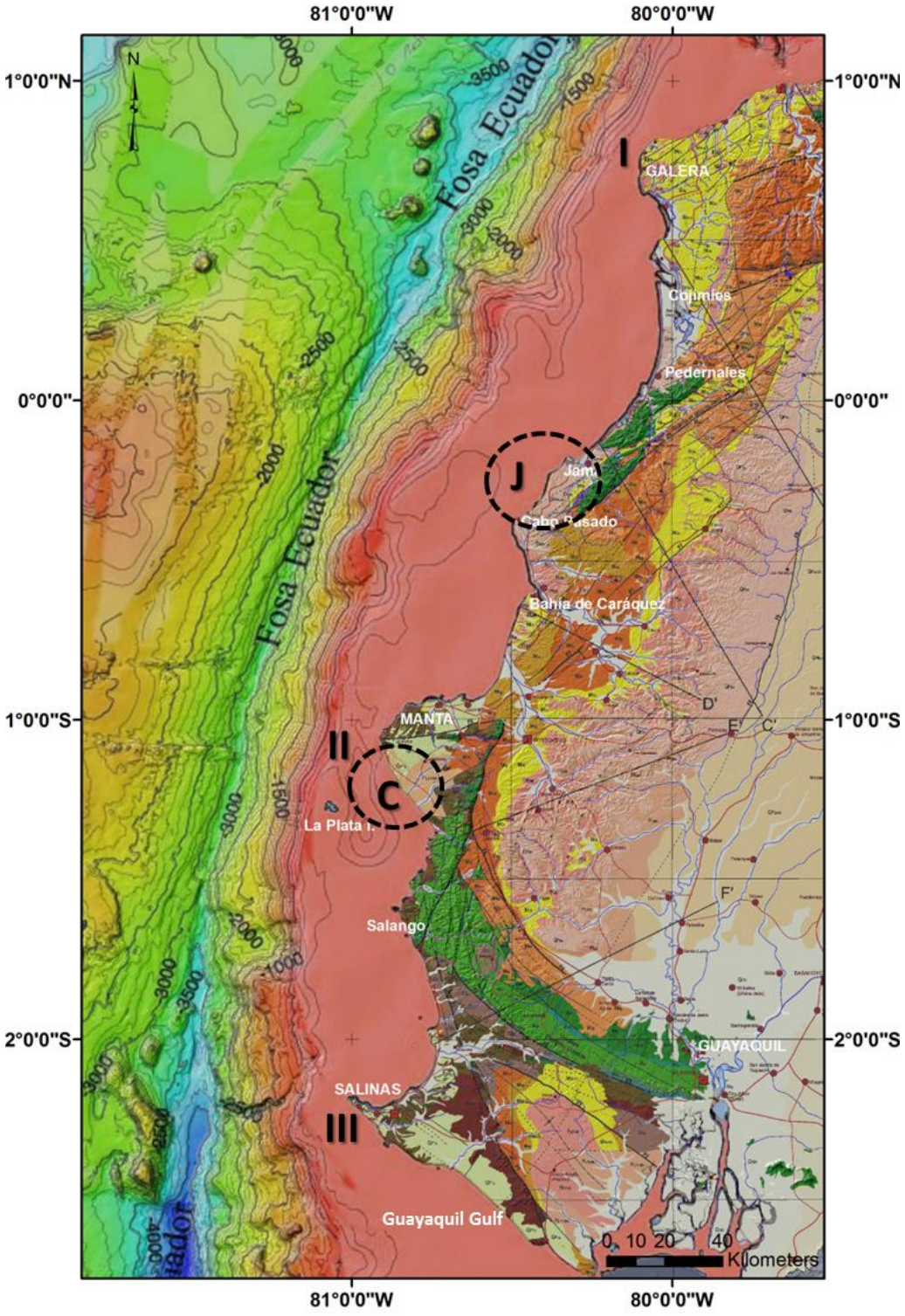

Figure 2.8: Geological map showing the onshore Quaternary outcrops. Composition map from Reyes (2013) and Michaud et al. (2006).

4.2.2. The Canoa Formation

The Canoa Formation lies unconformably over the Early Miocene Tosagua Formation and is divided by an extensive angular unconformity into two units: the Lower Canoa Formation (CnFlow) and Upper Canoa Formation (CnFupp) (Cantalamessa and Di Celma, 2004). According to Di Celma et al. (2005) the CnFlow crops out from a few hundred meters south of Santa Rosa to El Mangle, but it is best exposed and most accessible on the sea cliff south of Punta Canoa (***C*** in Figure 2.9). The 36 m thick lower unit of the Canoa Formation (CnFlow) consists essentially of bluish-gray silty or sandy shales in the offshore area and on the shelf. It is composed of four facies successions (C_{low} 1 to 4 in Figure 2.10C), which are inferred to be a sixth-order (ca. 40 ka) depositional sequence bounded by ravinement surfaces (Di Celma et al., 2002).

The upper Canoa Formation consists of 38 m thick shoreface and inner-shelf deposits including two top-truncated, fining-upward depositional sequences ($C_{upp}5$ and $C_{upp}6$ in Figure 2.10C). The deepening-shallowing upward facies succession that characterizes the depositional sequences of this formation follows regular vertical transition pathways and is referred to as a sheltered sequence architecture, developed in a sheltered, semi-enclosed basin (Di Celma et al., 2005). The age proposed for the Canoa Formation is from the Late Pliocene for CnFlow to the late Early Pleistocene for CnFupp (Cantalamessa and Di Celma, 2004). These ages correspond to the top of the Gelasian and the base of the Calabrian in the current Chronostratigraphic Chart (v.2015/01).

4.3. The Tablazos

The Tablazos Formation (TF) is Middle Pleistocene-Holocene in age. According to the description given by Cantalamessa and Di Celma (2004), around El Aromo (from Punta Canoa to Rio de Caña), the TF is composed of at least six cyclothems characterized by a deepening–shallowing upward facies succession (Tb1 to Tb6 in Figure 2.10C). This formation is referred to as an exposed sequence architecture developed in a more open setting than the sheltered or semi-enclosed basins (like CnFupp). Their deposits show high-energy features, such as trough cross-stratified, wave-winnowed, and lag concentrations formed by storm waves and currents along the bases of the transgressive shelf wedges; storm-wave related soft-sediment deformation structures; and a sharp erosional transition between the siliciclastic shelf wedges and overlying late-transgressive, epifaunal-dominated community backlap shell beds (Di Celma et al., 2005).

In the area between Cabo San Lorenzo to the north and Rio de Caña,according to Cantalamessa and Di Celma, (2004), the CnFupp and TF sequences (from Tb1 to Tb5) have been related to one of the flat morphological features that slopes gently southward with progressively lower angles - surface CII. These authors consider that this surface CII resulted from the progressive south-westerly migration of the depocenter caused by the synsedimentary upwarping of the northern margin (in the Aromo zone on Manta Peninsula). The two other surfaces in this area - CI with a proposed Early Pleistocene age (Calabrian in the Chronostratigraphic Chart v.2015) and CIII related to the MIS 5e- are considered as marine terraces.

However, in this zone (Manta Peninsula), Pedoja et al. (2006a) consider the presence of five levels of marine terrace from T5 for the oldest to T1 for the youngest. These marine terraces have been analyzed as geologic and geomorphic records of repeated glacio- eustatic sea-level highstands superimposed onto a rising coastline. These marine terraces have proposed ages from MIS 37 for T5 to MIS 5e for T1 (II in Figure 2.10A).

There are three other zones along the Ecuadorian margin where the marine terraces outcrop; as the marine terraces in these areas have been dated as from the Pleistocene, generally from MIS 13 to MIS 5e (Table 2 in Pedoja et al., 2006b), they are usually represented as the Tablazo formation in geological maps (Reyes, 2013, pp. 38-39). These zones are: La Plata Island (Cantalamessa and Di Celma, 2004; Pedoja et al., 2006a), Galera Point, and to the north of the Gulf of Guayaquil (Pedoja et al., 2006b).

La Plata Island (II in Figure 2.9) presents a sequence of four marine terraces cut in Cretaceous basaltic basement rocks, with a thin discontinuous sedimentary cover. The altitudes and proposed age of these marine terraces differ between Cantalamessa and Di Celma (2004) and Pedoja et al. (2006), as shown in Table 2.1; but in any case, both assume a rate of uplift between 0.35 and 0.4 mm/y, obtaining a similar age for the oldest marine terrace related to MIS 13.

La Plata	Cantalamessa and Di Celma (2004)		Pedoja et al (2006)	
Terrace	**Altitude (m)**	**Proposed MIS**	**Altitude (m)**	**Proposed MIS**
1	55	5e	47	5e
2	80	7	73	7
3	160	11	145	9
4	175	13	170	13

Table 2.1: Comparison of the altitudes and ages proposed for La Plata Island between Cantalamessa and Di Celma (2004) and Pedoja et al. (2006).

On Galera Point (I in Figure 2.10), three marine terraces T1, T2 and T3, are carved in the Onzole Formation (Upper Miocene–Lower Pliocene). They are locally covered by marine sediments that are 2–3 m thick, with maximum altitudes and a proposed age of: T1 45 ± 2 m – MIS 5e; T2 61 ± 3 m – MIS 7; and T3 101 ± 3m – MIS 9 (Pedoja et al., 2006b). To the north of the Gulf of Guayaquil (III in the Figure 2.9), the marine terraces are on the northern flank of the graben constituted by the Gulf of Guayaquil (Deniaud et al., 1999), from the Santa Elena Peninsula to Puna Island. According to Pedoja et al. (2006b), three marine terraces have been identified in this zone with the following proposed altitudes: T1 15 ± 5 m – MIS 5; T2 35 ± 10 m – MIS 9 and/ or 11; and T3 80 ± 10 m; and ages related to the sea-level highstand of the early–middle Pleistocene (between the Calabrian and Middle Pleistocene in the Chronostratigraphic Chart v.2015).

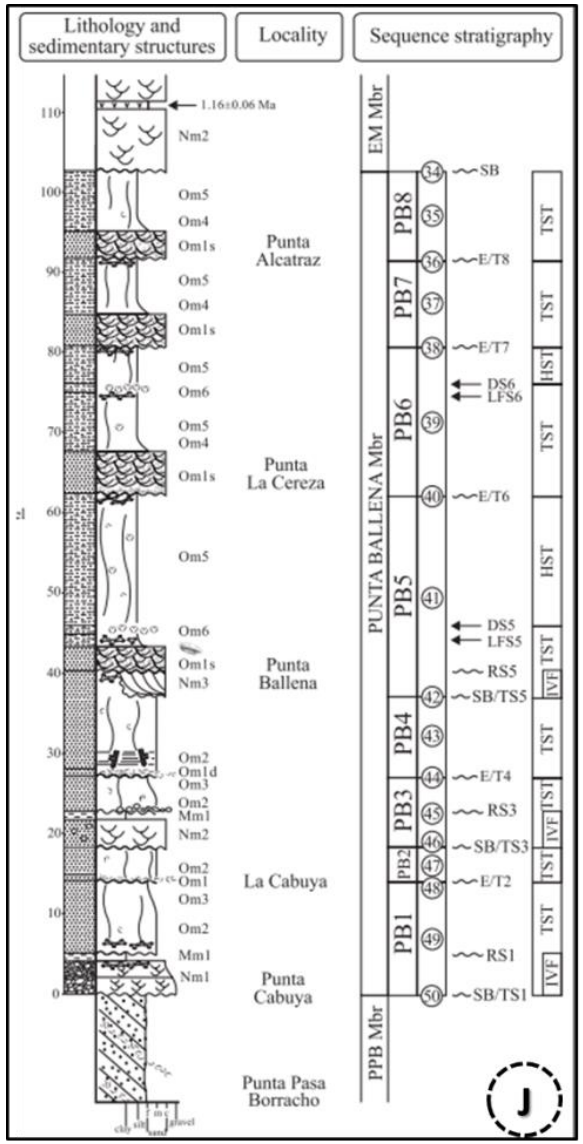

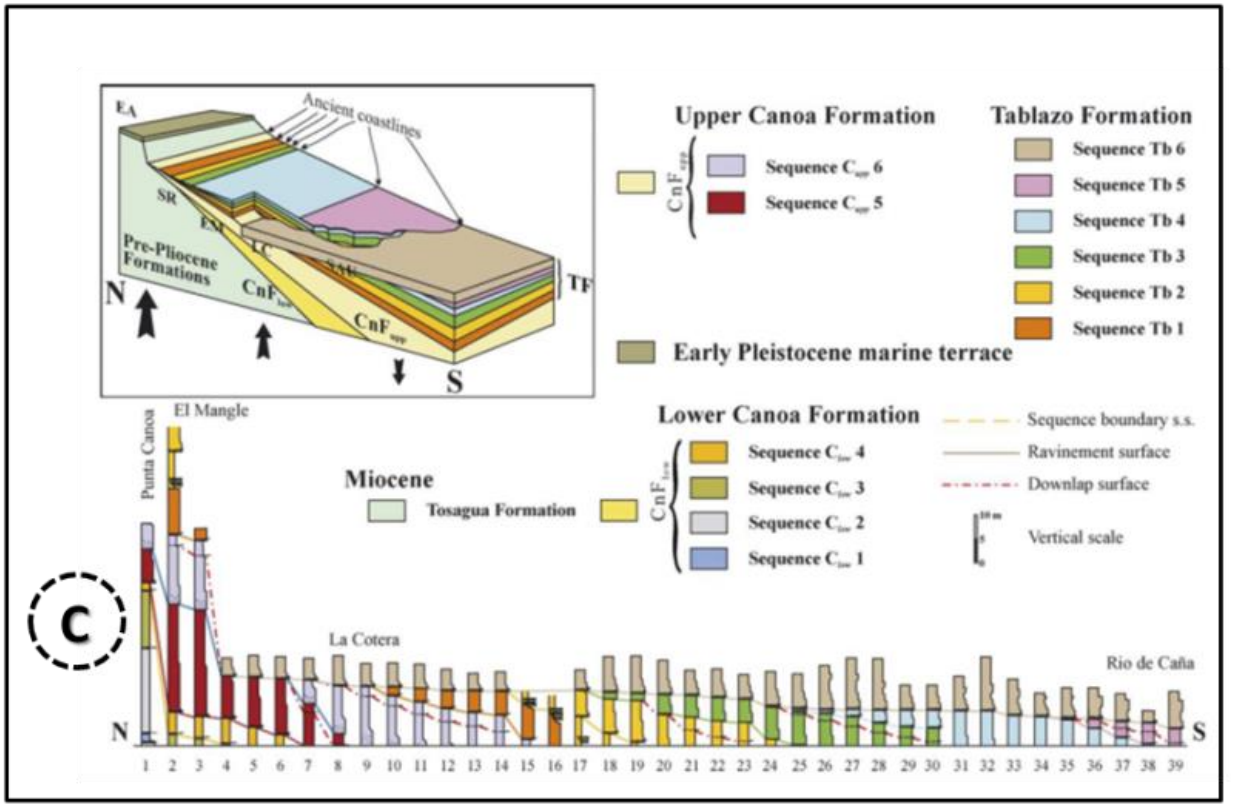

Figure 2.9: Jama and Canoa Formations. J) Stratigraphic section of the Punta Ballena Member of the Jama Formation (from Cantalamessa et al. 2005, see the location in Figure 2.8). C) Stacking pattern and block diagram of the depositional sequences of the Canoa and Tablazo Formations (from Cantalamessa and Di Celma, 2004; see the location in Figure 2.8).

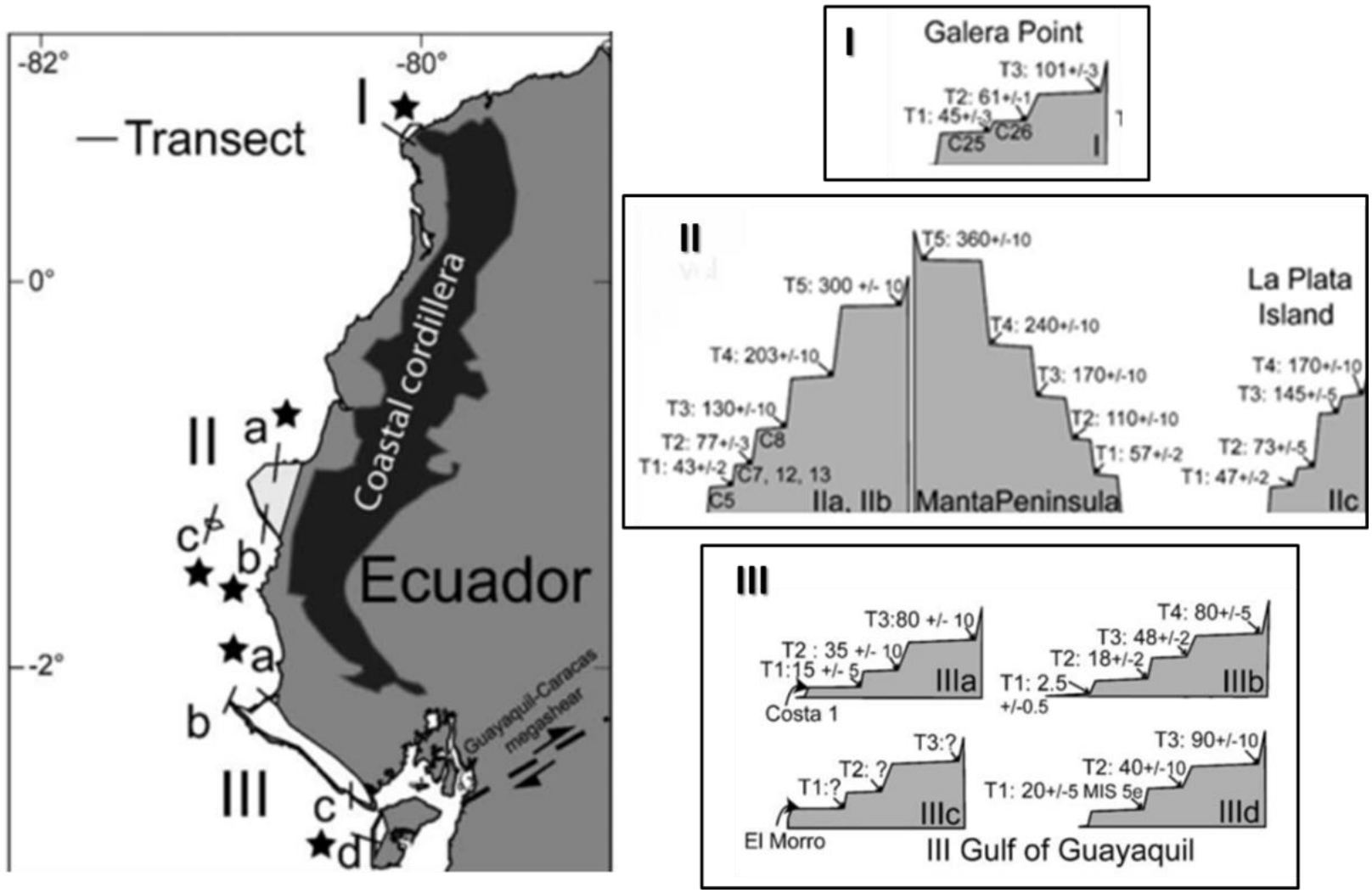

Figure 2.10: Altitudes of the marine terraces along the Ecuadorian margin (from Pedoja et al., 2006b). Their location in the geological map (Figure 2.8) can be identified with I, II, III.

4.4. Offshore quaternary basins

Offshore, the Quaternary deposits are poorly known. In the literature, some maps propose the location of the Neogene basins as along the Ecuadorian margin (Cantalamessa and Di Celma, 2004; Deniaud, 2000), but they are not specific to the Quaternary. Collot et al. (2009) tentatively present a map of the repartition of the Quaternary sediments along the margin (Figure 2.11A). In this map, the most important accumulations of Quaternary sediments are located to the north and south of the margin, i.e. in the Bay of Ancon de Sardinas (between Cabo Manglares and Punta Galera) and in the Gulf of Guayaquil, respectively.

The best studied is the offshore quaternary Gulf of Guayaquil basin (GGB), which develops at the southern end of the Guayaquil Caracas Megashear (GCM) (Dumont et al., 2005). The GCM is the structural contact between the North Andean block (NAB) and the South American plate. The GGM evolved along the shelf area through two main tectonic steps. The first one, during the Mio-Pliocene, is characterized by low subsidence-low sedimentation rates; the second one, during the Pleistocene, is characterized by an abrupt increase of subsidence leading to a maximum deposition of ~3500 m of sediments at the site (Witt et al., 2006) (Figure 2.11B).

The basin was developed in the dextral transcurrent regional context of the northward escape of the NAB. Normal faults belonging to this regional transcurrent frame control the depocenters on the platform and on the upper-slope (Figure 2.12) (Calahorrano, 2005). Taking into account the strong dependence of the subsidence in the GGB area with respect to the northward drifting of the NAB, Witt et al. (2006) assume that the Pliocene–early Pleistocene boundary is associated with a major change in the northward migration rate of the NAB, produced by the increase of the interplate coupling probably caused by the Carnegie Ridge subduction (or the collision of an along-strike positive relief of the ridge). During the upper Pleistocene, the subsidence is significantly less and the normal faults are sealed by the sediment.

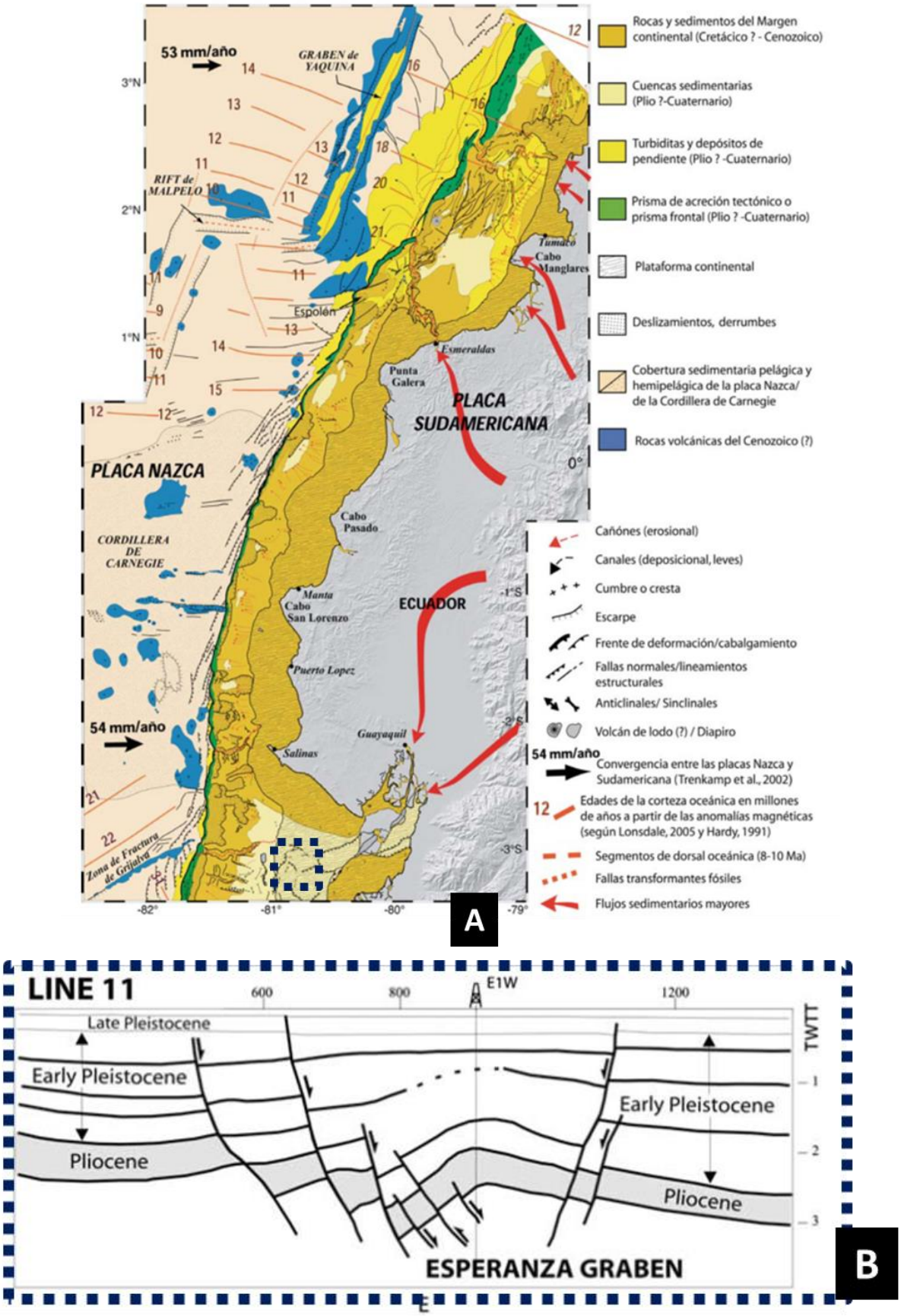

Figure 2.11: Quaternary deposits along the margin. A) Map of the Ecudorian margin proposed by Collot et al. (2009) showing a significant Quaternary sedimentary accumulation in the Bay of Ancon de Sardinas and Gulf of Guayaquil. B) Seismic line showing the thickness of the basins in the Gulf of Guayaquil (more than 3 seg TWTT) (from Witt et al., 2006).

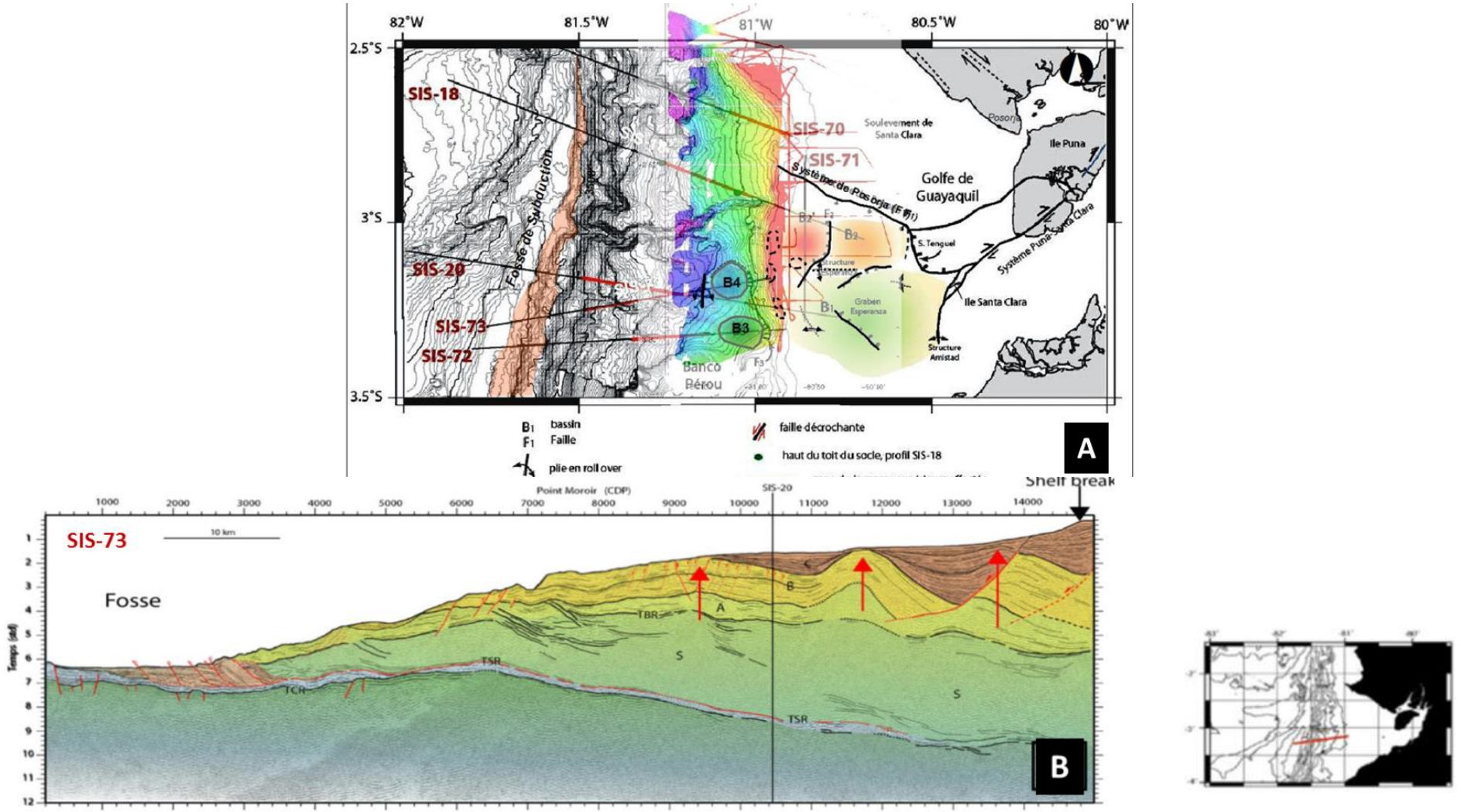

Figure 2.12: Regional context of the Gulf of Guayaquil basin. A) Bathymetric map of the Gulf of Guayaquil with the location of the principal depocenters in the Gulf of Guayaquil Basin, from Calahorrano (2005) and modified by Loayza (2013). The depocenters are located on the platform and along the slope. Red color = platform. B) Seismic profile SIS-73 (location in A). Unit C (brown) corresponds to the Pleistocene deposits and they show two stages. During the first stage, the lower-middle Pleistocene deposits are controlled by normal faults showing significant subsidence. During the second stage, the faults are sealed and the deposits are much thinner (Calahorrano, 2005).

5. The regional faults system on the Ecuadorian coast

The costal domain, and most specifically the Coastal Cordillera, is divided by several regional fault systems. The more recent compilation of these faults was carried out by Reyes (2013). Regionally, these faults can be grouped into two sets: one northern set from 1°S until 1°N where the faults trend SW-NE, and second southern set where the faults trend NW-SE (Reyes, 2013) (Figure 2.13).

The northern set includes the Galera fault system and Jama fault system.

=> The Galera faults are poorly known. In the Galera area, several SW-NE trending faults are reported (Pedoja et al. 2006a; Reyes and Michaud 2012), including the Galera fault that might be a transcurrent dextral fault (Eguez et al., 2003). These onshore faults do not seem to extend across the shelf. Nevertheless, based on a preliminary seismic data interpretation, Michaud et al. (2015) show that some offshore faults have a similar geometry to the onshore Galera fault system. This suggests that these offshore faults might reflect the surface expression of a negative flower structure, and could represent a northward onshore prolongation of the Galera fault system.

=> The Jama fault system is underlined by a relief that includes what we have named the “Jama Massif” where the cretaceous basement outcrops (Piñon formation). The nature of this fault system is not well defined but Eguez et al. (2003) suggest that some faults of this system are transcurrent dextral faults.

The southern set of faults control the Chogon Colonche Cordillera. These faults are poorly known and the offshore prolongations there have not yet been established.

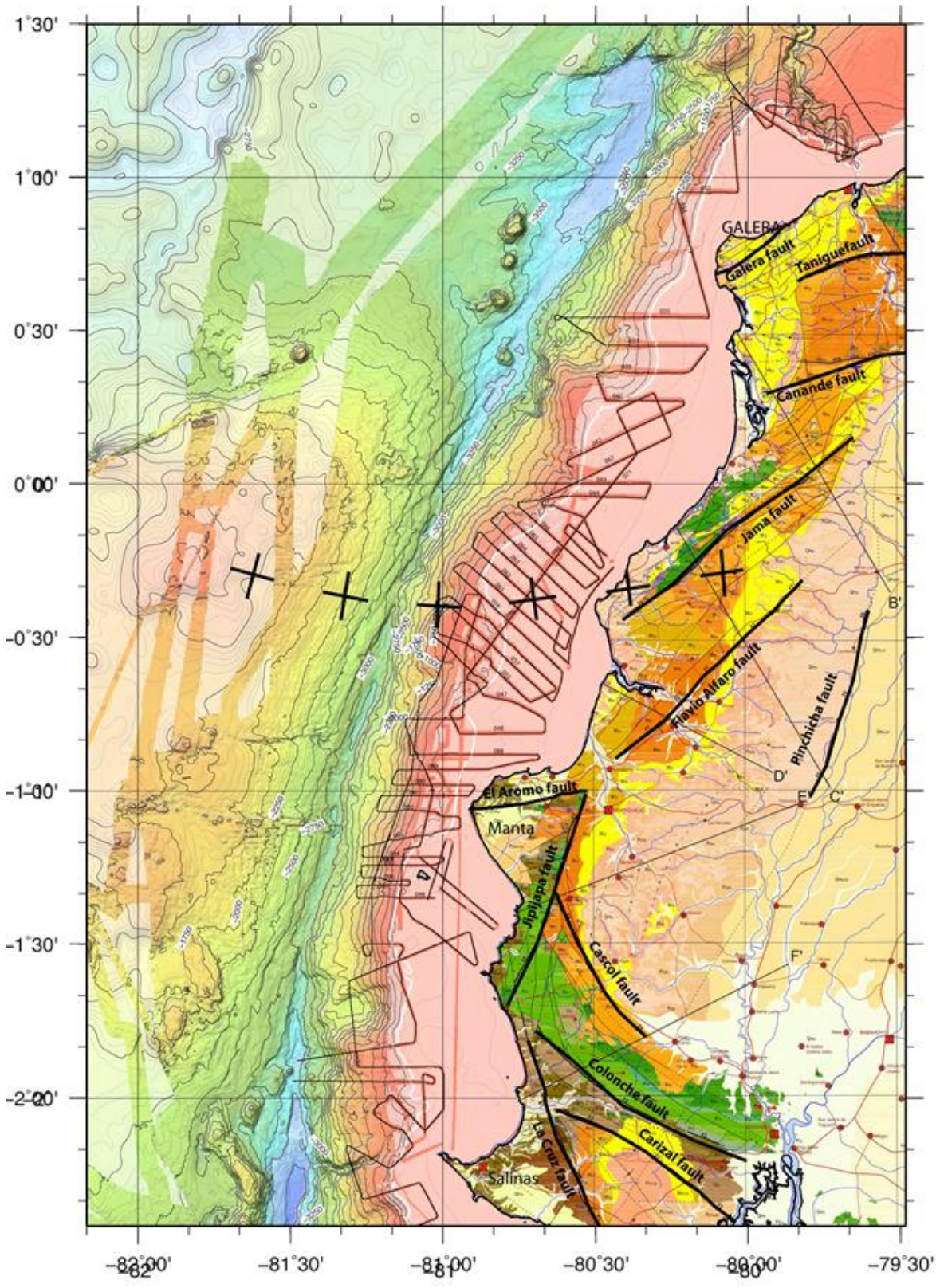

Figure 2.13: Geologic map showing the principals faults onshore (From Reyes, 2013). The crosses underline the supposed prolongation of the crest of the Carnegie Ridge beneath the upper plate (from Collot et al., 2004). The small black lines are the locations of the Atacames seismic profiles. The white line is the platform boundary (=-150 m isobaths). The green color corresponds to the cretaceous basement outcrops (Pinon formation). Along the Jama fault, the basement outcrops along the so-called Jama Massif.

Based on a seismic data interpretation, to the west of Bahia de Caraquez, Collot et al. (2004) evidenced an offshore flower structure with a NE orientation, as a major crustal transtensional strike-slip fault, suggesting that it corresponds to the continuity of the Jama fault system (Figure 2.14).

In the same area, the SCAN seismic data show a deformed sedimentary basin controlled by highly dipping faults (Hernandez et al., 2014); these faults tend to coalesce downward supporting the ‘‘flower structure’’ hypothesis. This supports the suggestion of the offshore prolongation of the active Jama fault system.

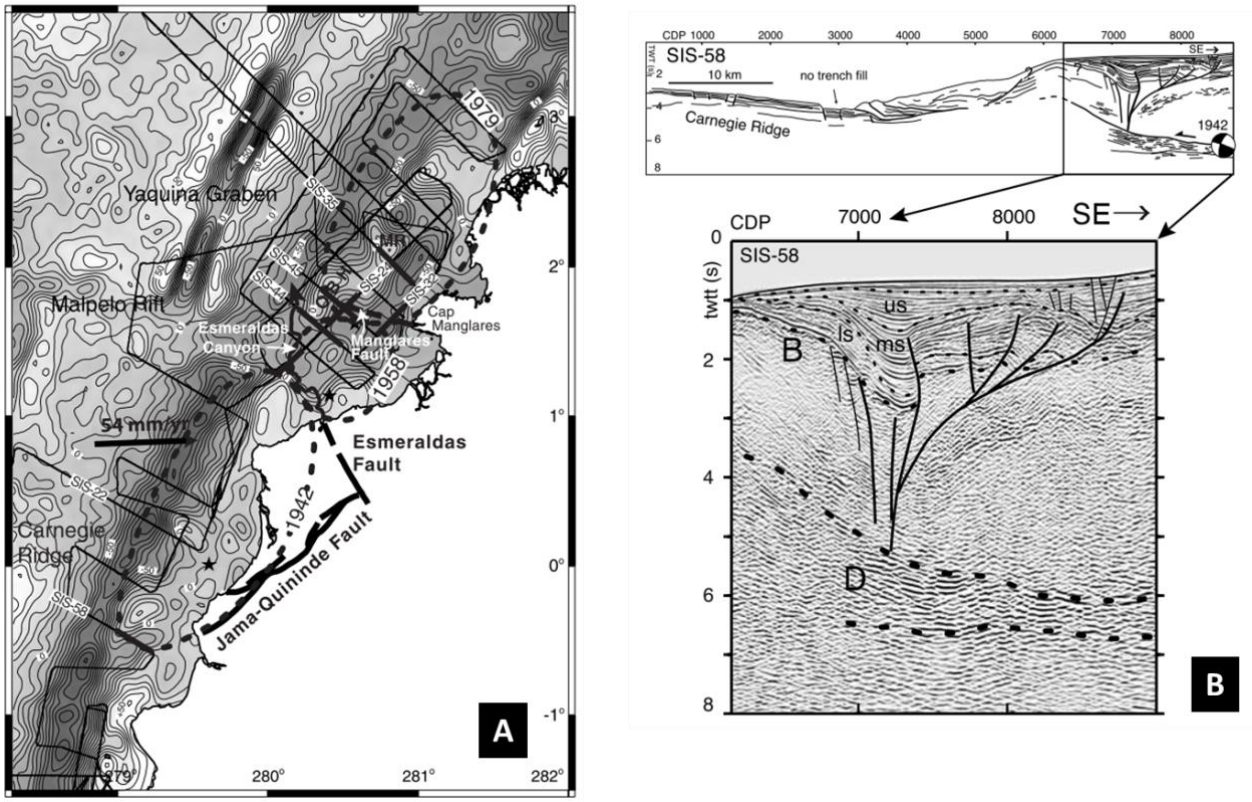

Figure 2.14: Offshore prolongation of the Jama fault system (Collot et al., 2004). A) Gravity anomaly map and location of the Jama fault system (Jama-Quininde Fault). B) Seismic profile showing a flower structure, which prolongs the offshore the Jama fault system.

6. Evidence of Pleistocene faulting

Above, we mentioned the possibility that some faults, that were active during the Pleistocene, extend offshore, such as the Galera fault system and Jama fault system (Michaud et al., 2015). In addition to these faults, the neo-tectonics is poorly known; however, the literature indicates that the Jipijapa and Manta faults are also active.

The Jipijapa fault, located onshore on the eastern side of La Plata Island (Figure 2.13), is defined as a dextral strike-slip fault with a reverse component. Its activity was confirmed by focal mechanisms which provide rupture planes parallel to its superficial projection (N10°-N25°) (Bethoux et al., 2011).

Pedoja et al. (2006) assume that two faults affect the terraces, on the Manta Peninsula, i.e. the Montecristi fault (=Aromo fault of Reyes, 2013) and the Rio Salado fault. The Quaternary marine terraces are approximately horizontal. Thus, a striking variation in the elevation of a shoreline angle could be interpreted as an offset due to the motion of a fault (Figure 2.14), in accordance with the other observations of faults on the geological map or in the field.

The motion of the Montecristi fault is assessed by the different elevations of the correlated terraces observed north and south of the Manta Peninsula. The total maximum offset observed through the uppermost T5 marine terrace ranges between 40 and 80 m (Figure 2.15).

The Rio Salado fault is assumed to cross the Manta Peninsula from north to south and it was interpreted from a sharp offset of the marine terrace elevation to the north of the Manta Peninsula. However, we can note that this fault is not reported in the work of Reyes (2013).

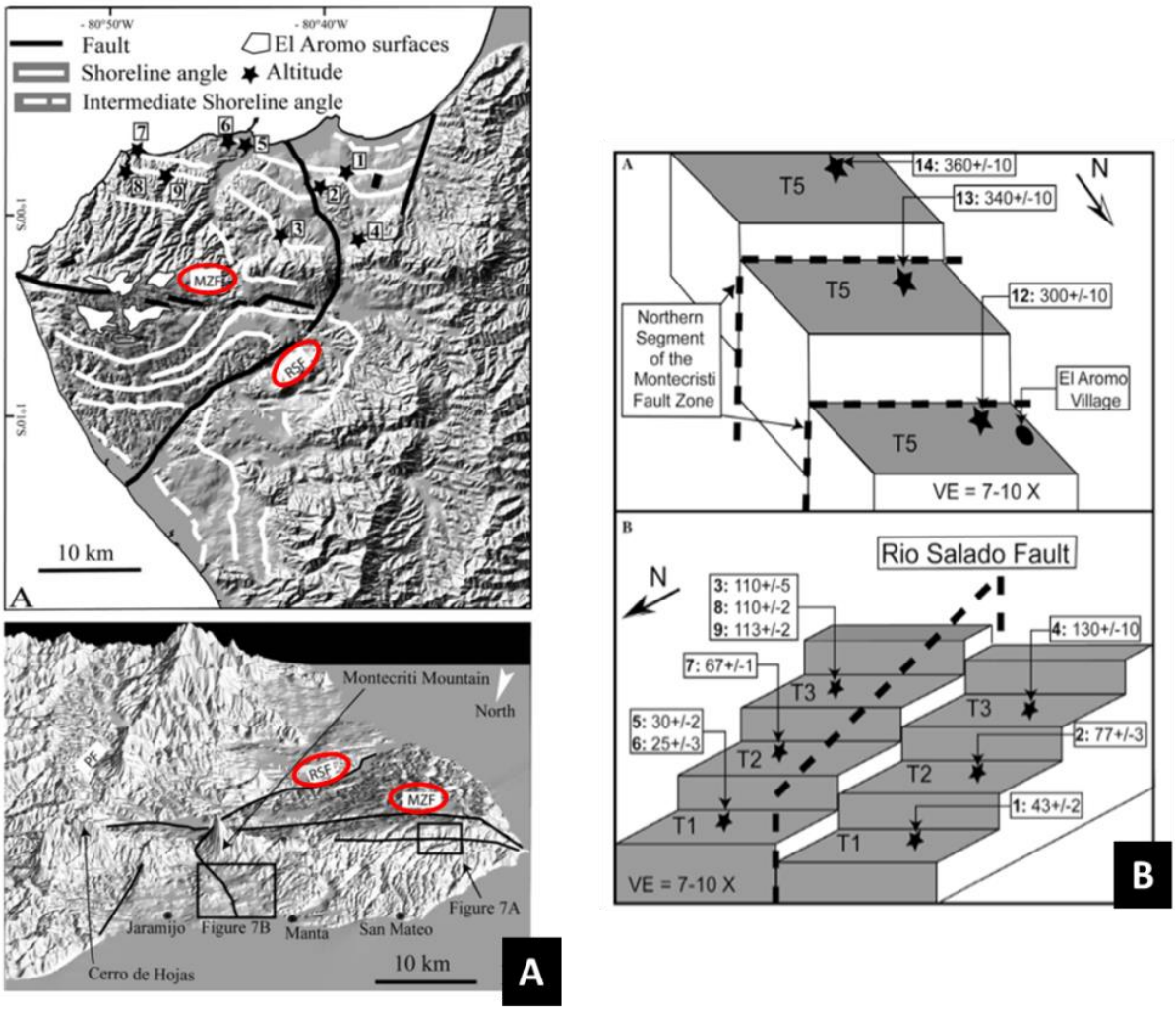

Figure 2.15: Faults of Manta Peninsula. A) Montecristi (MZF = Aromo fault on Figure 2.13) and Rio Salado (RSF) fault trace (from Pedoja et al., 2006). B) Illustration of the offset of the marine terraces caused by these faults (Pedoja et al., 2006).

CHAPTER 3: Data and methods. *A Quaternary deposits record in the Ecuadorian margin: the Atacames data set.*

"La nature est remplie d'une infinité
de raisons dont l'expérience
n'a jamais vu la trace"

Leonardo De Vinci (1452 – 1519)

1. *Introduction*

The main data used in this work were collected during the ATACAMES scientific cruise. The ATACAMES campaign (Archivage de la Tectonique Active et du Climat le long de la Marge d'Équateur en Subduction) had as scientific goals to register and analyze the Pleistocene evolution of the Ecuadorian shelf in response to the climate change and tectonic deformation (Michaud et al., 2012).

It was conducted onboard the research vessel L'Atalante (IFREMER, http://www.ifremer.fr/flotte) in January–February 2012. During this campaign about 20000 km^2 of seafloor were mapped, from shallow to deep marine areas (between 50 and 1000 m of water depth using multibeam bathymetry, back scatter imagery, 3.5 kHz mud penetrator, high-resolution seismic reflection (~4500 km of profiles) and magnetics. In addition, 44 sites both in deep and shallow waters were cored for sediment analysis (Figure 3.1).

All this data allow us to describe the nature and the geometry of the sedimentary architecture to build a stratigraphic succession of reference showing the successions of transgression and regression during the Quaternary (Michaud et al., 2015). As well as, to interpret the record of the deformation in the marine forearc basins, for proposing a tectonic evolution caused by the subduction process of the Nazca plate, with its different types of asperity, beneath the Central Ecuadorian Margin.

2. *Data description*

2.1. The bathymetry data

The principal bathymetry data used in this work was the high-resolution multibeam bathymetry data obtained from the ATACAMES scientific cruise. The data were acquired by using a Kongsberg EM122 (11 to 13 kHz) and Simrad multibeam echosounder EM710 (73 to 97 kHz) (http://flotte.ifremer.fr/Presentation-de-la-flotte/Equipements/Quelques-animations/Sondeur-multifaisceau), allowing the construction of a 25 m-resolution digital elevation model (Figure 3.1C). This bathymetry data were collected around the platform and the slope of the Ecuadorian margin, mainly in perpendicular direction to the coastline (Figure 3.1A).

The Atacames bathymetry data were complemented with the following data sets: a bathymetry grid from the Amadeus campaign (2005), multibeam bathymetry data from GEMAC campaign (INOCAR-2009) and single beam bathymetry data from I.O.A.-1:100.000 nautical charts (INOCAR- different years) (Figures 3.3 and 3.4).

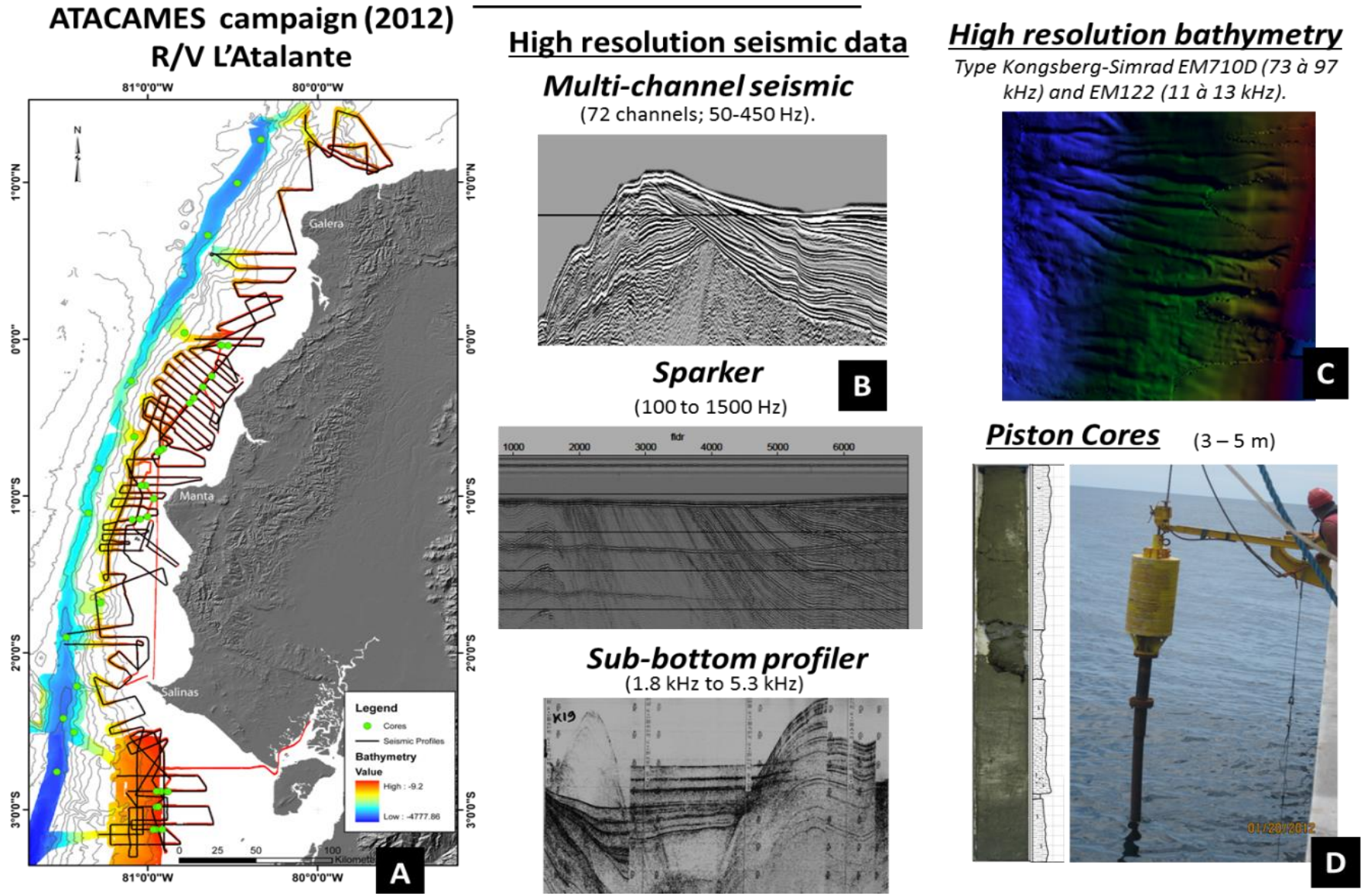

Figure 3.1: Atacames campaign data set. A) Navigation track and location of the core data. B) The different types of seismic data. C) The multibeam bathymetry data. D) The piston core data.

2.2. The seismic data

The main seismic profiles used in this work, came from the ATACAMES seismic reflection data, which were recorded using a 72-channels digital streamer towed at 2 m of water depth (channel length 6.25 m). The source array towed at 2.1 m of water depth consisted of two ramps mounted with three 13/13 Ci plus three 24/24 Ci mini GIgun. Shots were fired at 140 bars every 25 m. Given this shot rate and the streamer configuration this seismic reflection system ensures a nine fold stack (Figure 3.1B).

These seismic lines were processed on board with the Seismic Unix (SU) software (Center of Wave Phenomena, Colorado School of Mines) for Band Pass Filtering, spherical divergence correction (water velocity)—NMO velocity analysis and correction, nine fold stack and constant velocity time migration (1,490 m/s).
Other seismic data sets collected during the ATACAMES cruise and used along of this work are the sub-bottom profiler (1.8 kHz to 5.3 kHz), and Sparker (100 to 1500 Hz) with 5 m streamer with 8 hydrophones (Figure 3.1B).

2-D multichannel seismic reflection data, collected during the SCAN Campaign (2009), was used to complement seismic data from Atacames (Figure 3.2). These data was acquired from the Secretaria de Hidrocarburos del Ecuador (S.H.E. in Spanish) and consist of 78 multichannel profiles in E-W direction and 12 profiles with N-S direction. The acquisition parameters were: compressed air cannon at 400 in^3 as source, distance source-receptor 183 m, shooting interval between points of 25m. Flute length streamer 8000 m, streamer depth 8m, number of traces 640, record time 9s, sampling rate 2 ms. (Hernández, 2012; 2014).

The SCAN multichannel data were used in several zones along the Ecuadorian margin where the Quaternary basins are very thick and difficult to identify with the ATACAMES seismic profiles. These data can be used thanks to the cooperation agreement between IRD and SHE.

2.3. Sediment cores data

From the 44 sediment cores collected during the ATACAMES Expedition, 17 of them were taken from the central margin with an average length of 2m. They were obtained using the Kullenberg corer (Figure 3.1-D). The principle of the Kullenberg corer is based on the free fall of a steel core barrel into the soft sediment. The device crosses vertically the water column attached to a cable. When approaching the seafloor, the trigger corer hits the bottom. This leads to the trigger of the core barrel that falls down into the sediment along the cable. The presence of a cable loop between the trigger arm and the core barrel permits the acceleration of the corer at trigger. The piston that is put at the head of the corer stays stable at the contact of the seafloor during the fall of the corer (http://flotte.ifremer.fr/Medias-Ifremer/Mediatheque-Flotte/flotte/Equipements-et-logiciels/Quelques-animations/Medias/carottier)

A core catcher at the end of the tube prevents sediment from flowing down the tube during recovery of the corer, and maintains the pressure and inhibits upwards sediment expulsion from the tube. The sediment fills a plastic tube that is positioned into the core barrel. This plastic tube is collected onboard and cut into 1 m-long sections before splitting and study into the lab.

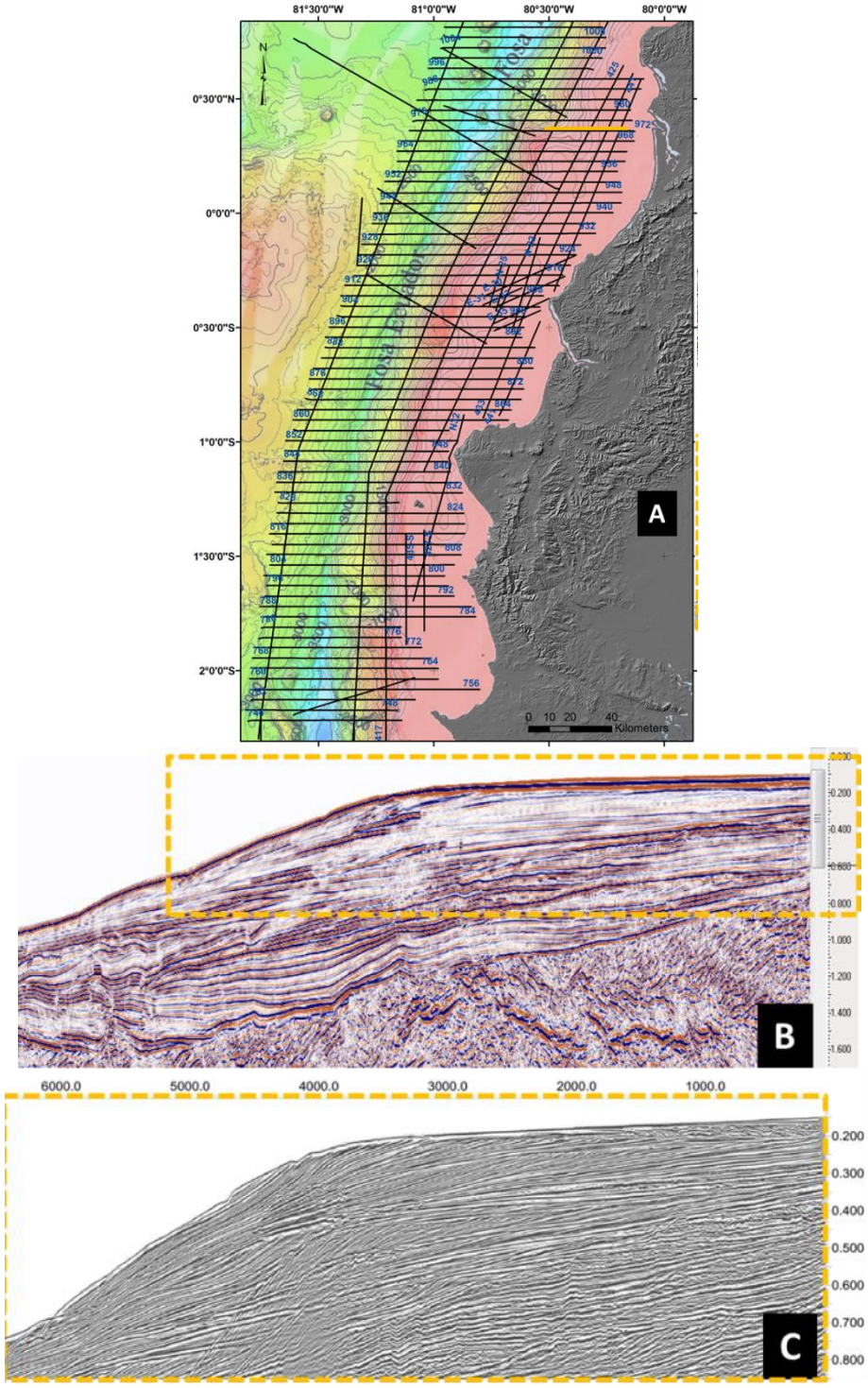

Figure 3.2: A) SCAN multichannel seismic data location. B) Example of the SCAN seismic profile. C) Example of the ATACAMES seismic line. We can note the significant differences in resolution and penetration between the SCAN and ATACAMES seismic data. SCAN data were used in places where Quaternary basins are very thick and difficult to identify with the ATACAMES seismic profiles.

3. Methods

3.1. Bathymetry data

The high resolution bathymetry data acquired during the ATACAMES campaign were processed on board with the software Caraibes, (TM Ifremer). In order to obtain a general bathymetric grid that permits the geomorphological analysis of the central Ecuadorian margin, we complemented the ATACAMES bathymetry grid with multibeam bathymetry data from previous multibeam campaigns such as: Amadeus campaign (2005) compiled by Michaud et al. (2006), GEMAC campaign (INOCAR-2009), and single beam bathymetry data from I.O.A.-1:100.000 nautical charts from INOCAR (different years – Figure 3.3).

All bathymetry data was homogenized to 30m-resolution grid, and they were integrated using the Global Mapper G.I.S. application. The Amadeus bathymetry grid covers principally the slope and trench of the Ecuadorian margin, and the front side of the Carnegie subduction (Figure 3.4A). The INOCAR grid includes data from the coastline to the edge of the continental shelf (Figures 3.3 and 3.4B); and the ATACAMES data comprises the platform, the slope and the trench (Figure 3.4C).

The grid obtained by merging the data presented some gaps around the shelf break (ovals in the Figure 3.4D). These gaps were filling using the Inverse Distance Weighting (IDW) interpolation method from the Spatial Analyst Application of the ArcGIS software. The interpolation was generated for each zone with a gap, using the bathymetry data from the three sources (ATACAMES, AMADEUS and INOCAR). In this way we obtained a general 30m-resolution bathymetric grid of all Ecuadorian central margin, located in front of the Carnegie Ridge subduction (Figure 3.4E).
In this way it was possible to obtain a homogeneous bathymetric grid with spatial resolution of 30m. This grid preserves the original “visual” resolution of the original data, but it allowed us to have a general morphologic context of the margin, as well as to identify some important geomorphological features of the seafloor, principally at platform and around the shelf break where there were not until this moment a spatial model of the seafloor. Thus, the best details of the grid are the places covered by the ATACAMES data, and for this reason the bathymetry cross sections used for the geomorphology analysis in this work were obtained only over these sites.

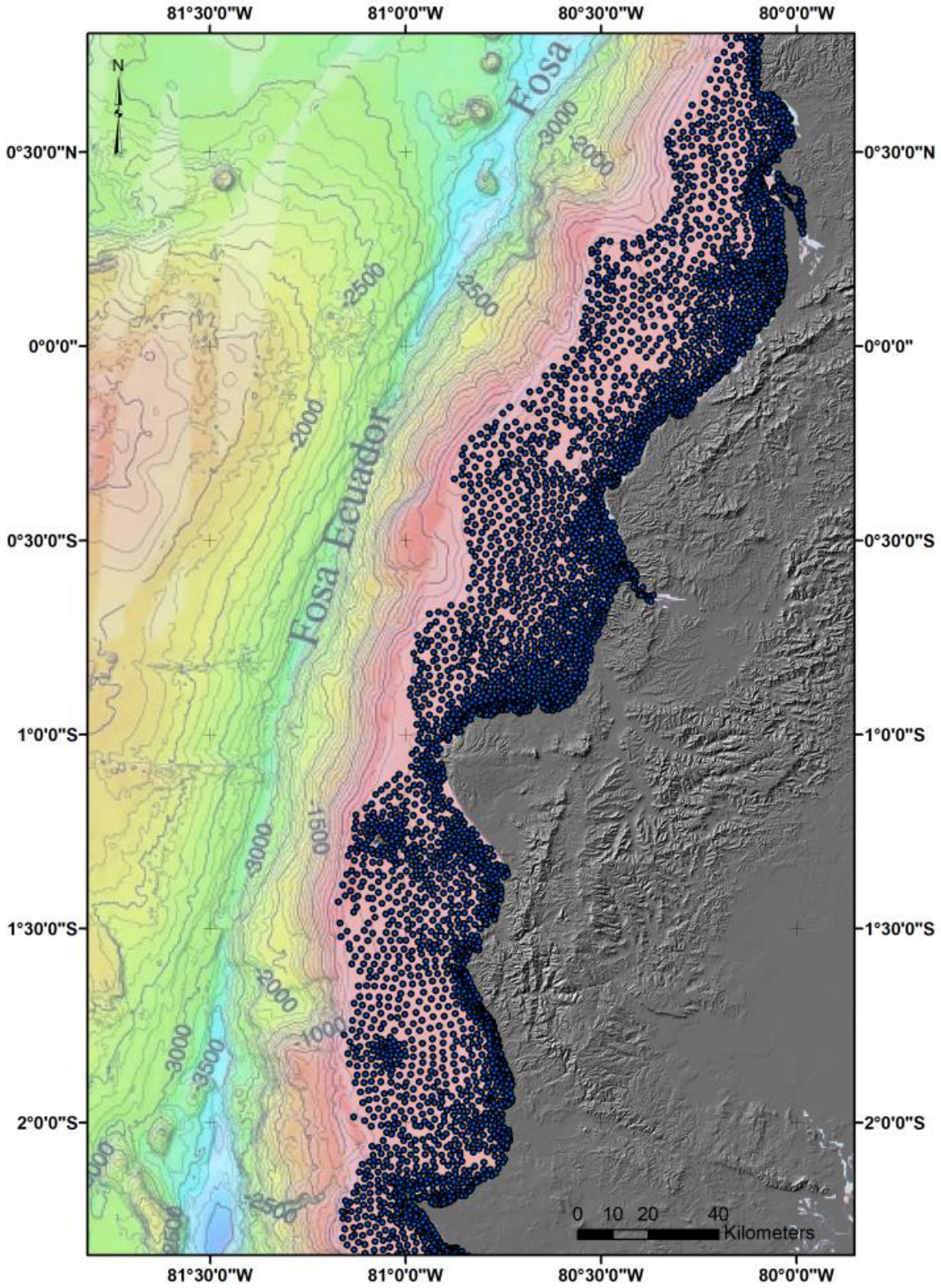

Figure 3.3: Single bean bathymetry data at the Ecuadorian central shelf. Data obtained from I.O.A.- 1:100.000 nautical charts (INOCAR- different years).

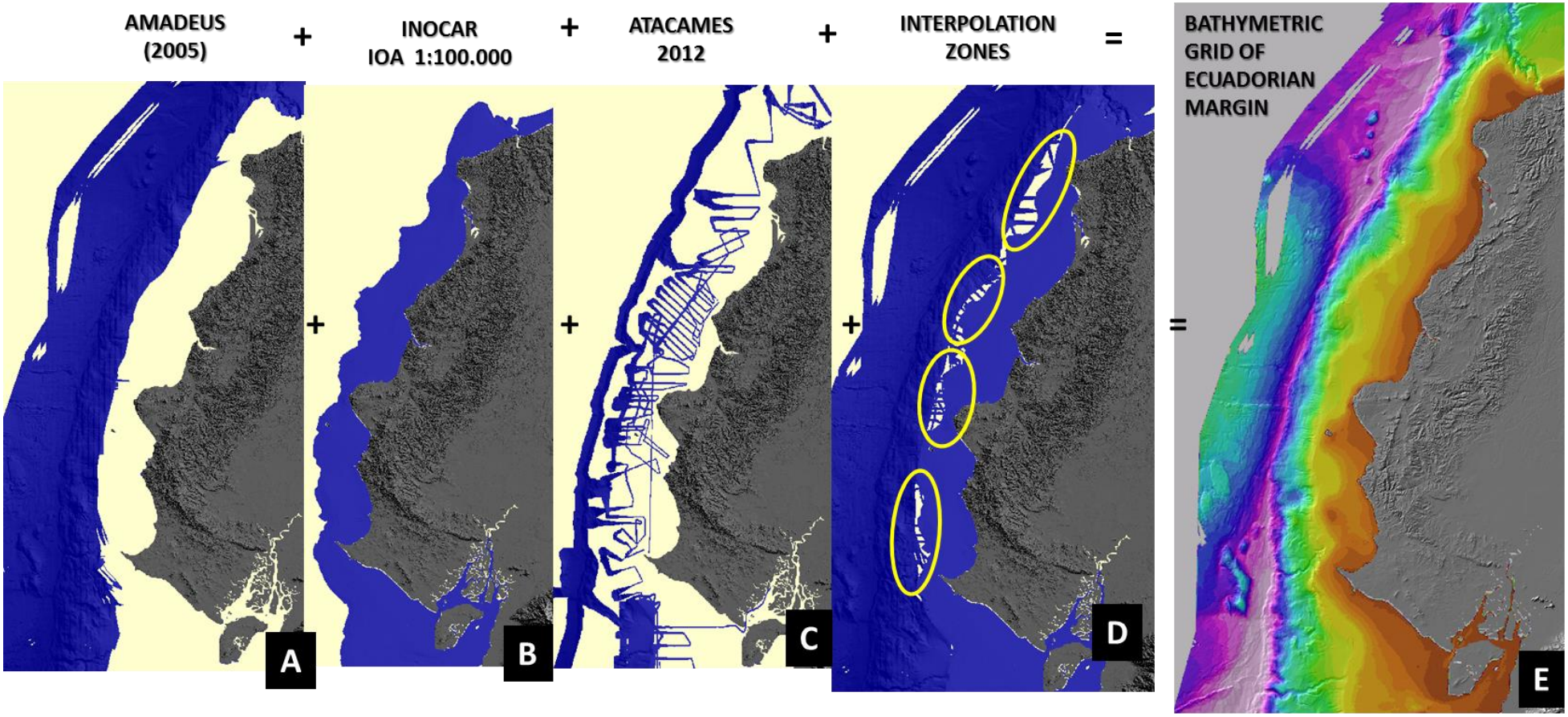

Figure 3.4: Zones covered by different sources of bathymetry data used to build a 30m-bathymetry grid of the Ecuadorian margin.

3.2. The seismic data Interpretation

The interpretation of the seismic data was realized following several steps:

The first step consisted in a very detailed interpretation of one seismic line through the thickest and best preserved part of each basin depocenter, in order to obtain a "state of the art" seismic stratigraphic interpretation according to the principles of seismic stratigraphy (Mitchum et al., 1977) and the sequence stratigraphy (Catuneanu et al., 2009a).

In this seismic profile we identified the stratal termination patterns (onlap, toplap, downlap, truncation and offlap) to discriminate the main seismic unconformities, which bound the systems tract that compose the depositional sequences (Vail et al., 1977) (Figure 3.5A). The seismic facies were interpreted in each systems tract, using the criteria of configuration, amplitude, continuity and frequency of the internal seismic reflectors (Sangree and Widmier, 1977) (Figure 3.5C). From the analysis of the shorelines trajectories and the vertical trend of the seismic facies changes, we interpreted the transgression (T), the normal regression (NR) and the forced regression (FR) (Figure 3.5B) that triggers the shifts of facies and the stacking patterns shown in the different types of the system tracts.

The surfaces that bound the systems tract were named after Catuneanu (2006): *the* Maximun Regressive Surface (MRS) at the end of the regression, the Transgressive Surface (TS) at the beginning of the transgression, the Maximum Flooding Surface (MFS) at the end of the transgression, the Basal Surface of Forced Regression (BSFR) at the onset of the forced regression with its Correlative Conformity (CC) at the end of the forced regression. The systems tracts are named accordingly with the Highstand Systems Tract (HST) above the MFS, the Falling Stage Systems Track (FSST) above the BSFR, the Lowstand Systems Track (LST) above the MRS and the Transgressive Systems Tract (TST) above the TS (Catuneanu et al., 1998) (Figure 3.5D and 3.5E) (for details see Chapter 1).

Following the definition of the T-R sequences proposed by Embry (1995) we grouped the set of regressive system tracts (Highstand, Falling-Stage and Lowstand) as a unique "Regressive System Tract" and the transgressive in a "Transgressive System tracts". This allowed us to locate the limits of T-R sequences on MRS. The T-R sequences were re-grouped, using the unconformities showing the largest lateral extend as boundaries between sets of sequences, in Low T-R, Medium T-R and Upper T-R (see Chapter 5).

The *second step* involved the correlation of the T-R sequences boundaries along the entire Ecuadorian central margin. To make this some tools from the Kingdom software were used. This interpretation was made using the ATACAMES seismic data in two way travel time (TWTT), and in some zones we have used the SCAN seismic lines also in TWTT (Figure 3.6A)

The *third step* was to obtain the isobath and isopach maps. These charts were made using the Flex Gridding interpolation algorithm of the Kingdom software. The depth conversion was performed using specialized tools from the Arcgis software and assuming a regular sound velocity of 1900 m/s (Figure 3.6B)

The *fourth step* was to obtain the ages of the sequences, passing from sequence stratigraphy to the chronostratigraphy. To do this it was assumed that each T-R sequence saves the eustatic transgression and regression records related to the interglacial-glacial stages of the Milankovitch cycles. The top layer of the T-R sequences of some basins, along of the margin, were dated from C14, obtaining a correlation with the current Marine Isotopic Stage (MIS 1). From this, we have correlated each sequence boundary (MRS) by counting them downward and comparing them with the MIS and the ages proposed by Lisiecki and Raymo (2005). At the end the proposed ages for the sequences were correlated with the Quaternary onshore outcrops available in each zone.

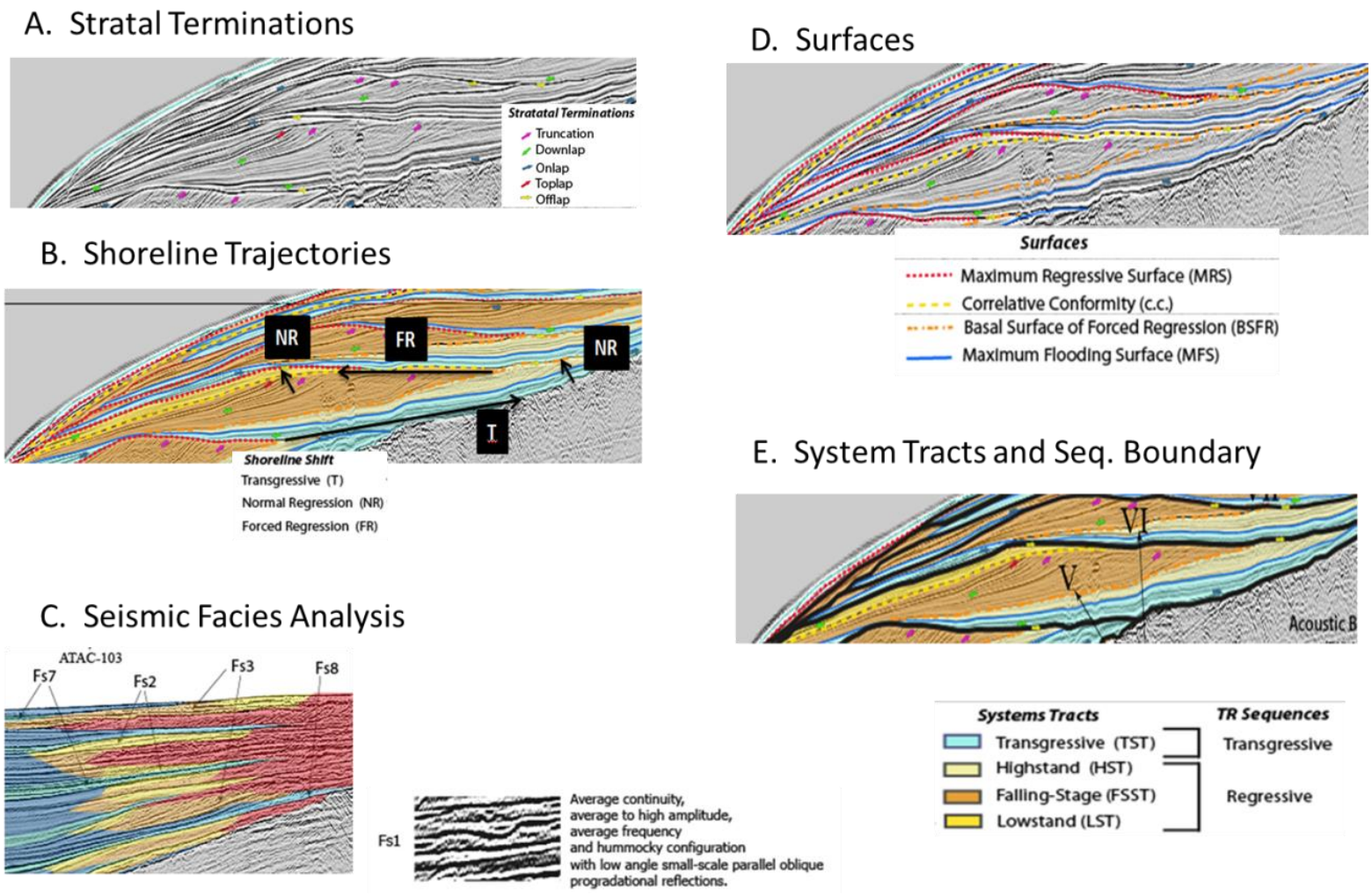

Figure 3.5: Steps followed for the seismic data interpretation.

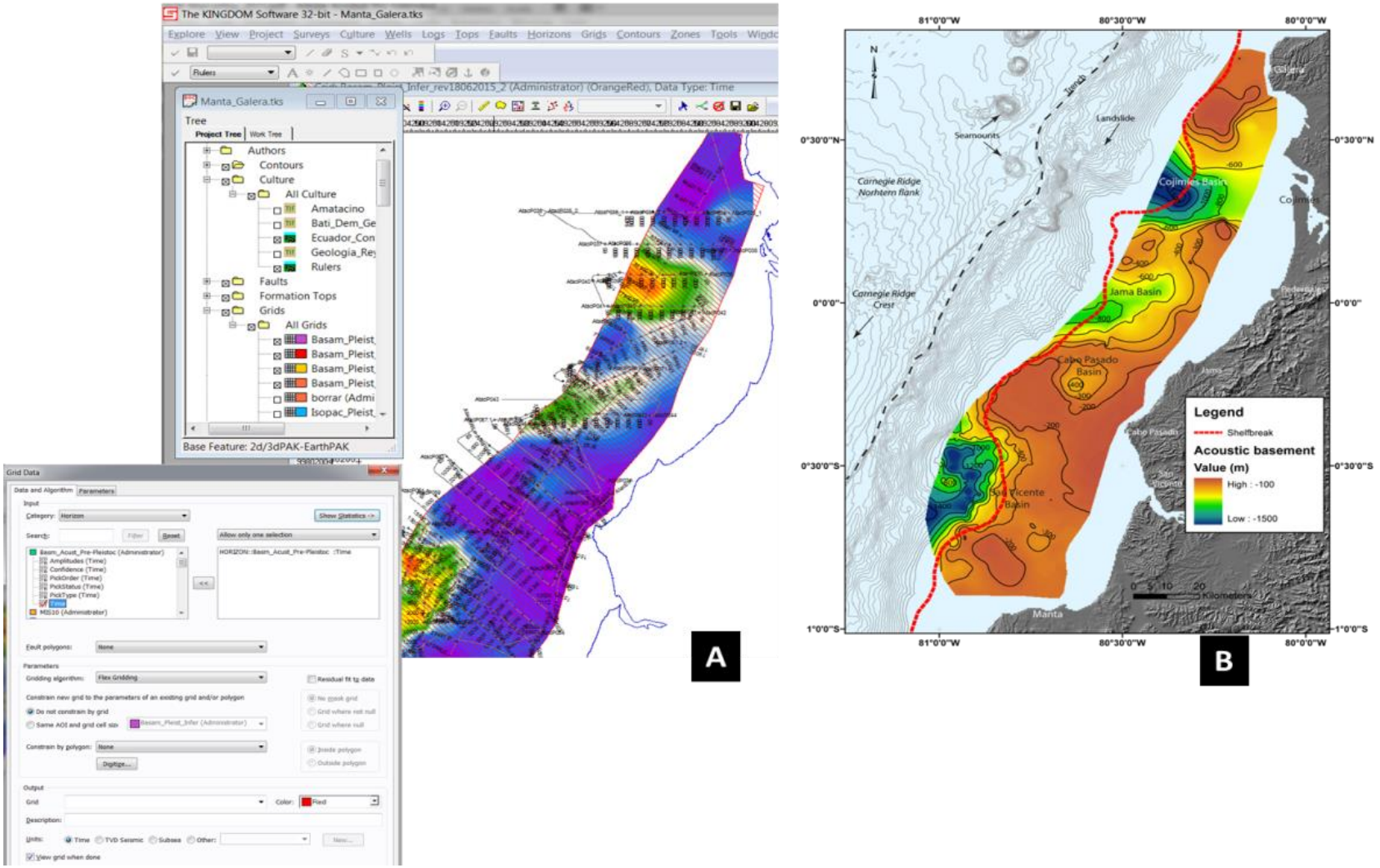

Figure 3.6: A) The Quaternary bottom-grid deduced from seismic data using the Kingdom software. B) The depth conversion of the grid was carried out using the Arcgis software, assuming a sound velocity of 1900 m/s.

3.3. The Sediment cores data interpretation

Sedimentary cores were cut in 1m-long sections and then split for visual descriptions and photographic record (Figure 3.7A). Visual assessment involved description of the following parameters: photography, general aspect of the core, lithology, grain size, presence of bioturbation and sedimentary structures description (Figure 3.7B).

After visual description some cores were selected for microfossils sampling (Figure 3.7C) for age dating using C14 radiometric method. In this way it was possible to set the ages to the upper sequence interpreted in the ATACAMES seismic profiles (Figure 3.7D). The age dating was carried out in Poznan Radiocarbon Laboratory (http://radiocarbon.pl/index.php?lang=en).

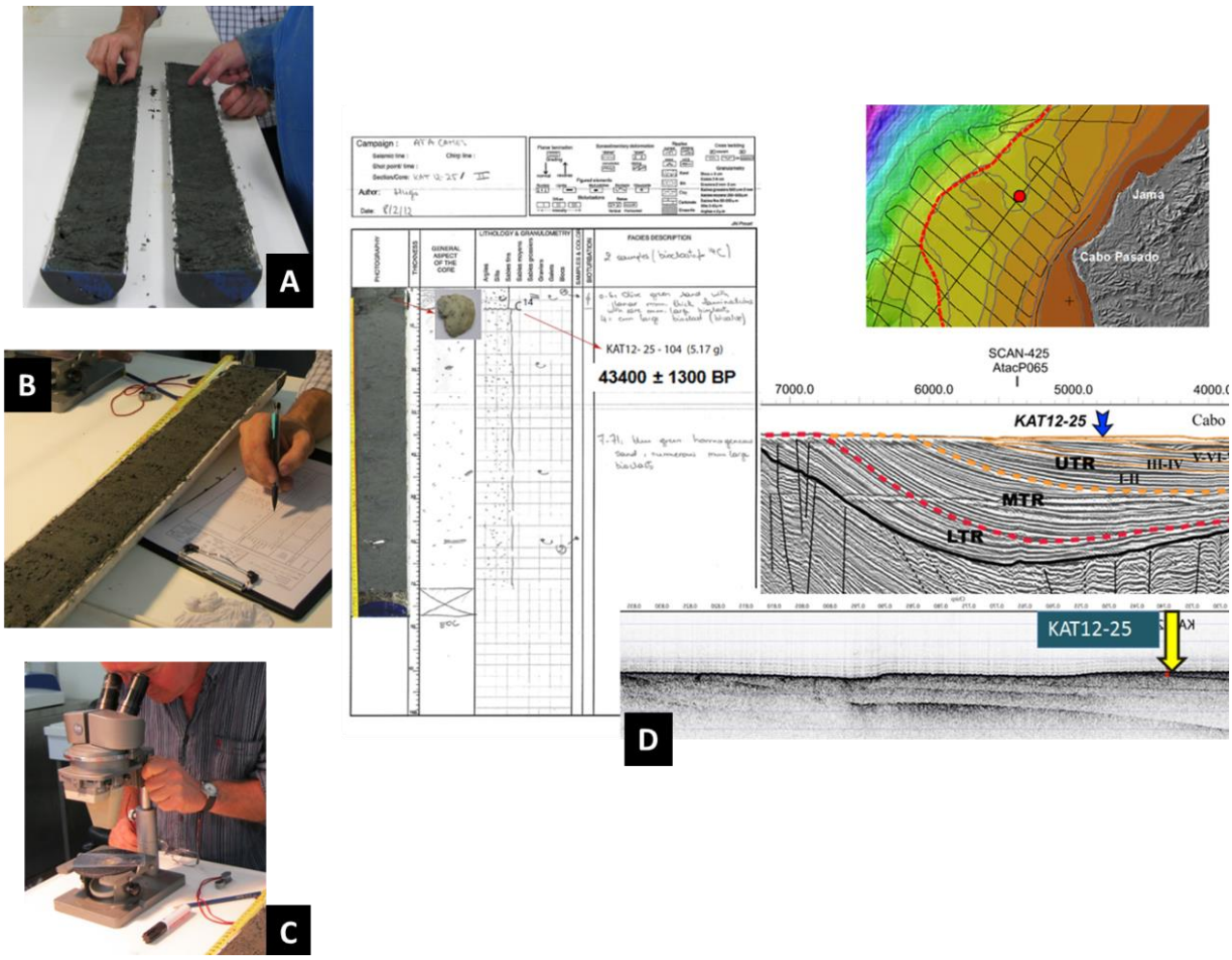

Figure 3.7: Proceeding followed for the interpretation of cores.

Radiocarbon dates were calibrated using the nearest and the most recent measurement of marine reservoir age obtained from the Marine-13 dataset (http://calib.qub.ac.uk/marine/) (Stuiver and Reimer, 1993) with a reservoir age of 434 years with Delta R: 132 and Delta RErr:40 (Etayo-Cadavid et al., 2013) (Figure 3.8). This correction was made using the CALIB Rev 7.0.2 software for windows (http://calib.qub.ac.uk/calib/). The calibrated ages were assigned to their respective T-R sequence.

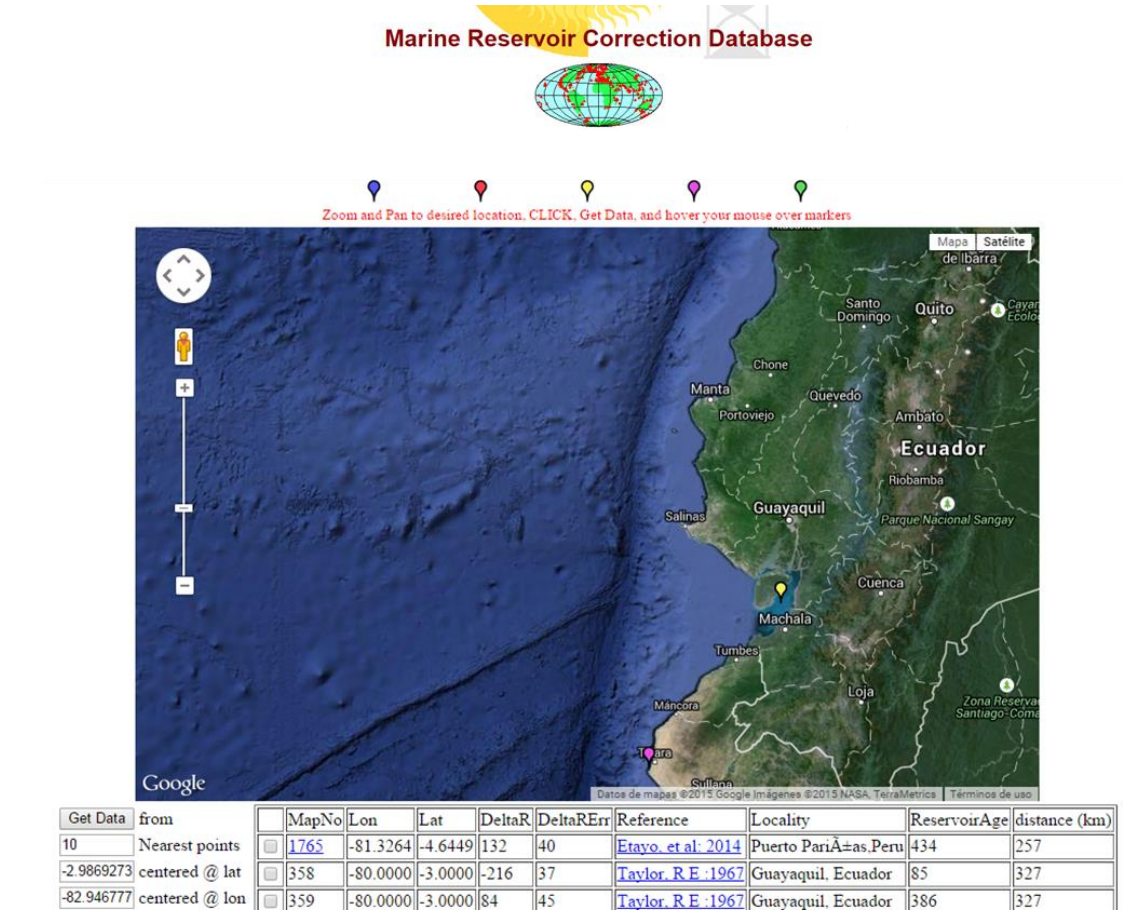

Get Data	from		MapNo	Lon	Lat	DeltaR	DeltaREr	Reference	Locality	ReservoirAge	distance (km)
10	Nearest points		1765	-81.3264	-4.6449	132	40	Etayo, et al: 2014	Puerto PariÃ±as,Peru	434	257
-2.9869273	centered @ lat		358	-80.0000	-3.0000	-216	37	Taylor, R E :1967	Guayaquil, Ecuador	85	327
-82.946777	centered @ lon		359	-80.0000	-3.0000	84	45	Taylor, R E :1967	Guayaquil, Ecuador	386	327

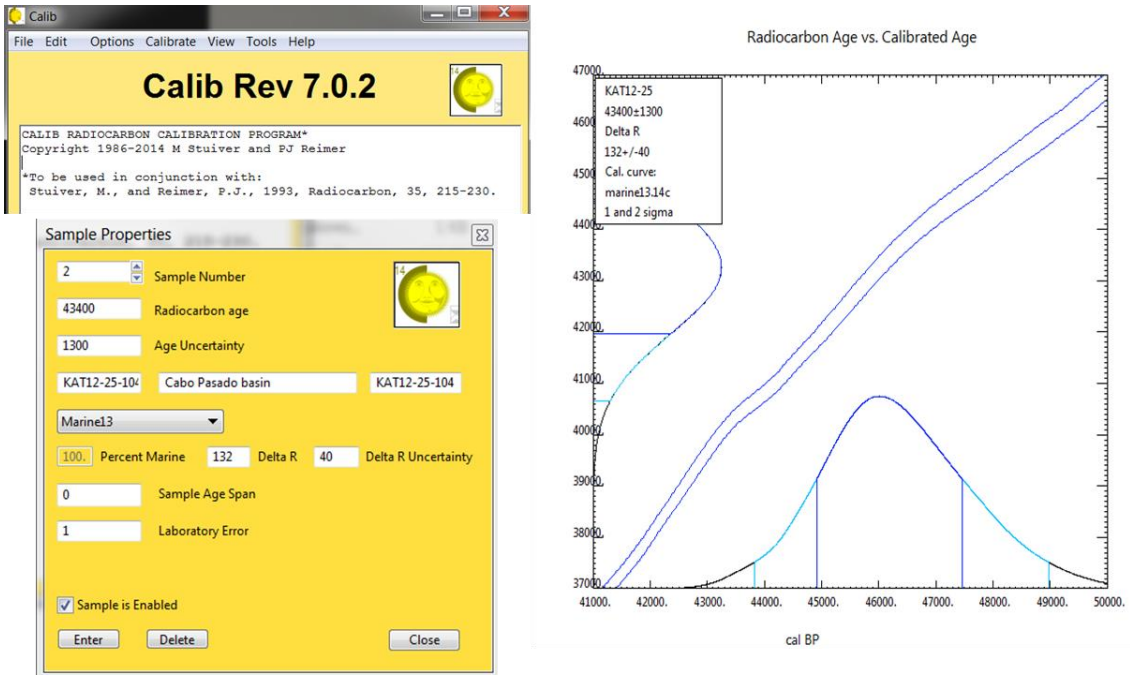

Figure 3.8: Software and marine reservoir database used for calibrating the laboratory-measured ages from the shell. The used correction parameters were taken from the nearest and most recent measurement of marine reservoir age obtained from the Marine13 dataset located near of Talara (Etayo et al. 2014).

4. Age validation

To validate the ages proposed to the sedimentary sequences, we carried out correlation of data in different scales. The location of sedimentary cores, and in some case the internal stratigraphy contacts shown into the cores, were correlated with the boundaries of T-R sequences interpreted in the sub-bottom profiler data. This allowed us: 1) to assure which sequences has been dated, and 2) validate if the obtained age from C14 corresponds well with the transgressive or regressive systems tract interpreted into the sequence. For this validation we did the correlation with the curve of the eustatic-climatic changes.

The sub-bottom profiler data were correlated with the Atacames multichannel seismic data, in some cases also with the SCAN seismic data, for assigning the obtained age to respective sequence.

To check the consistency between the proposed ages to the lower T-R sequences with the eustatic-climatic changes curve, we tried to compare the changes of amplitudes of the shifts of the offlap-break, at zones where the forms of the depositional stacking patterns have been preserved from deformation, with the changes of amplitude of the curve of eustatic variation from Lisiecki and Raymo (2005) (Figure 3.9B).

At the end, to verify the consistency of the ages proposed to the sedimentary sequences interpreted in the seismic data, we correlate the T-R sequences with the onshore Quaternary outcrops. In some case these correlations were possible to do using the ages and the stacking patterns of the sequences shown in the seismic lines with the geometry of the onshore deposits displayed or proposed in the literature. In some other cases this correlation has been realized only by comparison between the seismic T-R sequences with the ages of the coastal outcrops proposed by the scientific publications (Figure 3.9 A).

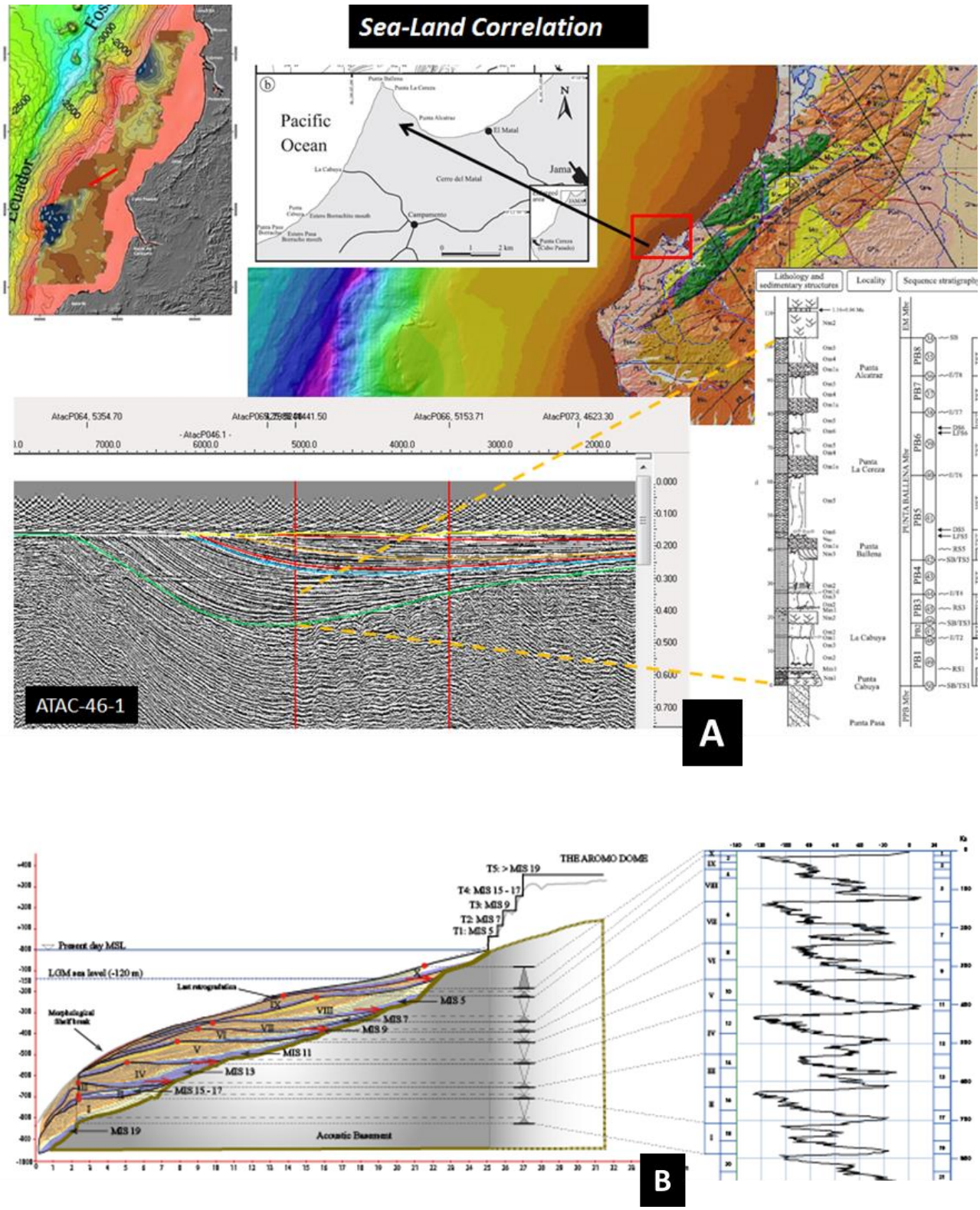

Figure 3.9: Some of the procedures done for the data interpretation validation. A) Seismic data were correlated with the onshore outcrops in some zone of the margin. B) We have tried to link the depositional sequences and climatic change curve.

CHAPTER 4: Detailed stratigraphic analysis of the active margin shelf sediments of Central Ecuador (Article Manta-Plata Zone)

Subduction of seafloor asperities revealed by a detailed stratigraphic analysis of the active margin shelf sediments of Central Ecuador

(Scientific article accepted in Marine Geology on March, 24 2016)

Subduction of seafloor asperities revealed by a detailed stratigraphic analysis of the active margin shelf sediments of Central Ecuador

Jean Noël Proust[1], Carlos Martillo[1, 2,3], François Michaud[2], Jean Yves Collot[2, 4], Olivier Dauteuil[1],

(1) Géosciences Rennes, CNRS, Université de Rennes 1, Campus de Beaulieu, 35042 Rennes cedex, France
(2) Géoazur, Université Pierre et Marie Curie, Université de Nice-Sophia-Antipolis, IRD-CNRS-OCA, 250 avenue Albert Einstein 06560 Valbonne/Sophia Antipolis, France
(3) Escuela Politécnica del Litoral, Grupo de Investigación de Geociencias Marinas y Costeras, FICT -, km 30.5 Vía PerimetralCampus "Gustavo Galindo", Guayaquil, Ecuador.
(4) Investigador Prometeo, Instituto Geofísico, Escuela Politécnica Nacional, Ladrón de Guevara E11-253, Ap. 2759, Quito, Ecuador.

Corresponding author: Jean Noel Proust, email address jean-noel.proust@univ-rennes1.fr

ABSTRACT

The uplift of the coastal cordillera of central Ecuador is likely consequence of the subduction of the Carnegie Ridge, a 400km-long and 2km-high topographic asperity. This study aims at analysing the impact of the subduction of the Carnegie Ridge on the continental shelf sedimentation during the Quaternary. We interpret high-resolution (50- 450Hz frequency) multi-channel (72 channels) and single channel (Sparker) seismic data, piston cores, sediment profiles (3.5khz) and high-resolution multibeam bathymetry acquired during the ATACAMES cruise with the RV L'Atalante in 2012. In the La Plata Island – Cabo San Lorenzo Peninsula region, the results show a full and detailed record of the last ten Quaternary sedimentary sequences deposited in intra-shelf basins, at and -just seaward of the shelf break. These 100ka-scale sequences are tied to piston core data,to well-dated Quaternary onshore exposures and to a flight of coastal marine terraces on Cabo San Lorenzo Peninsula and La Plata Island. These sequences correlate with the global ice volume and deep marine temperature changes (d18O) for the last 0,7Ma, which points to a strict climatic control on depositional sequence development and preservation. However, the subsidence of the continental shelf acoustic basement, estimated by the stepwise backstripping of the sedimentary record, exhibits a complex deformation pattern with uplifting and subsiding regions. Deep marine seismic data, currently under processing, show evidences for a subducted seamount beneath La Plata Island and GPS data indicate an important interplate coupling in the same area with the potential to generate an Mw 7-7.5 earthquake. The pattern of the continental shelf deformation is consistent with the shape of this seamount. We tested the hypothesis of a link between the deformation and the subduction of the seamount, by comparing a stepwise subduction of the seamount to the palinspastic restoration of the deformation of the continental shelf for the last 1Ma. This comparison shows that the collision probably started c.500ka ago, together with the syntectonic sedimentation, and drastically slowed down by c.50ka, with the sealing of most of the deformation on the shelf.

AUTHOR KEYWORDS: Active Margin, Seamount Subduction, Quaternary Stratigraphy, Ecuador, Continental Shelf

1. Introduction

The Earth's surface is shaped by the interaction of tectonics and climate, and is also the result of surface processes (sediment fluxes, *i.e.* erosion and sedimentation). Active changes in topography occur at subduction margins due to both important tectonically induced vertical movements and high climatic variability as for example, during Pleistocene times (Hoffman and Grotzinger, 1993; Willet, 1999; Montgomery et al., 2001; Whipple, 2009; Paquet et al., 2011). The uplifted sediments destabilized during dry glacial periods by local landslides are remobilized and transferred to sedimentary basins during wet interglacials (*e.g*. Paquet et al., 2009, Pouderoux et al., 2012; Marden et al., 2014; Bilderback et al., 2015 and references herein). Sediment unloading by erosion increases basement uplift and relief (e.g. Willet et al., 2006; Proust et al., 2005; Braun et al., 2014), shift in drainage areas (Bonnet, 2009) and local seismicity (Steer et al., 2014). But tectonic forcing is certainly the primary player, as for example the topography of the subducting plate, which influences the location of creeping and locked interplate areas and hazards, such as the occurrence of the infamous megathrust earthquakes (*e.g.* Scholz and Small et al., 1997; Mochizuki et al., 2008; Von Huene, 2008; Duan, 2012; Hicks et al., 2012). The nature and the amplitude of the deformation caused by the subduction of lower plate asperities is a poorly explored area of tectonic forcings in active margins (*e.g.* Dominguez et al., 1998; von Huene et al., 2004; Watts et al., 2010, Von Huene et al., 2012).

Most of the information on tectonic forcing is recorded in sedimentary archives and marine terraces preserved in sedimentary basins adjacent to the orogens. However, the backstripping of subsidence and the reconstruction of the deformation history require to tie confidently the sedimentary record to a well-dated template of climate chronicle, taking into account the influence of eustasy and continental erosion. These ties are usually difficult to obtain and examples are scarce (e.g. Paquet et al., 2009, 2011). In the following, we propose to unravel the tectonic deformation of the continental shelf of the Ecuadorian active margin in relation with the subduction of asperities of the lower plate during Pleistocene times. The study area is located off the coast of the Cabo San Lorenzo Peninsula, where the 2000 m-high Carnegie Ridge generated by the Galapagos hotspot subducts beneath the North Andean sliver for at least several Ma (Collot et al., 2002; Graindorge et al., 2004). Significant vertical movements are well documented along the slope, with subduction erosion and subsidence of the trench inner-wall (e.g. Sosson et al., 1994; Mercier de Lepinay et al., 1997; Collot et al., 2002, 2008, 2009; Clift and Vannuchi, 2004; Sage et al. 2006; Ratzov et al., 2012), and onland, with the continuous uplift of marine terraces over the last 700 ka (e.g. Pedoja et al., 2006a, 2006b). Vertical movements are less documented on the platform itself.

We analyze and interpret the seismic data collected on the platform during the ATACAMES oceanographic campaign (Michaud et al., 2015). We correlate these data to piston core, coastal exposure (Di Celma et al., 2005) and marine terrace data (Pedoja et al., 2006a, 2006b). The aim

is to define the nature of the lithofacies and depositional sequences and finely date sediment deposition. After correction of the eustatic changes and compaction, we reconstitute the history of tectonic deformation of the continental shelf and discuss the link between the subduction of lower plate asperities and the deformation of the Ecuadorian continental shelf.

2. Geologic and tectonic settings

In Ecuador, the Nazca Plate is subducting at a velocity of about 4.7 cm/y with respect to the South American Plate, (Trenkamp et al., 2002, Kendrick et al., 2003) (Figure 4.1). The evolution of the margin is strongly influenced by the subduction of the Carnegie aseismic Ridge, which corresponds to the track on the Nazca plate of the Galapagos Hot Spot (Lonsdale, 1978, 2005; Sallarès and Charvis, 2003). The subduction of the Carnegie Ridge (CR) and the obliquity of the subduction influence the motion toward the North of the North Andean Block (NAB) (Ego et al., 1996; Dumont et al., 2005; Nocquet et al., 2009), the Nazca Plate subducting at only 4.7 cm/y below the NAB.

The subduction of the CR generates an excess of coastal uplift of 0.2-0.3 mm yr^{-1} of the northern part of the Talara Arc - a 1000-km-long stretch of the coast of Ecuador and northern Peru, characterized by subduction with a concave landward plane-view (Pedoja et al., 2006b) and the segmentation of the Ecuadorian margin into three morphological zones, i.e. Northern, Central and Southern segments (Gailler et al., 2007; Collot et al., 2009). The northern segment, north of Punta Galera point, and the southern segment, south of Salinas, are located respectively to the north and south of the CR whereas the central segment, from Punta Galera to Salinas, which includes our study area, faces the top of the CR (Figure 4.1).

Figure 4.1*- Study area map. A- Map view of the main structural elements of the Nazca Plate subduction margin in NW South America (modified from Gutscher et al., 1999). The thick black line with arrows shows the location of the interplate fault between the Nazca Plate and the North Andean block. The continuous black lines show the location of the active spreading centers and the discontinuous lines figure the location of the magnetic anomalies in a schematic way. The black circle indicates the location of the study area in Ecuador (see details in B). B- Detailed map of the Ecuadorian subduction margin. The figure shows the 2000m-high Carnegie Ridge subducting at 56 mm/yr below the North Andean Block, which escapes northward along the Guayaquil-Dolores Megashear. Flights of marine terraces show that the margin is strongly uplifting especially in the study area between Manta peninsula and Puerto Lopez (black square, 0,45mm/year). To the North, the margin experienced megathrust earthquakes (7.7<Mw<8.8) when the central Ecuador recorded less intense earthquake swarms (4.0<Mw<6.2) and slow slip events. Dashed white lines show the major tectonic features i.e. the interplate fault and the Guayaquil Dolores megashear; White arrows indicate the uplift rates as gathered from the marine terrace record in Salinas, Manta Peninsula and Punta Galera. White stars show the location of the epicenter of the three largest earthquakes that occurred during the last century. Bathymetry is from Michaud et al. (2006). C- Simplified cross-section through the margin showing the main structural elements and their present day deformation.*

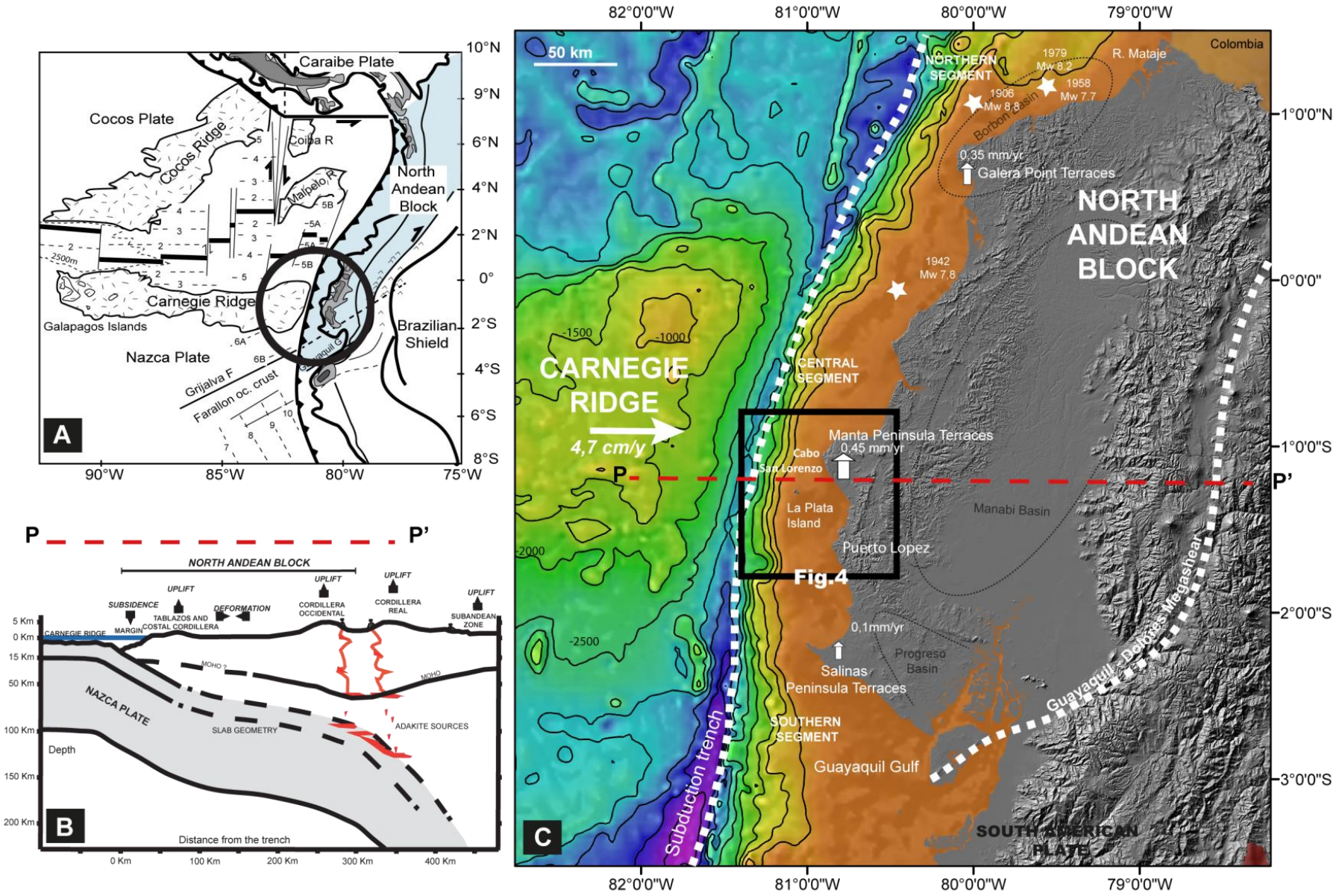

Figure 4.1: Location map of the study area.

The oceanic Nazca plate in front of our study area, shows a wrinkled morphology with blade reliefs (5000m large and 400m high) (Figure 4.2A), scarps of NS-oriented normal faults and seamounts (Figure 2), (Collot et al., 2009). This roughness participates in the destabilization of the slope of the continental margin (Sage et al., 2006) which is characterized by a poorly developed accretionary prism, e.g. presence of 5km-large fans of recent sediments, landslides, scarps and rubbles, gullies, promontories and a canyon (Figure 4.2) with consequences on the seismicity in this zone (Bethoux et al., 2011; Font et al., 2013; Vallée et al., 2013a). Offshore La Plata Island, between 1°25'S and 1°05'S, the bathymetric curves of the lower slope are concave toward the trench (Figure 4.3A); this connfiguration was interpreted by Sanclemente (2014) as the trace of a subducting seamount. The platform is relatively flat and narrow, 40-50 km wide, offshore La Plata Island and 5 km wide, west of Manta area, forming a landward curved re-entrance (Figure 4.3A), (Michaud et al., 2015). It generally bathes in less than 140m of water but the shelf break is at 140m in water depth, offshore La Plata Island, and at 500m in water depth, west of Manta Peninsula.

Little is known of the geology of the continental shelf. Onshore, the coast shows Cretaceous age basalts (Piñon Formation) overlapped by marine volcaniclastics (Cayo Formation) and Mio-Pleistocene sediments filling the Borbón, Manabí and Progreso forearc basins (Benitez, 1995; Jaillard et al., 1996; Deniaud et al., 1999), (Figure 4.1). Some large NE-SW and EW regional faults can be observed on land but only a few of them show a well-established offshore extension (e.g. Jama fault, Montecristi fault). The Pleistocene marine deposits of the Canoa and Tablazos formations, which drape most of the shelf, are well exposed along extensive cliff exposures at the coast (Di Celma et al., 2005; Reyes, 2013). The marine terraces of the Tablazos formation crop out along the Talara Arc and record the vertical ground motion superimposed on Quaternary global sea level oscillations (Pedoja et al., 2006b, 2014). The highest marine terraces are located in Manta Peninsula and La Plata Island study areas (Cantalamessa and Di Celma, 2004; Pedoja et al., 2006a). The main part of the Manta peninsula is covered by eight, flat and gently dipping marine terraces at elevations of 25–360 m (Cantalamessa and Di Celma, 2004; Pedoja et al. 2006a). Each successively younger terrace dips to the SSW at a shallower angle, from 5° for the oldest to 1° for the youngest, pointing to synsedimentary tilting (Di Celma et al., 2005). Four marine terraces at elevations ranging from 47 to 160 m are observed on Plata Island where they are cut in the basalts and dolerites of the Pinon Formation (Cantalamessa and Di Celma, 2004; Pedoja et al. 2006a).

_____

***Figure 4.2**- Geomorphology of the slope of the continental shelf in Manta Plata area. The shelf edge shows a wrinkled morphology with a shelf break bathed in 120 to 500m in water depth. See the numerous features on the slope (scarps, landslides, gullies, accretionary prism and promontories) and on the Carnegie Ridge in the trench (seamounts, blade asperities and fault scarps). The land is figured in green color when the shelf, slope and trench are in grey shaded relief. Numbers (1) and (2) indicate the location of two 3D detailed and shaded views of the continental slope presented on figure 3C. All bathymetry data were homogenized to 30m-resolution grid, and integrated using the Global Mapper G.I.S. application (Martillo et al., 2011). The multibeam bathymetry grid includes CNRS-IRD (ATACAMES and previous campaigns) and INOCAR data.*

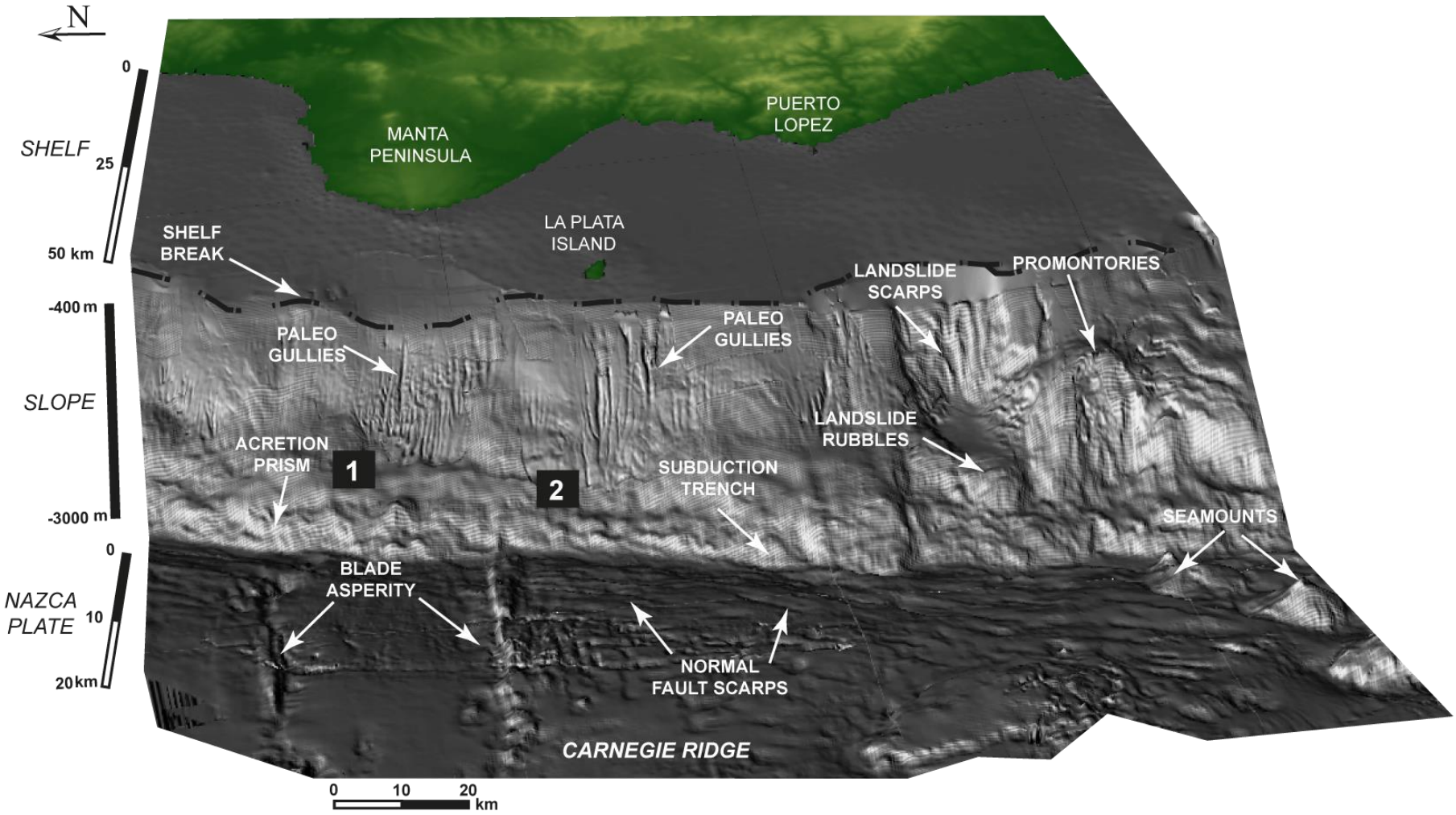

Figure 4.2: Geomorphology of the slope of the continental shelf in Manta Plata area

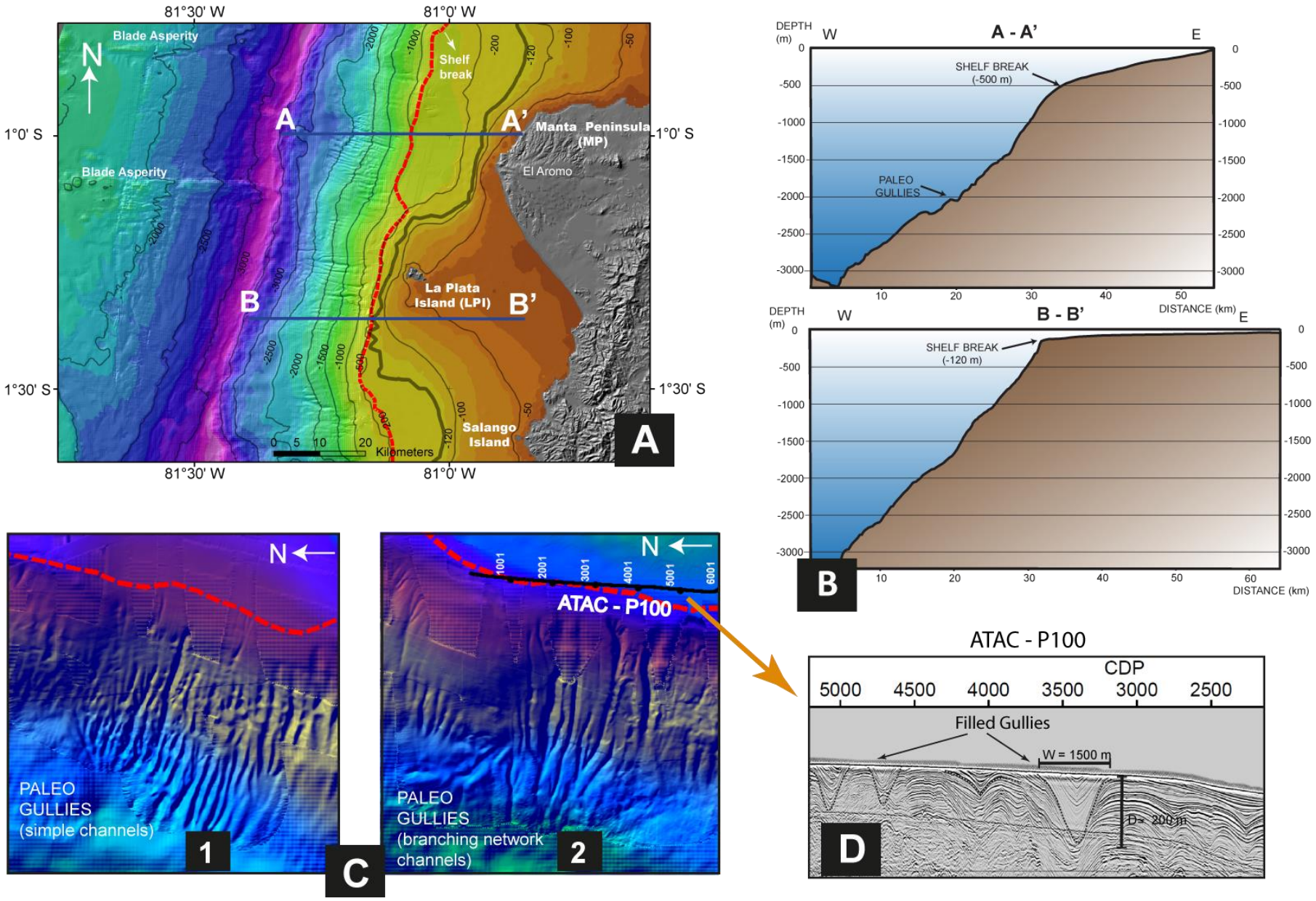

Figure 4.3: Map of Manta Peninsula-Plata area shows the bathymetry of the shelf, the slope, the trench and the eastern flank of the Carnegie Ridge.

Figure 3- *Map of Manta Peninsula-Plata area shows the bathymetry of the shelf, the slope, the trench and the eastern flank of the Carnegie Ridge (A). The red line indicates the location of the shelf break, whereas the grey line shows the location of the 120m isobath. Lines AA' and BB' show the location of the two bathymetric profiles presented in (B). The emerged land is in grey shaded relief when the submarine shelf and slope are figured in colors graded from brown to pink. (B) Bathymetric profiles transverse to the shelf and the slope. Note that the shelf break is bathed at very different water depths: 500 m on AA' and 120m on BB'. See location of profiles AA' and BB' in (A). (C) These two blowouts (1) and (2) show the shape and distribution of the gullies (see location on figure 2) and the location of the shelf break (red line). The thin black line with CDP white numbers in blowout 2 shows the location of the seismic line ATAC P100. (D) See gullies filled by sediment just beyond the shelf edge on seismic line ATAC_P100.*

_____

3. Data and methods

This work is based on data collected by the ATACAMES Expedition in the L'Atalante research vessel (Michaud et al, 2015) (Figure 4.4). The data are comprised of c.700 km of high resolution multi-channel seismic data (72 channels; 50-450 Hz) acquired with a 450 m-long streamer of 72 active sections, 6.25 m-long each; c.110 km of very high resolution single channel sparker seismic data (100 to 1500 Hz) with 5 m streamer with 8 hydrophones; c. 900 km of sub-bottom profiler (1.8 kHz to 5.3 kHz); high resolution bathymetry type Kongsberg-Simrad EM710D and EM122 along all seismic lines and two piston cores collected in 150-160m of water depth (KAT12-36; 1,06 m-long and KAT12-37; 2,07 m-long). We obtain a bathymetric grid with a 25 m large cell-grid size. This grid was completed by older multibeam of 50 m resolution (Michaud et al., 2009).

We use Caraibes (©Ifremer), ArcGis (®ESRI), Seismic Unix (©Colorado School of Mines) software to process respectively the bathymetric, the D-GPS and the seismic data and Kingdom Suite (©IHS) and Petrel (©Schlumberger) to interpret the seismic data. The depth conversion of the seismic data recorded in time was run by using a velocity of 1600 to 1900 $m.s^{-1}$ of sound in the sediment (*i.e*., a velocity range used for seismic data processing) depending on the depth in the sedimentary record.

The seismic profiles were interpreted applying the criteria of seismic stratigraphy as originally defined by Mitchum et al. (1977) *i.e*. configuration, amplitude, continuity and frequency to identify seismic facies and the stratal termination patterns *i.e.* onlap, toplap, downlap, truncation and offlap, to discriminate the main surfaces bounding genetically related packages of seismic facies called systems tracts (Vail et al., 1977), which register the changes in shoreline trajectories (transgression, T; normal regression, NR; and forced regression, FR).

The surfaces are named after Catuneanu (2006) and Catuneanu et al., (2009) *i.e.* Maximun Regressive Surface (MRS) at the end of the regression, Transgressive Surface (TS) at the start of the transgression, Maximum Flooding Surface (MFS) at the end of the transgression, Basal Surface of Forced Regression (BSFR) at the onset of the forced regression capped by the Subaerial Unconformity (SU) and its Correlative Conformity (CC) at the end of the forced regression. The systems tracts are named accordingly with the Highstand Systems Tract (HST) above the MFS, the Falling Stage System Track (FSST) above the BSFR, the Lowstand Systems

Track (LST) above the SU and CC and the Transgressive Systems Tract (TST) above the TS and MRS (Mahieux et al., 1998; Proust et al., 2001; Braaksma et al., 2006; Catuneanu et al., 2009). Following the T-R sequences proposed by Embry (1993, 1995) we have grouped the set of regressive systems tracts (Highstand, Falling-Stage and Lowstand) in a "Regressive Systems Tract" and the Transgressive Systems tracts in the "Transgressive Systems Tract" locating the limits of T-R sequences on MRS.

The cores were cut in 1m-long sections, then split for visual descriptions, photographed and sampled for ^{14}C age dating. The radiocarbon dates were calibrated to calendar years with a 399 ±30 yr marine reservoir age (Etayo-Cadavid et al, 2013) using CALIB Rev 7.0.2/Marine13 dataset (Stuiver and Reimer, 1993). The calibrated ages were assigned to their respective T-R sequence. Because of the lack of significant erosion between sequences, each T-R sequence is then correlated to the Marine Isotope Stages (MIS) (Waelbroeck et al., 2002; Siddall et al., 2003; Lisiecki and Raymo, 2005) by counting down the section starting from the age dated reference point sampled by coring at the sea floor.

The construction of the subsidence maps was carried out by using the backstripping method Allen and Allen (2013), modified to take into account for aerial deposits and erosion events. We defined 120 virtual wells crossing through the entire set of sequences regularly distributed 4km apart in a 50x50km large area, offshore along the main seismic lines and onland through the exposed marine terraces (Figure 4.5). In each well and at the top of each sequence, we plotted the lithology (mud or sand) used for decompaction law, the depth in meters, the age, and the paleobathymetry or paleoaltitude. The ages were determined by correlation of the transgressive surface at the top of each sequence to the Marine Isotopic Stage (MIS, Lisiecki and Raymo, 2005) tied to several dated points in cores (see below). The precision of the ages and paleobathymetries or paleoaltitudes is estimated at 10kyrs and 10 m, respectively.

_____

***Figure 4.4**- (A) Location map of the bathymetry, 3.5 KHz chirp, sparker and MCS seismic data acquired during the ATACAMES (CNRS-IRD) campaign in 2012 in Manta-Plata area as well as the location of the two piston cores considered in this study (Kat12-036 and KAT12-037). MCS seismic data are noted "ATAC_P". Sparker seismic profiles are noted "ATAC_SP". (B) Location map of the 120 virtual wells used for backstripping and subsidence calculation. Regional contour data are from Michaud et al. (2006).*

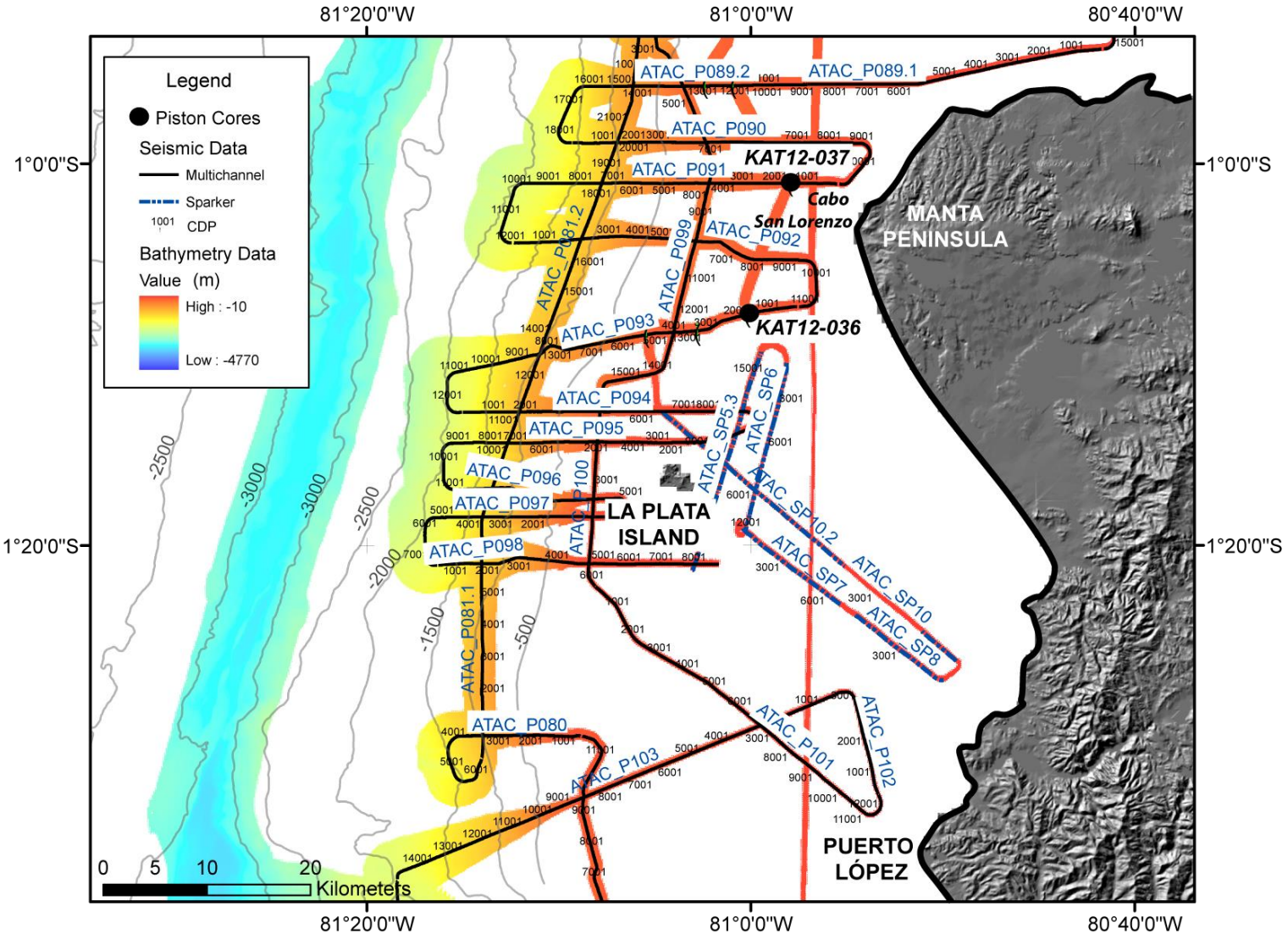

Figure 4.4: Location map of the bathymetry, 3.5 KHz chirp, sparker and MCS seismic data acquired during the ATACAMES (CNRS-IRD) campaign in 2012 in Manta-Plata area as well as the location of the two piston cores considered in this study.

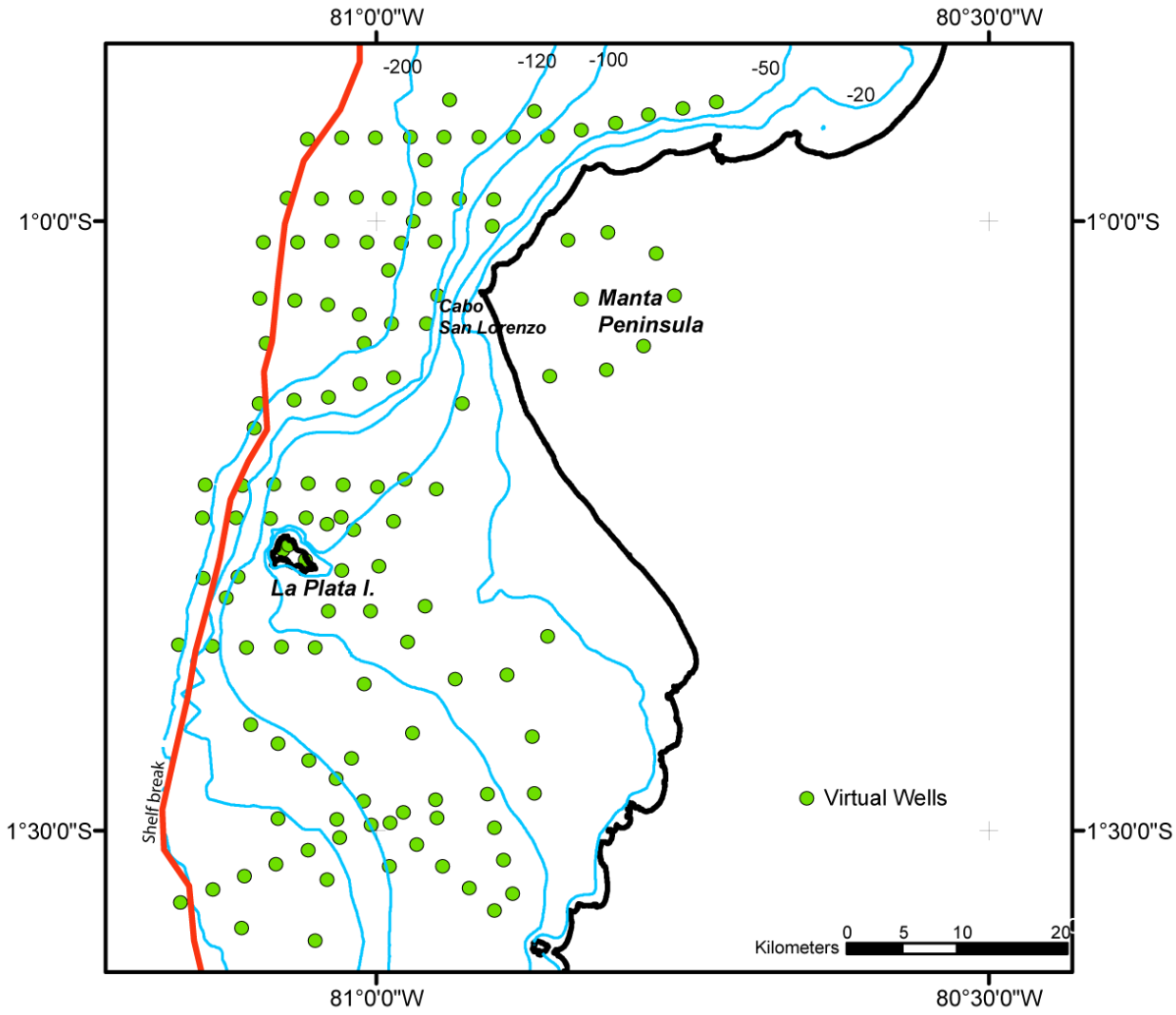

Figure 4.5: Map showing the location of the 120 virtual wells used to build the subsidence maps. The wells are regularly distributed 4km apart in a 50kmx50 km large area along the mains seismic lines.

4. Results

This section shows the results obtained from the analysis of bathymetry, seismic and core data collected during the ATACAMES campaign in 2012 (Michaud et al., 2015) between Manta Peninsula and Puerto Lopez (Figure 1).

4.1. Bathymetry data

The bathymetry of the upper slope and on the shelf between Manta Peninsula (MP) and La Plata Island (LPI) shows a rather complex morphological pattern (Figure 4.2 and 4.3). The shelf break is oriented in a NS direction, subparallel to the trench orientation. The shelf break varies in water depth between 500m in the North (A-A' bathymetry profile Figure 4.3B), in front of MP, to 200m in the South, with local rises at 120 m in front of LPI (B-B' bathymetry profile Figure 3B). The orientation of the shelf break differs drastically from the sinuous shape of the last glacial maximum (LGM) 120m-lowstand shoreline (Siddall et al., 2003), which in turn, is out of phase with the present day 0m-shoreline (Figure 4.2). The 120m isobath underlines a submarine rise bathed at 20km to the SW of the Manta Peninsula promontory in LPI area (Figure 4.3A).

The multibeam data acquired on the upper slope show three zones of gullies facing the three main regional promontories *i.e.* offshore MP, LPI and Salango Island (SI) respectively (Figure 4.2 and 4.3C). The heads of the gullies are located beyond the shelf break at water depths that vary from 800m in the North, in front of MP, to 500 m in front of LPI and SI (A-A' and B-B', Figure 4.3C). The gullies exhibit different shapes from straight (MP), to branched (LPI) and sinuous with slope failures (SI) (Figure 4.3C). The straight gullies in front of MP and SI are 5,000-8,000 m in length, 500-700 m in width, and 20-100 m in depth. The branching gullies in front of LPI are 5,000-10,000 m in length, 500-1,000 m in width, and 60-140 m in depth. A few hundred meters below the shelf break, the bathymetry data show open gullies that, on seismic section, appear filled by sediment (Figure 4.3D). The disconnection of the gullies from the shelf break indicates a recent uplift of the shelf break in areas facing the main promontories (MP, LPI, SI). Gullies with sealed heads suggest that the active sediment transfer from the shelf to the slope through the gullies stopped recently (Izumi, 2004; Gales et al., 2013), but is not active now (Peñafiel, 2012).

4.2. Seismic Data

4.2.1. Seismic Facies

This section describes the seismic facies and provides an interpretation for their main characteristics in term of lithologies and depositional environments according to principles outlined in Mitchum et al. (1977) and Sangree and Widmier (1977). We identified nine seismic facies end members in the ATACAMES seismic sections (Table 4.1).

Facies of the Regressive Systems Tract

Fluvial meandering sands and flood plain clays - Seismic Facies 1 (Sf1) displays an average continuity, average to high amplitude, average frequency, and hummocky configuration with low angle small-scale parallel oblique progradational reflections. The high amplitude of the seismic facies suggests sharp changes in impedance character, which might correspond to the interbedding of high velocity coarse-grained sediment and low velocity clayey sediments. The low continuity and the hummocky character of the reflection suggest localized deposition of coarse sediment in channel forming sediment bodies. The channel forms are filled by low angle progradational reflection patterns, which might correspond to lateral accretion bedding as observed in meandering river channel deposits wandering in a fine-grained flood plain.

Wave influenced delta front sands and coastal plain - shoreface seismic facies 2 (Sf2) appears in the upper part of large wedge-shaped sets of progradational reflectors with offlap and toplap terminations. This facies shows a low to average amplitude, low continuity and frequency, with divergent and progradational configuration. The low amplitude, continuity and frequency of the facies suggest a poorly bedded, homogeneous lithology that can be either sands, silts or clays but more likely sand in an overall progradational geometry. The divergent progradational pattern of homogeneous sediment is commonly observed in rapidly prograding delta lobe with high sediment supply at, or just beyond, the rollover of steep and active clinoform fronts. The depositional environment is interpreted as the seaward edge of the delta plain in the transition zone with the marine environment where shoreline sands accumulate in wave-dominated barrier islands and aeolian dunes (Boggs, 2010).

Mouth bar sands and subtidal channels pebbly sands- Seismic Facies 3 (Sf3) develops in the upper part of the large wedge-shaped sets, along the clinoform fronts, a few meters downslope of the seismic facies 2. Sf3 shows an average to high amplitude, an average to low continuity, a low frequency and a hummocky configuration. The relatively high amplitude of the reflections points to high impedance and to high lithological contrasts between discontinuous and thick beds as shown by the low continuity and low frequency of the reflectors. Because of the lack of carbonate sediment on the margin, these beds are probably coarse or pebbly sand beds lying on homogeneous mixture of sandy silts or silty clays. The hummocky configuration of coarse sand beds might correspond to discontinuous channel and bar sediment bodies encased in silts or clayey silts. These sediment bodies

seated in the upper segment of clinoforms might correspond to stacks of mouth bars and subtidal channels settled in the upper delta front.

Wave-influenced, clinoform delta lobe sands and silts - Seismic Facies 4 (Sf4) is located in the lower section of wedge-shaped sets of progradational reflectors a few meters below of Sf3 in a downslope direction. Sf4 displays an average to high continuity and frequency, low amplitude reflector packages bounded by high amplitude single reflectors and a subparallel to divergent configuration. The relatively high continuity and frequency points to thin- and well-bedded series deposited in a quiet depositional environment. The low amplitude of the reflectors indicates that the contrasts of impedance, *i.e.* the contrasts between adjacent lithologies, are quite poor. This sediment probably corresponds to well-bedded sand (or sandy silts) and silts (or clayey silts) deposited in a lower shoreface or shoreface transition setting. The occurrence of high amplitude reflections separating packages of lower amplitude reflectors is indicative of the deposition of coarser-grained lithologies during periods of reactivation of the progradational slope very similar to what may happen with delta lobe switching before avulsion.

Offshore marine, prodelta silts - Seismic Facies 5 (Sf5) occurs at the base of the wedge-shaped set, at the foot of the clinoforms, a few meters downslope of Sf4. The reflections display an average to high continuity, average amplitude and average to high frequency. The configuration of the reflectors shows tangential downlap geometries in their lower part, on the lower bounding surface, and a sub-parallel to divergent configuration in the upper part, in a landward direction. The high continuity, high frequency and average amplitude of the reflections can be interpreted as the seismic signature of thin-, well bedded fine-grained sediment deposited in a stable environment. The location at the toeset of a large prograding set of clinoforms seems characteristic of distal, deep marine, silty clays in an offshore prodeltaic setting.

Toe of slope debrites and mass flows - Seismic Facies 6 (Sf6) appears at the seaward edge and the toe of the progradational wedge, downslope of facies Sf5. Sf6 displays low continuity and low frequency reflectors that can be either of low amplitude or transparent or of high amplitude. The reflections display low angle to parallel, mound shape and chaotic configurations locally erosional on the lower bounding surface of the progradational wedge. The lithologies are probably a mix of (fine-grained?) homogeneous sediment, as shown by the transparent reflections, with intervening lenses of coarse-grained deposits as illustrated by the high amplitude reflectors. The deposition at the toe of the progradational wedge in discontinuous, mound shaped and chaotic configuration, points to the massive deposition of debrites or mass flow in a deep marine setting, at the foot of a depositional slope swept by along slope currents.

Facies of the Transgressive Systems Tract

Offshore marine silts and clays with debrites - Seismic Facies 7 (Sf7) drapes the slope of the clinoform progradational wedge. It is characterized by high continuity, average to high amplitude and average frequency reflections. The reflectors show a subparallel configuration with onlap terminations against the clinoform slope. The sediments correspond to thick- and well-bedded deposits of contrasting lithologies like coarse sands and silty clays. The subparallel configuration of the wedge, which drapes the clinoform slope, is similar to the "healing-phase" deposits, which accumulate during marine transgression (Catuneanu, 2006). These deposits might correspond to the deposition of offshore marine silt and clay that drape the slope during quiet times interbedded with coarse material ripped by the wave action of the transgressive sea on the platform.

Transgressive lag coarse bioclastic sands - Seismic Facies 8 (Sf8) covers the platform at the top of the progradational wedge and passes gradually to Sf7 in a seaward direction. Sf8 displays high continuity, high to average amplitude, and low to average frequency. The configuration of the reflections is divergent in a landward direction and convergent in a seaward direction where they downlap at low angle on the top of the progradational wedge. The high amplitude, high continuity and low frequency of the reflectors is interpreted as well- and thick-bedded, very coarse-grained sediment interbedded with fine grained deposits. The location of the facies on the platform, at the top of the progradational wedge, is indicative of shallow marine conditions. In such a setting, the coarse sediment may easily be remobilized and progressively sorted by storm and fair-weather wave ravinement during marine transgression. The balance between the rates of coastal aggradation and the rates of wave-ravinement erosion forms the transgressive lag deposits (Catuneanu, 2006).

Facies of the acoustic basement

Seismic Facies 9 (Sf9) lies below the entire well-stratified facies described above. Its lower part is masked by sea floor multiples. A high amplitude reflector underlines its top. Reflections show very low continuities, very high amplitudes and average frequencies in chaotic to transparent configurations with high angle diffractions. The chaotic configuration with highly inclined, disrupted reflections is indicative of thinly layered but deformed and dissected rock elements. The underlying transparent facies might be interpreted as massive rock bodies. This unit constitutes the acoustic basement and is attributed to the Tertiary sediments, underlain by Cretaceous volcanics.

Table 4.1- *Views of the main seismic facies observed on the MCS seismic profiles of the ATACAMES campaign with inferred lithologies and depositional environments.*

REGRESSIVE SYSTEMS TRACT

Fluvial meandering sands and flood plain clays

Sf1

Average continuity, average to high amplitude, average frequency and hummocky configuration with low angle small-scale parallel oblique progradational reflections

Delta front, wave-influenced shoreface sands

Sf2

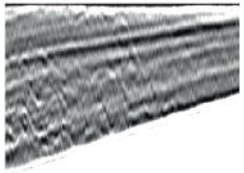

Low to average amplitude, low continuity and frequency, with divergent and progradational configuration

Mouth bar sands and subtidal channels pebbly sands

Sf3

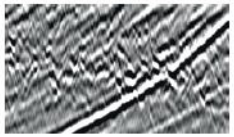

Average to high amplitude, average to low continuity and low frequency with hummocky configuration

Shoreface transition sands and silts

Sf4

Average to high continuity and frequency, low amplitude reflector packages bounded by high amplitude single reflectors and a subparallel to divergent configuration

Offshore marine, prodelta silts

Sf5

Averavge to high continuity, low amplitude and average to high frequency. The configuration shows tangential downlap geometries in their lower part and a sub-parallel to divergent configuration in the upper part

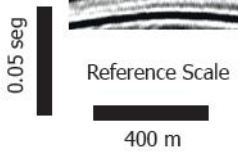

TRANSGRESSIVE SYSTEMS TRACT

Table 1

Toe of slope, debrites and mass flows

Sf6

Low continuity and low frequency reflectors that can be either of low amplitude to transparent or of high amplitude. The reflections display low angle to parallel, mound shape and chaotic configurations

Offshore marine silts and clays with debrites

Sf7

High continuity, average to high amplitude and average frequency reflections. The reflectors show a subparallel configuration with onlap terminations against the clinoform slope

Transgressive lag coarse sands

Sf8

High continuity, high to average amplitude, and low to average frequency. The configuration of the reflections is divergent in a landward direction and convergent in a seaward direction.

ACOUSTIC BASEMENT

Cretaceous volcanics and tertiary sediments

Sf9

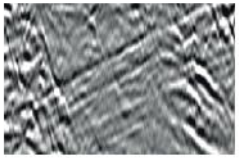

Reflections show very low continuities, very high amplitudes and average frequencies in chaotic to transparent configurations with high angle diffractions.

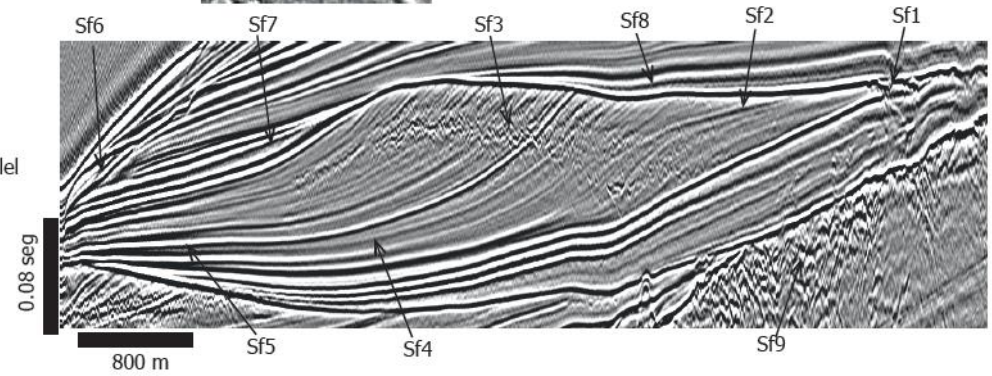

Table 4.1: Seismic Facies from Regressive and Transgressive Systems Tract

4.2.2. Architecture of the T-R sequences

The facies are arranged in T-R sequences, which are comprised of four systems tracts *i.e.* from base to top: the TST, the HST, the FSST and the LST. The Maximum Regressive Surface (MRS) was taken as the boundary of the T-R sequences.

The sequences are described below from the example of the AtacP092 reference profile located at the shelf edge, which shows the most complete record of the T-R sequences in the study area (Figure 6). Each sequence exhibits the superposition of a RST up to 100m-thick (120ms TWTT@1700m/s) overlain by a TST up to 30-40m-thick (40ms TWTT@1700m/s) (Figures 6 and 7). The RST shows a well-developed wedge shape while the TST exhibits two draping lenses on the landward and seaward sides of the RST rollover. We recognize ten seismic sequences above the acoustic basement in the ATACAMES seismic lines (Figure 4.6). They are named I to X from the oldest to the youngest.

The TST sits at the base of the T-R sequences (Figures 4.6 and 4.7). It is c.30-40m-thick and made up of a two-part body: one draping the toe and the base of slope of the regressive progradational wedge, the other covering its top (Figure 4). In places, these two sediment packages pass gradually to each other. They may also directly overlay the acoustic basement around basement highs and in a landward direction. The reflectors of the TST are generally sub parallels with a gentle onlap termination on the sharp erosion surface at the top of the underlying progradational wedge (MRS) or the acoustic basement. The top of the TST is a conformable surface (MFS) at the base of the next progradational wedge (Figure 4.6 and 4.7). These two surfaces are interpreted respectively as the MRS, and the MFS according to Catuneanu (2006)'s definitions. The TST is comprised of seismic facies Sf8 of the shelf and Sf7 on the slope that, locally, interfinger with Sf6 at the toe of slope. Seismic facies Sf8, Sf7 and Sf6 correspond respectively to wave ravinement deposits on the shelf, offshore mud interbedded with gravity flow and turbidites on the slope, and debrites and mass flows at the toe of the slope. Mass flows, debrites and turbidites are interpreted as reworked material of the underlying progradational wedge when the shoreline and the wave base migrate quickly in a landward direction during marine transgression. The seismic wedge draping the base of the slope closely resembles the healing-phase deposits formed by resedimentation of material eroded from the shelf seafloor and retreating shoreface (Posamentier and Allen, 1993). The healing-phase deposits are well developed on ramp margins with narrow shelves, which present a limited capacity to trap large quantities of terrigeneous sediments, such as the Southern California Shelf (Sommerfield et al., 2009).

The HST is c.50m-thick (Figures 4.6 and 4.7). It forms acute angle wedges of seismic reflector lying at low angle on the underlying TST. The internal reflectors are low-angle, progradational, sub-parallels to parallels. The reflectors show toplap terminations along the BSFR and the TS, and downlap terminations on the MFS, according to Catuneanu (2006)'s definitions. From the top to the base of the progradational clinoforms, the bulk of the HST is comprised of a suite of seismic facies including fluvial (Sf1), coastal plain to barrier island (Sf2), channel and mouth bars (Sf3) and shoreface deposits (Sf4). The toe of the wedge bathes into a thin Sf5, which is

interpreted as offshore marine silt and clay. The HST shows a suite of facies that can be interpreted as a prograding delta system with delta plain mudflats and meandering channels (Sf1), delta front sands with subtidal channels, mouth bars and shoreface sediments (Sf2, Sf3, Sf4) and prodelta mud (FS5).

The FSST is the thickest of the systems tracts with a maximum thickness of c.85m (Figures 6 and 7). It shows well-defined wedges with high angle progradational reflection patterns contrasting with the lower angle reflections of the underlying HST. The top boundary of the FSST is characterized by toplap to offlap terminations and erosional truncation. The lower boundary shows downlapping reflections with tangential terminations. The lower boundary is interpreted as a BSFR and the upper boundary as either a CC when overlain by a LST, or a MRS when the LST is absent. Along slope, from the top to the base of the clinoforms in the progradational wedge, the seismic data show a succession of facies similar to the HST (Sf1 to Sf5) interpreted as deltaic deposits. This set is complemented in the FSST by facies Sf6 located at the toe of the clinoforms. This facies corresponds to the deposition of mounded debrites and mass flow deposits reworked from the platform and upper depositional slope during the downward shift of the wave base due to the forced sea-level drop.

The LST sediments are scarcely preserved (Figures 4.6 and 4.7). They are recognized in sequences V and VIII where they form thin wedges of c.15m of sediment, which drape the slope and the rollover of the underlying FSST. The internal reflections are subparallel to slightly divergent, and show an overall progradational-aggradational pattern. The upper boundary is an offlap surface and locally a toplap. The lower boundary is characterized by downlap with very low angle tangential terminations. The upper and lower surfaces are interpreted as a MRS and a CC, respectively. In a downslope direction, along the clinoforms, the bulk of the LST seismic facies are comprised of the suite Sf1, Sf3, Sf4, which correspond to the lateral change from fluvial to stacks of subtidal channels and mouth bars, and delta front shoreface sands. In sequence V, the toe of the LST sediments is underlined by the seismic facies Sf6 that corresponds to small fans of debrites and mass flow deposits. The strong fluvial character of these deposits, the presence of debris flow at the toe of the progradational body and the lack of coastal plain and shoreline deposits show a strong continental signature and an efficient migration of the deltaic body to the shelf edge.

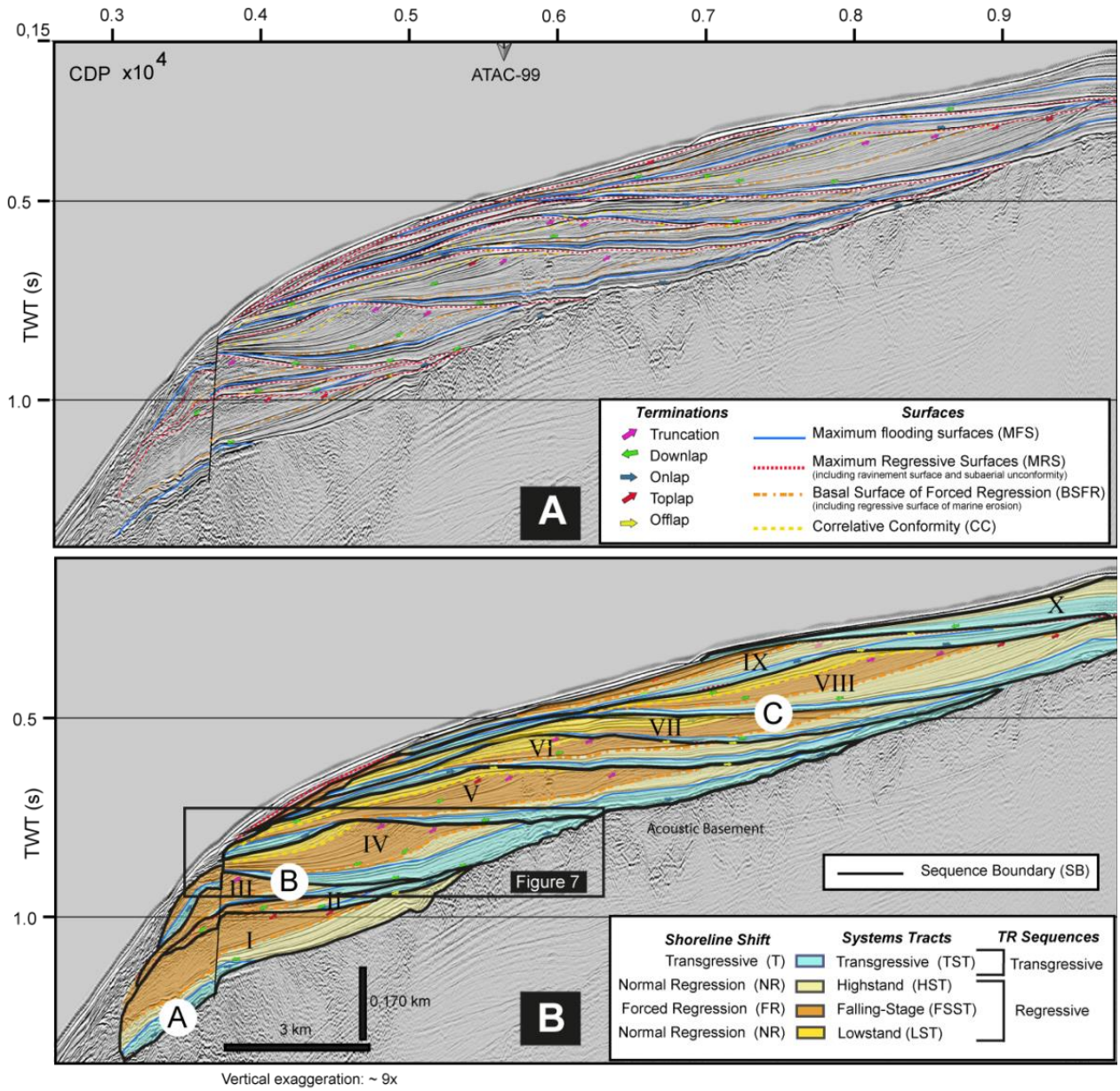

Figure 4.6: Seismic profile ATAC_P092 (see location map on figure 4) showing the seismic reflector terminations with interpreted surfaces (A), systems tracts, depositional sequences and regional unconformities labeled A,B, and C (B).

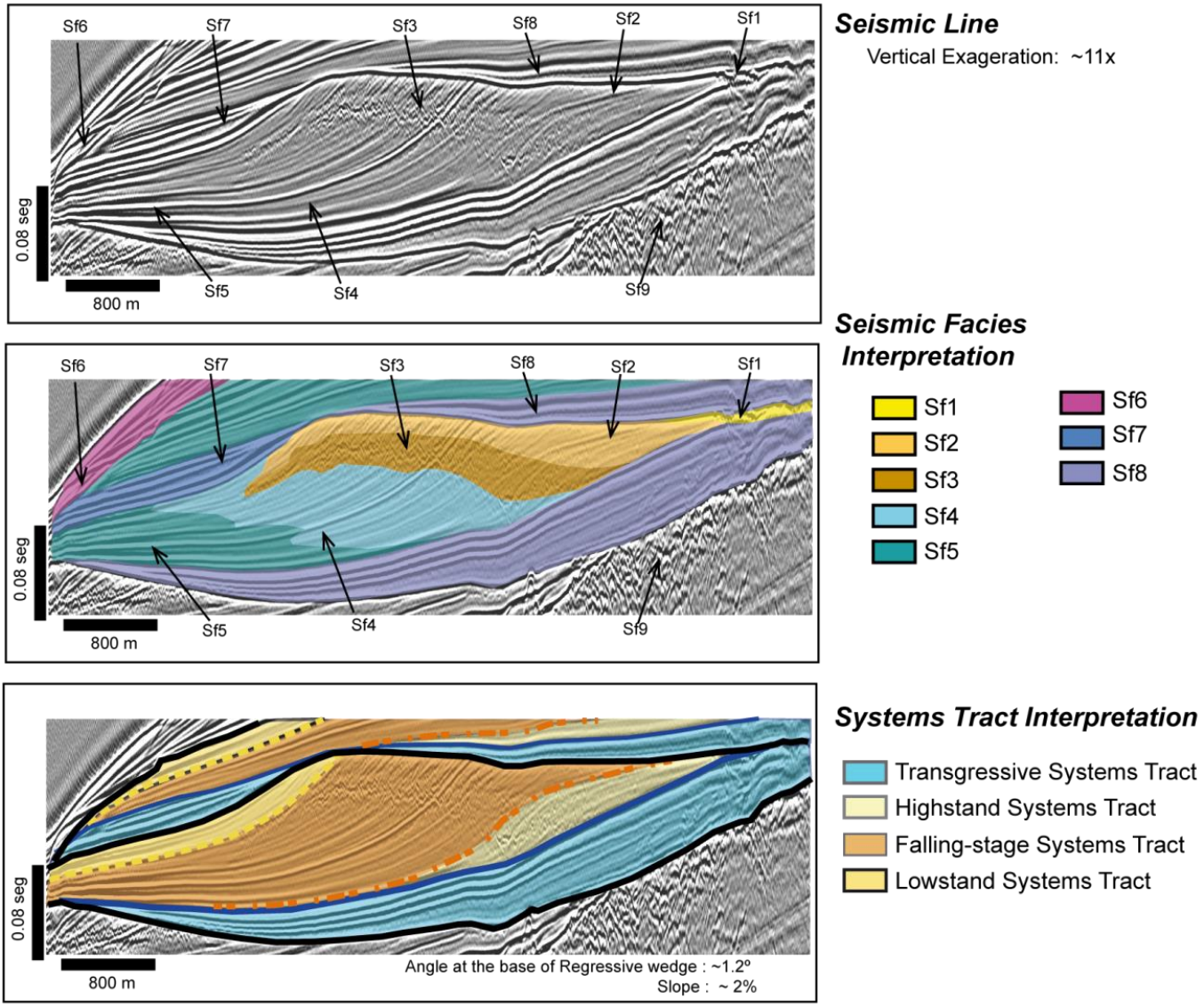

Figure 4.7: Detailed view of the facies and systems tract interpretations from the example of sequence IV (C). See location of sequence IV on figure 4.6.

4.2.3. T-R sequence stacking pattern and lateral and vertical variations

The 10 T-R sequences have been imaged and mapped throughout the Manta-Plata area. The stack of 10 T-R sequences is organized in three major packages (stacks 1, 2, 3) bounded by angular unconformities A, B and C of regional extend (Figure 4.6 and 4.8).

Stack 1 is comprised of T-R sequences I, II and III. It is c.265m-thick, widely distributed along the rim of the margin. It lies between 850 and 750 m-water depth, 200m below the present day shelf break (Figure 4.6), and also in the intra-shelf basins (Figure 4.8). At the shelf margin (Figure 6), three T-R sequences are vertically stacked with either no significant change in the lateral position of the clinoform rollover through time or a slight seaward stepping of the individual units. In the intra shelf basin of La Plata area, the three T-R sequences, imaged on a low-resolution industry seismic line, form the upper part of a large progradational set of reflectors. This progradational wedge downlaps on surface A and is sharply truncated by an erosion surface locally angular (surface B, Figures 4.6 and 4.8)

Stack 2 is comprised of T-R sequences IV to VII. It is c.360m-thick, widely distributed at the rim of the margin, between 750 and 420 m-water depth (Figure 4.6), and on the shelf (Figure 4.8). Stack 2 T-R sequences lie unconformably on stack 1 units and the acoustic basement, strongly stepping in a landward direction at a pace of 3 to 5 km/sequence. At the shelf edge (Figure 4.6), the T-R sequences are roughly thinning upward with a well-preserved LST in sequence V only. On the shelf (Figure 4.8), the T-R sequences of stack 2 T-R sequences are gently folded with a slight divergent character due to sedimentation during the growth of basement tectonic structures of the uplifting LPI and MP areas.

Stack 3 is comprised of T-R sequences VIII to X. It is c.250m-thick, widely distributed from the shelf edge, between 450 and 120 m-water depth (Figure 4.6), to the inner shelf (Figure 8). Stack 3 units unconformably overlie stack 2 units (surface C, Figure 4.6) and also the acoustic basement in a landward direction. At the shelf edge (Figure 6), the T-R sequences are strongly progradational, thinning upward with well-preserved LST in the thickest sequence VIII. Sequences VIII and IX step landward overlain by sequence X, drastically stepping seaward. Sequence X is comprised of a TST and a thin HST with no discernable FSST nor LST deposits. On the shelf (Figure 4.8), the T-R sequences of stack 3 are slightly folded at the very base, due to the continuous growth of basement tectonic structures, but largely drape previously deposited units, onlapping the shelf towards the present day shoreline. Sequence X does not clearly show any folding but rather a clear backstep.

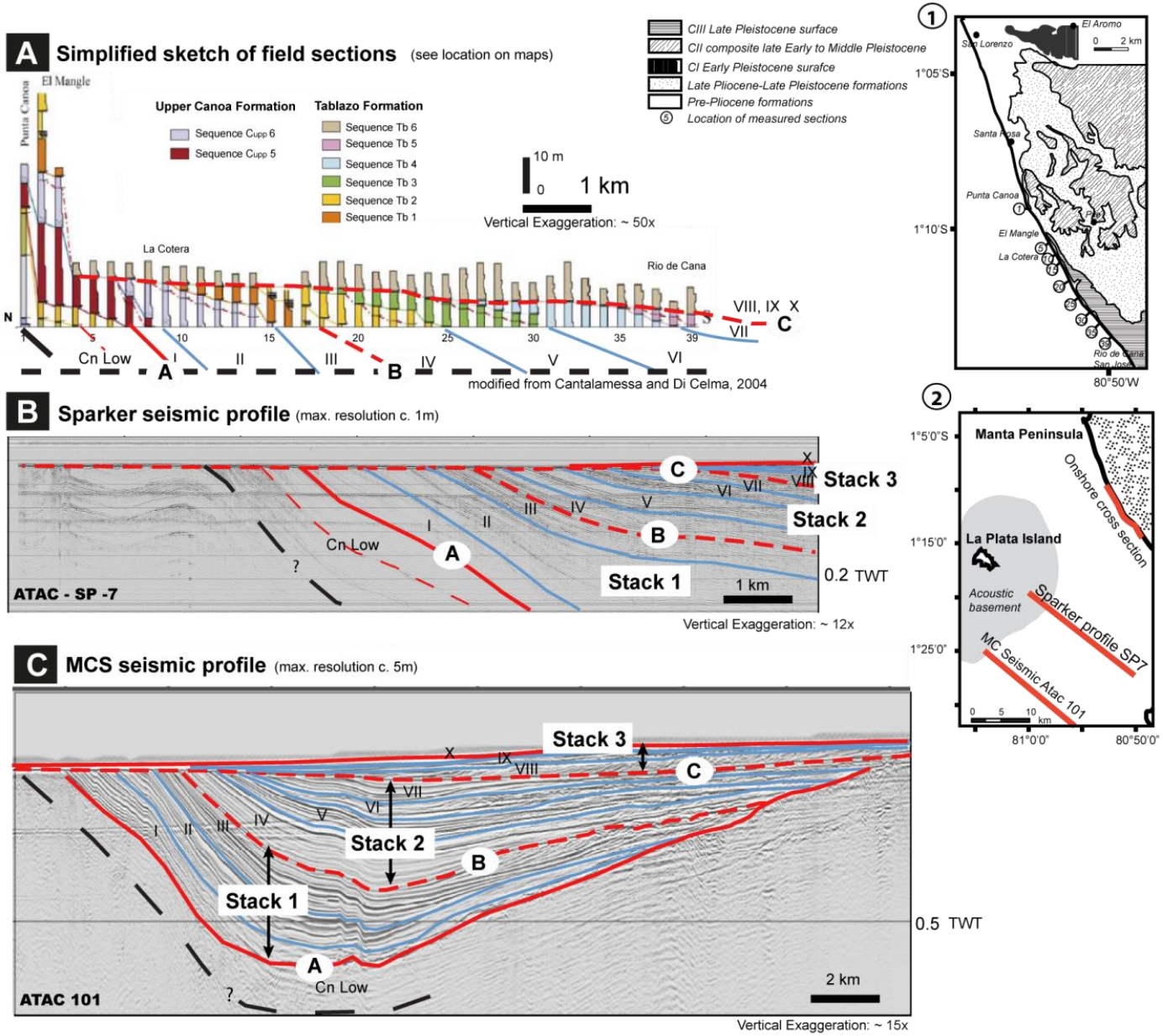

Figure 4.8: Correlation of the T-R seismic sequences described offshore with the depositional sequences described onshore along coastal cliffs by Cantalamessa and Di Celma (2004).

Figure 8- *Correlation of the T-R seismic sequences described offshore with the depositional sequences described onshore by Cantalamessa and Di Celma (2004) along coastal cliffs. The T-R seismic sequences I to VIII correlate with the eight depositional sequences exposed on land in the Upper Canoa and the Tablazos Formations. The T-R seismic sequences IX and X are not exposed in the coastal cliff sections as they plunge to the south below the sea- and ground floor. (A) Oversimplified sketch of field section showing the overall architecture of sequences described by Cantalamessa and Di Celma (2004) in the Upper Canoa (Cupp) and Tablazos (Tb) Formations. CnLow are the sequences of the Lower Canoa Formation, which are not well illustrated with the sparker seismic data in (B). Numbers I to X are seismic sequence names. A, B, C are regional unconformities as defined on seismic lines. (B) ATAC-SP7 is an example of very high-resolution sparker seismic line shot close to the coastal exposures with superimposed line drawing of seismic sequences boundaries. The seismic sequences correlate well to the depositional sequences described on the coastal exposures in (A). (C) Multichannel high-resolution seismic line showing the geometry of the three stacks of seismic sequences described the LPI basin depocenter. Insert 1 shows the location of the different field sections used to reconstruct the coastal exposure sequences architecture on a simplified geological map. Insert 2 shows the locations of the section of the coastal exposure, the very high-resolution sparker ATAC_SP7 seismic line and the high-resolution MCS seismic line ATAC_P101.*

_____

4.3. Piston Core data

We collected two piston cores in the inner to mid shelf location (Figure 4.4) in an attempt to determine the age of the observed sedimentary record and to confirm the seismic facies interpretation. As shown on the chirp and the seismic profiles, the two piston cores sample sequences VIII, IX and X (Figure 4.9). Piston core KAT12-37 is 1 m-thick. It samples the uppermost part of sequences VIII as well as sequences IX and X on seismic line AtacP091 (Chirp line AT0185). Piston core KAT12-36 is 2 m-thick. It samples the uppermost part of sequences IX and sequence X on seismic line AtacP093 (Chirp line AT0187).

Facies description. The facies successions in both piston cores are very similar. They show alternations of (1) light brown coquinoïd sands, (2) bioclastic silty sands and (3) greenish-grey, clayey sandy silts. (1) The coquinoïd sands are of two types. One is comprised of disarticulated and broken thick-walled bivalves and gastropods in a polygenic, medium-grained sand matrix. It is organized in cm to dm- thick fining upward beds with a sharp erosional base. The second type shows bioclastic, polygenic, fine-grained sand slightly coarsening up, largely bioturbated, with some low angle laminations. (2) The bioclastic silty sand is generally very massive (thoroughly bioturbated?) except for some laminated shell hash at the base, or occasional low angle lamination and rare infaunal bivalves in life position. (3) The greenish clayey sandy silts show dm-scale slight coarsening and fining upward trends in an overall fining upward tendency, with increasing and decreasing abundance of mm-scale bioclasts, foraminifera and polygenic silts and rare larger scale shells. Sedimentary and biogenic structures consist of ripple and hummocky cross-stratification and, in places, some burrows. Trace fossils include *Teichichnus*, *Rhizocorallium*, *Palaeophycus* of the *Cruziana* ichnofacies. The more clayey beds exhibit gas vugs.

Facies interpretation. In the first kind of coquinoïd sands, the disarticulated, sorted and broken, thick-walled shells are typical of a high-energy marine depositional environment. The erosion at the base of the beds, the upward fining trend capped by a bioturbated horizon are indicative of episodic bursts of hydrodynamic energy bringing, altogether, coarse material and faunas living in a shore proximal area, in the offshore environment. This kind of deposits resembles the

storm-graded layers formed by rip currents described by Aigner (1985). The second type of coquinoïd bed exhibits smaller and thinner shell faunas mixed with a finely bioclastic sand matrix. The bed is fine grained and shows a gradational basal contact and remnants of low angle to hummocky cross-lamination (*e.g.* Hunter and Clifton, 1982). Pervasive bioturbation reworks and disarticulates the autochthonous faunas. These sediments were deposited in a mid shelf environment under storm-influence. The bioclastic silty sands are massive with few but generally in life up infauna. The greenish clayey sandy silts show rare bioclasts, but it does show burrows, and remnant rippleforms and low angle laminations. These sediments are interpreted as mid shelf deposits laid down in current- and storm-swept sea floor environment. In the greenish facies, the local abundance of vugs due to the early maturation of buried organic matter in disoxic condition corroborates the interpretation of the overall low energy environment.

The two coquinoïds beds exhibit strong analogies respectively with the “onlap” and “backlap” shell beds described by Di Celma et al. (2005) in the Pleistocene strata exposed in the coastline exposures. These beds are thought to underline amalgamated maximum regressive surface and ravinement surface (i.e. sequence boundary, “onlap” shell bed) and maximum flooding at downlap surface (“backlap” shell bed), (Kidwell, 1991; Naish and Kamp, 1997; Di Celma et al., 2005; Carnevale et al., 2011). The “onlap” shell beds may indicate the base of sequence IX and X in core KAT12-37 and the base of sequence X in core KAT12-36 (Figure 5), whereas the “backlap” shell bed in core KAT12-36 highlights the base of the highstand of sequence X and the time of maximum flooding.

Age dating. Three samples were analyzed for ^{14}C age dating. The samples are carbonate shells of large bivalves collected in the coquinoïd sand facies in the lower parts of the two piston cores. The sample in core KAT12-36 provides an age of 20,270 ± 200 years (30,686 years cal BP) at 1,78 m bsf (below seafloor). The two samples in core KAT12-37 provide an age of 36,500 years ± 600 (40,227 years cal BP) at 0,48m bsf and 42,200 years ± 1300 (44,953 years cal BP) at 0,85m bsf. The c.40 ka ages fits into the window of the Marine Isotopic Stage (MIS) 3, whereas the c. 30 ka age is close to the boundary between MIS 3 and MIS 2 (Waelbroeck et al., 2002; Siddall et al., 2003). Nonetheless, as discussed above, most of the shells, including the dated ones, are reworked by storm-induced rip current from the shorelines and as such, they may be fairly older than the enclosing sediment. These shells are part of “onlap” shell beds formed along the merged subaerial unconformity and ravinement surfaces of sequences IX and X during marine transgressions. These ravinement surfaces very likely correspond to the transgressive stages MIS 3 and 1 despite the fact that the shells reworked in the coquinoïd beds are slightly older (Figure 4.9).

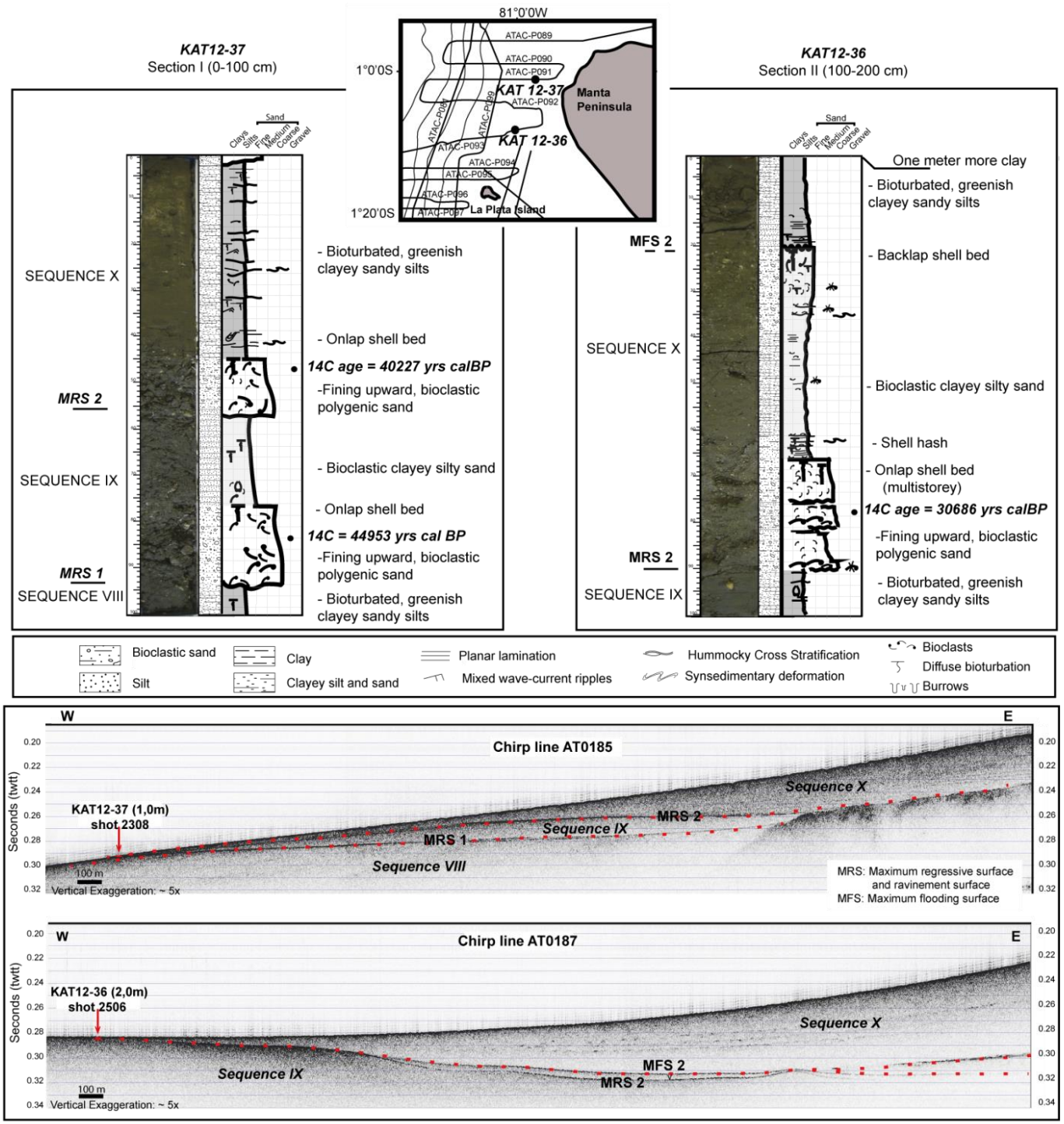

Figure 4.9: Piston core data collected in front of Manta peninsula. Piston core KAT12-37 samples T-R seismic sequences VIII to X, whereas piston core KAT12-36 samples T-R sequences IX and X as shown on the 3.5KHz chirp lines AT0185 and AT0187.
See text for details and the interpretation of shell beds. The shell beds underline stratigraphic surfaces that correlate to depositional sequences exposed along the coast.

5. Discussion

5.1. Correlation of the T-R seismic sequences with on land depositional sequences

To ground truth the seismic interpretation, the MCS seismic data were correlated to the coastal exposures by using very high-resolution single channel sparker data acquired in the shallow waters between the MCS survey grid and the shore exposures (Figure 4.8). The exposures are comprised of Pleistocene strata onlapping an angular unconformity at the top of the Miocene Tosagua Formation (Di Celma et al., 2002). The Pleistocene strata taper out to the north and diverge to the south with a progressively decreasing angle of 1° to 5°. The strata are made up of a 36m-thick, Lower Canoa formation unconformably overlain by a 38m-thick, Upper Canoa and a 70 m-thick, Tablazos formations of late early to late Pleistocene age (Di Celma et al., 2005).

The physical correlations show a good geometrical coherency between the seismic and field datasets (Figure 4.8) as well as with the piston core data (systems tracts, shell beds). The ten T-R seismic sequences, defined in front of Manta Peninsula (e.g. see SP7 and ATAC_P101 seismic lines on Figure 8) and correlated around the seismic grid in the intra shelf basins, correlate to the depositional sequences described onshore by Cantalamessa and Di Celma (2004) and Di Celma et al. (2005), (Figures 8). At a large scale, the unconformity A at the base of T-R sequence I (*i.e.* base of stack 1) corresponds to the angular unconformity reported onland between the Lower and Upper Canoa formations by Cantalamessa and Di Celma (2004). The sharp erosion and angular unconformity observed at the base of T-R sequence VIII (i.e. base of stack 3) correlates to the syntectonic angular unconformity reported on land at the base of the Tb 6 unit (also called SAU surface in Cantalamessa and Di Celma, 2004 and Di Celma et al., 2005). The sharp erosion surface B observed at the base of T-R sequence IV (i.e. base of stack 2) correlates onland to the base of sequence Tb2 of Di Celma et al. (2005).

In details, the T-R seismic sequences I to VIII correlate to the eight depositional sequences exposed on land in the Upper Canoa and the Tablazos formations (Figure 4.8 and 4.10). The overlying T-R seismic sequences IX and X are not exposed in the coastal cliff sections as they plunge to the south below the sea and ground floor. Each depositional sequence shows an asymmetric shape that fits with the T-R structure of the seismic sequences. The depositional sequences are comprised of a sand prone, transgressive lithosome overlain by a silt prone, regressive lithosome (Di Celma et al., 2005). A single erosion surface, interpreted as merged subaerial unconformity and wave ravinement surfaces, bounds the depositional sequences below, except at the base of the Tablazos (base of Tb2, Figure 4.10) where the two surfaces are distinguishable. The transgressive lithosome (“T” part of the T-R seismic sequence) is fining upward and consists of massive, intensely bioturbated and locally deformed, shoreface sands. The shoreface sands are underlain by either dispersing upward shell concentration in sheltered settings, or trough cross-bedded, wave-winnowed shell beds in open shelf conditions (OSB, onlap shell bed). The regressive lithosome (“R” part of the T-R seismic sequence) is a coarsening upward, almost always fossil-free sandy silts to silty fine sands underlain by a community shell bed (BSB, backlap shell bed). The shell bed is either gradational or it is lying on a disconformity surface at the boundary between the backstepping and the forestepping

sediment wedges (maximum flooding surface). In the suite of sequences, Tb1 and Tb5 are incomplete. The tops of Tb1 and Tb5 are deeply eroded by the overlying merged subaerial and ravinement unconformities in the seismic sections to surfaces B and C, respectively. Tb 6, which is not overlain by another sequence at the outcrop, is the least eroded and is capped by well-preserved coastal plain deposits as observed on seismic lines (Figure 4.8).

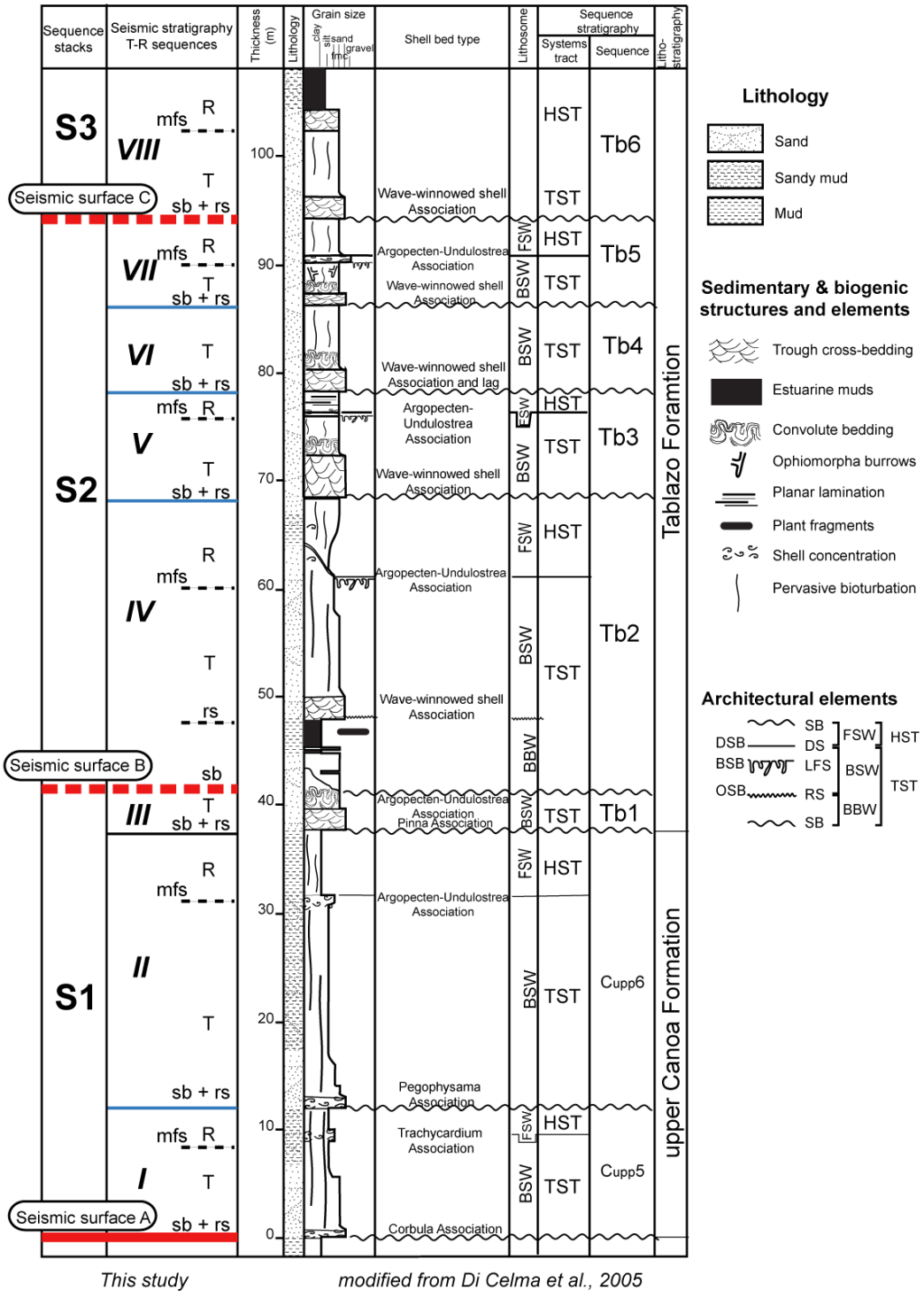

Figure 4.10: Details of the correlation of the T-R seismic sequences with the depositional sequences described onshore by Di Celma et al. (2005).
Unconformities A and C at base of stacks of T-R sequences 1 and 3, correspond on land to angular unconformities at base of depositional sequence Cupp5 and Tb6. Seismic surface B correlates to a sharp surface at base of Tb2. The

internal architecture of T-R sequences parallels the subdivision of the depositional sequences where the different systems tracts are bounded by specific shell beds. These shell beds are also found offshore in piston core data (see figure 5). The Upper Canoa (Cupp) and the Tablazo (Tb) Formations were formed landward of the lowstand shoreline in sheltered and exposed shelf conditions, respectively. They comprise interglacial TST and HST bounded by merged subaerial and ravinement erosion surfaces formed during LST and early TST. The sediments are comprised of bioturbated, fining or coarsening upward, shoreface and inner shelf silts and sands interbedded with wave-winnowed, trough cross-bedded shell beds. BBW—back-barrier wedge; BSW—backstepping shelf wedge; FSW—forestepping shelf wedge; TST—transgressive systems tract; HST—highstand systems tract; DSB—downlap shell bed; BSB—backlap shell bed; OSB—onlap shell bed; SB—sequence boundary; DS—downlap surface; LFS—local flooding surface; RS—ravinement surface; fmc—fine, medium, coarse.

_____

5.2. Climate control on the T-R seismic sequences deposition

Offshore, the piston core ^{14}C age dating provides an age of MIS 3 (57-14 ka, table 2) for the T-R sequence IX and MIS 1 (14ka to present, table 2) for sequence X (Figure 4.9). Onshore, the ravinement surface at the base of depositional sequence Tb6, which corresponds to the surface at the base of T-R sequence VIII, is dated from interglacial stage 5e (c.130ka) (Cantalamessa and Di Celma, 2004). Because each depositional sequence onland, and as such each seismic T-R sequence at sea, is inferred to represent a single Milankovitch sea-level oscillation due to orbital control on climate cyclicity (Di Celma et al., 2005), the age of the T-R seismic sequences can be postulated by counting the number of climatically controlled sequences down the stratigraphic record. In Table 4.2 and Figures 4.10 and 4.11, we suggest an age model for the ten T-R seismic sequences dating back to the late mid-Pleistocene climate transition (c.790 ka) to the Present. These rough estimates are in agreement with the Pleistocene ^{18}O-based sea-level curve (Lisiecki and Raymo, 2005) with the migration in space and time of the point of offlap break (*i.e.* maximum seaward shift of the shoreline) of each T-R sequence in the intrashelf basin (Figure 4.11). The offlap break migration curve mimics the shape of the Pleistocene eustatic sea-level curve, hence substantiating both the age dating and the strong climate control on the deposition of the T-R sequences (Figure 4.11). The possibility exists that the two thin T-R sequences II and III on ATAC_P092 (Figure 4.6) record the two 40ka sea level cycles that built the thick c.100ka sequence of MIS stages 15-14 (Figure 4.11C). However, sequences II and III are faulted at the shelf edge (Figure 4.6) and they are as thick as other 100ka sequences in the intrashelf basin (AtacP101, Figure 4.11A and B). Consequently we interpret sequences II and III as the two 100ka sequences of MIS stages 17-16 and 15-14 (Figure 4.11C).

5.3. Tectonic control on the T-R seismic sequences deposition

The ages of the marine terraces formed on LPI and MP at the maximum marine encroachment of the continental area compare to the ages of the maximum flooding surfaces of the T-R sequences (mfs, table 4.3). The marine terrace dataset (Cantalamessa and Di Celma, 2004; Pedoja et al., 2006a, 2014) shows a set of three to four terraces preserved between MIS 13 (533 ka) to MIS 5e (130 ka) and two isolated, older terraces, much less constrained in age at MIS 17 (712ka) and sometimes between MIS 27 to 31 (1060 to 966 ka), (Table 4.3). The suite of terraces is time correlative to the stack 2 (T-R sequences IV to VII) bounded below and above by two large unconformities in the offshore (surfaces B and C). Inland, the unconformities merge with the transgressive ravinement surfaces that underline the marine terraces deposits. Offshore, the stack 2 shows a divergent pattern of component seismic units indicative of synsedimentary deformation and differential uplift of the LPI area with respect to the basin depocenter (Figure 4.11). This uplift is observed onland with the differential tilting of the successive marine terraces (Pedoja et al., 2006a). Along with the high amplitude of sea-level changes, this deformation is probably at the origin of the set of marine terraces on the continental domain. Deformation is nevertheless the main driver as high amplitude of sea-level change started after the carving of the first terrace at MIS 11 and resumed later at MIS 1 - the set of terraces probably marking the peak of the tectonic activity in the area.

Name Seq.	*Seismic Facies (Profile 92)*	*Stratigraphic Surface (on Top)*	*Shoreline Shift*	*System Track*	*TR Sequence*	*MIS (proposed)*	*Age*
		Seafloor	T				
X	Sf5	MRS	FR	TST	Transgressive	1	14000
IX	Sf1, Sf3, Sf4, Sf6	MFS	T	FSST	Regressive	2	29000
	Sf5, Sf6	MRS	NR	TST	Transgressive	3	57000
VIII	Sf1, Sf3, Sf4	c.c.	FR	LST	Regressive	4	
	Sf1, Sf3, Sf4, Sf6	BSFR	NR	FSST			
	Sf1, Sf3, Sf4	MFS	T	HST			71000
	Sf5, Sf6	MRS	FR	TST	Transgressive	5	130000
VII	Sf1, Sf3, Sf4, Sf6	BSFR	NR	FSST	Regressive	6	
	Sf1, Sf3, Sf4	MFS	T	HST			191000
	Sf5	MRS	FR	TST	Transgressive	7	244000
VI	Sf1, Sf3, Sf4, Sf6	BSFR	NR	FSST	Regressive	8	
	Sf1, Sf3, Sf4	MFS	T	HST			300000
	Sf5, Sf6	MRS	NR	TST	Transgressive	9	337000
V	Sf1, Sf3, Sf4, Sf6	c.c.	FR	LST	Regressive	10	
	Sf1, Sf3, Sf4	BSFR	NR	FSST			
	Sf1, Sf3, Sf4	MFS	T	HST			374000
	Sf5, Sf6	MRS	FR	TST	Transgressive	11	424000
IV	Sf1, Sf2, Sf3, Sf4	BSFR	NR	FSST	Regressive	12	
	Sf1, Sf2, Sf3, Sf4	MFS	T	HST			478000
	Sf5	MRS	FR	TST	Transgressive	13	533000
III	Sf1, Sf2, Sf3, Sf4	BSFR	NR	FSST	Regressive	14	
	Sf3	MFS	T	HST			563000
	Sf5	MRS	FR	TST	Transgressive	15	621000
II	Sf4	MFS	T	FSST	Regressive	16	676000
	Sf5	MRS	FR	TST	Transgressive	17	712000
I	Sf1, Sf2, Sf3, Sf4	BSFR	NR	FSST	Regressive	18	
	Sf3, Sf4	MFS	T	HST			761000
	Sf5			TST	Transgressive	19	790000

Table 4.2: Summary of the seismic stratigraphy of the Ecuadorian continental shelf in Manta-Plata area.

Proposed correlation to Marine Isotopic Stages (MIS) and ages of the T-R sequences boundaries.

T-R sequences - MIS	Ages of MIS End Int* — Start Int**	La Plata Island marine terraces	Manta Peninsula marine terraces ***
X - MIS 1	6 ka mfs - - - - - - - - - - rs · 14 ka	- -	
IX - MIS 3	29 ka mfs - - - - - - - - - - rs · 57 ka		
VIII - MIS 5	71 ka mfs - - - - - - - - - - rs · 130 ka	**Plata 4** 124 ka 55 m	**T1** 76+/-9; -85+/-1,2 25- 57 m +/-2
VII - MIS 7	191 ka mfs - - - - - - - - - - rs · 243 ka	**Plata 3** 200 ka +/- 12 80 m	**T2** 203- 232 ka 67-77 m +/-10
VI - MIS 9	300 ka mfs - - - - - - - - - - rs · 337 ka		**T3** 272 =/- 38 ka 170 m +/-10
V - MIS 11	374 ka mfs - - - - - - - - - - rs · 424 ka	**Plata 2** 400 ka +/-12,5 160 m	
IV - MIS 13	478 ka mfs - - - - - - - - - - rs · 533 ka	**Plata 1** 438 ka +/- 12,5 175 m	
III - MIS 15	563 ka mfs - - - - - - - - - - rs · 621 ka		
II - MIS 17	676 ka mfs - - - - - - - - - - rs · 712 ka		**T4** 640 - 710 ka T4 203 m +/- 10
I - MIS 19	761 ka mfs - - - - - - - - - - rs · 790 ka		
MIS 27 to 31	1081 ka		**T5** 966 - 10600 ka T5 300m +/-10 m
	Lisiescki and Raymo, 2005	Cantalamessa & Di Celma, 2004	Pedoja et al., 2014 Pedoja et al., 2006

* top interglacial MIS, ** base interglacial MIS, ***combined IRSL U/Th age ranges

Table 4.3: Proposed correlation of the T-R seismic sequences with the La Plata Island and Manta peninsula marine terraces

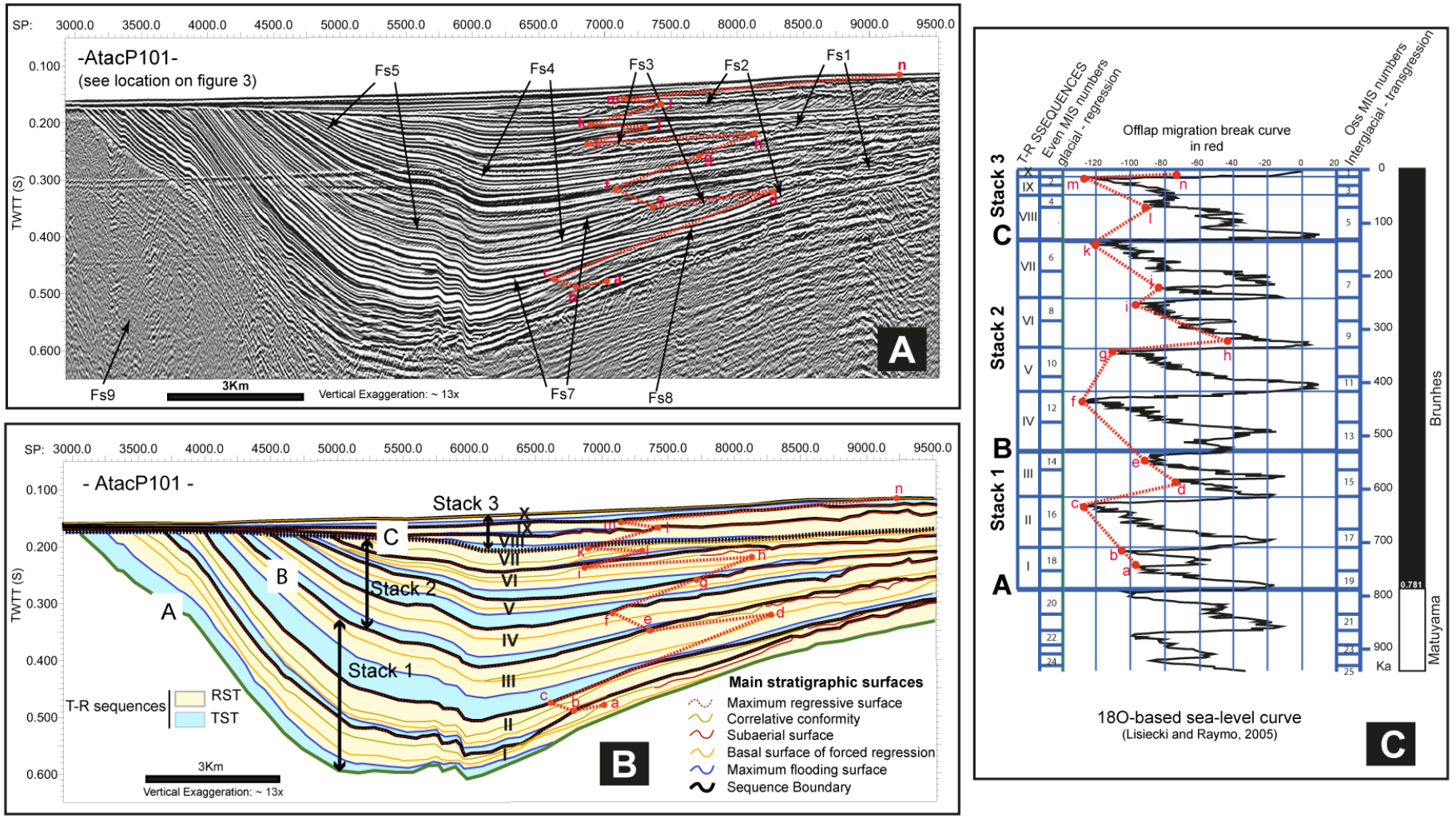

*Figure 4.11: Comparison of the Pleistocene ^{18}O-based sea-level curve (Lisiecki and Raymo, 2005) with the migration in space and time of the point of offlap break (*i.e. *maximum seaward shift of the shoreline) of each T-R seismic sequence picked along a seismic line perpendicular to the present day shoreline.*
The shape of the offlap break migration curve shows variations that compared to the eustatic sea-level curve for the last 800 Ka, which supports the age estimates for the T-R sequences and the climatic control on sediment deposition. (A) MCS seismic line ATAC_101 with the location of the main seismic facies (Fs, see table 1) and a line featuring the lateral and vertical migration of the offlap break. (B) Line drawing of seismic line ATAC_P101 showing the regressive (RST) and transgressive (TST) systems tracts, the seismic sequences and their stacking pattern, and the offlap break line migration. (C) The MIS and eustatic sea level curve of Lisiecki and Raymo (2005) with the proposed correlation to the offlap migration line (in red) and to the seismic sequences.

5.4. Subsidence history of the Manta-Plata area

The evolution of the subsidence of the acoustic basement of the Manta-Plata area portrays the continental platform's recent of the history. The cumulative subsidence of the acoustic basement was calculated, sequence-by-sequence, by using 120 virtual wells extracted from the seismic lines interpretation. They cover a 50 by 50 km-large area and are distributed at sea along the seismic lines, and in the onland marine terraces described in Pedoja et al. (2006a), (Figure 4.12). Nine maps shown in Figure 4.9 display the main results. Each map shows the cumulative subsidence calculated since the previous depositional sequence. The ages are the estimated ages of the basal surface of each sequence (see above, tables 4.2 and 4.3).

The maps show the succession of three main episodes of basement subsidence. The first episode T2-T3 shows the subsidence of the shelf break area in blue and the subsidence of an EW trough perpendicular to the shelf break, which parallels large EW-oriented faults on the shelf (Figure 4.12). Conversely, the T2-T3 episode exhibits a relative uplift in the MP area. The transition between the MP uplift to the North and the subsiding area to the South is coincident to a drastic dropdown of the Bouguer anomaly intensity (Feininger, 1977), which attests the presence of two blocks separated by a main E-W discontinuity. The second episode T4-T7 shows the development of an NE-SW subsiding area in the South of the uplifting LPI area. The subsiding trough progressively increases its curvature through time in a well-defined U-shape structure. To the North of the LPI area, in front of MP, the previously uplifted area subsides and the shelf break downwarps. This gives rise to a trough, which tends to merge progressively southward with the trough in the South of LPI. During the third episode T8-T10, the active subsidence of the shelf tends to resume and sediments progressively fill remnant topographies.

5.5. The role of the subduction of seafloor reliefs

At the Ecuador subduction margin, the Carnegie Ridge is subducting eastward at an average rate of 47mm/yr with respect to the NAB (Nocquet et al., 2014) beneath the Manta-Plata continental narrow shelf. Pre-stack, depth-migrated images along SIS05 and SIS09 seismic lines (SISTEUR campaign, Sanclemente, 2014; see lines location in 14krs-inset on Figure 4.12) show anomalous plate boundary topography at the top of the Carnegie Ridge, beneath the outer margin wedge, west of LPI. The 3D geometry of the plate interface relief shows a 55 km-large seamount with closely spaced, rounded and sharp asperities as high as 2.2km, with a few peaks at 3.2 km, beneath the sea-floor (Sanclemente, 2014). The present day morphology of the margin supports this interpretation with (1) a 50 km long and 10 km large re-entrant that scallops the base of the slope of the margin as a trace of the passage of the seamount, (2) a seaward protrusion of the shelf edge adjacent to LPI and marine terraces on LPI reflecting uplift, and (3) depressed northern and southern areas surrounding LPI.

By moving backward in space and time, at a rate of 47mm/yr, stepwise, sequence by sequence, the present day morphology of the observed seamount and its surrounding modeled interseismic coupling (Chlieh et al., 2014), one can figure out the impact of the seamount subduction on the continental shelf subsidence history (Figure 4.12). From TR-II to TR-III, the seamount sits on the oceanic subducting plate moving eastward toward the plate boundary.

The subsidence of the overriding plate seems largely controlled by EW oriented tectonic structures dissecting the shelf. EW compressive deformation might explain the synchronous downwarp of the shelf edge and uplift of Manta Peninsula. At TIV, the seamount collides the base of the continental slope and subducts beneath the continental shelf until it totally disappears from the surface at TR-VIII. At that time, the shelf shows a complex subsidence pattern with an uplift of the LPI and the subsidence of the surrounding areas, which mimics the gross shape of the subducting seamount. From TR-X to present day, subsidence tends to resume and relax, as the seamount can be too deep to influence the surface any longer.

6. Conclusions

The detailed analysis of the seismic and piston core data collected on the shelf of the active subduction margin of Ecuador during the ATACAMES campaign on the L'Atalante (Michaud et al., 2012) provides the opportunity (1) to describe the architecture of the Pleistocene sedimentary deposits of the continental platform (lithofacies, depositional environments and depositional sequences), (2) to tie the offshore dataset to the onshore interpretation of coastal exposure and marine terraces and (3) to determine an age and to trace time lines through the sedimentary record. The results show that despite the strong tectonic activity of this active margin, the sedimentary record is composed of a set of ten depositional sequences preserved during climatically controlled Milankovitch-scale, global sea-level variations (see other example in New Zealand, Proust and Chanier, 2004). Stacks of sequences correlate to sets of uplifted marine terraces, which points to the importance of tectonic deformation on the geometry of depositional sequences. Careful backstripping and mapping of tectonic deformation shows that the deformation of the continental shelf, in the Manta-Plata area during the Late Pleistocene, results from the subduction of topographic reliefs of Carnegie Ridge below the continental shelf.

Our knowledge of these shelf deformations is still rather limited but a better understanding of the timing and amplitude of upper plate deformation associated with the subduction of oceanic plate relief would drastically improve our knowledge of the evolution of the plate boundary. The subduction of oceanic plate reliefs indeed drastically influences (1) the relative uplifts and subsidence of the forearc and backarc domains, (2) the distribution of fluids along the plate interface and arc volcanism and (3) the dip of the slab: this results in an increase of the interplate coupling and a decrease in subduction velocity, which in turn enhances subduction erosion and participates in the formation of large barrier against the propagation of earthquake ruptures.

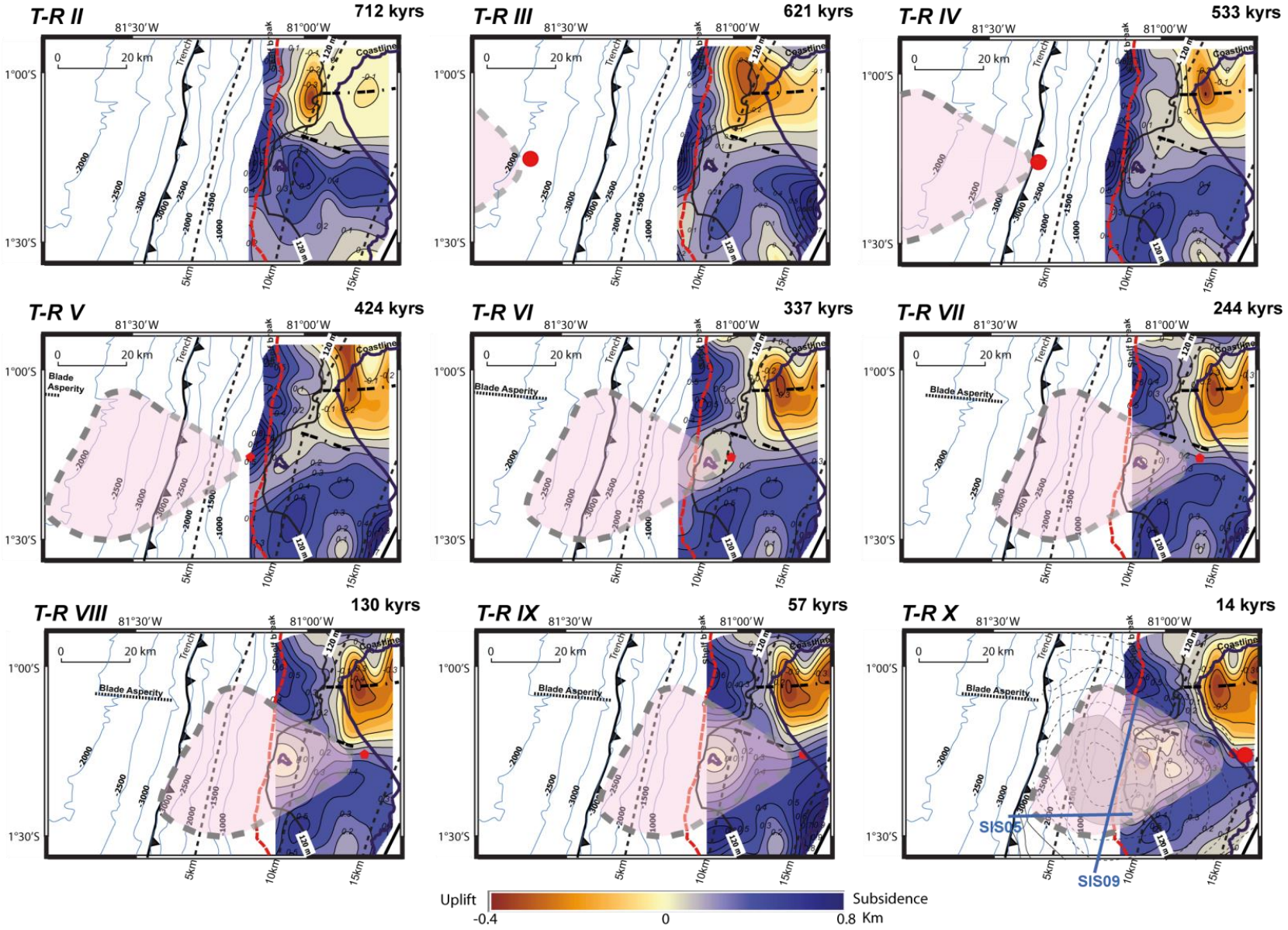

Figure 4.12: Oversimplified sketch showing the progressive eastward migration of a seamount entering in subduction at the top of the Carnegie Ridge and the possible consequences on the deformation of the continental shelf of the overriding plate.

Figure 12- *Oversimplified sketch showing the progressive eastward migration of a seamount entering in subduction at the top of the Carnegie Ridge and the possible consequences on the deformation of the continental shelf of the overriding plate. The transparent pink body bounded by a thick black contour is the broad subducted seamount with peaks reconstructed from Sanclemente (2014). Thin black lines contouring the seamount show the distribution of the interseismic coupling (0<ISC<1) (Chlieh et al., 2014). The highly coupled zone of the seamount (ISC>0.7) is shaded in grey. The blue green color map shows the tectonic subsidence of the continental shelf in Manta-Plata area at each sequence boundary, backstripped from seismic and field data. A map is drawn for each T-R seismic sequence from T-R sequence II (T-R II) to T-R sequence X (T-R X). The isodepth contour lines are in kilometers.*

_____

Acknowledgments

Data were acquired in 2012 during the IRD-CNRS oceanographic campaign ATACAMES on board the IFREMER research vessel *L'Atalante*. This work was carried out in the framework of the Joint French-Ecuador Laboratory LMI "Séismes et Volcans dans les Andes du Nord" with the financial support of the CNRS-INSU, IRD, Rennes 1 and Nice Universities and IFREMER. We thank SENESCYT (Secretaría Nacional de Ciencia y Tecnología del Ecuador) for the student scholarships; ESPOL and INOCAR for their support and also *Schlumberger* and *IHS* for making available respectively *Petrel* and *Kingdom Suite* seismic interpretation software. We thank Hugo Pouderoux, Gueorgui Ratzov and the ATACAMES Science Party for their help in gathering and processing the data during the campaign and for the fruitful scientific discussions at different stages afterwards. We thank also Fabien Paquet and the anonymous reviewer for their constructive comments as well as Camille Proust for her editorial work that largely improved the quality of the paper.

CHAPTER 5: Tracing the Pleistocene sequences in marine forearc basins along the central Ecuadorian margin using a stratigraphic sequences analysis

"Look deep into nature,
and then you will understand
everything better"

Albert Einstein (1879 – 1955)

1. Introduction

This chapter presents the results obtained from the analysis and interpretation of the ATACAMES dataset for the central Ecuadorian margin (see Chapter 3 for details), supplemented with 2D regional seismic lines (SCAN Geophysical ASA, 2009 & Secretaria de Hidrocarburos de Ecuador). The central segment of the Ecuadorian margin encompasses the area located between Galera Cape and Salinas Point, where Carnegie Ridge subducts below the North Andean block (see Chapter 2). In further detail, we subdivided the central segment into three zones: Northern, Central and Southern. The Northern zone extends from Galera Cape to Manta Peninsula, the Central zone from Manta Peninsula to Salango Island, and the Southern zone from Salango Island to Salinas Point.

We show the stratigraphic record of the eustatic-climatic changes, as well as the differential deformation record caused along the margin by the subduction of the various types of asperities present in the oceanic plate.

Based on 14C dating and by correlating the TR sequences with the eustatic-climatic change curve, we propose ages for the TR sequences interpreted in the different forearc marine basins. Based on these proposed ages, we use a correlation analysis to compare the T-R sequences to the onshore Quaternary outcrops described in the literature.

Last, we propose a structural scheme at the base of the Quaternary sequences, which attempts to explain the behavior of the deformation shown in the seismic lines.

2. Seafloor Morphology

The seafloor morphology is analyzed from the grid elevation model built from the data provided by different bathymetric campaigns (Figure 3.4). See Chapter 3 for more details regarding the source of the data and the construction method for the grid elevation model.

2.1. The Northern zone

- *The platform* is regular and flat with NNE-SSW isobaths following the general orientation of the coastline. In front of Galera Cape and Manta Peninsula, the shelf is narrow (10 km wide), and between them, the shelf is large (c. 40 km wide).

Between Galera Cape and Manta Peninsula, the shelf break shows three reentrants: from north to south, the first is in front of the Cojimíes estuary, the second is in front of the coastal village of Jama and the third in front of the city of San Vicente (Figure 5.1A).

The Cojimíes reentrant (CE) reaches the platform showing isobaths with a concave shape towards the coast. This morphology corresponds with the bathymetric low on the platform displayed in profile A-A' (Figure 5.1B, blue arrow pointing down). In the same profile, we can note that the Jama reentrant (JE) shows a shallow bathymetric low on the platform, while the San Vicente reentrant (SVE) does not have a low bathymetry expression on the platform.

However, the general trends of the bathymetric profile along the shelf break (continuous line in Figure 5.1C) show a similar bathymetry low between the SVE and CE.

Two promontories are located among the reentrants. The first is set in front of the coastal village of Pedernales, between the CE and JE; the second is situated in front of Cabo Pasado Point, between the JE and SVE. These promontories reach the platform, and are expressed as a bathymetric high in profile A-A' (Figure 5.1B). We can note in this profile that the highest promontory is the one in front of Cabo Pasado Point.

- *The continental slope* presents morphological irregularities in the north, while it is smooth in the south (Collot et al., 2009). From north to south, the continental slope presents a 25 km wide curved scarp in front of Cojimíes estuary (at the slope of the CE). In the trench in this area, the bathymetry exhibits a rough morphology with a convex trend, contrary to the concave tendency of the CE.

To the south, there is a bathymetric high as well as the scarp related to the subducted double-peak Atacames seamount (Collot et al., 2009; Marcaillou et al., 2016). At the foot of the scarp, the bathymetry shows a rough morphology similar to the foot of the slope of the CE, which has been interpreted as mass wasting deposits by Marcaillou et al. (2016).

To the south of the Pedernales promontory, the 50 km long coastward slope, which has a concave morphology, is underlined by a set of deep gullies disconnected from the shelf break. The concave slope connects to a smooth convex promontory in front of Cabo Pasado Point (Figure 5.1A). After this second promontory, the continental slope exhibits a 500 m high step corresponding to a 20 km wide reentrant of the shelf break that is arcuate in shape with a radius of approximately 9 km and is limited seaward by a morphological "indentation" (Figure 5.1D).

2.2. The Central zone

The seafloor morphology of the Central zone, from Manta Peninsula to Salango Island, was described in Chapter 4. The shelf break and slope are relatively smooth with a slight reentrant of the shelf break in front of Manta Peninsula (Figure 5.1A).

A bathymetric profile along the slope (A-A' in Figure 5.2) shows two areas with gullies separated by a 250 m high promontory. One gully area is in front of Manta Peninsula and the other is in front of La Plata Island. The promontory between these two gully areas is located in front of a blade asperity of Carnegie Ridge that arrives in the trench, between Manta Peninsula and La Plata Island (Chapter 4).

2.3. The Southern zone

The seafloor morphology of the Southern zone, between Salango Island and Salinas Cape, presents a slightly wavy platform shape and a very rough slope.

- The platform shows two bathymetric highs: one is in front of the coastal town of Montañita (the Montañita bathymetric high) and the other is around Salinas Cape (the Salinas bathymetric

high; Figure 5.3A). Both highs rise to 80 m above the average seafloor. These two bathymetric highs are separated by a landward reentrant of the platform corresponding to the upper "valley" of Santa Elena Canyon (SEC; Figure 5.3A).

- The slope exhibits some important bathymetric irregularities, with a broad 17 km wide trough in front of the town of Ayampe (Figure 5.3A). The eastward boundary of the Ayampe trough extends until the shelf break. On the middle slope, the Ayampe trough is dissymmetrical and it is limited to the south by a peak (crest of the escarpment in Figure 5.3B). This peak is 2 km high and 8 km wide, and it is limited seaward by a 2250 m high scarp (seamount subduction scarp, Figure 5.3C) and landward by a 200 m high scarp (back-scarp, Figure 5.3C). The peak is underlain by a subducted seamount (Sage et al., 2006). To the south, the bathymetry shows 100 m high curved scarps (bathymetric notch in Figure 5.3A) facing seaward, defining a gentle stepped morphology and extending in an S-shape from north to south (Figure 5.3A).

Finally, southward, the slope is sharply cut by the Santa Elena Canyon (SEC), which shows a NNE-SSW trend oblique to the shelf break direction (Michaud et al., 2015). The SEC incision is 45 km long, extending from the shelf break to the trench, and with a maximum depth of 800 m. The valley shows a "V"-shape from the shelf break to a depth of approximately 1000 m and a "U"-shape morphology from 1000 m to the trench (Coronel, 2002). North of Santa Elena Canyon, the slope exhibits a landslide. The head of the landslide exhibits an E-W trending straight morphology that is approximately 4 km in length. This morphological element draws a "V" shape in the bathymetry, corresponding to a 50 m deep valley (Figures 5.3B, straight head of the landslide).

Figure 5.1: A) The seafloor grid shows: a smooth platform, the shelf break around the 150 m isobaths, and an irregular slope with some morphological features, i.e. landslide scarp, subducted seamount scarp, gullies, promontories, terrace and indentation, as well as the three reentrants displayed in this zone: in front of Cojimíes (CE), in front of Jama (JE) and in front of San Vicente (SVE). B) The bathymetric profile A-A' displays the bathymetric low in front of Cojimíes and the bathymetric high in front of the Cabo Pasado zone. C) Curve of the heights of the shelf break, displaying its irregular position along the margin. Its general behavior (filled line) also shows the bathymetric low in the Cojimíes area and the bathymetric high in the Cabo Pasado area. This profile also presents a bathymetric low in front of San Vicente. D) Bathymetric profile B-B', in front of the San Vicente area, presents a step at the slope (terrace) with an indentation at its border.

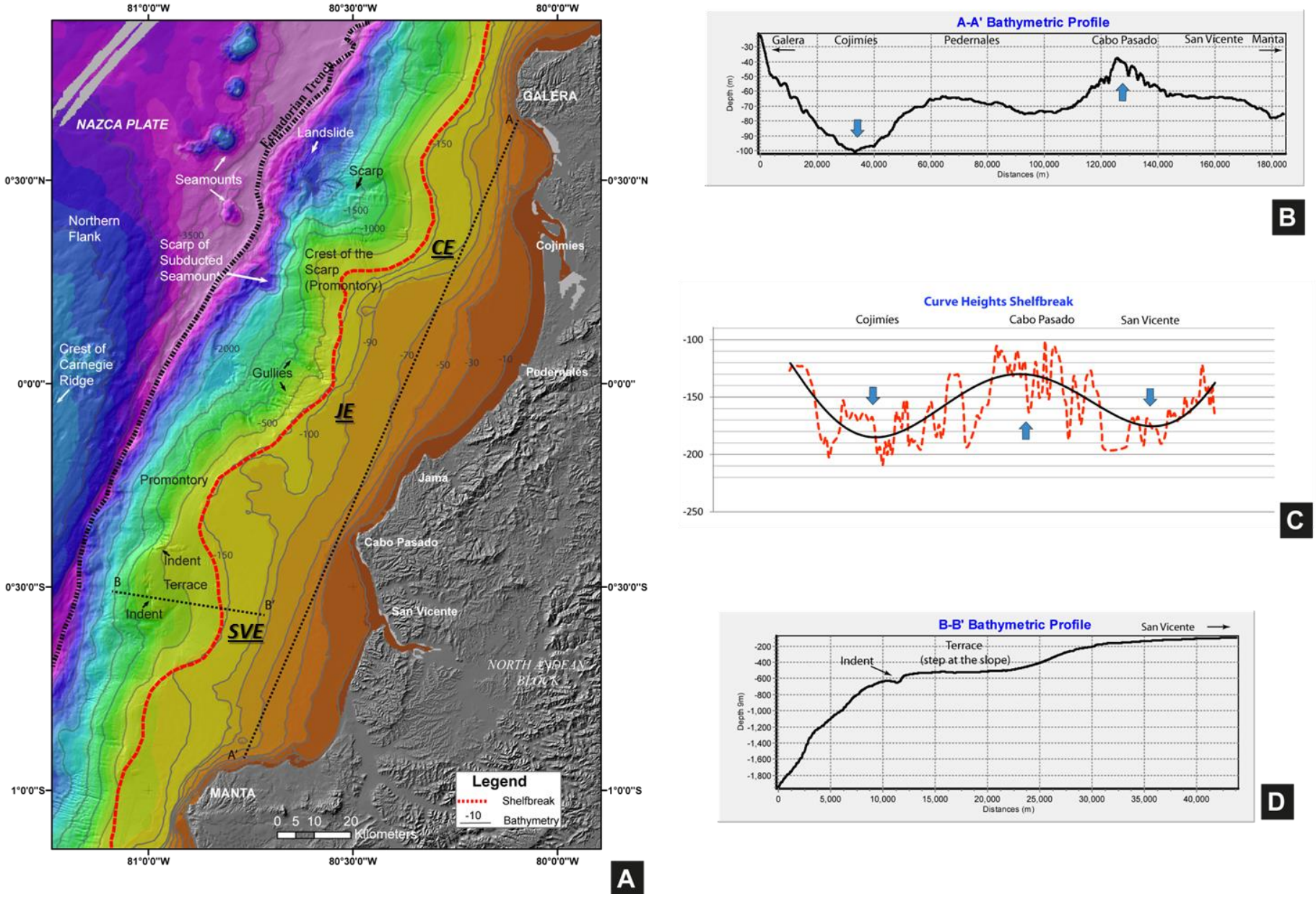

Figure 5.1: Seafloor morphology of the Northern zone (Galera Cape-Manta peninsula).

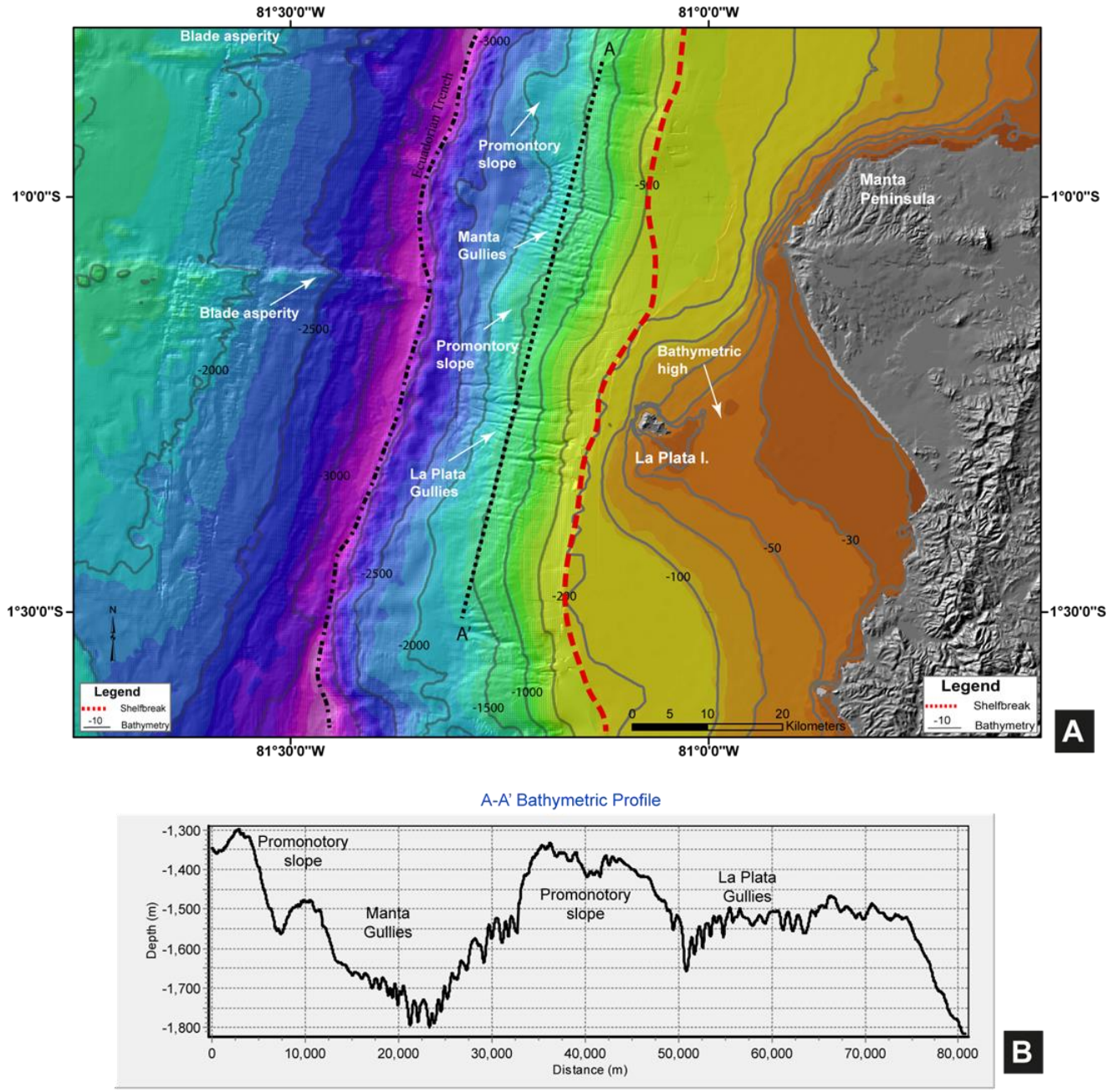

Figure 5.2: Seafloor morphology of the Central Zone (Manta Peninsula-La Plata Island).
A) It shows the gullies at the slope in front of Manta Peninsula and La Plata Island, as well as the subduction of the blade asperity in front of the two zones. B) The bathymetric profile shows the promontory on the slope located just in front of the blade asperity, which divides Manta gully from La Plata gully.

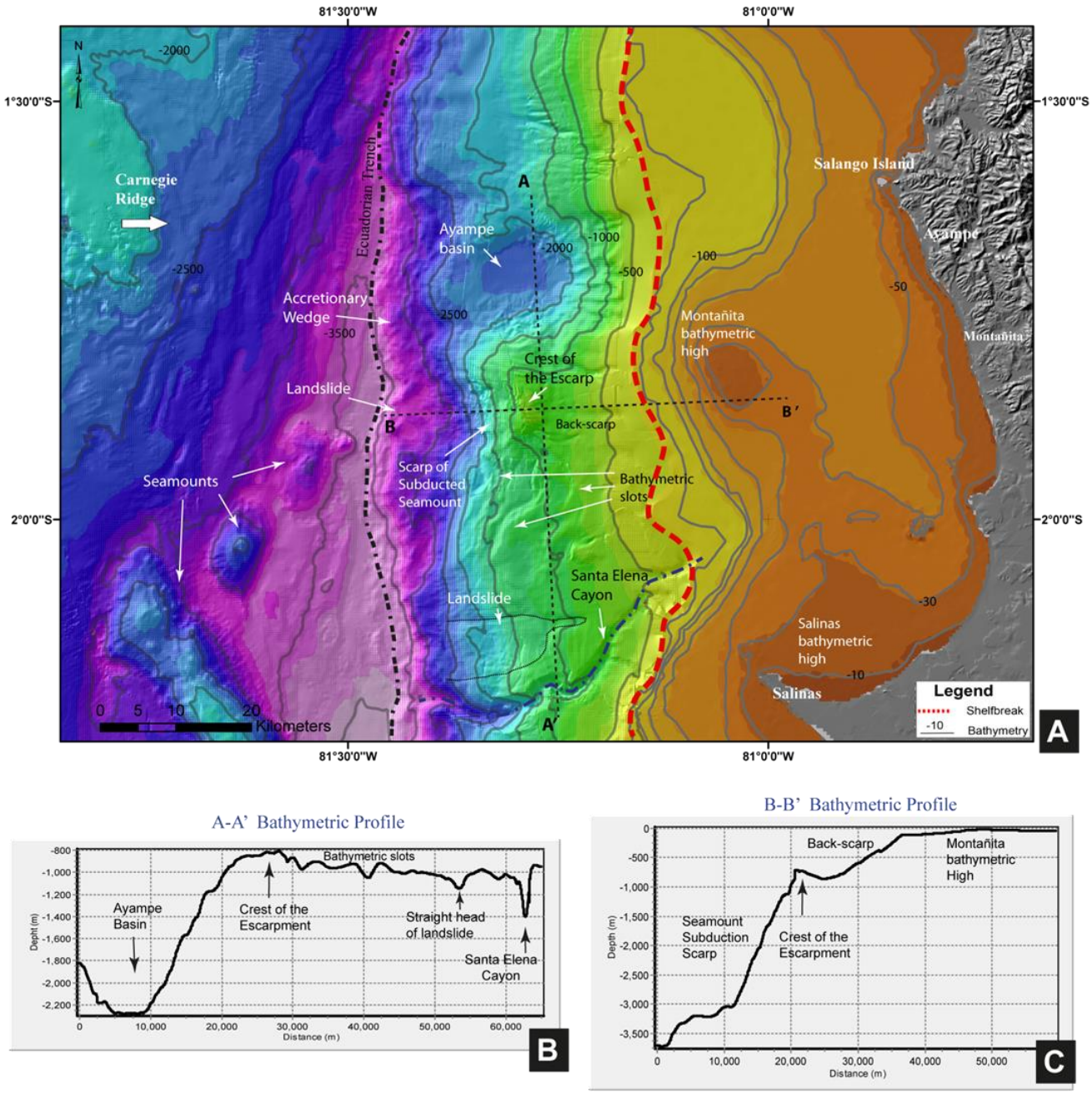

Figure 5.3: Seafloor morphology of the Southern zone (Salango Island-SalinasCape).

A) The bathymetric grid shows the main morphological features in the margin: 1) the bathymetric highs on the platform in front of Montañita beach and around Salinas Cape. 2) On the slope: Ayampe basin, the subducted seamount scarp, the bathymetric notches, a landslide and Santa Elena Canyon. B) N-S bathymetric profile A-A' along the slope displaying: Ayampe basin, the crest of the scarp, the bathymetric slots, the "straight head" of the landslide and Santa Elena Canyon. C) W-E bathymetric profile B-B' showing: the subducted seamount scarp, the crest of the scarp, the back-scarp and the bathymetric high in front of Montañita beach.

3. Seismic Data Analysis and Interpretation

The acoustic basement grid (isodepth map), which was generated for the entire central Ecuadorian margin, corresponds to the acoustic basement interpreted from the Atacames seismic data (Figure 5.4A). See Chapter 3 for explanations of how this isodepth grid was constructed. This basement grid allows us to define the basins (areas in blue) and uplifted areas (red to yellow area). The isopach map (Figure 5.4B) shows the thickness (m) of the offshore sediment filling in these basins between Galera Cape and Salinas Point: the thickest area is shown in blue and the thinnest in brown (see Chapter 3 for explanations of how this grid was constructed). Below, we present the principal characteristics of these basins.

The Northern zone (Galera-Manta zone) shows four basins from north to south: Cojimíes, Jama, Cabo Pasado and San Vicente. The Central zone is characterized by two basins: San Lorenzo and La Plata. The Southern zone (Salango-Salinas zone) shows: the Ayampe basin sited on the middle slope; the Montañita and Salinas basins, which are small slope basins connected to the platform; and sedimentary deposits linked to Santa Elena Canyon.

Some of the basins in the three zones are superimposed on the deeper basins identified in the low resolution, high penetration SCAN seismic profiles provided by Hernandez (2014). Table 5.1 indicates the different names of basins used in the two studies.

Using the methodology given in Chapters 3 and 4, we interpreted the seismic facies in each basin -in terms of the lithology and depositional environments- and we discerned the principal unconformities used to identify the T-R sequences and their boundaries. The T-R sequences were grouped into three sets of sequences to build mega-sequences. These mega-sequences are from base to top: the Lower T-R (LTR), the Middle T-R (MTR) and the Upper T-R (UTR). The LTR and MTR mega-sequences are well exposed in the Jama basin, while the UTR is well developed in the San Lorenzo and Cojimíes basins. The LTR and MTR include 16 TR sequences. The UTR shows 10 TR sequences that have already described in Chapter 4.

The interpretation and correlation of the mega-sequences from one basin to another allowed us to analyze the regional evolution of the sedimentary accommodation caused by the tectonics in the margin, from Galera Cape to Salinas Point. In the following, we describe the characteristics of the mega-sequences in the different basins found in the study area.

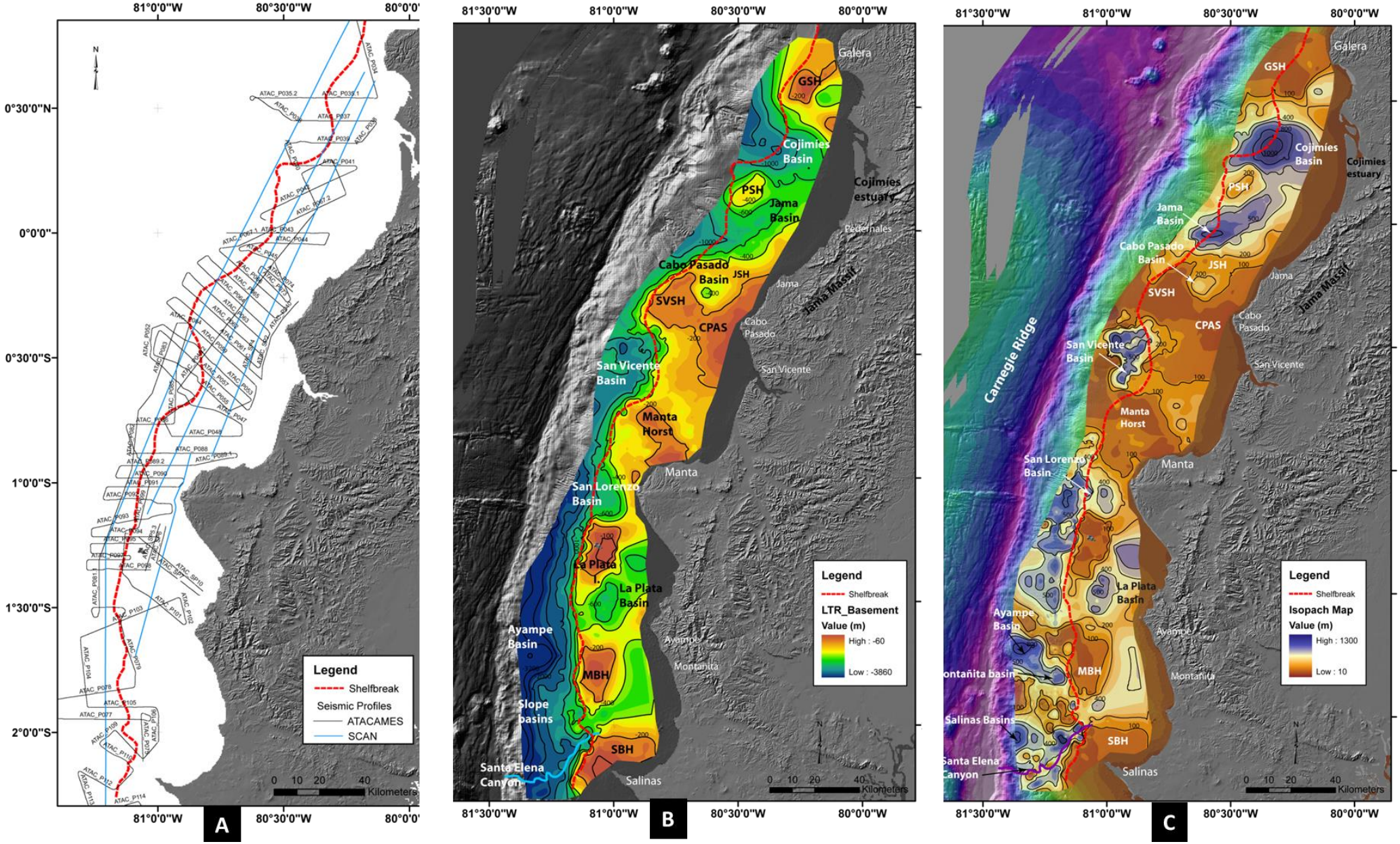

Figure 5.4: Isobath grid for the Pleistocene acoustic basement (left) and Isopach grid of the Pleistocenic deposits along the central Ecuadorian margin.

Figure 5.4- *A) Isobath grid for the Pleistocene acoustic basement (depth in meters). It shows the location of the Quaternary basin in the central Ecuadorian margin, as well as the structural highs. GSH: Galera Structural High; PSH: Pedernales Structural High; SVSH: San Vicente Structural High; CPAS: Cabo Pasado Anticline Structure; Manta Horst; La Plata Island; MBH: Montañita Bathymetric High; SBH: Salinas Bathymetric High. B) Isopach map of the Quaternary deposits along the central Ecuadorian margin. The thickest deposits are shown in blue and the thinnest ones in brown.*

_____

Quaternary basins (This work)	***Socle Map basins (Hernández, 2014)***
Cojimíes	Pedernales
Jama	
Cabo Pasado	
San Vicente	Bahía-Jama

Table 5.1: Table showing the names of the Quaternary basins identified in this work and names of the older basins interpreted by Hernández (2014)

3.1. The Northern zone

3.1.1. The Cojimíes basin

The Cojimíes basin is located in front of the Cojimíes estuary (Figure 5.4), where the shelf break shows a large landward reentrant (CE in Figure 5.1A). The isodepth map (Figure 5.4A) shows that its depocenter is 1500 m deep (1600-ms TWTT @ 1900 m/s). The basin is 48 km long in the E-W direction and extends from the upper slope to the inner shelf in the Cojimíes estuary. In the N-S direction, the basin encompasses the zone limited by the Galera structural high (GSH) to the north and by the Pedernales structural high (PSH) to the south (Figures 5.4 and 5.5), and is approximately 40 km long. The PSH location is related to the zone where the subduction of the Atacames double-peak seamount, described by Marcaillou et al. (2016), is located (Figure 2.4). The basin is filled with the three mega-sequences: LTR, MTR and UTR (Figures 5.5, 5.6 and 5.7D).

-The *LTR* group of sequences is at the base of the mega-sequences. It shows, around all the basins, an angular unconformity with the acoustic basement. In the N-S SCAN-425 seismic line onlap, it displays stratal terminations against the GHS and PSH (Figure 5.5A). However in the N-S SCAN-433 seismic line (Figure 5.5C), at the southern border of the basin, it displays reflectors truncated by the K9 fault. These reflectors seem to come from the Jama basin over the PSH. In the W-E direction, the seismic reflectors of the LTR show some onlap terminations against the acoustic basement, with a sheet drape external form (SCAN-972, Figure 5.7D). At the top, the LTR seismic reflectors show erosional truncations with an angular unconformity contact with

the overlaying MTR sequences. In the N-S direction, this group of sequences shows divergent concave and bag-shape seismic reflection configuration patterns (Figure 5.5A).

-The *MTR* group of sequences sits on the LTR sequences and displays an angular contact (Figure 5.5A). At the base, it displays onlap terminations against the LTR sequences in the N-S direction and a downlap stratal termination in the W-E direction (Figures 5.5 and 5.7). At the top, the seismic reflectors appear to be highly truncated by the upper contact with the UTR sequences (black arrows in Figure 5.7D). In the N-S direction, the MTR sequences show divergent concave and bag-shape reflection configuration patterns, similar to the LTR sequences (Figures 5.5A and C). In the W-E direction, it exhibits prograding clinoform seismic reflection patterns (on the eastern side of the basin) and a migrating wave to chaotic seismic reflection configuration (on the western side of the basin) (Figure 5.7D).

-The *UTR* sequences are over the MTR sequences with an angular unconformity. In the N-S SCAN 425 seismic line, the UTR are on top of the GSH and the PSH showing a direct angular discordance with the acoustic basement. In the landward direction, in another N-S seismic line (SCAN-433, Figure 5.5C), this group of sequences appears to cross the southern structural border of the basin (PSH) coming from the Jama basin. In the W-E seismic profiles, it shows downlap terminations against the eroded contact with the lower MTR sequences, showing an angular unconformity (black arrows in Figure 5.7C and D).

The Atacames seismic profile AtacP039 (Figure 5.7A) allowed us to detail the UTR sequences identifying the transgressive systems tract (TST) and regressive systems tract (RST) of the 10 T-R sequences numbered from I to X (Figure 5.7C), similar to the San Lorenzo basin (Chapter 4, Figure 4).

The 10 T-R sequences display an aggradational wedge external form, but internally there are different types of prograding clinoform seismic reflection patterns (Mitchum et al., 1977).

Sequences I to III present internal oblique tangential progradational seismic reflection patterns, with sheet drape to wedge external forms. Internally, these sequences display an angular unconformity contact between them, with truncations at the top of the sequences. However, at the top of sequence III, there is a sharp erosional truncation of the seismic reflectors, displaying an angular discordance with the upper sequence IV (white arrow in Figure 5.7C). In the N-S SCAN-425 seismic line, sequences I to III appear to display prograding clinoforms. These clinoforms are at the southern border of the basin, over the PSH. They seem to prograde towards the north (to the basin's depocenter) and appear to be truncated at the top by the seafloor.

Sequences IV and V lay on the truncated sequence III, showing downlap terminations and forming an angular unconformity with the lower sequences I to III (white arrow in Figure 5.7C). At the top of the two sequences (top of sequence V), they show toplap stratal terminations against the upper sequence VI. In general, they present a complex sigmoid-oblique seismic reflection configuration with a wedge to bank external form. These lower five T-R sequences present an overall progradation stacking pattern in the Cojimíes basin, which is shown in the W-

E Atac039 seismic line (purple dotted line in Figure 5.7C). However in the N-S SCAN-433 seismic profile, sequences I to V display prograding clinoforms that come down from the Jama basin (Figure 5.5C). These clinoforms are over the PSH, crossing the structural boundary between the Cojimíes and Jama basins.

In the Atac039 seismic line, sequences VI and VII exhibit a significant landward migration of the offlap break with respect to the lower five sequences (see the purple dotted line in profile Atac039C). Sequences VIII and IX are prograding seaward with respect to sequences VI and VII, showing a complex sigmoid-oblique stacking pattern. Sequence X is a thin sequence that sits at the top of eastern side of the UTR, with an angular unconformity above sequence IX. The N-S seismic lines (Figures 5.5B and C) show that sequences VI to X are not connected to the Jama basin; they are totally developed in the current depocenter of the Cojimíes basin.

The principal structures around the Cojimíes basin provide a framework for the general behavior of the basin. To the north of the basin, there are some faults related to the GSH (Figure 5.6). Some of them cross the acoustic basement and the LTR, MTR and UTR sequences before reaching the seafloor.

Figure 5.5- A) SCAN 425 seismic line interpretation. It displays the quaternary basins and the principal structures in the Galera-Manta zone. The Cojimíes, Jama and Cabo Pasado basins appear to be separated from the San Vicente basin by the CPAS (the SVSH does not crossing this seismic line). The San Vicente basin is limited to the south by the Manta Horst. The northern basins of the CPAS show a decrease in their thickness from north to south (from Cojimíes basin to Cabo Pasado basin). B) Details of the configuration of the T-R sequences in the northern zone of the Pedernales Structural High (PSH), related to a seamount subduction. It shows that sequences I to III are divergent and thickest towards the south (just above the seamount location), while sequences IV to X are divergent and thickest towards the northern side (actual depocenter of the Cojimíes basin). C) SCAN-433 seismic line interpretation around the Jama and Cojimíes basins. It shows the union between the two basins on the eastern side of the PSH. D) Location of the SCAN-425 and SCAN-433 seismic profiles.

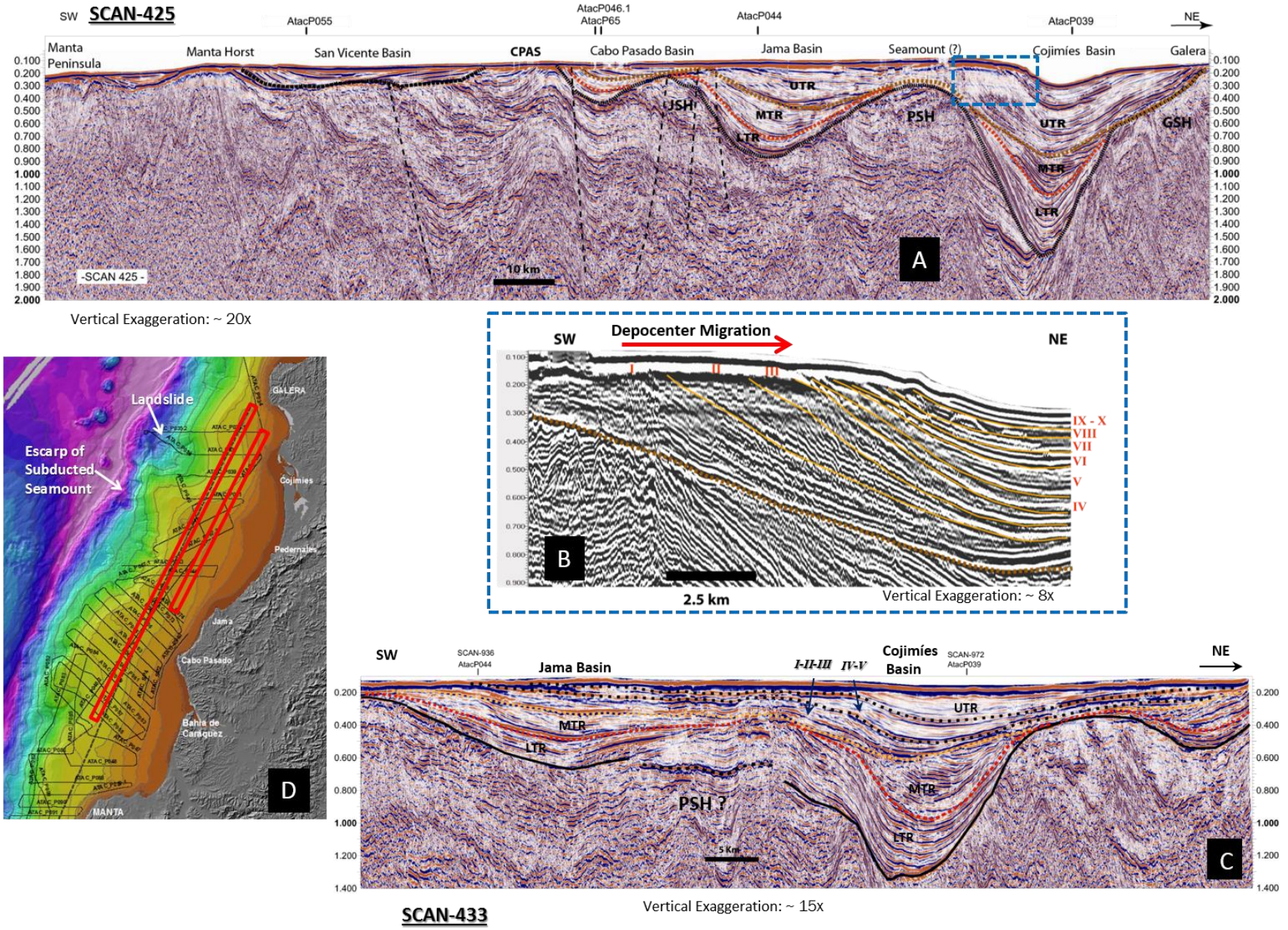

Figure 5.5: The NE-SW multichannel seismic lines along of the Nortern zone basins.

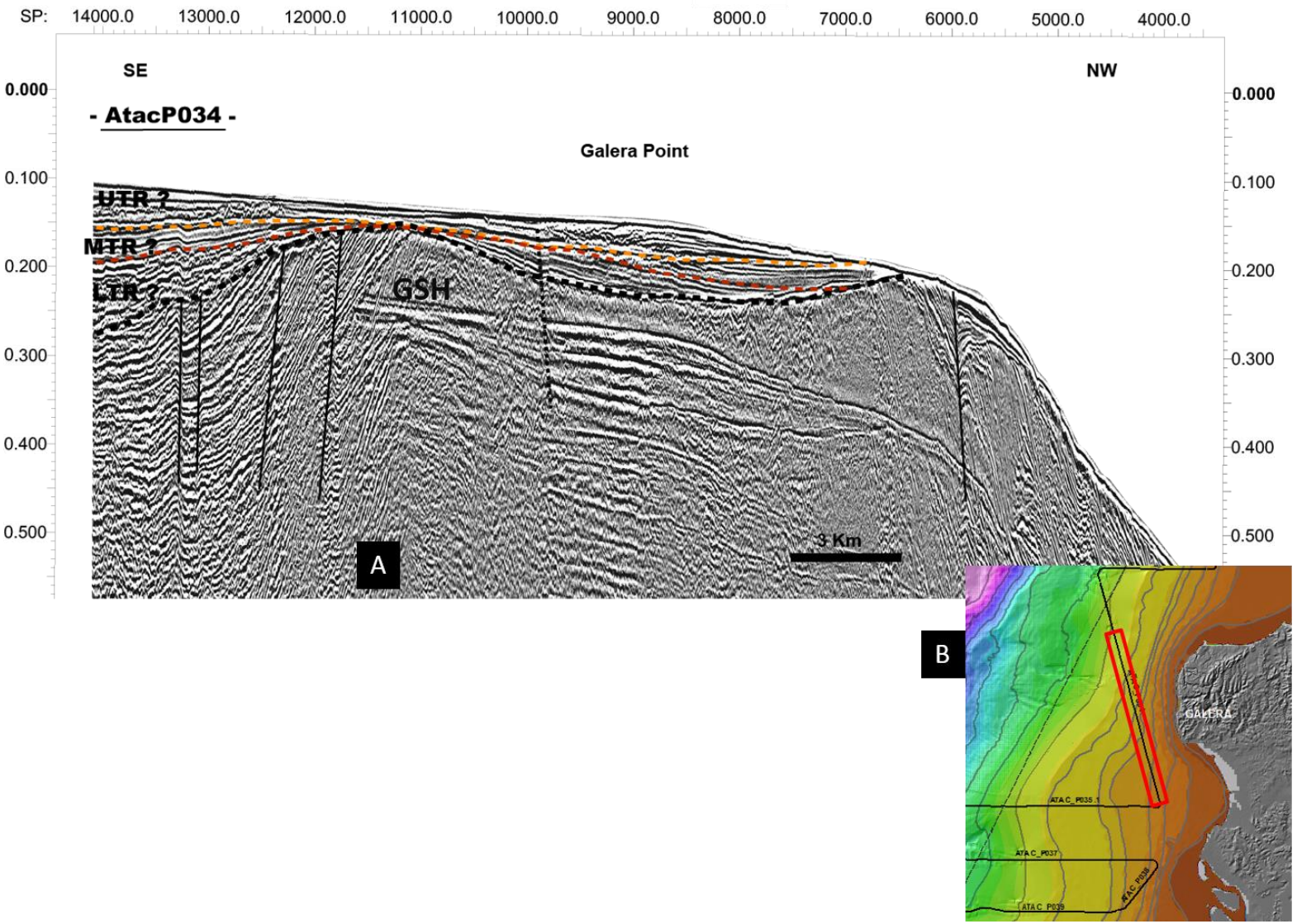

Figure 5.6: Seismic profile interpratation showing the interpreted TR sequences in front of Galera Cape.
A) AtacP034 seismic profile, showing the interpreted TR sequences in front of Galera Point. We can note the uplift of the Galera Structural High (GSH), which borders the Cojimíes basin on the northern side. B) Location of the seismic line in the margin.

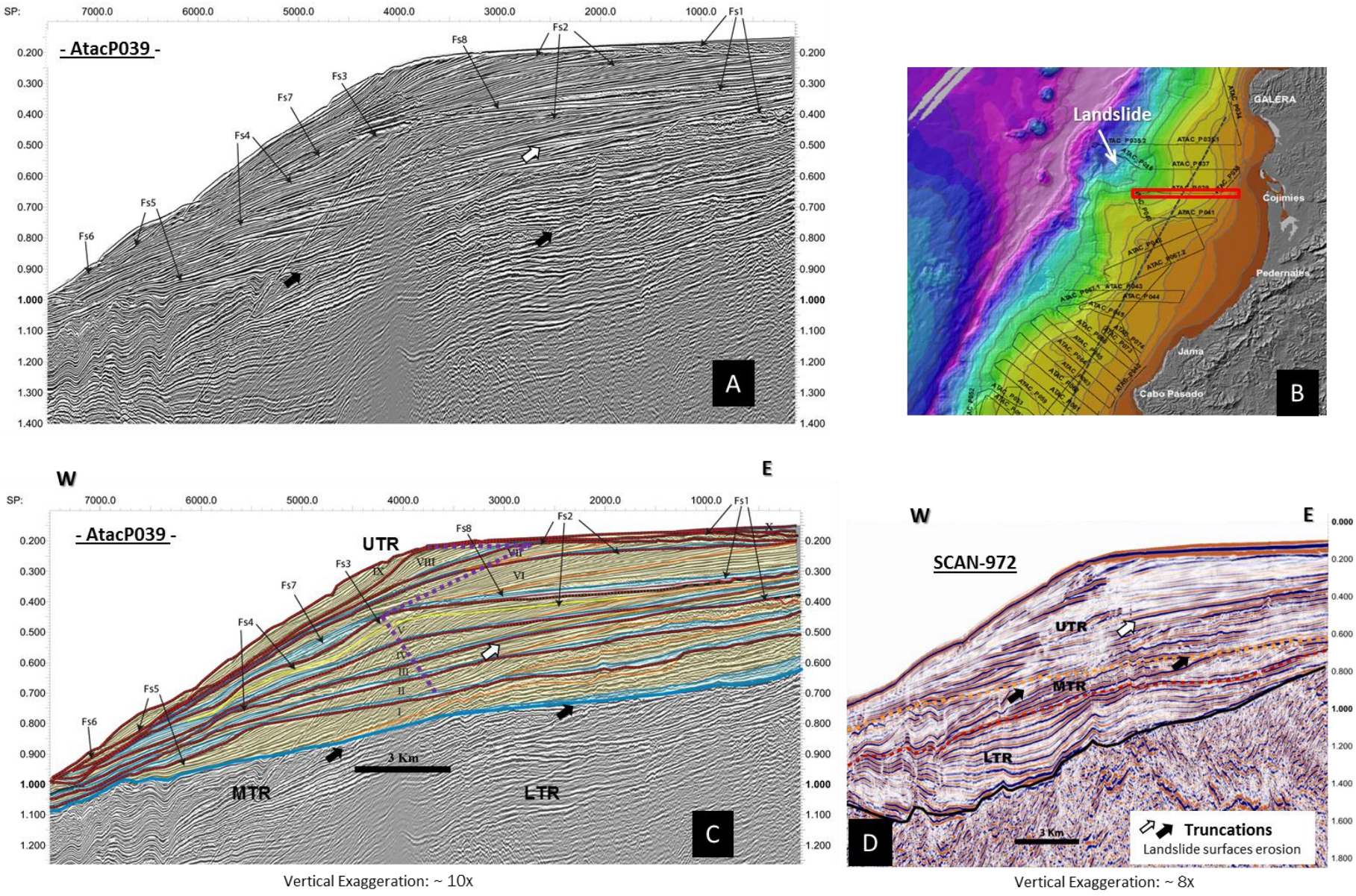

Figure 5.7: Seismic profile showing in the Cojimíes basin: the seismic facies, the T-R sequences and System Tracts

Figure 5.7- *A) AtacP039 seismic profile showing the interpreted seismic facies in the Cojimíes basin. B) Location of the AtacP039 and SCAN-972 seismic profiles (one above the other). C) Interpretation of the T-R system tracts for the upper set of sequences (UTR). The transgressive systems tracts are shown in light blue and the regressive systems tracts are shown in yellow. The purple dotted line shows the progradation-aggradation trend of the sequences from I to V, the landward migration of the offlap break in sequence VI, and the progradation from sequences VII to IX. D) Interpretation of the SCAN-972 seismic line. This line shows the LTR and MTR groups of sequences, which could not be identified in the Atacames seismic line.*

_____

3.1.2. The Jama basin

The Jama basin is located in the offshore area between the coastal cities of Pedernales and Jama. The basin is oriented in a NE-SW direction parallel to the onshore Jama Massif and to the dextral Jama Fault System (Figure 5.4). The basin deepens towards the edge of the continental platform reaching 850 m in depth (900 ms TWTT @ 1900 m/s). It is bounded to the north by the PSH and to the south by the Jama structural high (JSH) (Figure 5.5A).

Like the Cojimíes basin, the Jama basin is filled by the three mega-sequences LTR, MTR and UTR. In this basin, the LTR and MTR are very well exposed and they are comprised of 16 interpreted T-R sequences (see the Atacames profile P044, Figure 5.9). From base to top, the LTR is comprised of sequences Q to F (11 T-R sequences), the MTR cover is made up of sequences E to A (five T-R sequences). The UTR encompasses the 10 upper T-R sequences I to X (Figure 5.8B).

-The *LTR* presents a set of progradational T-R sequences from oblique tangential (Q to J) to complex sigmoid-oblique (H to F) reflection patterns (Figures 4.8A and 4.9A). Some of the T-R sequences are truncated and incomplete, but it was possible to identify their internal reflection patterns (Figure 5.9A): from high continuity, high to average frequency, high to average amplitude with a parallel configuration linked to the Fs8 of the TST (See Table 4.1, Chapter 4) to average continuity, high amplitude with a hummocky configuration related to the Fs1 of the RST (see Table 4.1, Chapter 4). These set of sequences show apparent onlap to tangential downlap terminations against the acoustic basement (orange arrows in Figure 5.9). The LTR mega-sequence is internally truncated by three unconformities: one is between P and O, another is between M and L and the last is between J and H. These unconformities separate four groups of TR sequences (QP-OM-LJ-HF), which show a progressive landward migration of the successive offlap breaks (Figure 5.8A). The clinoforms are tilted in a landward direction and their offlap break is above the flat of the bank, at least from the LJ group of sequences (the OM group also seems to be inclined, but this is not very clear) (Figure 5.8A).

In the SW-NE seismic profile (Figure 5.8B), the LTR set of sequences shows a divergent reflector pattern towards the center of the basin, together with changes in the thickness of the TR (observe the differently sized red arrows between the southwest edge of the basin and the middle of it).

-The *MTR* is comprised of sequences E to A, which present an overall complex sigmoid-oblique progradational configuration pattern. The internal reflections of the TR sequences show a high amplitude subparallel configuration overlain by a sigmoid to complex sigmoid-oblique configuration. The best-developed sedimentary wedge is sequence E, which shows a transgressive-lag seismic facies (Fs8) at the base, overlain by regressive seismic facies tracts Fs5, Fs4, and Fs3 (Figure 5.9A). At the top of this sequence, it is possible to distinguish seismic facies Fs1, suggesting a fluvial environment (like in Table 4.1, Chapter 4). This succession is probably a general pattern for all of the T-R sequences, at least in the MTR. This set of sequences shows landward tilted clinoforms, similar to the LTR sequences, stacked vertically with an internal progradation trend (Figure 5.8A). However, all together, the set of MTR sequences displays an uplift and landward shift of the offlap break, following the general trend shown in the LTR sequences (Figure 5.8A), as well as a landward migration of the depocenter.

On the SW-NE profile (Figure 5.8B), the MTR sequences display the same pattern as the LTR sequences, i.e. divergent seismic reflectors from south to north, with sequences thickening in the central zone of the basin (see the different heights between the blue arrows located at the southwest border of the basin and its central part).

-The *UTR* presents a set of oblique tangential to shingled prograding TR sequences (Figure 5.9A). The internal configurations of the TR sequences, when they are not obscured by multiple reflections, are similar to the LTR and MTR sequences. This group of sequences shows three internal well-marked unconformities: a lower one, between III and IV; a middle one between V and VI, and an upper one between VII and VIII. These angular unconformities subdivide the UTR into four sets of TR sequences: I-III, VI-V, VI-VII and VIII-X (Figure 5.9A). In sequence set I-III, only sequence I displays a well-preserved clinoform pattern with a well-defined offlap break, while sequences II and III are partly eroded. The best-preserved zone of sequence II exhibits sigmoid reflection patterns. Sequence III shows a shingled reflection configuration (Figure 5.9). The set of sequences IV-V displays a wedge external form, overlaying sequence III with onlap stratal terminations (Figure 5.9A). Sequences VI and VII are over sequence V, displaying onlap terminations and showing a bank external form with their thickest zone oriented towards the east (landward direction). Typically, they show parallel to divergent seismic reflection configurations with hummocky reflection patterns at the top of each sequence in a landward direction, (Figure 5.9A). Sequences VIII-X show a wedge shape external form (Figure 5.9A) with a pinch-out to the west. The sequences are thin and truncated; the best and thickest is sequence VIII, which displays a landward divergent reflection configuration. Sequences IX and X show hummocky reflection configuration patterns at the top of the sequences (Figure 5.8A).

In the UTR group of sequences, only sequence I shows a clear offlap break (Figure 5.9). This offlap break is shifted 3 km in a landward direction with respect to the MTR offlap break. The other sequences do not show evidence of offlap breaks, which have been eroded out at the seafloor, but the general trend of the overall UTR sequences shows a progressive tilt and depocenter migration in a landward direction. This suggests that the UTR sequences followed the uplift tendency of the offlap break observed in the LTR and MTR mega-sequences.

The SW-NE seismic profile (Figure 5.8B) shows that the UTR depocenter migrates in a northern direction with respect to the LTR and MTR depocenters, as well as a differential thickness between the rim of the basin and its central part, as in the LTR and MTR sequences (see the different highs between the yellow arrows located in the different zones of the basin).

The SCAN-425 seismic line shows some faults that delimit the Jama basin from the Cabo Pasado basin. These faults dip towards the north and towards the south. They appear to reach the seafloor and to be related to the origin of the JSH.

Figure 5.8- A) SCAN-936 seismic line interpretation. It shows the general behavior of the LTR, MTR and UTR sequences in the W-E direction in the Jama basin (see the details in the text). B) Zoom of the SCAN-425 seismic line (shown in Figure 5.5A), which displays the interpretation of the sequences in the Jama basin in a N-S direction. The red, blue and yellow arrows displayed in both profiles show the different thicknesses of the LTR, MTR and UTR mega-sequences in the basin.

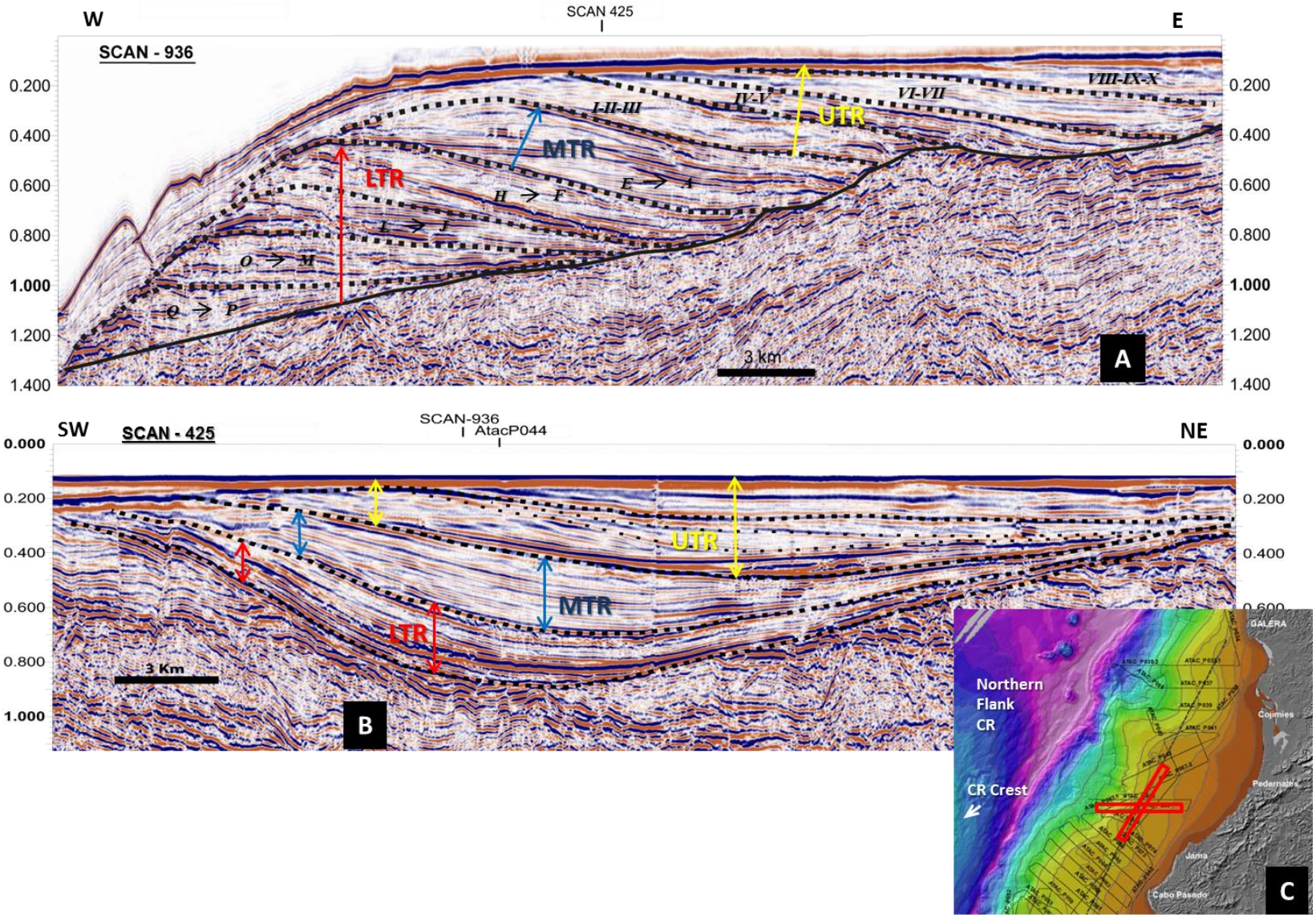

Figure 5.8: SCAN-936 seismic line interpretation in the Jama basin. It shows the general uplift of the LTR, MTR and UTR sequences in the W-E direction and the different thicknesses of the mega-sequences in N-S direction.

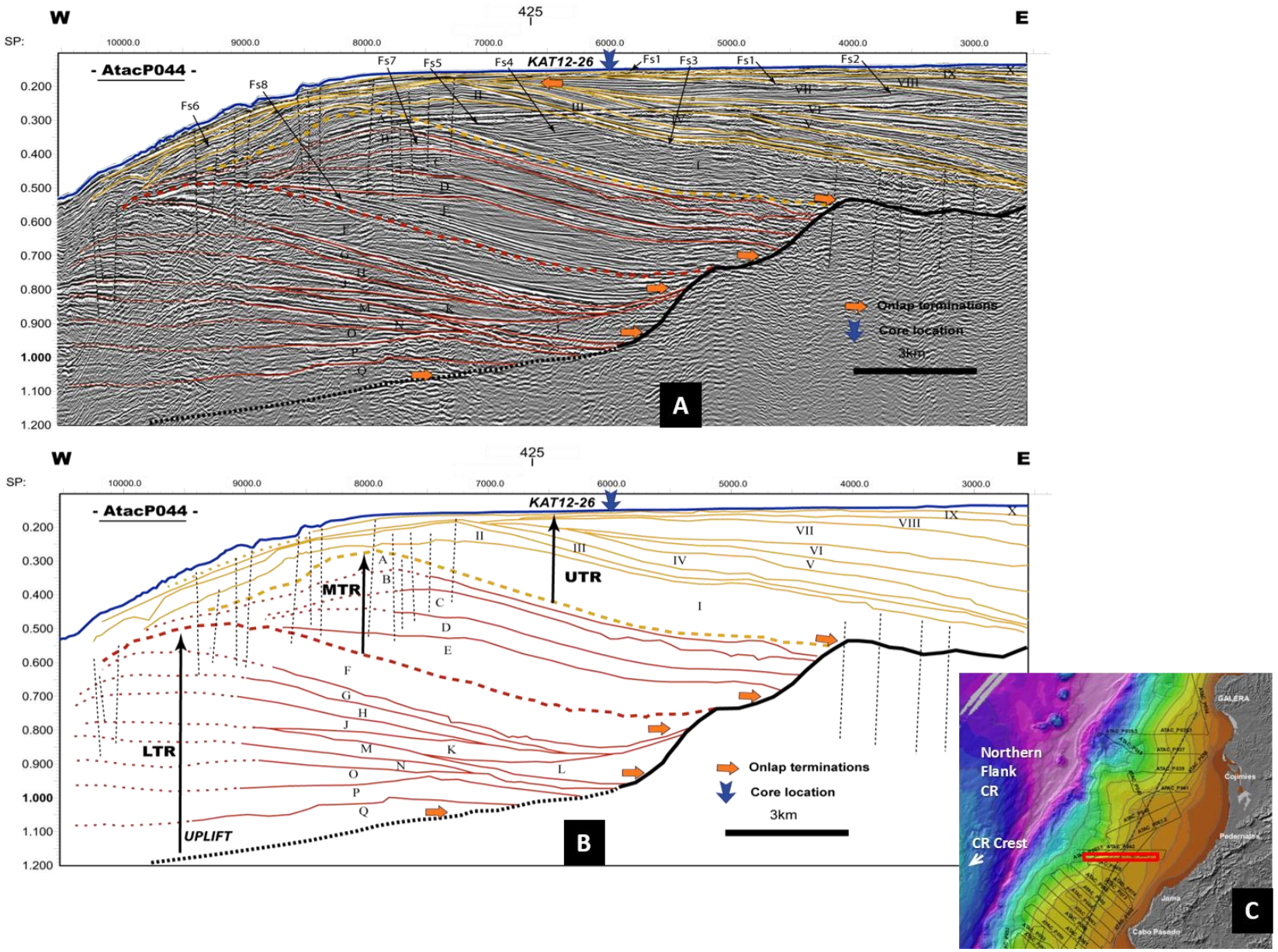

Figure 5.9: AtacP044 seismic profile with the interpretation of the seismic facies and the T-R boundaries in the Jama basin.

Figure 5.9- *A) AtacP044 seismic profile with the interpretation of the seismic facies and the T-R boundaries in the Jama basin. B) Interpreted groups of stacking patterns for the T-R sequences (mega-sequences). They are limited by the dashed Lower T-R (LTR), Middle T-R (MTR) and Upper T-R (UTR). These groups of stacking patterns show, in general way, a constant uplift of their offlap break (shown with vertical arrows), as well as a constant shift in the depot center for the three groups of mega-sequences in a landward direction. C) Location of the AtacP044 seismic profile.*

_____

3.1.3. The Cabo Pasado basin

The Cabo Pasado basin shows a thin sedimentary fill, reaching a maximum depth of 420 m (450 ms-TWTT @ 1900 m/s) (Figure 5.4A). This basin exhibits a circular shape with a central depocenter located to the northwest of Cabo Pasado Cape (Figure 5.4). It is bounded to the north by the JSH and to the south by the Cabo Pasado Anticline Structure (CPAS) (Figures 5.5A and 5.10A). The CPAS, which is located close to the onshore Jama Massif, appears to be a fold in the SW-NE seismic profile (AtacP-046 in Figure 5.10A) with its hinge zone outcropping at the seafloor in an E-W direction. The limbs of the anticline are at the base of the Quaternary sequences and they show divergent reflection configuration patterns towards the north and south.

To the west, this basin is bounded by an uplift of the edge of the platform (Figure 5.10B). This uplift of the border of the platform, called the San Vicente Structural High (SVSH) here, is separated from the CPAS by strike-slip faults according to the structural scheme proposed by Hernández (2014). The basin thins towards the east and it seems to reach the coastal zone between village of Jama and Cabo Pasado Cape (Figure 5.10B).

We recognize all three groups of TR sequences, i.e. LTR, MTR and UTR, as shown on the SW-NE AtacP046.1 and NW-SE AtacP065 seismic profiles (Figure 5.10).

-The *LTR* sequences in the SW-NE profile overlay the CPAS following the arched shape of the anticline. These sequences present a bank external form with their thickest part facing to the west (red arrows in Figure 5.10A), while their thinnest part and tip are directed towards the east. The sequences show divergent seismic reflection configurations towards the west. The basal contact with the acoustic basement is concordant around the CPAS, but it shows an angular unconformity with the underlying mega-sequence at the toe of the anticline.

On the NW-SE seismic line, the LTR sequences overlay the uplifted border of the platform, displaying a similar external form as in the SW-NE profile, i.e. a bank following the arched shape of the acoustic basement with the thickest part facing westwards. On the NW-SE profile, the reflectors also appear to be divergent towards the west, but are always in angular unconformity with the acoustic basement. In both profiles, on the uplifted side of the sequences (where the LTR sequences outcrop on the seafloor), the reflectors appear to be sharply truncated, but in the NW-SE seismic profile, the LTR seems to have crossed the uplifted acoustic basement.

-The *MTR* sequences display a wedge external form along the SW-NE seismic section (Figure 5.10A), which thickens to the west and thins to the east, with a downward arched shape as observed in the LTR sequences. They show a slightly divergent configuration reflection pattern towards the east. In the NW-SE profile (Figure 5.10B), this group of sequences displays a sigmoid-sheet external form with a divergent internal reflection pattern towards the east. In both seismic profiles, the internal reflectors of these sequences are generally concordant with the LTR sequences; however, the MTR sequences show an eastward displacement of the depocenter with respect to the LTR (see the blue arrows in both profiles). The reflectors of this group of sequences are also sharply truncated at the seafloor, in both profiles, but as seen with the LTR, the MTR seems to have crossed the uplifted acoustic basement in the NW-SE seismic line.

-The *UTR* sequences show a sigmoid-sheet external form. The two seismic profiles, SW-NE and NW-SE, show internal unconformities in the UTR bounding sets of subparallel to divergent reflections configuration patterns towards the east. These sets are interpreted as the 10 sequences of the UTR. These sequences are thin, but when correlated with the Jama basin, they can be subdivided into four groups of sequences: I-III, VI-V, VI-VII and VIII-X (Figure 5.10). The internal reflectors from sequences I to V appear to be arched downward, while the reflectors from VI to X appear to be sub-horizontal. Altogether, the four groups of sequences present a general movement of the depocenter towards the east with regards to the MTR depocenter (see the yellow arrows in both profiles).

The SCAN-425 seismic profile shows a series of faults that limit the southern side of the Cabo Pasado basin with the CPAS. The Atac46.1 seismic profile (Figure 5.10A) additionally shows some faults at the base of the Cabo Pasado basin, which appear to be sealed by the three groups of mega-sequences. The AtacP065 seismic line (Figure 5.10B) displays some structures related to the SVSH that cut the acoustic basement and reach the seafloor. Another group of faults appears on the eastern side of the SVSH, cutting the LTR sedimentary sequences. These groups of structures seem to be related to deep faults with an unknown behavior.

Figure 5.10- *A) AtacP046.1 seismic profile interpretation. The Cabo Pasado Anticline structure (CPAS) is located on the southwestern side of the line, acting as a southern barrier for the Cabo Pasado basin (CPb). The CPb shows the same stacks as the Jama basin: LTR, MTR and UTR. B) The interpretation of the AtacP065 seismic profile shows the uplift of the border of the platform, called the San Vicente Structural High (SVSH) in this work. The red, blue and yellow arrows locations indicate the shift in the depocenter for the three groups of sequences, in both lines, towards the east. C) Location of Atacames seismic profiles AtacP046.1 and AtacP065.*

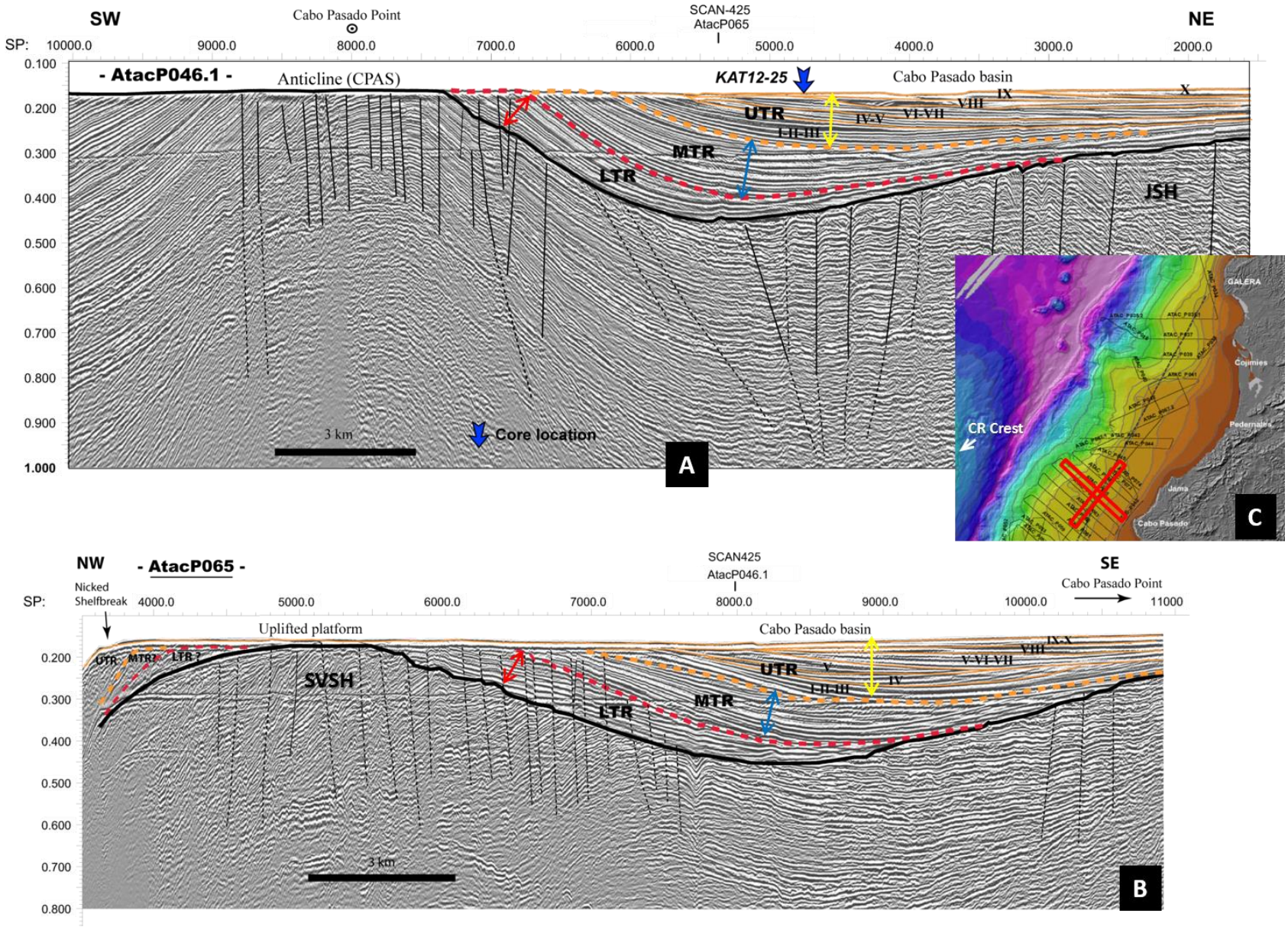

Figure 5.10: AtacP046.1 seismic profile interpretation in the Cabo Pasado basin.

3.1.4. The San Vicente basin

The San Vicente basin is located in front of the city of San Vicente (Figure 5.4). It crosses through the platform and stepped terrace of the upper slope (Figure 5.1). The deeper zone of the San Vicente basin sits from the shelf break to the stepped slope until a water depth of 1500 m (1580 ms-TWTT @ 1900 m/s) (Figure 5.11A). The basin is filled by c. 850 m of sediments (900 ms-TWTT @ 1900 m/s). The thinnest zone of the basin is 95 m thick on the platform (100 ms-TWTT @ 1900 m/s) (Figures 5.11B and 5.4).

This basin is limited to the north by the SVSH and CPAS, which isolate this basin from the other northern basins, and to the south by the Manta Horst, which separates this basin from the Central basins (Figures 5.4 and 5.5A; Hernández, 2014). The western side of the basin is bounded by an uplifted wall of the acoustic basement which forms the bathymetric indentation shown on bathymetric profile B-B' (Figure 5.1D). The eastern side the basin is close to the coastal zone (Figure 5.11B).

The three groups of sequences, LTR, MTR and UTR, were identified in the thickest sector of the basin, but only the thinnest zone records some UTR sequences.

- The *LTR* sequences were interpreted in the zone between the shelf break and stepped slope. They were also identified in some areas on the western side of the uplifted wall of the slope, crossing the morphological indentation (Figure 5.11A). In the W-E 896-SCAN seismic line (Figure 5.11B), they display an angular unconformity with the acoustic basement; in general, they show a concave bank external form with a low amplitude sub-parallel to a bag-shape reflection configuration pattern. Some localized areas in the sequences show a low-amplitude chaotic reflection pattern, e.g. on the eastern side of the uplifted wall. This group of sequences shows a thickness variation between the border of the basin and its central part (see the red arrows in Figure 5.11B). In the Atacames profiles, they appear to be obscured at the base of the basin by the multiple reflections; however, in the zone below the shelf break, the LTR sequences appear to be uplifted and perturbed by the acoustic basement, showing some knolls which seem to be diapirs (Figure 5.11C).

- The *MTR* set of sequences were also only interpreted on the western side of the shelf break, in the stepped slope zone of the basin and in some areas on the western side of the uplifted wall of the slope (crossing the bathymetric indentation) (Figure 5.11A). As in the LTR sequences, they are not well distinguished in the Atacames seismic line due to the multiple reflections, but it is possible to also describe the MTR from the W-E SCAN-896 profile (Figure 5.11B). They overlay the LTR sequences showing a relative concordance with a downward curved sheet external form. They present average to high amplitude reflectors with a subparallel seismic reflection configuration pattern that is tight on the border of the basin and loose in the depocenter zone. The MTR sequences, like the LTR sequences, show an internal thickness variation between the depocenter and the border of the basin. The MTR sequences also appear below the shelf break, for which the contact with the LTR sequences is hidden by the multiple reflections, but they present a sub-vertical contact with the acoustic basement.

- The *UTR* sequences display an overall sigmoid-sheet external form overlaying the MTR sequences with an apparent concordance in some sectors of the basin (e.g. around the depocenter); but when examined in further detail, they show an angular discordance (e.g. at the edges of the thicker zone) (Figure 5.11B). This group of sequences is well identified on the W-E Atacames seismic line, where we found the 10 T-R sequences in the thicker zone of the basin. The 10 T-R sequences broadly show high amplitude, average to high continuity and average frequency reflectors with a subparallel seismic reflection configuration. The reflectors appear to be tight on the border of the stepped slope of the basin and separated in the depocenter zone (Figure 5.11C). In further detail, the UTR show three marked internal unconformities, i.e. between sequences III and IV, between sequences IV and V and between sequences VII and VIII, which are well distinguished in Figure 5.11B (black points in the UTR) and on the Atacames seismic line (red arrows in Figure 5.11C). On the steeped slope zone of the basin, the UTR sequences show a thickening from its border to the depocenter, as observed in the LTR and MTR.

Around the shelf break, sequences I to V display angular discordances with the MTR and do not reach the platform. Sequences VI and VII appear on the platform and have a direct angular contact with the acoustic basement, showing subparallel horizontal reflection configuration patterns. Sequences VIII to X overlay sequences VI and VII and the T-R sequences with a relative concordance.

There is a series of faults around the San Vicente basin that presents a different behavior from the platform to the slope. A principal positive flower structure with diapirs underlines a zone around the shelf break. Some of these faults outcrop close to the seafloor. Further downslope, in the stepped part, negative structure flower seems to control the deepest sector of the basin, which corresponds to the negative structure flower shown by Collot et al. (2004). On the western side of this negative structure flower, at the limit of the basin, there are reverse faults that outcrop at the seafloor and which seem to be related to the bathymetric indentation.

Figure 5.11- *A) SCAN-896 seismic profile interpretation. In this zone, there are a series of faults that control the geological framework from the shelf to the slope. B) Zoom of the SCAN-896 at the thickest area in the San Vicente basin (into the steeped slope zone), which shows the three groups of T-R sequences interpreted in this basin (from LTR to UTR). The red, blue and yellow arrows indicate the different thicknesses of the LTR, MTR and UTR mega-sequences in the basin. C) AtacP057 seismic line interpretation, where the details of the UTR sequences on the slope and platform are shown. D) Location of the seismic lines.*

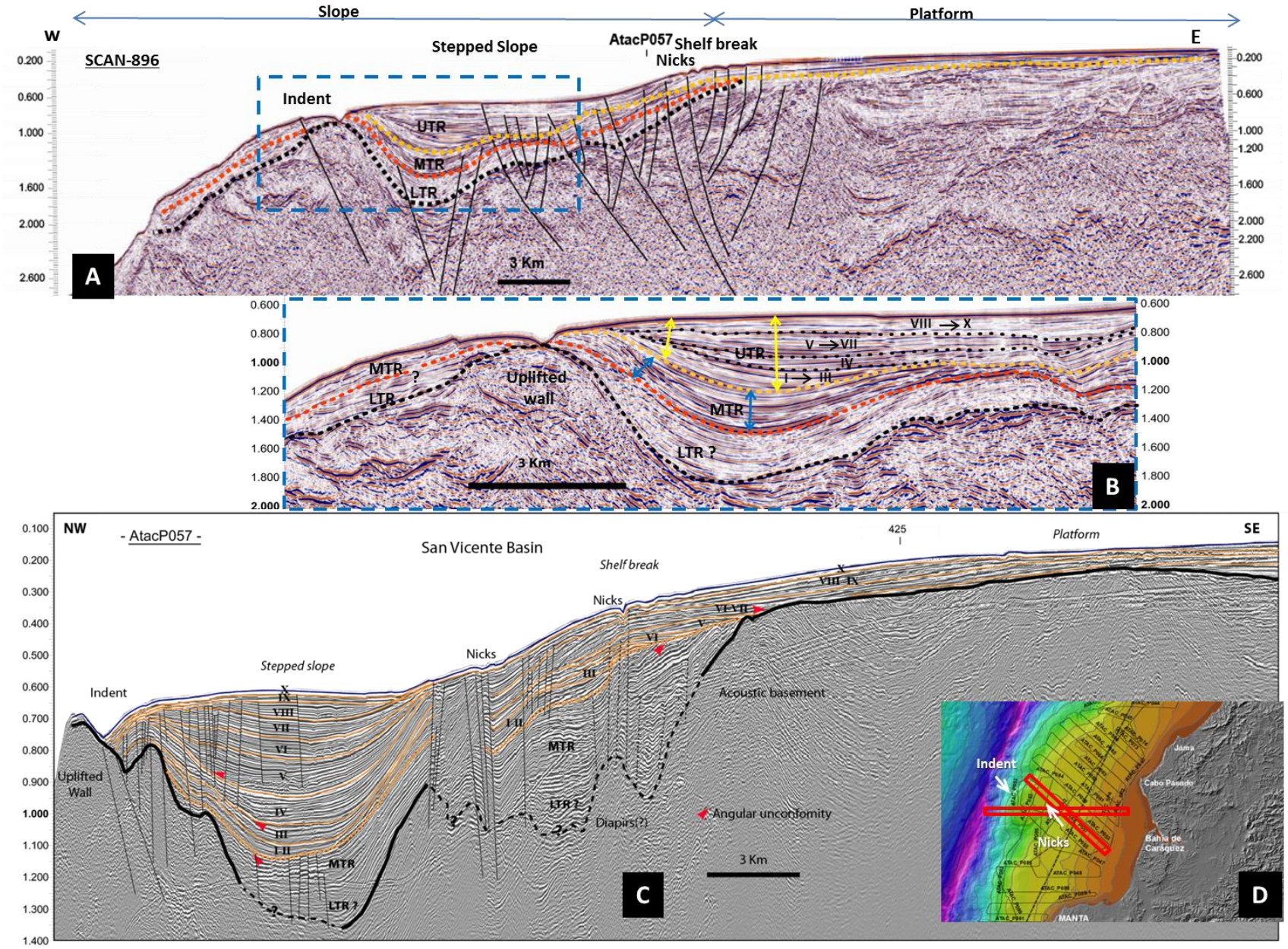

Figure 5.11: SCAN and Atacames seismic profiles interpretation in the San Vicente basin.

3.2. The Central zone

The Central zone comprises two main basins: the San Lorenzo basin, sitting in front of Manta Peninsula, and the La Plata basin, located to the SW of La Plata Island (Figure 5.4).

3.2.1. The San Lorenzo basin

In general, the San Lorenzo basin has a convex landward external morphology, with a depocenter as deep as 1000 m in terms of water depth (1100 ms-TWTT @1900 m/s) and 380 m thick (400 ms-TWTT @ 1900m/s). This basin encompasses the present day platform and the slope in front of Manta Peninsula (see the SCAN-844 profile in Figure 5.12). It extends in a north to south direction, from the Manta Horst to La Plata Island (Figure 5.4). The three groups of sequences, LTR, MTR and UTR, were identified in this basin (Figure 5.12A), but the best-preserved group of sequences is the UTR, which were well described in Chapter 4. Below, we present some general characteristics of these three sets of sequences.

- At the base, the *LTR* sequences show an angular unconformity with the acoustic basement. This group of sequences is present mostly on the slope. On the platform, they are located in small specific or local zones, like small cavities, controlled by normal faults according the SCAN-844 seismic line (Figure 5.12A). On the slope, they extend from the shelf break to the trench; however, they are thickest in the middle slope affected by normal faults. They present a subparallel seismic reflection pattern, which follows the shape of the contact surface with the acoustic basement. However, around the faulted zone on the middle slope, the sequences show a hummocky to chaotic reflection configuration pattern.

- The *MTR* sequences overlay the UTR sequences with an angular unconformity, and they were interpreted at the same places as for the LTR, i.e. mainly at the slope, from the shelf break to the trench, and at the platform into the local cavities. Contrary to the LTR, the thickest zones of the MTR sequences encompass the zone from the shelf break to the middle slope. In a general manner, this set of sequences shows a subparallel reflection configuration, as in the LTR sequences.

- The *UTR* sequences sit through an angular unconformity on the MTR sequences. They were identified from the platform to the foot of the slope, but they are well preserved on the platform. On the platform, they present the 10 T-R sequences described in Chapter 4.

The differential preservation of the LTR and MTR between the platform and the slope in this basin is shown in the N-S seismic profiles provided in Figure 5.13. SCAN-N32 (Figure 5.13A), located in the platform zone (Figure 5.13C), shows in front of Manta Peninsula the deposition of the UTR sequences only, which are deposited in an angular unconformity with the acoustic basement, while SCAN-417 (Figure 5.13B), located in the slope zone (Figure 5.13C), displays the LTR and MTR below the UTR.

The structural geology in this zone is complex, and it encompasses deep structures as shown in the N-S seismic profiles (Figure 5.13). In addition, we can also note that some of these structures cut the UTR sequences and seem to reach the seafloor. One of these structures is the

fault located just in front of Manta Peninsula. However in a seaward direction along the SCAN-844 seismic line (Figure 5.12A), we identified some normal faults on the platform and slope that cut the acoustic basement to the base of the UTR sequences without going to the seafloor.

3.2.2. La Plata basin

La Plata basin is located around La Plata Island, from the platform to the slope (Figure 5.12B). On the platform, the basin is located between the island and coast (see the AtacP101 seismic line in Figure 4.7). To the southeast of La Plata Island, the basin shows a circular shape measuring 15 km wide, 660 m deep (700 ms-TWTT @ 1900 m/s) and 430 m thick (450 ms-TWTT @ 1900 m/s) (Figure 5.4). Near the coast, the depth and thickness of the basin are difficult to evaluate because the single-channel sparker data do not show the acoustic basement, but we interpolate a depth of approximately 500 ms-TWTT, i.e. a depocenter with a depth of approximately 475 m.

On the platform zone of La Plata basin, the 10 UTR sequences (Figure 5.12B) show an angular unconformity with the acoustic basement (Figure 5.13A). However, as in San Lorenzo basin, some local zones could present the LTR and MTR, as shown in the deepest zone of the AtacP103 seismic profile (Figure 5.12B) or on the southern side of La Plata Island in the SCAN-N32 seismic line (Figure 5.13A), but this is not clear. On the slope zone of the basin, on the western side of La Plata Island, the three groups of sequences, LTR, MTR and UTR, are shown in the SCAN-417 seismic profile (Figure 5.13B), which shows a lateral continuity with the groups of sequences from the San Lorenzo basin.

- The *LTR* sequences show an angular unconformity with the acoustic basement. Based on the SCAN-417 seismic line, the internal configuration of the sequences is not clear, but we believe that they present a similar configuration to the LTR sequences of the San Lorenzo basin, through a lateral correlation.

- The *MTR* sequences overlay the LTR sequences with an angular unconformity. Like the LTR sequences, the internal configuration should be similar to the MTR sequences of the San Lorenzo basin.

- The *UTR* sequences show the 10 T-R sequences on the platform with a W-E lateral variation, from clinoforms with hummocky seismic reflection configuration patterns on the eastern side of the basin (towards the land) to bag-shape external forms with subparallel reflection configuration patterns on the western side of the basin (towards the sea; Figures 4.7 and 5.12B). The UTR have been well described in Chapter 4.

The SCAN-N32 seismic profile (Figure 5.13A) shows some groups of faults on the platform, which seem to be deep and associated with the uplift of the acoustic basement. Some of these faults appear to reach the seafloor after cutting the sedimentary sequences, which seem to dip towards the north. On the slope, it is important to note that some of the structures are related to the two gully zones (see the bathymetric description above): in front of Manta Peninsula and

La Plata Island. Between these gully zones, there is a knoll that corresponds to the bathymetric promontory slope, shown in Figure 5.2, and which is located in front of the blade asperity.

_____

Figure 5.12- *A) SCAN-844 seismic line interpretation in the San Lorenzo basin. This profile shows the three groups of sequences in the slope zone of the basin. UTR sequences are primarily deposited on the platform, which have been well described in Chapter 4. B) AtacP103 seismic line interpretation in the La Plata basin. In this basin, only the UTR sequences are found (see their description in Chapter 4). C) Location of the seismic profiles.*

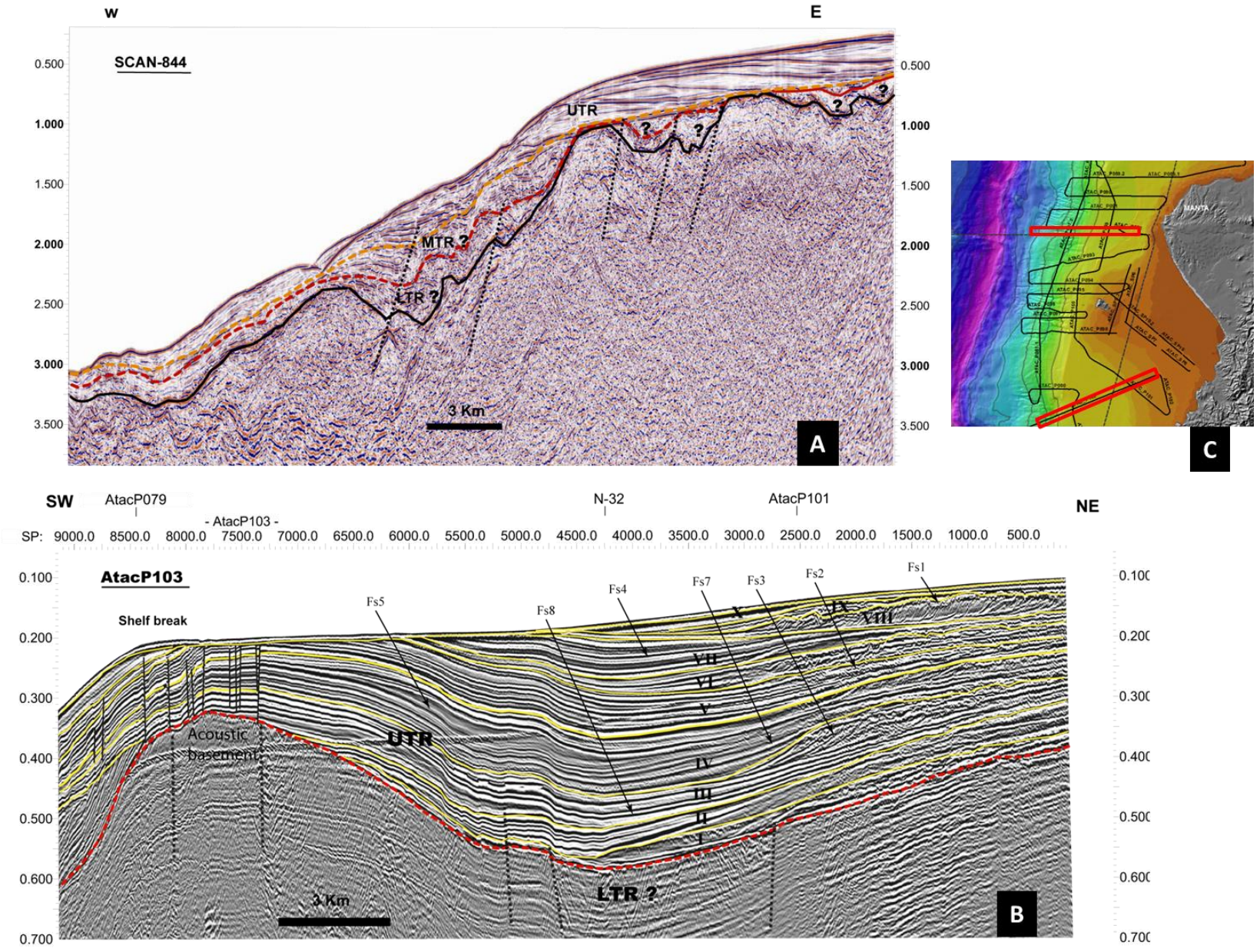

Figure 5.12: A) SCAN seismic line interpretation in the San Lorenzo basin. B) ATACAMES seismic line interpretation in La Plata basin.

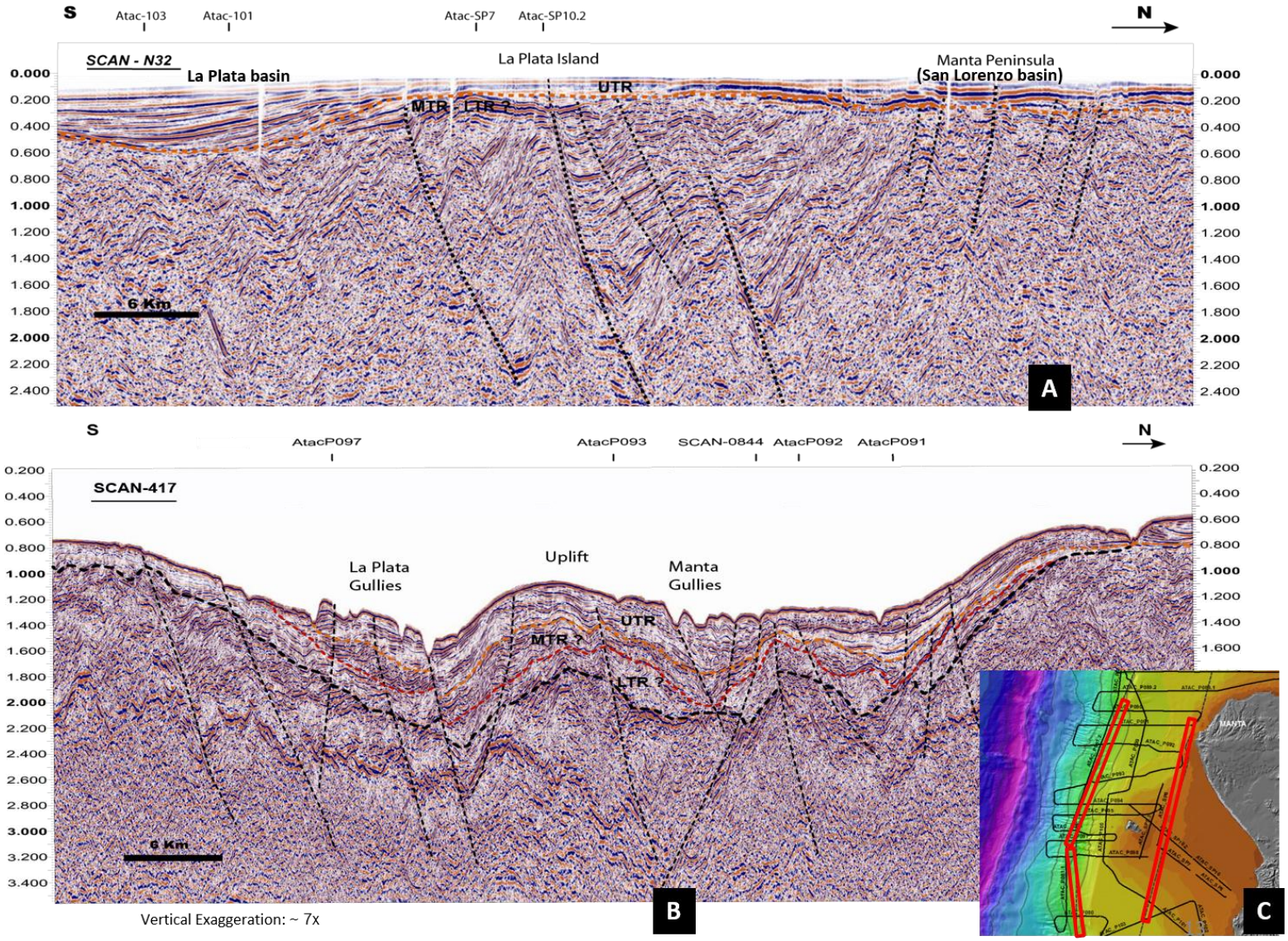

Figure 5.13: Interpretation of the SCAN seismic profiles located at the slope and at platform between Manta Peninsula and La Plata Island.

Figure 5.13- *A) The SCAN-N32 seismic line, located on the platform between Manta Peninsula and La Plata Island. It shows the lateral continuity of the UTR sequences between the San Lorenzo and La Plata basins, as well as the local presence of the LTR or MTR sequences on the shelf. B) SCAN-417 seismic profile, located on the slope of the margin, showing the lateral continuity of the LTR, MTR and UTR between the San Lorenzo and La Plata basins. It also shows the gullies located in front of Manta Peninsula and La Plata Island, controlled by structural faults, and separated by a promontory which is located in front of the blade asperity. C) Location of the oil seismic line.*_____

3.3. The Southern zone

3.3.1. The Ayampe basin

The Ayampe *basin* corresponds to a cavity and circular bathymetric shape on the middle slope, in front of the coastal city of Ayampe (Figure 5.3). It is an isolated basin (Figure 5.4B), the basement of which is located 3800 m below the sea surface (4000 ms-TWTT @1900m/s), with c. 660 m of sediment infilling (700 ms-TWTT @1900 m/s) (Figures 5.14, 5.15). A morphological high (crest of the scarp on Figure 5.15B), formed by a subducted seamount (Sage et al., 2006; Sanclemente, 2014; Villamar, 2001), bounds the basin to the south. The three groups of sequences, LTR, MTR and UTR, fill the basin (Figure 5.14A), creating a terrace into the trough.

- The *LTR* sequences lay on the basement through an angular unconformity. This set of T-R sequences show a chaotic to reflection-free seismic reflection pattern; whereby it is not possible to discriminate their internal deposition events (Figures 5.14 and 5.15). The W-E SCAN-788 seismic profile (Figure 5.14) shows the thickest zone of the LTR on the western border of the basin, which thins in a landward direction (see the sizes of the red arrows). The LTR set of sequences shown in the N-S AtacP104 seismic line (Figure 5.15) corresponds to the deposits from the landward side of the basin; this is why it appears to be thin in the Atacames seismic data (see the intersection of AtacP104 in the SCAN-788 profile).

-The *MTR* sequences overlay the LTR sequences with an angular unconformity. In the W-E seismic line (Figure 5.14A), they present, from base to top, a set of sequences with high continuity, high amplitude and subparallel to divergent to landward seismic reflection configuration patterns. Overlaying these sequences, there is another group of sequences that show a seismic facies with low amplitude or semi-transparent reflectors with chaotic reflection configurations. The sequences with a subparallel to divergent reflection configuration extend everywhere at the base of the MTR in a W-E direction, while the sequences with a chaotic reflection pattern cover an area extending from the center to the eastern border of the basin. The SCAN-788 seismic profile shows that the thinnest zone of the MTR sits at the rim of the terrace, while the thickest zone is on the eastern border of the basin, contrary to the LTR sequences (see the sizes of the blue arrows).

The N-S AtacP104 seismic profile (Figure 5.15) shows the same two groups of sequences described in the W-E seismic line, i.e. sequences with a subparallel reflection configuration pattern, and sequences with a chaotic to transparent reflection configuration. However, on the N-S line, we can observe the first group of sequences (the sub-parallel sequences) located from

the center to the northern side of the basin, while the second group of sequences (the chaotic sequences) extends from the center of the basin to the south of it. The chaotic sequences present middle to high amplitudes at the center of the basin, while to the south, they show low to transparent amplitudes.

At the center of the basin, the subparallel reflection sequences for the MTR have a sub-vertical and sudden contact with the chaotic sequences. In fact, we can observe that the sequences with chaotic configuration patterns intrude into some levels of the sequences with subparallel reflection patterns.

- The *UTR* sequences show a detailed stratigraphy with 10 T-R sequences, as in the San Lorenzo and La Plata basins (see Chapter 4). In the W-E seismic profile (Figure 5.14), the 10 T-R sequences show, from the border of the terrace in a landward direction, a seismic facies with a high continuity, high amplitude and subparallel to divergent reflection configuration. Around the eastern wall of the basin, almost all of the sequences display seismic facies with low to transparent amplitude, low continuity and chaotic reflection configuration patterns, intercalated into the subparallel seismic reflection configuration. In this seismic line (SCAN-788), the UTR sequences show their thinnest part at the edge of the terrace and their thickest part on the eastern side of the basin (see the different heights of the yellow arrows between the base and top of the UTR on the western and eastern sides of the basin).

The AtacP104 seismic profile (Figure 5.15), with a N-S direction, shows the 10 T-R sequences stacked vertically with a general concordance contact between them. They present three groups of seismic facies: 1) high continuity, high frequency, average to high amplitude with a subparallel reflection configuration pattern; 2) low continuity, average frequency, average to high amplitude with a chaotic seismic reflection configuration pattern; and 3) a low continuity, low frequency, low amplitude to transparent chaotic reflection configuration pattern.

The three groups of facies share characteristics with the seismic facies described in Table 4.1 (see Chapter 4). The first group of seismic facies is similar to Fs5 or Fs7 and the second and third groups are similar to facies Fs6.

- Sequence I is located at the base of the UTR. Its depocenter is c. 80 m thick (78 ms-TWTT @ 1900 m/s) and is composed of the first group of subparallel seismic facies. On the southern side of the basin, sequence I passes laterally to chaotic seismic reflection patterns. In fact, it seems that a c. 280 m thick (300 ms-TWTT @ 1900m/s) section of the chaotic seismic facies change suddenly into the sub-parallel facies.

- Sequence II shows, in the central zone of the basin, the subparallel seismic facies at the base, overlain by the transparent seismic facies. In the southern zone of the basin, it displays the same chaotic seismic facies as in T-R sequence I. The distinction between the two sequences is difficult on this side of the basin.

- Sequence III is exposed all around the basin; in the N-S direction, it shows subparallel seismic facies, discordantly overlaying the chaotic and transparent facies shown in sequence II. Around

the center of the basin, sequence III shows, at the base, some thin levels of transparent facies intercalated with the subparallel facies. However, on the southern side of the basin, sequence III seems to seal the large chaotic depositions. From this sequence to sequence X, there are no intercalations of the chaotic deposits present on this side of the basin (Figure 5.15A)

-The TR sequences from IV to X show, at the center of the basin, an interbedding of the subparallel seismic facies and chaotic and transparent seismic facies (Figure 5.15A). Some sequences show a thick chaotic seismic facies (e.g. V, VIII), while others present a thicker subparallel seismic facies (e.g. VI, VII, IX, X). On the W-E seismic profile (Figure 5.14A), the UTR sequences exhibit this facies intercalation on the eastern border of the basin.

_____

Figure 5.14- *A) SCAN-788-s seismic line interpretation in the Ayampe basin. It shows the thickness variations for each group of sequences, from the border of the basin for the LTR to a landward direction for the MTR and UTR. The red, blue and yellow arrows indicate the different thicknesses of the LTR, MTR and UTR mega-sequences in the basin. It also indicates the relationship between the chaotic and subparallel to divergent reflection configuration patterns in the different levels of the basin (see the details provided in the text). B) Seismic line location.*

_____

Figure 5.15- *A) AtacP104 seismic line interpretation, with a N-S direction, showing the 10 upper T-R sequences in the Ayampe basin, as well as the MTR and LTR at the base of the UTR. We can note how the chaotic to hummocky reflection configuration seismic facies have extended into the sub-parallel seismic reflection configuration facies of the MTR sequences and UTR sequences I and II. We can also observe some levels of the intercalation of the chaotic reflection configuration seismic facies in T-R sequences V and VIII. B) The Atac-104 seismic line shows that the crest of the scarp borders the southern side of the Ayampe basin. C) Location of the Atac-104 seismic line and its spatial relationship with the bathymetric features.*

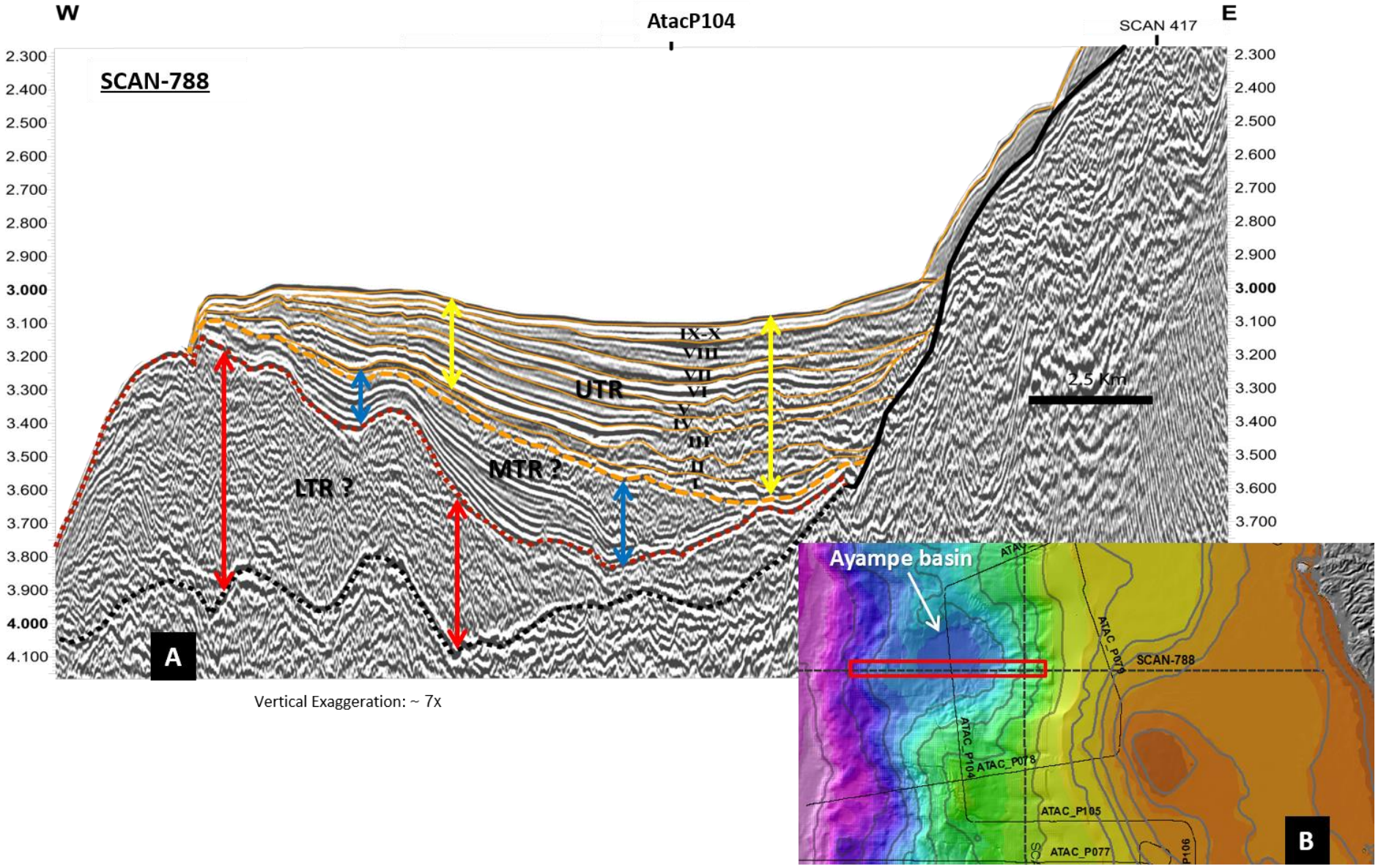

Figure 5.14: SCAN-788-s seismic line interpretation in the Ayampe basin (W-E direction).

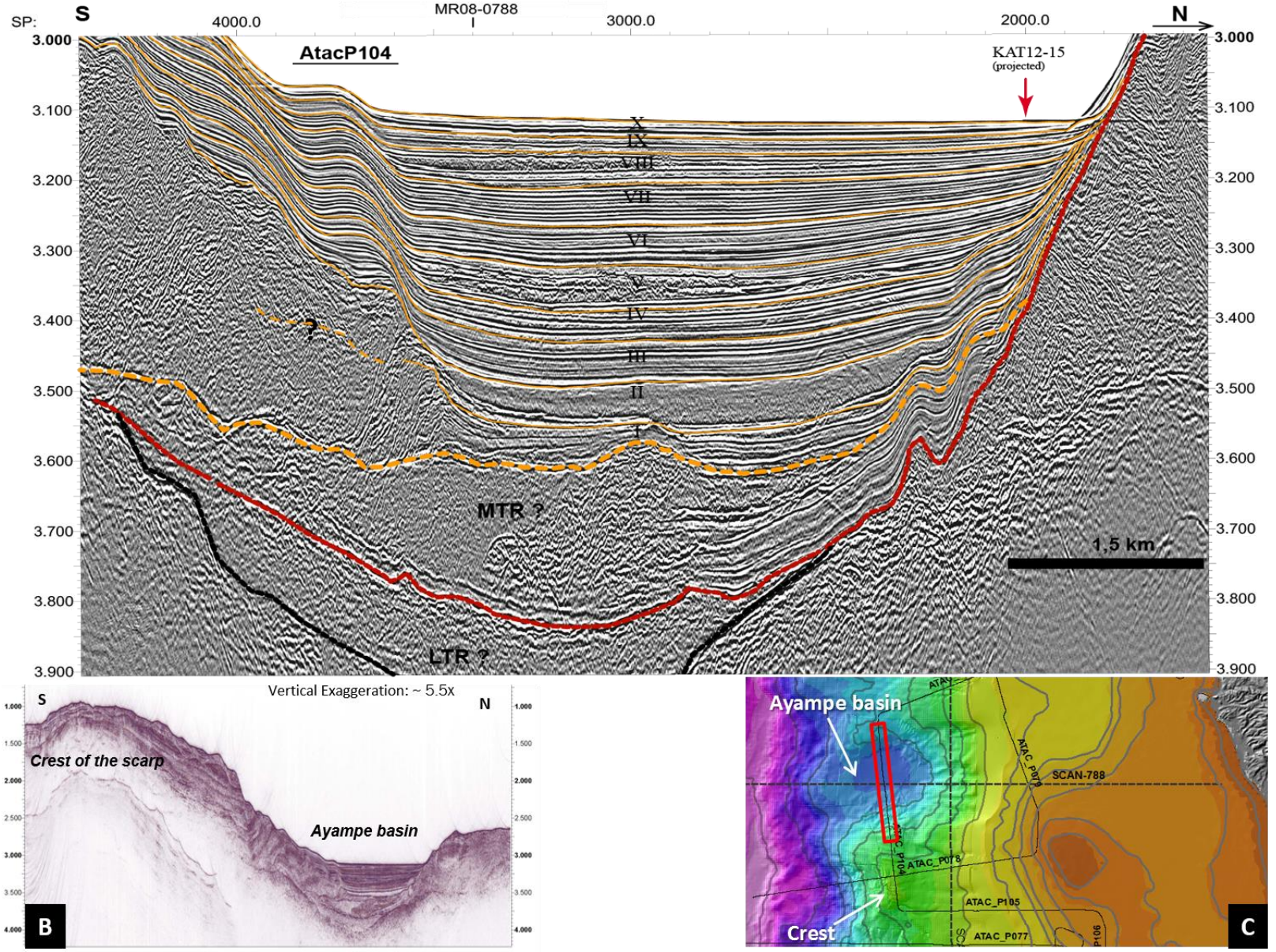

Figure 5.15: AtacP104 seismic line interpretation, with a N-S direction, showing the 10 upper T-R sequences in the Ayampe basin.

3.3.2. Slope basins

Slope basins are shown to the south of the Ayampe basin. They correspond to a set of small basins encased in fault-controlled areas of the slope.

- The Montañita basin is located on the southern side of the Ayampe basin and on the western side of the Montañita bathymetric high (MBH; Figure 5.3). This sediment accumulation is located between the crest of the scarp caused by a seamount subduction and the Montañita bathymetric high (Figure 5.16A). The LTR, MTR and UTR are mainly located between the crest of the scarp and the shelf break, but they are poorly exposed on the platform, over the MBH.

- The *LTR* group of sequences appears at the base of the three groups of sequences. The seismic data do not show their characteristics very well, but they seem to present a subparallel reflection configuration that is folded and truncated by normal faults.

-The *MTR* set of sequences overlays the LTR sequences with a discordant contact. They are characterized by a sub-parallel to wavy seismic reflection configuration and are truncated by normal faults.

- The *UTR* sequences onlap the unconformity at the top of the MTR and present a sub-parallel to divergent seismic reflection configuration. This group of sequences is the thinnest of the three groups of sequences in this basin (see the different heights of the arrows for each group of sequences in Figure 5.16A).

There are some reverse faults on the outer shelf which match the external border of the Montañita bathymetric high (see the paragraph on the seafloor morphology in this chapter); however, there are also some normal faults from the shelf break to the crest of the scarp (Figure 5.16A).

- The Salinas basins are located further south. In this zone, the sediment accumulates in the small slope basins principally controlled by normal faults dipping seaward (Figure 5.17). Some of these faults reach the seafloor and coincide with the bathymetric curved scarp evidenced above (see Figures 5.3 and 5.17A). They cover the slope zone from the crest of the scarp of the subducted seamount in the north to the “straight head” bathymetric shape in the south (Figure 5.17C). The SCAN-756 seismic profile shows that the upper sector of Santa Elena Canyon is influenced by the faults that form the slope basins (Figure 5.17B). The LTR, MTR and UTR group of sequences are exposed in all of these slope basins.

- The *LTR* sequences are at the base of the sequences. In the SCAN-756 (Figure 5.17B) seismic profile, this group of sequences shows a subparallel reflection configuration pattern. In places, the sequences appear to be folded and uplifted (Figures 5.17A and B).

- The *MTR* sequences overlay the LTR sequences with an angular discordance. In the SCAN-756 profile (Figure 5.17B), they present a subparallel to divergent landward seismic reflection pattern with a concave external form. They appear to be strongly controlled by the faults.

- The *UTR* sequences were interpreted at the top of the MTR as downlapping onto an angular unconformity (SCAN-756, Figure 5.17B). In this seismic profile, they appear to be cut by the upper zone of Santa Elena Canyon. The sequences display sub-parallel to divergent seismic reflection patterns. On the eastern side of the seismic profile, above Santa Elena Canyon, the seismic reflectors show onlap terminations against the vertical wall of the Santa Elena Structural High (SSH).

_____

Figure 5.16- *A) Atac-078 seismic line interpretation. It displays some of the principal features of the seamount subduction described by Dominguez et al. (1998): the scarp, the crest of the scarp, the normal and strike-slip faults and the backthrust (?). The sediments deposited in the back-scarp have been correlated with the LTR, MTR and UTR sequences, and have been called the Montañita basin in this work. The red, blue and yellow arrows indicate the different thicknesses of the LTR, MTR and UTR mega-sequences in the basin. B) Location of the seismic line.*

_____

Figure 5.17- *A) Atac-077 seismic line interpretation. It presents some normal faults on the slope which create some local sedimentary accommodation, the Salinas basins. On the platform, the sedimentary deposits are related to Santa Elena Canyon (the Santa Elena basin). B) SCAN-756 seismic line interpretation, which also displays the normal faults on the slope controlling the sedimentary deposition in this zone. C) Seismic location and its spatial relationship with the bathymetric steps, which are the morphological expression of the slope faults.*

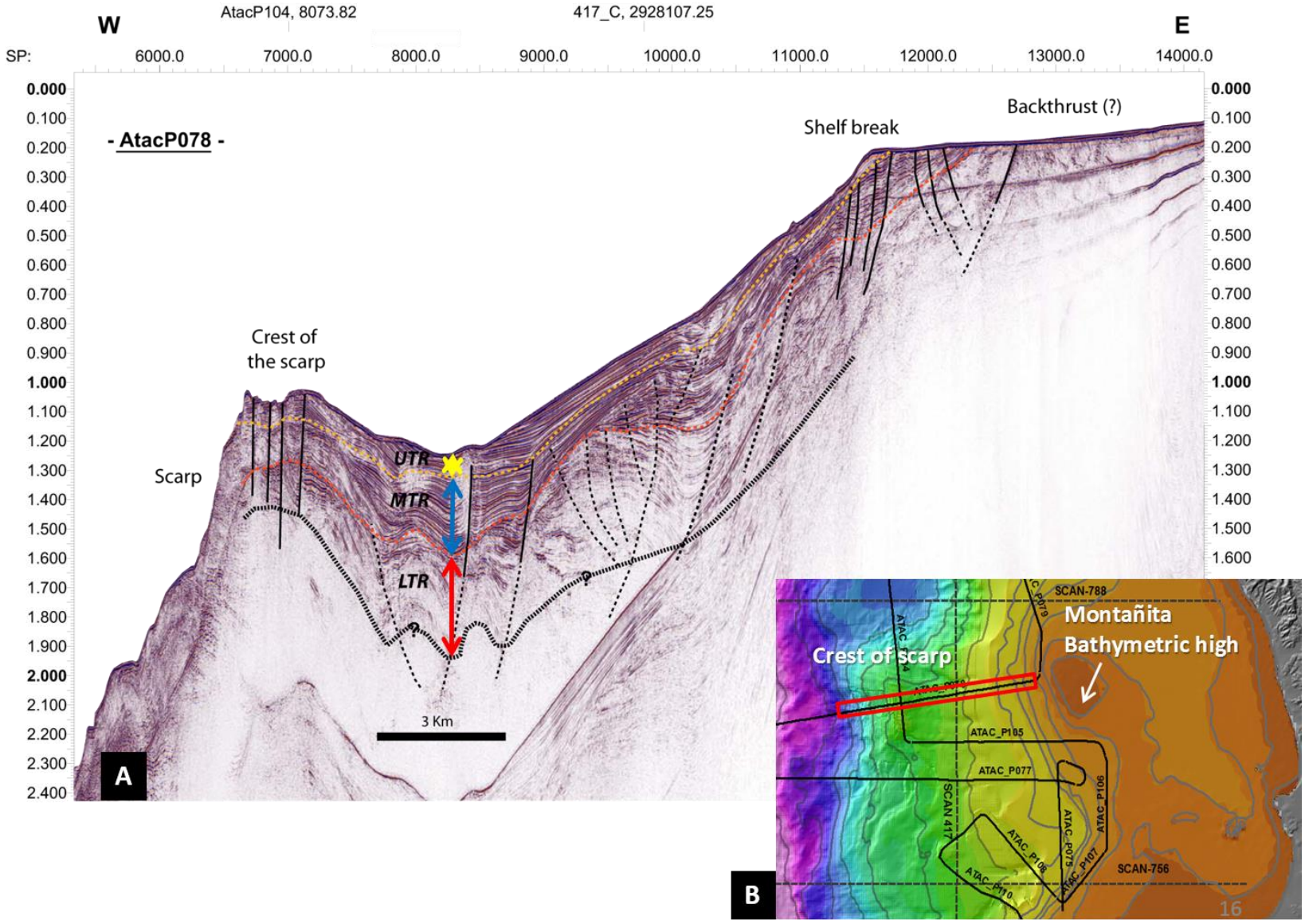

Figure 5.16: Atac-078 seismic line interpretation. It displays some of the principal features of the seamount subduction described by Dominguez et al. (1998).

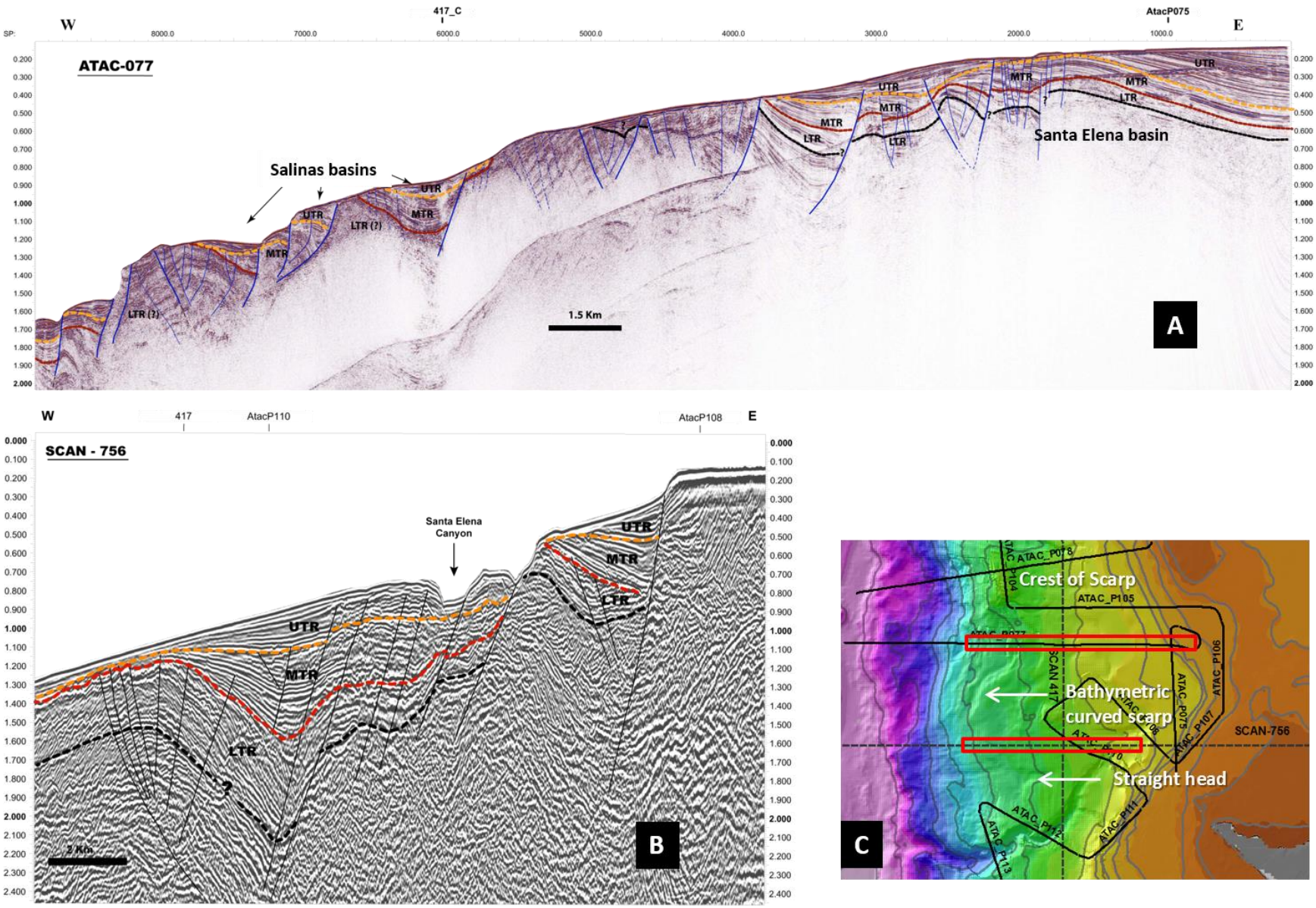

Figure 5.17: Atac-077 and SCAN-756 seismic lines interpretation, showing the normal faults that control de slope basins.

3.3.3. The Santa Elena basin

The Santa Elena basin surrounds Santa Elena Canyon, covering both the platform and slope (Figure 5.18). On the platform, it is located between the Montañita and Salinas bathymetric highs (Figure 5.4), and on the slope it follows the trend in Santa Elena Canyon. The basin infill is c. 480 m thick (500 ms-TWTT @ 1900 m/s) on the platform (Figure 5.17A), and c. 380 m thick (400 ms-TWTT @ 1900 m/s) on the slope (Figure 5.18C).

The three groups of sequences, LTR, MTR and UTR, were interpreted in the basin, but as this basin encompasses various zones, and each of them shows different features, we show the characteristics of the LTR, MTR and UTR and their relationship with each zone.

On the platform, the sequences fill the head and shelf edge that surrounds Santa Elena Canyon (Figures 5.18A and B). In general, the LTR, MTR and UTR sequences show sub-horizontal and parallel reflection configuration patterns to the north of the channels. In the head of the canyon, the LTR and MTR show seismic facies with a divergent reflection configuration. The UTR show seismic facies with complex fill-reflection configuration patterns (Mitchum et al., 1977). The UTR sequences show sharply truncated reflectors at the top of sequence VII. On the southern side of the filled channels, the sequences show a sub-vertical contact with the acoustic basement, which was interpreted as a structural contact (Figure 5.18).

On the upper slope, on the northwestern side of Santa Elena Canyon the MTR sequences were interpreted at the base. The UTR set of sequences overlay the MTR sequences with a divergent reflection pattern oriented towards the S-E and displays a wedge external form. The thickest part of the UTR is 760 m thick (800 ms-TWTT @1900 m/s) and the canyon truncates it. The UTR deposits thin to the north due to the uplifting of the acoustic basement controlled by reverse faults (SE2). On the southeastern side of the canyon, the UTR show onlap terminations against the steep structurally controlled (SE1) acoustic basement.

On the middle slope, the N-S SCAN-417 seismic profile crosses through the southern limit of the Salinas basin to Santa Elena Canyon (Figure 5.19). It passes over the “straight head” of the landslide described in the bathymetry (Figures 5.17C and 5.19C). On the seismic line, we identified from north to south: a syncline (Point 1 in Figure 5.19), a filled paleo-channel (Point 2), and Santa Elena Canyon (Point 3). The syncline geographically corresponds to the southern border of the Salinas slope basins (see the description above) and the filled paleo-channel with the “straight head” of the landslide. In this zone, the Santa Elena basin deposits present the three groups of TR sequences. This seismic profile also shows some faults that cut some levels of the sequences.

At the base, the LTR group of sequences display a seismic facies with high amplitude, average frequency, and average continuity reflectors with hummocky to subparallel reflection configuration patterns. In general, the LTR sequences drape the wavy acoustic basement. They show sub-parallel to divergent reflection configuration patterns (see the borders of the syncline and the filled channel). However, in the filled channel zone, the upper reflectors (above the light blue dotted line in Figure 5.19A) seem to be sub-parallel to the U shape of the contact with

the upper MTR sequences. In Santa Elena Canyon, the LTR sequences are incised by the V morphology channel.

In general, the MTR sequences present average to high amplitude, average to high continuity and high frequency with sub-horizontal to divergent fill reflection configuration patterns into the syncline and filled channel (Points 1 and 2, Figure 5.19). In the syncline, the reflectors seem to be concordant with the LTR seismic reflection configuration, but in the filled channel, the reflectors show onlap terminations against the U shape of the LTR sequences at this point. The MTR sequences are not displayed below Santa Elena Canyon, but rather on the southern side of the canyon.

The UTR sequences present an average to high amplitude, low to average continuity and low to average frequency with sub-parallel reflection configuration pattern. They seal the syncline and filled channel. In the Santa Elena channel, the UTR sequences show sub-parallel reflectors that mimic the V shape of channel, and they appear to be in angular unconformity with the LTR sequences.

_____

Figure 5.18- *A) The Atac-075 seismic line shows two filled channels on the border of the platform that are related to Santa Elena Canyon. B) Interpretation of the filled channels. It shows the deposit of the LTR and MTR groups of sequences at the base and the 10 UTR groups of sequences at the top. The UTR sequences show the truncation of the reflectors at the top of some of their sequences. C) The Atac-P108 seismic line shows the deposits of the Santa Elena basin in the slope zone. D) Seismic line location and their spatial relationship with Santa Elena Canyon.*

_____

Figure 5.19- *A) SCAN-417 seismic line interpretation. It shows from north to south: 1) a syncline, 2) a filled channel and 3) Santa Elena Canyon (see the explanation of the interpretation in the principal text). The syncline and filled channel are composed of the LTR, MTR and UTR sequences. The light blue dotted line between the base of the LTR and MTR (black and red dashed lines) may correspond to the base of the filled channel. In this seismic line, the Santa Elena Canyon levee displays the UTR sequences at the top, with reflectors that are sub-parallel to the V morphology of the canyon. B) Seismic line location. It shows that the filled channel (2) is connected to the "straight head" morphology of the landslide, described above in the bathymetry section.*

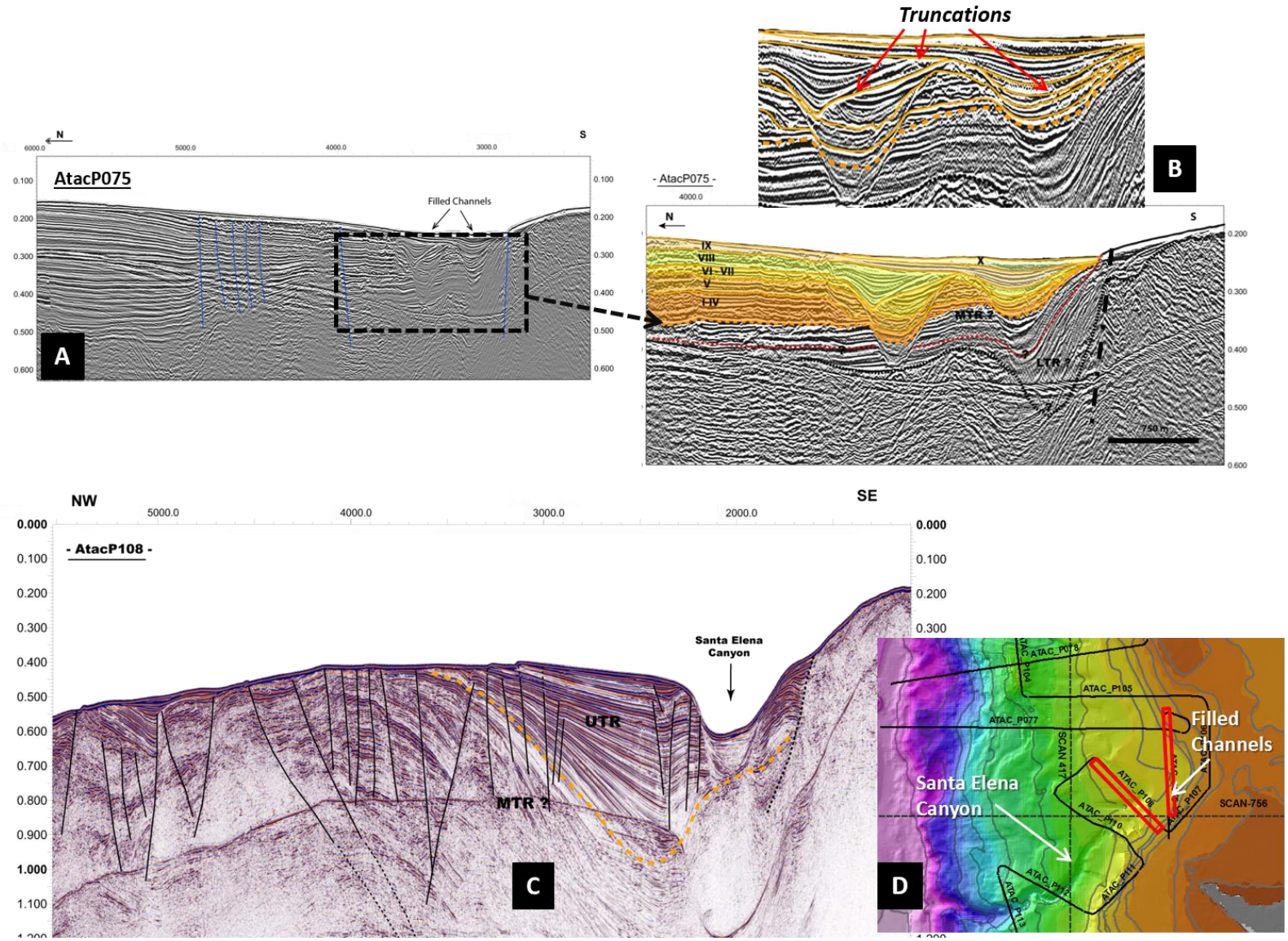

Figure 5.18: The Atac-075 seismic line shows two filled channels on the border of the platform that are related to Santa Elena Canyon, and The Atac-P108 seismic line shows the deposits of the Santa Elena basin in the slope zone.

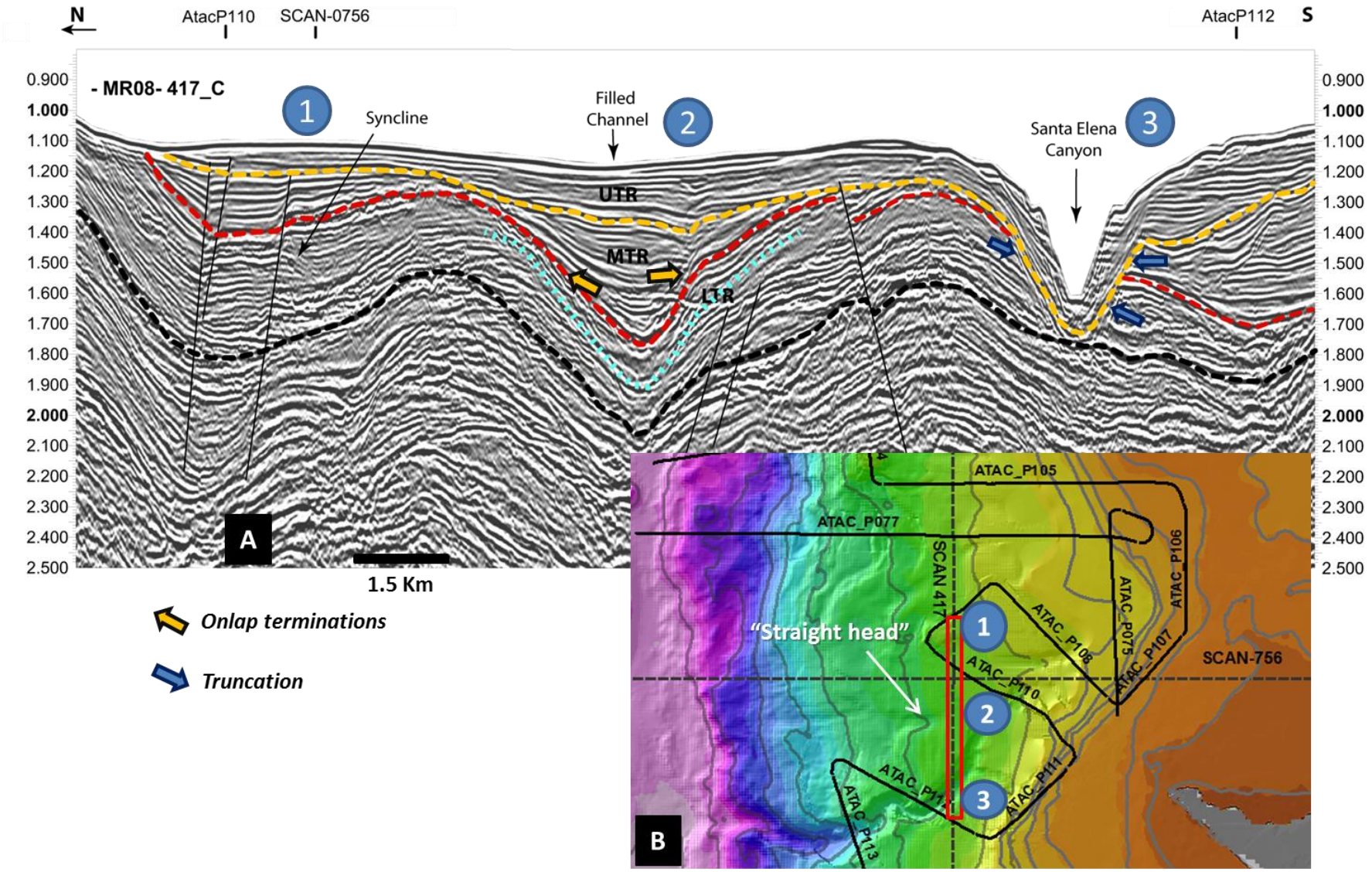

Figure 5.19: SCAN-417 seismic line interpretation. It shows from north to south: 1) a syncline, 2) a filled channel and 3) Santa Elena Canyon (see the explanation of the interpretation in the principal text).

4. Sedimentary record

Cores were collected at Atacames in order to try to sample and date the unconformities at the location where they intersect the seafloor. In this work, we used one core each from the Cabo Pasado, Jama, and Ayampe basins and two cores from the San Lorenzo basin. The cores from the San Lorenzo basin are described in Chapter 4.

The 1.70 m long KAT12-25 core was collected in the Cabo Pasado basin (Figure 5.20A) and on the AtacP-046.1 seismic line (Figure 5.20B) at the location where UTR sequence IX was interpreted (Figure 5.19C). The Chirp data are consistent with the seismic data, showing that the core has sampled the contact between sequence VIII and sequence IX (Figure 5.20D). The lower section of the core, from 1.70 m to 1.05 m, displays homogeneous facies with medium sand grains and the presence of mm-large bioclasts. At 1.05 m, an erosional unconformity separates the lower homogeneous facies from the upper olive-green fine sand facies. The latter presents heavy bioturbation from 1 to 0.50 m with cm-scale burrows infilled by dark sand (Figure 5.20A). A carbonate shell sample was selected for 14C dating at 1.04 m (Figure 5.20D) just above the unconformity. This sample provided an age of 43400 ± 1300 BP in the laboratory, and an age of 46400 cal yr BP with correction of the marine reservoir effects.

The 1.68 m long *KAT12-26* core was collected in the Jama Basin (Figure 5.21A). The core is located on the AtacP-044 seismic profile (Figure 5.9A), at the location where UTR sequence X was interpreted (Figure 5.21B). The Chirp data (Figure 5.21C) show that the core was collected in a zone with a wavy to subparallel concave reflection configuration interpreted as a channel fill. The presence of the channel is consistent with facies Fs1 described at the top of the AtacP-044 seismic line. The core exhibits a homogeneous facies with medium sand grains that are grey to olive-green in color, with some intercalations of mm-thick shell hash and coarse sands. Cm-scale shells are dispersed throughout the core from which we took out a bivalve shell located at a depth of 0.70 m for 14C dating (Figure 5.21D). This shell was dated at 13320 ± 60 BP in the laboratory, corresponding to an age of 15280 cal yr BP after the correction of the marine reservoir effects.

The 6.50 m long KAT12-15 core was collected in the Ayampe basin (Figure 5.15A). The detailed study of this core (Durand, 2014) shows the interbedding of bioturbated hemipelagic clay, yellowish clayey volcanic ash (tephra), rippled silt to fine sand (contourite) and silt to sand turbidites (Figure 5.22A). This core was collected 2000 m to the east of the AtacP-104 seismic line (Figure 5.22B). Its projection on the Chirp line and AtacP-104 seismic line suggests that it samples sequence X of the UTR (Figure 5.22C). Several levels of this core were dated using 14C dating of the carbonate of the planktonic foraminifera. The results provide an age of 6349 cal yr BP at the base of the core and age of 582 cal yr BP at its top (Durand, 2014).

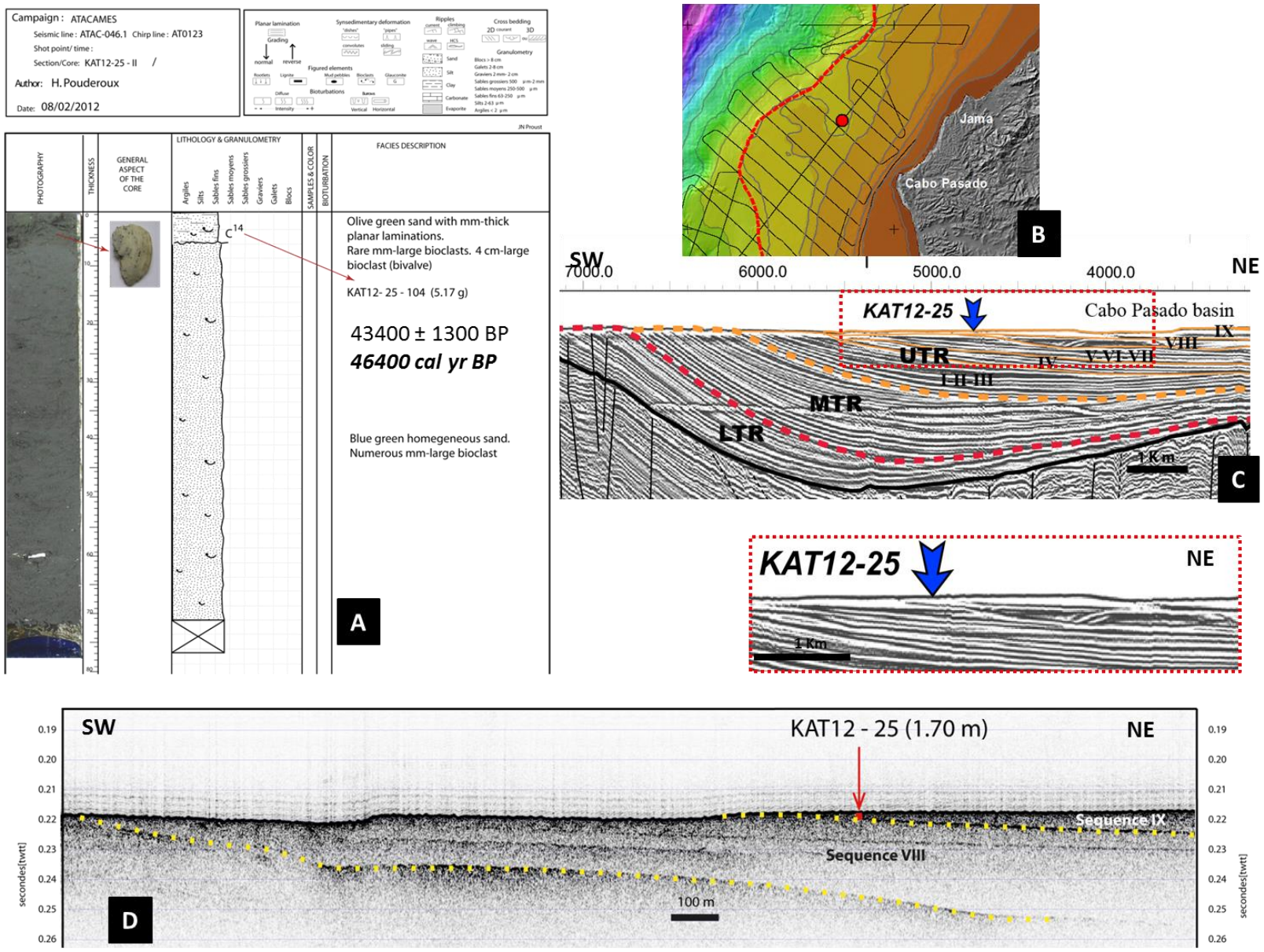

Figure 5.20: Core KAT12-25-II located in Cabo Pasado basin. Facies description and sample location of the carbonated shell for 14C dating.

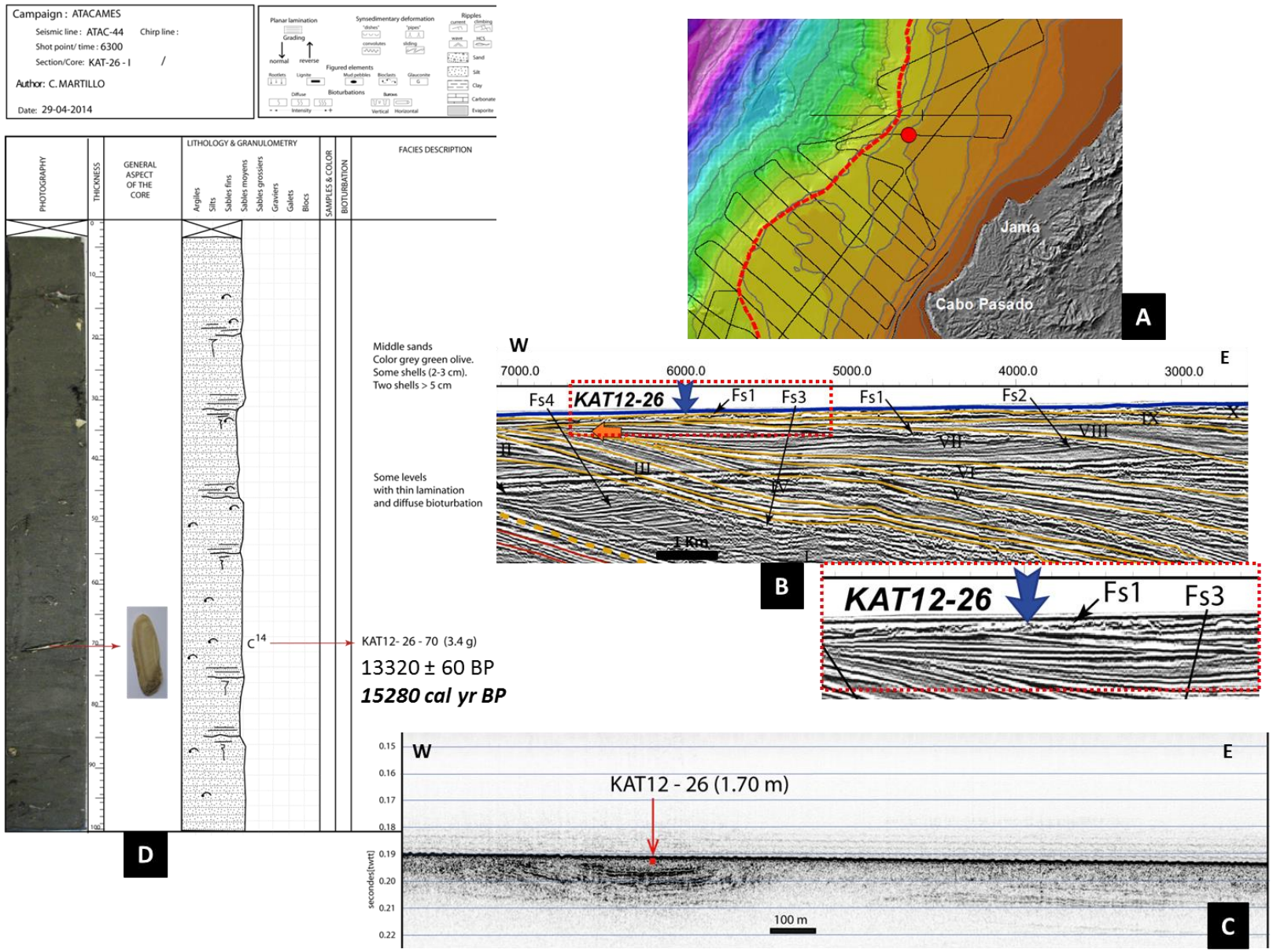

Figure 5.21: core KAT12-26-I located in the Jama basin. Facies description and sample location of the carbonated shell for 14C dating.

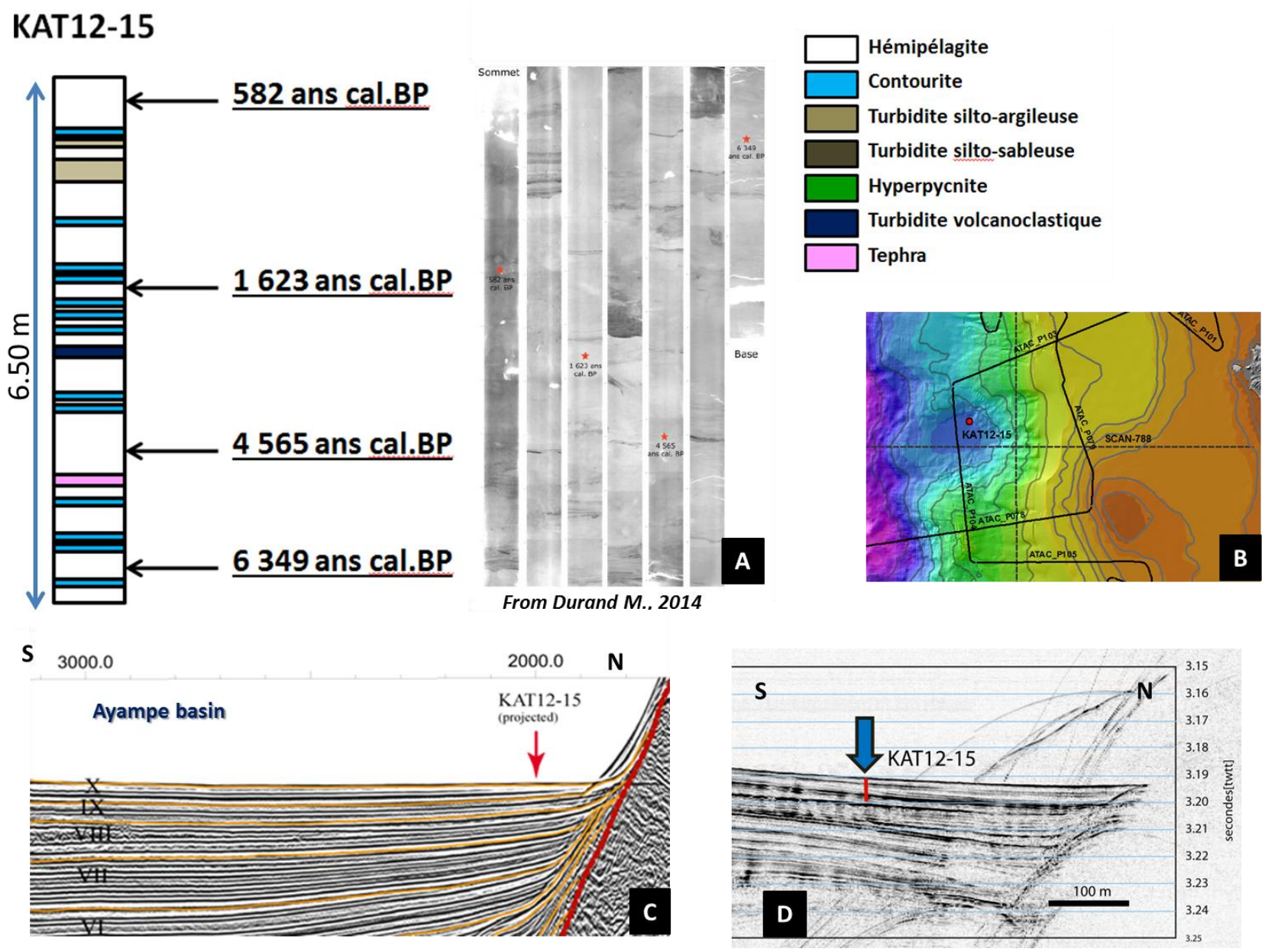

Figure 5.22: Facies description, X-rays of the core and dating of core KAT12-15, located in the Ayampe basin (from Durand 2014).

Figure 5.20- *A) Core KAT12-25-II. Facies description and sample location of the carbonated shell for 14C dating. B) Seafloor position of the core. C) Core location in relationship to the interpreted stratigraphic sequences in the AtacP46.1 seismic line in the Cabo Pasado basin. D) 3.5 KHz seismic data interpretation. We can note that the core is located at the top of the unconformity between sequences VIII and IX.*

_____

Figure 5.21- *A) Seafloor position of core KAT12-26-I. B) Core location in relationship to the interpreted stratigraphic sequences in the AtacP-044 seismic line in the Jama basin. Its position links with the interpreted sequence X and with the interpreted facies FS1 C) 3.5KHz seismic data interpretation. We can note that the core is located in a zone with a wavy to subparallel concave reflection configuration, suggesting that is in the channels filled by seismic facies Fs1. D) Core KAT12-26-I. Facies description and sample location of the carbonated shell for 14C dating.*

_____

Figure 5.22- *A) Facies description, X-rays of the core and dating of core KAT12-15, located in the Ayampe basin (from Durand 2014). The ages correspond to the actual Marine Isotopic Stage (MIS 1). B) Spatial location of the core (Ayampe basin). C) Core location in the interpreted AtacP-104 seismic line. D) Core location in the 3.5 KHz seismic data*

_____

5. Discussion

5.1. Ages of the sequences

The 14C dates obtained from the collected cores allow us to propose ages for some of the TR stratigraphic sequences. However, it is important to remember that most of the shells, including the dated ones, could be brought and reworked by rip currents from the shorelines. They can be older than the sequences that bury them, as was discussed in Chapter 4 in the Manta-Plata zone.

According to the seismic interpretation, in the Jama and Ayampe basins, we have supposed that we have cored the top of the interpreted T-R sequences: sequence X. The C14 ages confirm this interpretation. In the Jama basin, the measured C14 age in the core KAT-12-26 is 13320 ± 60 BP (15280 cal yr BP). The ages obtained in the Ayampe basin range from 6349 cal yr BP at the base of the KAT12-15 core to 582 cal yr BP at the top of the core (Durand, 2014). These ages are within the age interval for Marine Isotopic Stage MIS 1 (0-14 ka; Lisiecki and Raymo, 2005). In the Cabo Pasado basin, we suppose that we have cored the boundary between sequences IX and VIII. The measured age in the core KAT12-25 is 43400 ± 1300 BP (46400 cal yr BP), which is within the window of the ages for MIS 3 (29-57ka, Lisiecki and Raymo, 2005).

Based on the ages obtained from the cores, sequence X correlates with the ages for MIS 1, and sequence IX with the ages for MIS 3. These ages agree with the ages proposed for the basins in the Manta-Plata area, considered as the reference site in this work (Chapter 4). Therefore, for all of the basins discussed in this work, we propose a range of ages for MIS 1 (from 14 ka to present) for sequence X, and an age range for MIS 3 and MIS 2 (from 57 ka to 14 ka) for T-R sequence IX.

Based on these ages and following the criteria given in Chapter 3 (4th step of the seismic data interpretation) and applied in Chapter 4, in order to attribute an age to the T-R sequences that are older than sequences X and IX, we have correlated the T-R sequences with the MIS for the transgression-regression eustatic cycle and assigned the ages for the MIS proposed by Lisiecki and Raymo (2005).

In this way, the group of UTR sequences, from X to I, is correlated from MIS 1 (for X) to MIS 19 (for I). This corresponds to an age range from the present to 781 ka (Table 5.2) (from the Holocene to the Middle Pleistocene) according to the International Chronostratigraphic Chart ICSC–v. 2014/10 (www.stratigraphy.org)

Using the Atacames seismic profiles, the 10 UTR sequences were clearly identified in all of the Quaternary basins along the Ecuadorian margin. We were not able to reach the same level of detail for the sequences corresponding to the MTR and LTR.

We were only able to reach the same level of detail for the MTR and LTR as for the UTR in the Jama basin. In the Jama basin, in addition to the 10 T-R sequences of the UTR, we found 16 older T-R sequences: five in the MTR and 11 in the LTR (Figure 5.9). We cannot exclude that

some of the LTR or MTR sequences were eroded out (see the Jama basin explanation) and therefore, there could have been more than 11 sequences.

Following the same way of thinking as for the UTR, we propose that the set of MTR sequences, from A to E, corresponds to MIS 20 to 29, with ages ranging from 814 ka to 1031 ka; while the group of LTR sequences, from F to Q, corresponds to MIS 30 to 51 and consequently corresponds to ages ranging from 1062 ka to at least 1530 ka (Table 5.2). If some of the LTR sequences are missing in the Jama basin, this set of sequences could be as old as the base of the Calabrian, i.e. the base of the Pleistocene MIS 63 (1782 ka).

5.2. Onshore correlation ages

The onshore Quaternary deposits are principally located on the coast in the cape, i.e. Galera Cape, Cabo Pasado Point, Manta Peninsula, La Plata Island and Salinas Cape, with the exception of the Quaternary deposits in the Cojimíes estuary. The outcrops from Galera Cape, Manta Peninsula, La Plata Island and Salinas Cape were described by Pedoja et al. (2006) and Reyes (2013). The outcrops around Cabo Pasado Point, Manta Peninsula and La Plata Island are described by Di Celma et al. (2002), Cantalamessa and Di Celma (2004), Cantalamessa et al. (2005) and Reyes (2013).

In the Manta-La Plata region (Chapter 4), the 10 UTR sequences correlate in age and geometrically to the onshore exposures of the Upper Canoa and Tablazos depositional sequences described to the south of Cabo San Lorenzo (Cantalamessa and Di Celma, 2004) (Figure 4.8). Additionally, the marine terraces exposed on Manta Peninsula and La Plata Island correlate with some of the UTR sequences for the San Lorenzo and La Plata basins (Table 4.3). The older marine terrace of Manta Peninsula (T5), is correlated with MIS 27 to 31 (966 ka to 1060 ka) by Pedoja et al. (2006). This is consistent with the age we have assumed for the boundary between the MTR and LTR sequences, which is interpreted in this zone along the SCAN-844 seismic line (Figure 5.12A)

The Jama Formation is exposed onshore between Punta Ballena and Cabo Pasado (around the city of Pedernales; Reyes, 2013) (Figure 5.24A). According to Cantalamessa et al. (2005), the Jama formation is comprised of the Punta Paso Borracho Member (PPB) overlain by the Punta Ballena (PB) and El Matal (EM) Members (Figure 5.24C). The interpretation of the depositional sequences led Cantalamessa et al. (2005) to attribute an age of 1160 ± 0.06 ka to the erosional unconformity at the base of the El Matal member (MIS34) and an age of 1492 ka (MIS 50) to the base of the Punta Ballena member (Figure 5.24C). The AtacP46.1 seismic line shows that the set of LTR sequences extends from the CPAS until the zone in front of Punta Ballena (between Punta Cabuya and Punta Alcatraz), close to where Cantalamessa et al. (2005) made the stratigraphic description of the Punta Ballena member (Figure 5.24C). The Atac-65 seismic line, where the LTR sequences were identified, is located just in front of Cabo Pasado Cape (Figure 5.10C) where it is reported on the geological map outcrops for Punta Ballena (Reyes, 2013). We propose ages ranging from MIS 51 to MIS 30 for the LTR sequences, which are well defined in the Jama and Cabo Pasado basins (Table 5.2). These ages are concordant with the ages proposed for the Punta Ballena member (Figure 5.24).

The geographical correlation and the age concordances between the seismic interpretation and outcrop description allow us to propose that the LTR sequences correlate to the Punta Ballena member (1160-1492ka) and that the MTR sequences correlate to the El Matal member (1160 ka top unknown; Figure 5.24).

The ages for the marine terraces of Salinas Cape range from the early middle Pleistocene for the oldest terraces to MIS 5a age for the youngest terraces (Pedoja et al., 2006). Close to Salinas Cape, the MTR and UTR sequences are exposed in the AtacP-075 seismic line. The UTR shows multiple channel fills at the head of Santa Elena Canyon. The ages of the MTR and UTR sequences range from 1031 ka to present. This fits well with the ages proposed by Pedoja et al. (2006) for the onshore Quaternary deposits, represented by the marine terraces of Salinas Cape.

Groups of T-R Sequences	*T-R Sequences*	*Even MIS Number Glacial - Regression*	*Odd MIS Number Interglacial - Transgression*	*Edad (ka) (Lisieki & Raymo , 2005)*	*Stage/ Epoch*
UTR	X		MIS 1	14	Holocene
	IX	MIS 2	MIS 3	29-57	Upper Pleistocene
	VIII	MIS 4	MIS 5	71-130	
	VII	MIS 6	MIS 7	191-243	Middle Pleistocene
	VI	MIS 8	MIS 9	300-337	
	V	MIS 10	MIS 11	374-424	
	IV	MIS 12	MIS 13	478-533	
	III	MIS 14	MIS 15	563-621	
	II	MIS 16	MIS 17	676-712	
	I	MIS 18	MIS 19	761-790	
MTR	A	MIS 20	MIS 21	814-866	Calabrian Pleistocene *(Early Pleistocene, before 2009)*
	B	MIS 22	MIS 23	900-917	
	C	MIS 24	MIS 25	936-959	
	D	MIS 26	MIS 27	970-982	
	E	MIS 28	MIS 29	1014-1031	
LTR	F	MIS 30	MIS 31	1062-1081	
	G	MIS 32	MIS 33	1104-1114	
	H	MIS 34	MIS 35	1141-1190	
	J	MIS 36	MIS 37	1215-1244	
	K	MIS 38	MIS 39	1264-1286	
	L	MIS 40	MIS 41	1304-1320	
	M	MIS 42	MIS 43	1344-1362	
	N	MIS 44	MIS 45	1383-1405	
	O	MIS 46	MIS 47	1424-1452	
	P	MIS 48	MIS 49	1469-1492	
	Q	MIS 50	MIS 51	1510-1530	

Table 5.2: T-R sequences with their correlation to the Marine Isotopic Stages (MIS) and with the MIS age range proposed by Lisieki & Raymo (2005).

Figure 5.24*- A) Location of the Cabo Pasado basin, seismic lines and Punta Ballena. B) Interpreted Atacames seismic lines AtacP065 and AtacP46.1 (see the details of the interpretation in the section on the Cabo Pasado basin). C) Stratigraphic column for the sedimentary succession of the Punta Ballena Member, between Punta Cabuya and Punta Alcatraz, from Cantalamessa et al. (2005). The dashed lines show the proposed correlation between the LTR sequences and Punta Ballena Member.*

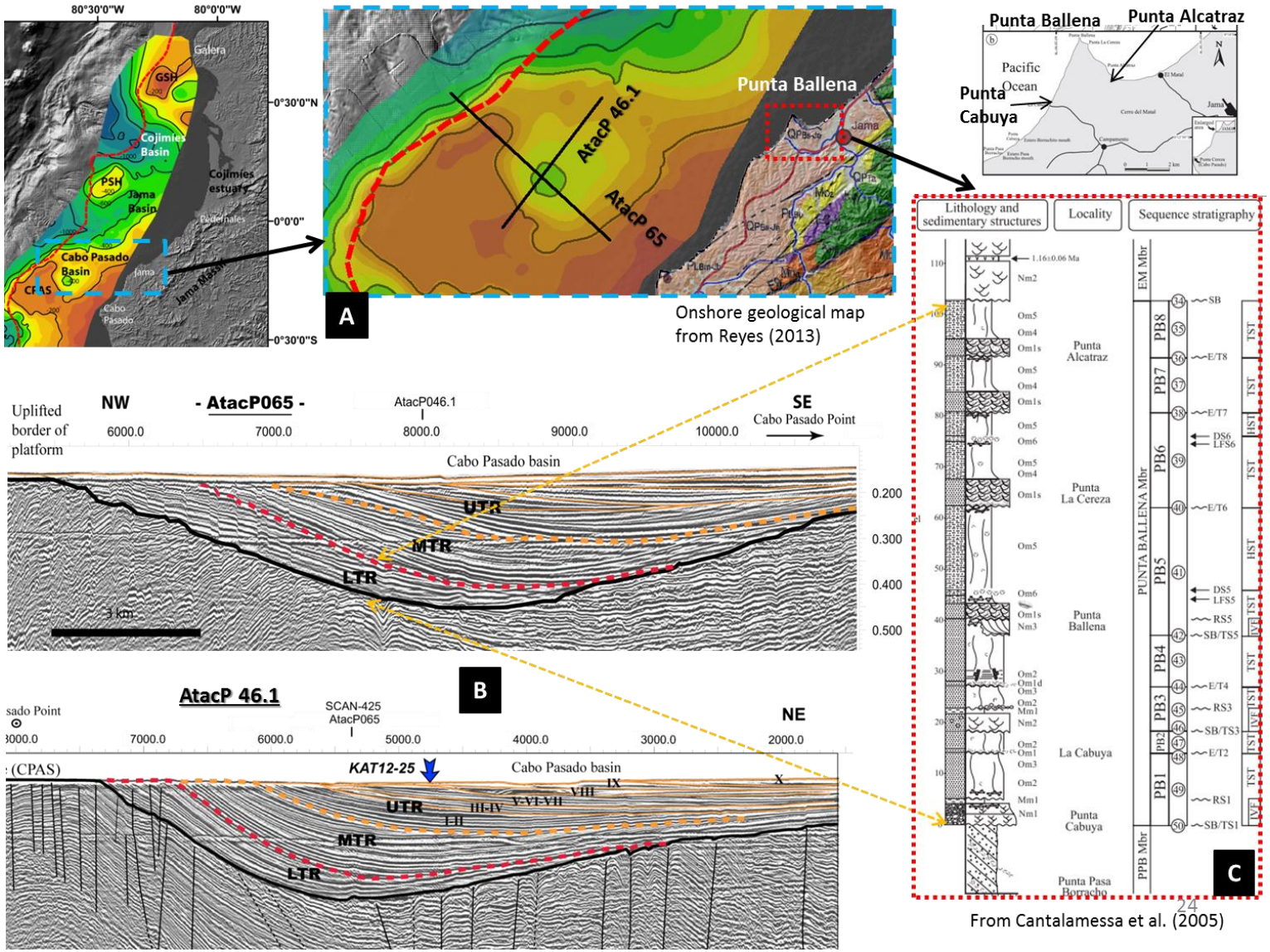

Figure 5.23: Sea-Land age correlation between the LTR mega-sequence from Cabo Pasado basin and Punta Ballena Member described by Cantalamessa et al. (2005), located onshore between Punta Cabuya and Punta Alcatraz.

CHAPTER 6: The Evolution of the Ecuadorian margin during the Calabrian Pleistocene

1. Introduction

A variety of processes are involved in forming large forearc basins along the subduction margins (e.g. Dickinson, 1995). These basins may form as a result of enhanced thinning of the upper plate through significant basal subduction tectonic erosion of the overriding plate (Von Huene and E. Suess, 1988; Von Huene and Lallemand, 1990), as well as by the influences of the structures of the upper plate (Collot et al., 2004).

The sedimentary archives preserved in the forearc basins record the deformations caused by the subduction processes and their interactions with the structures of upper plate (Laursen et al., 2002). But at the same time, sedimentary archives record eustatic-climatic changes caused by orbital forcing (i.e. Milankovitch cycles) during Pleistocene Epoch (Paquet et al., 2011; Proust and Chanier, 2004; Proust et al., 2005). These records, in the Ecuadorian forearc, have just been studied in the coastal zone (Cantalamessa and Di Celma, 2004; Pedoja et al., 2006).

The data set collected during the Atacames scientific cruise is an opportunity to study the record of tectonics and climate changes from the submarine zones, i.e. from the shelf and the slope of the central Ecuadorian margin, and to discuss the following points:

- The chronostratigraphic distribution of the Mid-Late Pleistocene sediments on the margin,
- The climatic versus tectonic controls on sedimentation,
- The chronology and spatial distribution of the Quaternary marine basins,
- The age, geometry and influence of the Carnegie ridge subduction along of the margin.

2. Chronostratigraphic distribution of Mid- Late Pleistocene sediments on the margin

The basic building block of the Ecuadorian mid- to late Pleistocene stratigraphy is the T-R sequence, as defined in the San Lorenzo basin (Manta-Plata area). But the most complete set of TR-sequences is observed in the Jama Basin. The stack of T-R sequences is comprised of 26 sequences in total but shows internal, angular unconformities of regional extend. From the largest to the less extensive, these unconformities are the followings.

Three large regional unconformities, which bound three sets of sequences called mega-sequences i.e., from base to top: Lower T-R (LTR), Middle T-R (MTR) and Upper T-R (UTR) (Figure 6.1). LTR encompasses the sequences, from base to top, F to Q (11); MTR from A to E (5), and the UTR from I to X (10) (Figures 5.8 and 5.9).

Two less extensive unconformities, which truncate the UTR sequence set between T-R sequences III and IV and between T-R sequences VII and VIII (surface B and C respectively, figure). These unconformities are observed in Cojimíes, Jama, San Lorenzo and La Plata basins but cannot be tied confidently to the South, in Santa Elena basin and Guayaquil Gulf (Figure 6.1).

One local unconformity is noted in the northern basins from Cojimíes to San Vicente basins between T-R sequences V and VI.

Six unconformities are observed in the Jama Basin: four in LTR, which bound Q-P, O-M, L-J, H-F and two in MTR sequences between E-D and C-A. The sedimentary record in the Jama basin is complete and unique. This record explains the apparent local extend of these unconformities.

Age dating was obtained by 14C measurement of the two uppermost sequences (IX and X) and geometrical correlation of sequences to Quaternary onshore exposures and marine terraces (Cantalamessa and Di Celma, 2004; Cantalamessa et al. 2005; Pedoja et al., 2006) (see details Chapters 3 and 4). Age dating was comforted by the correlation of the T-R sequence - interpreted as a continuous record of the eustatic climatic changes (see details in item 3.2 of chapter 3) - with ages of MIS from Lisiecki and Raymo (2005), (see details of method in chapter 3).

The ages proposed for LTR sequences range from 1.53 Ma (MIS 51) to 1.06 Ma (MIS 30), for MTR sequences from 1.03 Ma (MIS 29) to 0.81 Ma (MIS 20), and for UTR sequences from 0.790 Ma (MIS 19) to present (MIS 1) (Table 5.2). The age of the unconformity between UTR and MTR is well-defined due to the nice exposure in the seismic sections of the ten upper sequences (see Figure 6.1), but the age of the unconformity between MTR and LTR as well as between LTR and the acoustic basement is less certain as it is defined in only one basin. At the end, T-R sequences can probably cover ages from Calabrian (Early Pleistocene, before 2009) to present day (See item 6.1 in chapter 5, and Figure 6.1), i.e. from the 1782 Ka (MIS 63) onward.

_____

Figure 6.1- *Stratigraphic scheme of the forearc marine basins on the slope (A) and on the platform (B). The LTR and MTR mega-sequences are well-defined in the Jama basin. The UTR mega-sequence is well-defined in San Lorenzo and La Plata basins.*

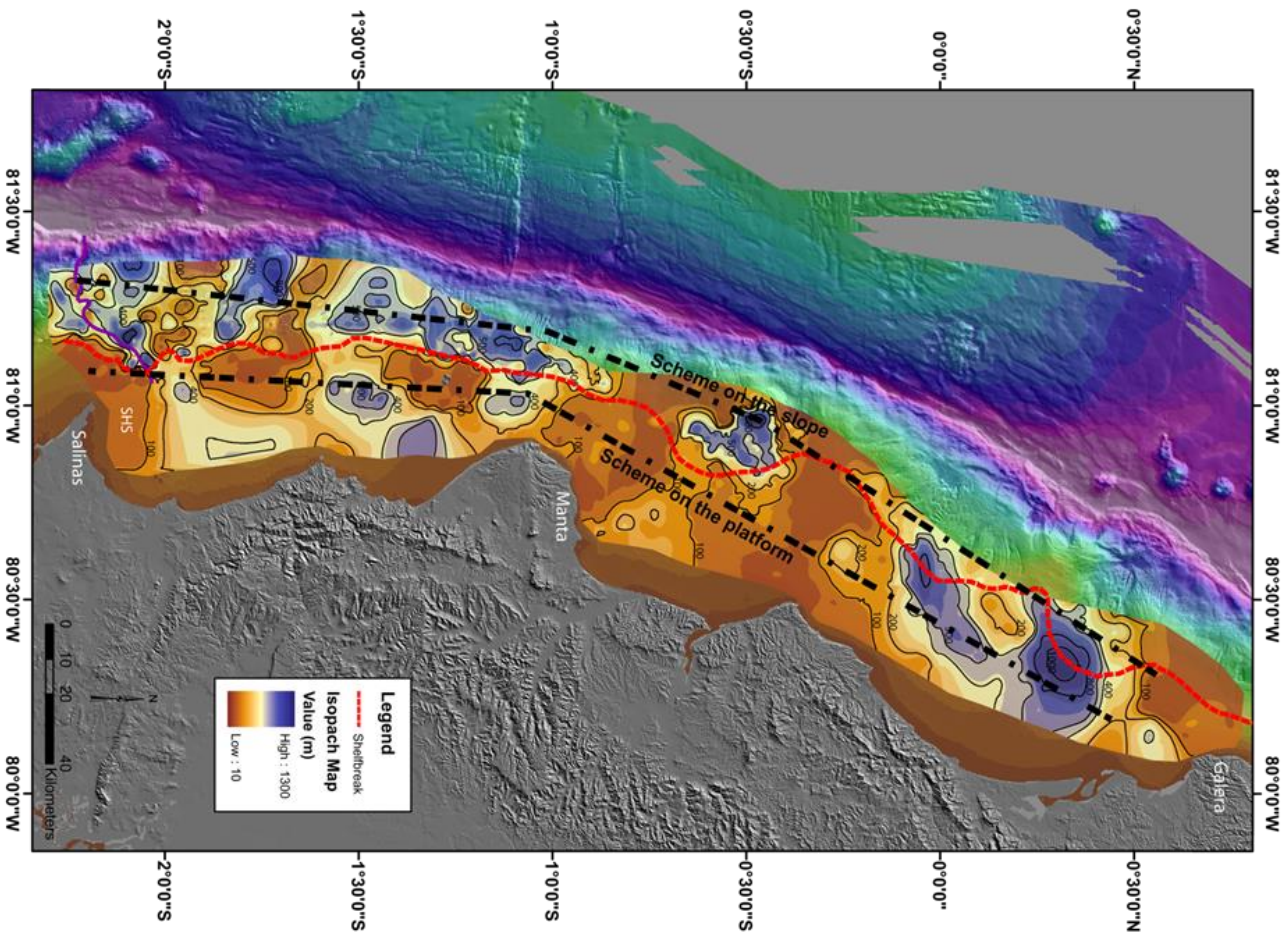

Figure 6.1: Stratigraphic scheme profiles on the slope (Figure 6.1A) and on the platform (Figure 6.1B). See the profile in the two next pages.

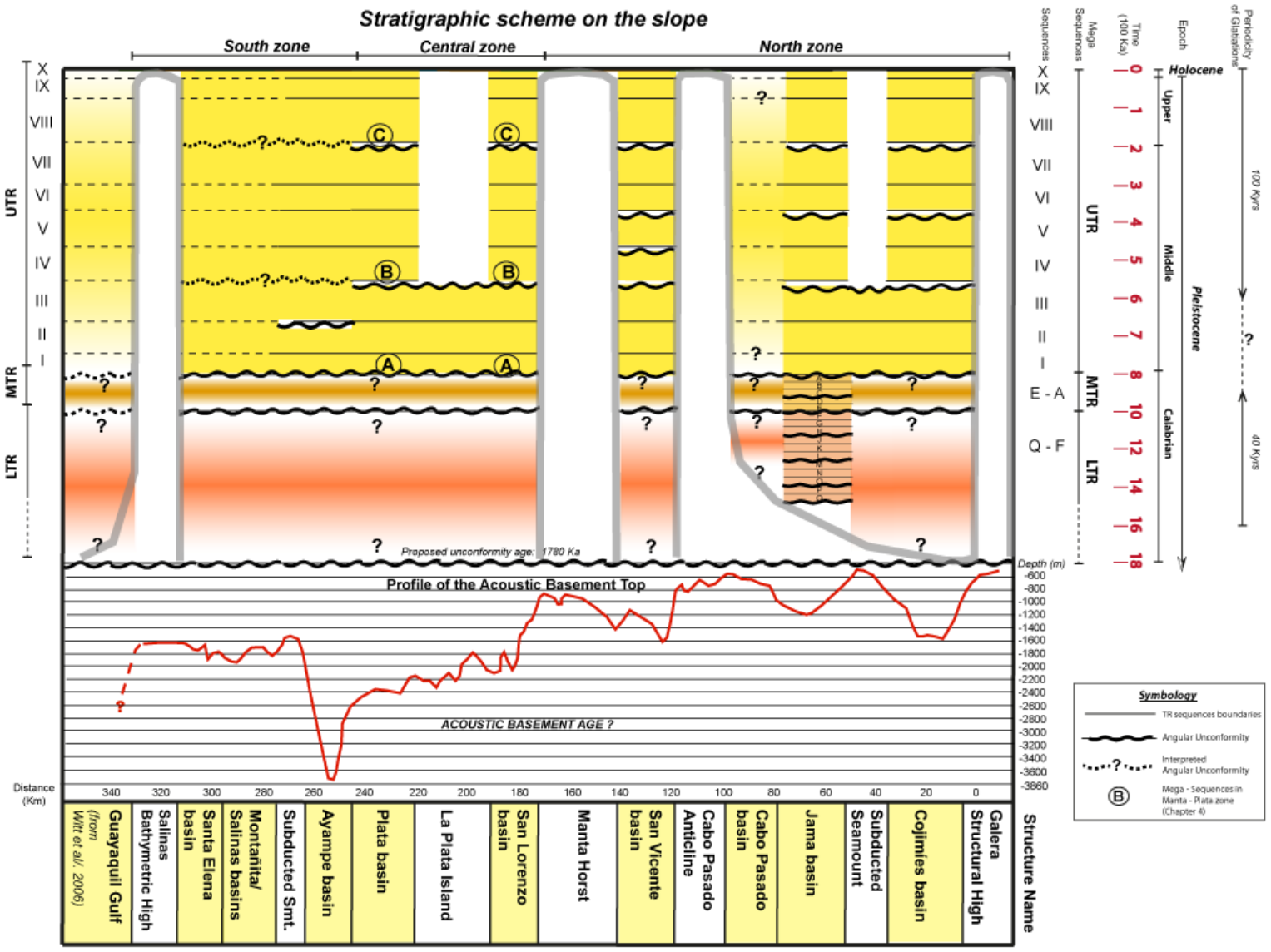
Stratigraphic scheme on the slope
South zone
Central zone
North zone
UTR
MTR
LTR
Proposed unconformity age: 1780 Ka
Profile of the Acoustic Basement Top
ACOUSTIC BASEMENT AGE ?
Distance (Km)
Depth (m)
Sequences
Mega Sequences
Time (100 Ka)
Epoch
Periodicity of Glaciations
Holocene
Upper
Middle
Pleistocene
Calabrian
100 Kyrs
40 Kyrs
E - A
Q - F
Symbology
TR sequences boundaries
Angular Unconformity
Interpreted Angular Unconformity
Mega - Sequences in Manta - Plata zone (Chapter 4)
Structure Name
Guayaquil Gulf (from Witt et al/ 2006)
Salinas Bathymetric High
Santa Elena basin
Montañita/ Salinas basins
Subducted Smt.
Ayampe basin
Plata basin
La Plata Island
San Lorenzo basin
Manta Horst
San Vicente basin
Cabo Pasado Anticline
Cabo Pasado basin
Jama basin
Subducted Seamount
Cojimies basin
Galera Structural High

Figure 6.1A

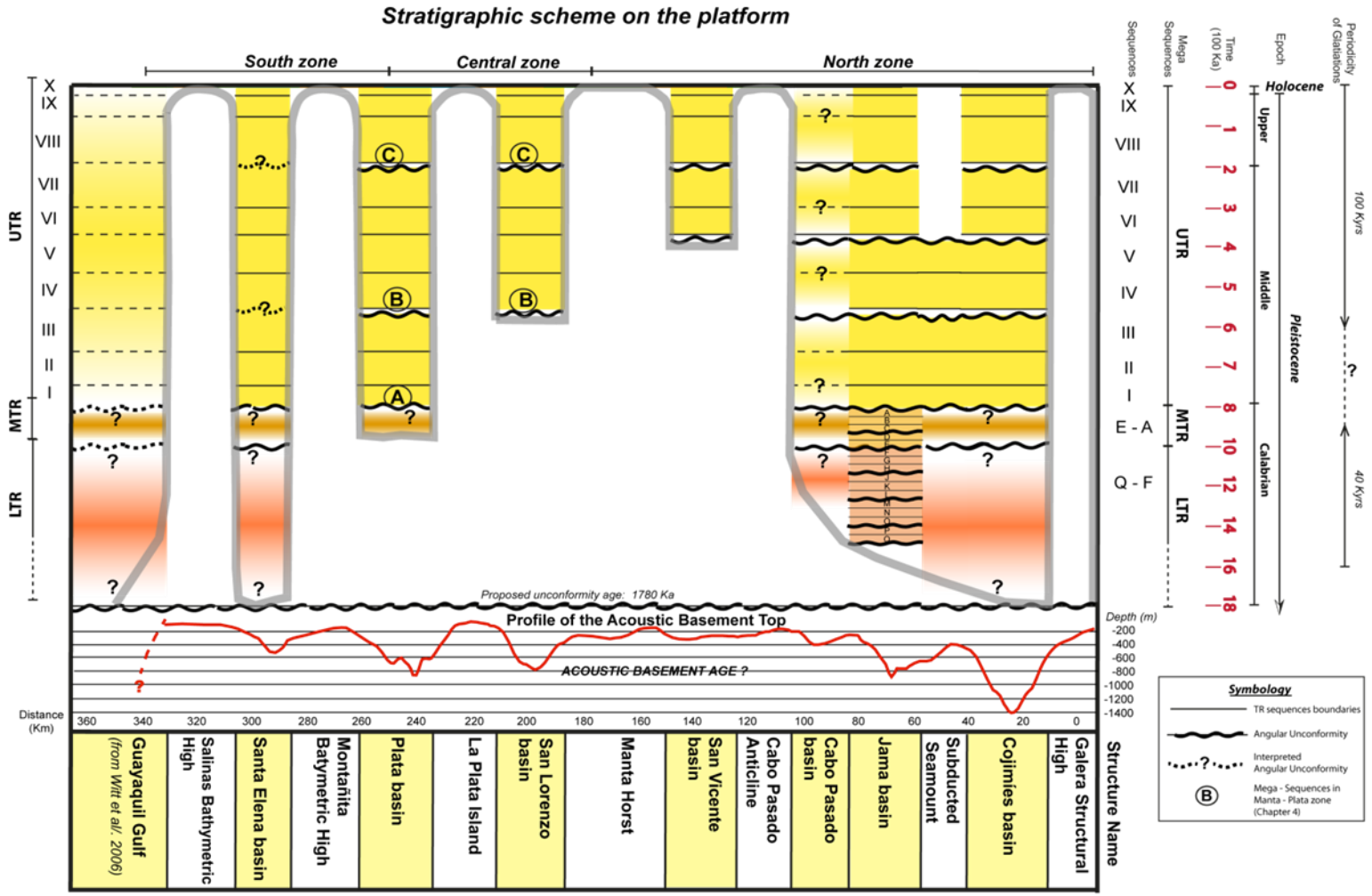
Stratigraphic scheme on the platform
South zone
Central zone
North zone
UTR
MTR
LTR
Proposed unconformity age: 1780 Ka
Profile of the Acoustic Basement Top
ACOUSTIC BASEMENT AGE ?
Distance (Km)
Depth (m)
Sequences
Mega Sequences
Time (100 Ka)
Epoch
Periodicity of Glaciations
Holocene
Upper
Middle
Pleistocene
Calabrian
100 Kyrs
40 Kyrs
E - A
Q - F
Symbology
TR sequences boundaries
Angular Unconformity
Interpreted Angular Unconformity
Mega - Sequences in Manta - Plata zone (Chapter 4)
Guayaquil Gulf
(from Witt et al/. 2006)
Salinas Bathymetric High
Santa Elena basin
Montañita Batymetric High
Plata basin
La Plata Island
San Lorenzo basin
Manta Horst
San Vicente basin
Cabo Pasado Anticline
Cabo Pasado basin
Jama basin
Subducted Seamount
Cojimies basin
Galera Structural High
Structure Name

Figure 6.1B

3. Climatic and tectonic controls on sedimentation

The tectonic and climate interactions create or eliminate space for sediment to accumulate (i.e. accommodation space). These changes can easily be measured by careful analysis and interpretation of change in paleo-water depths from seismic, core and exposure data. However, this analysis does not take into account the variation of the amount of sediment coming from land (or a potential offshore redistribution along the platform), which is erroneously but conveniently, considered constant.

3.1. The eustatic-climatic control

The T-R sequences are comprised of four systems tract: Transgressive systems tract (TST), Highstand systems tract (HST), Falling Stage systems tract (FSST) and Lowstand systems tract (LST). See seismic lines: AtacP092 (Figures 4.6, 4.7 and 6.2B) in the San Lorenzo basin; AtacP039 in the Cojimíes basin (Figures 5.7C and 6.2A); and the AtacP101 seismic line in La Plata basin (Figure 4.11). The preservation of these systems tracts is triggered by the cyclical change of the accommodation space during the glacio-eustatic falls and rises of sea-level due to global climatic changes, related to orbital forcing (e.g. Milankovitch cycles). The unconformity at the top of the regressive part of the TR sequences reflects the change from regression to transgression times.

The ages of LTR and MTR sequences range from 1.53 Ma (MIS 51) to 0.810 Ma (MIS 20), and for UTR sequences from 0.790 Ma (MIS 19) to present (MIS 1) (Table 5.2). The global sea-level curve for the Pleistocene (Lisiecki and Raymo, 2005) shows 40 ka-long periodicities from c.1500 to 790-Kyrs and 100 ka-long periodicities from c.600 ka to the Present. Between 790 ka and 600 Ka, the periodicity is less well defined. Those variations observed despite a strong tectonic overprint, in other active subduction margins (Proust and Chanier, 2004), are attributed to climatically controlled changes in ice volumes that could fit with our observations. The T-R sequences in Ecuador record global changes in sea level due to variations of ice volumes with an average 40 ka periodicity in LTR and 100 ka periodicity in UTR. In details however, LTR and MTR (from 1500 Ka to 790 Ka) show angular unconformities every two or three T-R sequences. This periodicity fits into a 120- 80-ka age-window, with a mean periodicity of 100-Kyrs, pointing to a climate-orbital control on the origin of the unconformities in LTR and MTR.

3.2. The tectonic control

3.2.1. Evidences of deformation

The lateral migration of the offlap break of the successive T-R sequences shows different patterns depending on its location along the margin. In La Plata basin (AtacP101, Figure 4.7) and in the San Lorenzo basin (AtacP092, Figure 4.4), the offlap break shifts progressively in a landward direction. On AtacP039, at the same time, in the Cojimíes basin, the offlap break shows a seaward migration (progradation) from sequences I to V, and from VIII to IX; and a landward migration (transgression) between sequences VI and VII. These shifts in different directions of the offlap break (the shoreline), at the same time, cannot depend on global eustatic changes but rather to a local tectonic influence at the origin of a differential

subsidence. In other words, nevertheless both basins record eustatic-climatic changes, they present a dissimilar record of shoreline shift, suggesting a differential tectonic control between the different basins.

Additionally, the irregular shape of the acoustic basement at the base of LTR - shown in the isodepth map (Figure 5.4A)- with structural heights and lows with different depths; as well as, the lateral changes in thickness of Quaternary deposits along of the margin -shown in the isopach map (Figure 5.4B)- confirms the heterogeneous influence of tectonic on the deposition of the T-R sequences along the margin.

3.2.2. The stratigraphic record of tectonic control

The Jama basin shows the most complete record of T-R sequences from Early-Mid Pleistocene to Holocene along the study zone. The T-R sequences are uplifted and tilted at the rim of the basin and they are truncated by regional scale unconformities, which bound the mega-sequences LTR, MTR and UTR (Figures 5.8 and 5.9). The three groups of mega-sequences do not show any large scale periodicity that can be directly associated with any known climate-control except the Mid-Pleistocene Climate Transition MPT, which encompass the MTR stratigraphic record. These large-scale unconformities, which extend from Galera to Salinas are more likely a manifestation of tectonic events (Figure 6.1).

Some large-scale angular unconformities are also observed in the mega-sequence UTR at the boundary between sequences V and VI in Cojimíes and Jama basins and between: sequences III-IV, as well as VII-VIII, in the basins of the Central zones (San Lorenzo and La Plata and named here as B and C, respectively) and the North zones (Cojimíes and Jama). They are not identified in the Southern basins, which show a thin sedimentary record. In the thick Ayampe basin, where we interpreted the ten T-R sequences of UTR, we did not find clear “angular unconformities” between sequences III-IV and between sequences VII-VIII. In the Ayampe basin, a high-resolution seismic line AtacP104 (Figure 5.15) cuts the basin in N-S direction, i.e. parallels to the direction of deposits. A low resolution SCAN-788 seismic line cuts the basin in a W-E direction, i.e. perpendicular to de direction of deposits (Figure 5.14). None of them offer the opportunity to see with no doubt the internal angular unconformities in UTR.

So, although the boundaries between III-IV and VII-VIII (B and C unconformities) are not correlated around in all basins, like acoustic basement-LTR, LTR-MT and MTR-UTR boundaries, the B and C unconformities were probably caused by regional scale tectonic events.

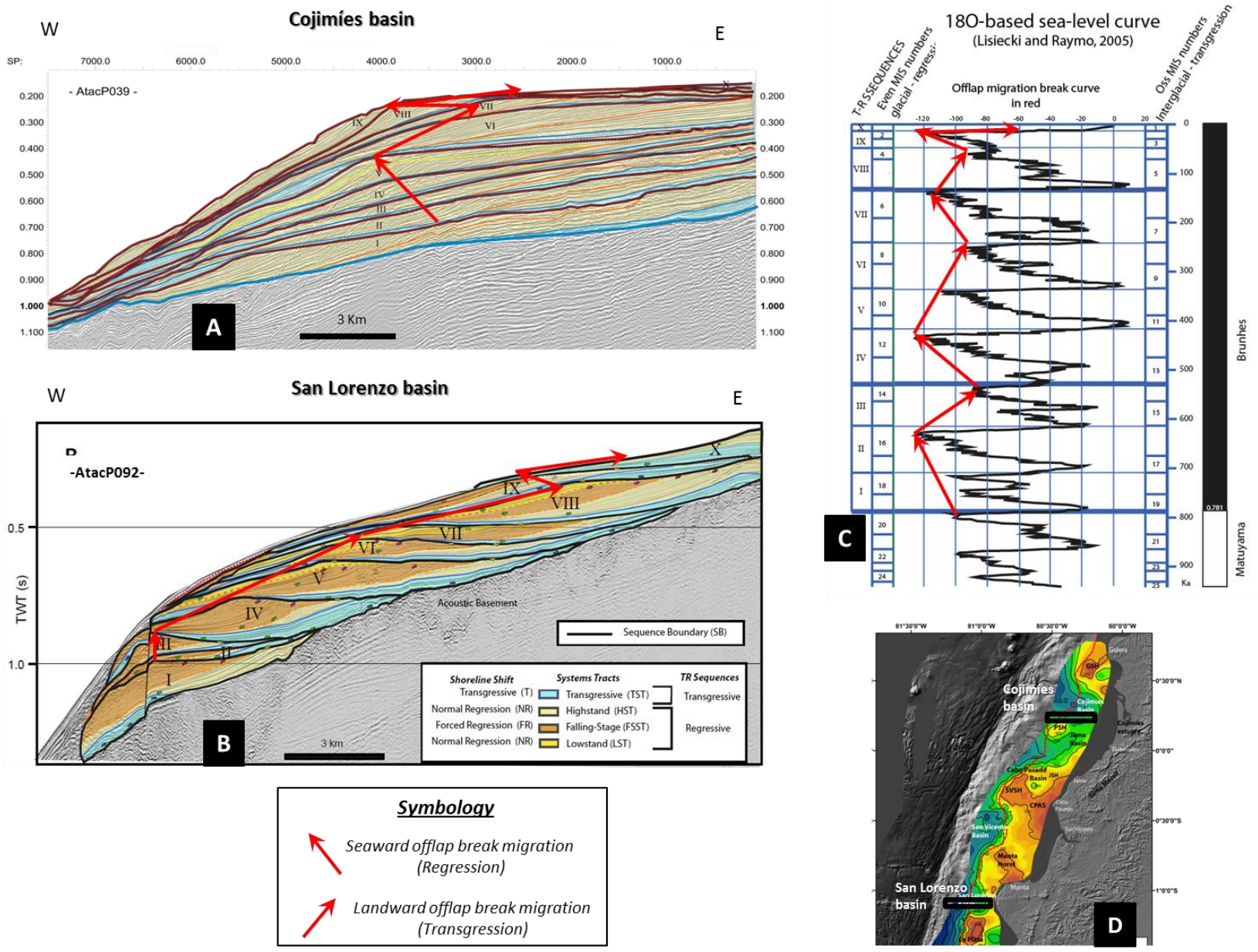

Figure 6.2: Tectonics vs. Climatic control.

Figure 6.2- *Tectonics vs. Climatic control. A) Seismic profile from the Cojimíes basin. B) Seismic line from the San Lorenzo basin. C) Eustatic-climatic curve, from the MIS19 to MIS1 (Lisiecky and Raymo, 2005). D) Map with the location of the seismic lines. We can observe that, despite the two seismic lines show the record of the eustatic climatic changes of the last ten interglacial-glacial cycle, they display different behavior of the offlap break shift. This different record of the shift of the offlap break is related to tectonics.*

_____

4. Evolution of the Northern basins

In the North zone we identified four basins. Three of them, the Cojimíes, the Jama and the Cabo Pasado basins, are located on the platform. The San Vicente basin is located on the upper slope and separated from the platform-basins by the Cabo Pasado Anticline Structure (CPAS) and by the San Vicente Structural High (SVSH) (Figure 5.4).

4.1. The platform basins

The three basins of the platform are filled by the three mega-sequences LTR, MTR, and UTR (Figure 6.1). Each mega-sequence thickens from Cabo Pasado basin to Cojimíes basin (Figure 5.5A). The imaginary line that joins the deepest point of the three basins (the lowest contact between the base of LTR and the acoustic basement) on seismic line SCAN-425 (Figure 6.3A), dips from south to north, *i.e.* there is an increasing depocenter depths toward the North. This structural behavior is also shown in the isodepth grid of the acoustic basement (Figure 5.4A) and reflected in the divergent reflection configuration pattern observed from the south to the north on the N-S seismic line (Figures 5.5A, 5.8B and 5.10A). This increasing accommodation space to the north together with the progressive tilt of the reflectors suggests a differential tectonic subsidence to the north, which occurred during sedimentation.

This differential subsidence to the North seems to be reflected also in the seafloor morphology (Figure 5.1). In the North, in the zone of higher subsidence (Cojimíes basin), the bathymetry shows the largest re-entrant of the platform edge (Cojimíes re-entrant, CE); while southward, in the zones of lower subsidence (Jama and Cabo Pasado basins), the isobaths show a smoother re-entrant (Jama re-entrant, JE). It seems that the subsidence of the basins drives the platform edge retreat and that this phenomenon might still be active.

4.2. Lateral continuity of the platform basins

The isodepth grid map of the acoustic basement and the isopach map show that the basins are separated by structural highs (Figure 5.4). The Pedernales Structural High (PSH), and the Jama Structural High (JSH) separate the Cojimíes from the Jama basins and the Jama from the Cabo Pasado basins, respectively. However, the increasing

subsidence to the north, as well as the divergent configuration reflection patterns of the mega-sequences, discussed above, suggests a lateral continuity of the stratigraphy between the three basins.

4.3. The Cojimíes and Jama basins continuity

On the platform, close to the coast, the mega-sequences LTR to UTR are continuous from the Cojimíes to the Jama basins (profile 433 of Fig. 5.5 C). Seaward, LTR and MTR are separated by the PSH (profile 425 of Fig. 5.5 A and Figure 6.3A), which influence increases close to the slope.

Figure 6.3- *NE-SW seismic lines of the North basins. A) Seismic line SCAN-425, showing the north basins Cojimíes, Jama, and Cabo Pasado. We can observe in this seismic line the concave and bag-shape reflection configuration patterns of the mega-sequences into Cojimíes basin, which suggest constant X-Y location of the depocenter along the time. While the divergent toward north of the seismic reflection patterns of the mega-sequences of Jama basin suggest a northward migration of the depocenters along the time. B) Seismic profile SCAN-433 suggests a lateral continuity between Jama and Cojimíes basin. The both seismic lines show a deepening of the depocenters toward north C) Map with the location of the seismic lines over the acoustic basement grid, which show the lateral continuity of the basins toward the inner platform. The Cojimíes, Jama and Cabo Pasado basin seem to have opened as a single basin and after divided by a the subduction of the Atacames seamount and by the marine prolongation of the Jama Massif.*

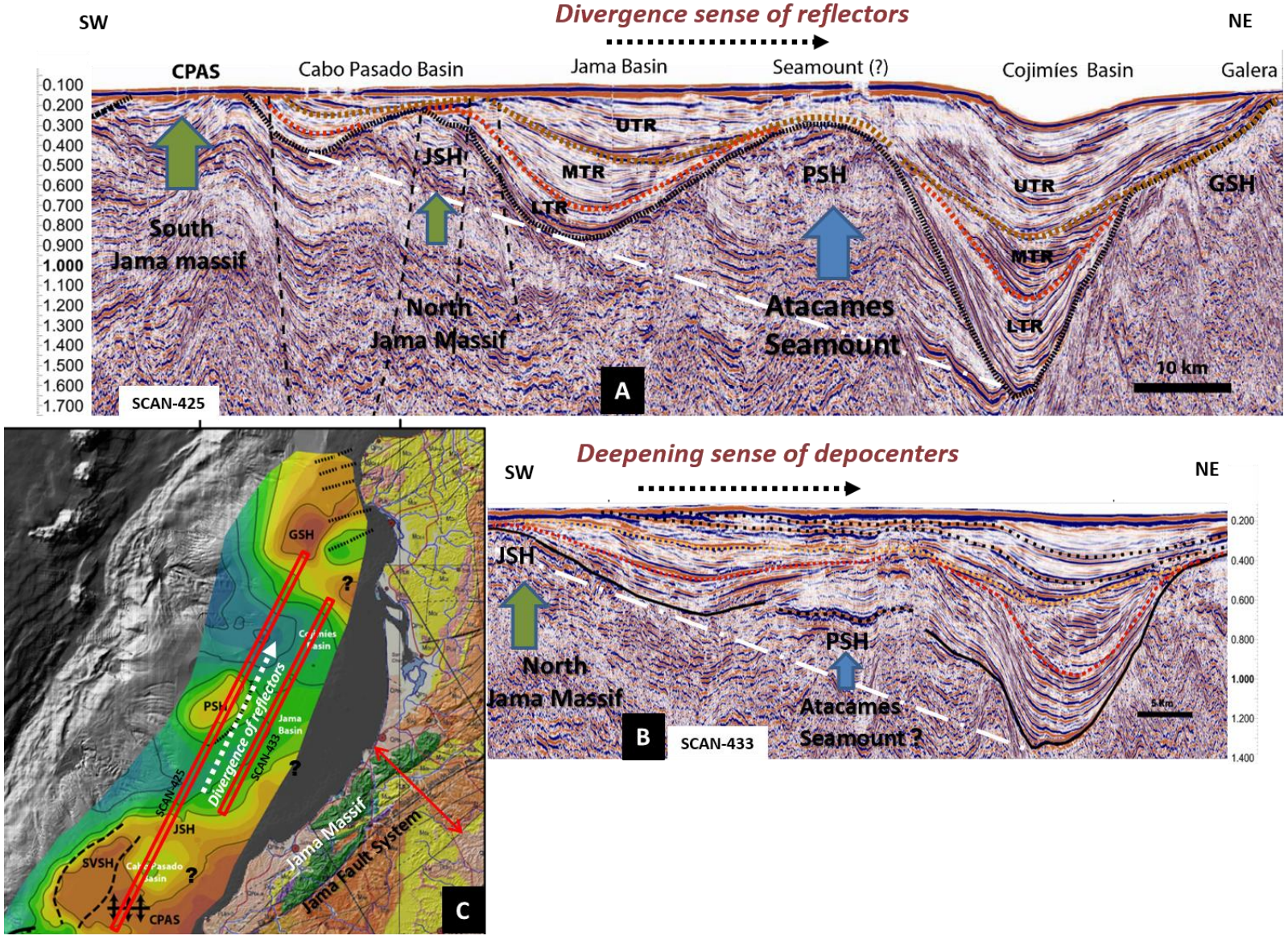

Figure 6.3: NE-SW seismic lines of the North basins.

4.3.1. The relationship between PSH and the subducted Atacames seamount

As discussed above, the PSH plunge below LTR, MTR and UTR sediments of the inner shelf when it is sealed by UTR (T-R IV to X) at the shelf break (Figure 5.5). Considering that:

PSH is closed to the area of the subducting double-peak seamount observed by Marcaillou et al. (2016),(Atacames seamounts chain, Figure 6.5A);

The flanks of the eastern peak (Ep) of the subducted seamount encompasses the PSH (dotted red line in Figure 6.5A);

The bathymetric data show deformation affecting more the slope than the inner platform: scarp of the subducted seamount on the eastern side of the PSH, landslides at the foot of the scarp and at the foot of the slope, in front of the Cojimíes basin (figure 6.5A);

As well as these deformations are similar to modeled features (Dominguez et al., 1998; Hampel, et al., 2004), it is very likely that the PSH corresponds to the deformation of the upper plate caused by the eastern peak of the double-peak Atacames subducted seamount (Marcaillou et al., 2016).

The distance between the two peaks (red stars in Figure 6.2A) and the trench are about 17 km for the western peak (Wp) and 25 km for the eastern peak (Ep) (Marcaillou et al., 2016). Considering a subduction velocity of 4.7 cm/yr (Nocquet et al., 2014), we obtain an age of 362-Ka for the start of the subduction of the western peak, and 532-Ka for the eastern peak. We examine below the chronology of the deformation caused by this seamount subduction.

- *The eastern peak:* the calculated-age of the eastern peak subduction fits to the age window of the regional unconformity between the sequences III and IV of UTR, i.e. 533-Ka (MIS 14 and MIS 13, see Table 5.1). The contact between the sequences III and IV is sharply erosive causing the truncation of the sequence III as described in Chapter 5 (Figure 5.7C) and possibly some landsliding with some relics sediment bodies preserved at the foot of the slope. The regional unconformity at the base of T-R IV underlines the sediments that seal the PSH. This regional unconformity marks also a landward shift of the T-R sequences in the Cojimíes basin (see the southern border, close up of SCAN-425, Figure 5.5B), an increase in accommodation space and subsidence rate. This supports the idea that the subduction of the eastern peak of the seamount caused the uplift of the acoustic basement, forming the PSH, the drowning of the basin and then the change in the depocenter geometry of the Cojimíes basin after the deposition of the sequence III.

However, it is important to note that, according to the stratigraphic scheme (Figure 6.1), the boundary between the sequences III and IV is a regionally correlative tectonic event. So, the two events, local and regional, could be somehow related.

- *The western peak:* the calculated-age for the subduction of western peak of the Atacames seamount fits with the age of the sequence V, i.e. window at 424-Ka. (MIS 11 - MIS10). The unconformity does not correspond neither recognized erosional and regional event, like at the

top of sequence III, nor specific landsliding, but the unconformity is sharply erosive and caps the sediment pile at the top of the PSH at the shelf break. In the Cojimíes basin, the unconformity marks a drastic landward migration of the offlap break of the T-R sequences which suggests a rejuvenation of the local depositional profile, an increase of accommodation space and an increase in the subsidence rate (see Atac039 seismic profile, Figure 5.7C). This evolution is similar to the one described above for the eastern peak.

4.3.2. A proposed evolution of the Cojimíes Jama basins boundary

The prograding clinoforms from the sequences I to V that cross the PSH between the Jama basin and the Cojimíes basin (N-S seismic profile SCAN-433 of the Fig. 5.5C) indicate that these two basins were connected until the deposition of sequence V. The subduction of the eastern peak of the Atacames seamount caused the separation between the Cojimíes and Jama basin at the shelf break after the deposition of the sequence III, but these basins were still connected on the inner side of the platform. The subduction of the western peak, after the deposition of the sequence V, increased the uplift of the high, which reaches the inner side of the shelf. The acoustic basement grid as well as the isopach map (Figures 5.4A and B) suggests that they are still connected today near the coastline, probably reaching the coastal zone in the Cojimíes estuary (Figure 6.5A).

All these considerations suggest that the Jama and Cojimíes basins were a single basin for a long time, until the subduction of the double-peak Atacames seamount. The subduction of this asperity caused the division of this single basin in two basins. The migration of the high occurred in two steps, each controlled by the subduction of two prominent asperities (eastern and western peaks).

4.4. The Jama and Cabo Pasado basins continuity

The Cabo Pasado and Jama platform basins are partially separated by the JSH (seismic line SCAN-425 of the Figure 5.5A). JSH does not show any bathymetric morphology that could be interpreted as the recent subduction of a seamount, like PSH (Figure, 5.1A). However, it is located offshore of the northern edge of the Jama massif (Figure 5.4), which is related to the Jama fault system (Reyes, 2013).

In the Cabo Pasado basin, LTR-MTR-UTR shows a divergent character, a general onlap with progressive thinning on JSH, and a progressive migration of the depocenter location to the north (Figure 5.10A). UTR lies with a sharp angular unconformity on MTR and shows internal unconformities and high angle clinoforms that sign changes in the progradation directions. These changes appear clearly close to CPAS on seismic profile AtacP046.1 (Figure 5.10A). In the Jama basin, LTR-MTR-UTR shows exactly the same features (Figure 5.8B). These observations suggest a strong control on south Cabo Pasado and north Jama basins sedimentation by the uplift of JSH. It might have been reactivated however during UTR altogether with CPAS.

The CPAS and the Jama System faults relationships at the southern border of the platform basins

CPAS bounds to the south the northern platform basins (Cojimíes, Jama and Cabo Pasado - Figures 5.4 and 5.5). CPAS, as described in Chapter V, is an anticline structure draped by places by Quaternary sequences (LTR, MTR and UTR). The reflection configuration on both sides of the anticline (Figure 5.10A), suggests that the axis of the anticline is oriented in E-W direction (Figures 5.23 and 6.5A). Its hinge zone crops out at the seafloor, in front of Cabo Pasado cape (Figures 5.10 A and C) where the southern side of the Jama massif, controlled by the strike-slip Jama fault system, is exposed (Figure 6.6A). The anticline axis is sub-perpendicular to the Jama fault system. The location of this anticline and the relative geometry of its axis allow us to suggest that this anticline (CPAS, and possibly JSH) corresponds to a possible trans-pressional structure related to the Jama fault system. CPAS cropping out at the seafloor, was uplifted higher (faster?) that JSH.

Given that the SE boundary of the three basins is close to the NE orientation of the Jama massif (Figure 6.1A), and the divergent reflection configuration patterns toward north shown in the three basins (see the N-S seismic lines of Figure 5.5), we infer that the uplift of the southern boundary of the basins formed at the same time as their opening. This opening could be related to the dextral transforms displacements along the Jama faults system. This process probably began by the opening of a single basin, progressively segmented by fault-controlled basement highs whose rise was locally enhanced by the subduction of oceanic asperities (Ep and Ew of the Atacames seamount), (Figure 6.3).

4.5. Uplift of the border of the platform

4.5.1. Geometric evidences

The W-E seismic profiles in the Cojimíes basin show a vertical stack of prograding clinoforms (see description in Chapter 5) without any deformation at the shelf break (Figure 6.4A). On the contrary, the W-E seismic lines in the Jama basin display groups of prograding clinoforms that are progressively tilted in a landward direction. The offlap breaks of these sequences (rollover) are uplifted above the flat part (topset) of the clinoforms (Figure 6.4B). In Cabo Pasado basin, the W-E seismic data show also a landward migration of the depocenter of the three groups of mega-sequences (Figure 6.4C). The LTR thickest zone is located on the western side of the basin, while the UTR thickest zone is displaced 9 km landward of the LTR depocenter (see description in the Chapter V). The acoustic basement outcrops at the seabed, close to the shelf break, bounding the basin to the west. This uplift and landward stepping pattern of the offlap breaks appears from sequences L-J of LTR to sequence X of UTR in Jama basin but started as early as sequences O-M and the very base of LTR Q-P (Figure 5.8A) to the North, in the Cabo Pasado basin. These different sequence patterns observed at the border of platform, without any uplift of the platform edge in the Cojimíes basin, and an uplift of the border of the shelf in the Jama and Cabo Pasado basins (Figure 6.4), suggest an additional W-E tectonic control aside the subduction of seamounts observed in the North, and the Jama fault system dextral shear seen in the South.

PSH relates to the Atacames seamount subduction, that extents 20 km south of the eastern peak location (red doted frame over SIS 55, in Figure 6.4A), (Marcaillou et al., 2016) but the

uplifted platform edge is located 40 km south of the eastern peak position (AtacP044 and the AtacP065, Figure 6.3), (Figure 6.5A). The age of the Atacames seamount subduction is bracketed by the ages of the UTR sequences III and V (533-Ka and 424-Ka, respectively). The age of the uplift of the border of the shelf is recorded by the offlap break migration of the O-M of the LTR sequences, dates back to 1452-Ka or possibly 1530-Ka.

- If the subducted CR retains the same N-S geometrical shape as the one described by Lonsdale (1978) in a longitudinal bathymetric section of the trench (Figure 2.3): the steep northern flank of CR started at latitude 0º, at the current location of the highest part of the CR. This northern flank of CR is observed in seismic data (see the multichannel seismic line SIS-55, blue dotted frame in Figure 6.5B), (Marcaillou et al., 2016), and below Cabo Pasado cape (Figure 6.5A), (Collot et al., 2004).

The subduction of the highest part of the CR fits with the observed uplift of platform edge at SVSH and Jama basin (white dashed line on borer of platform in Figure 6.5A). The subduction of its northern flank is probably responsible for the northward divergent reflection pattern of the mega-sequences together with the progressive drowning of the depocenters to the North (Figure 6.3).

Thus, we suggest that the forearc marine basins located between Cabo Pasado to Galera points were formed by the interaction between the Jama faults system and the subduction of the northern flank of the CR. These basins were locally deformed by the subduction of seamounts.

***Figure 6.4**- Uplift of the Platform edge. A) Seismic line from Cojimíes basin showing that there is not uplift of the platform edge in this zone . B) Seismic line from Jama basin showing uplifted sequences at the border of platform. C) Seismic profile from the Cabo Pasado basin showing the uplift at the edge of platform, where the acoustic basement crops out to the seafloor. D) Map with the acoustic basement grid and the location of the seismic lines.*

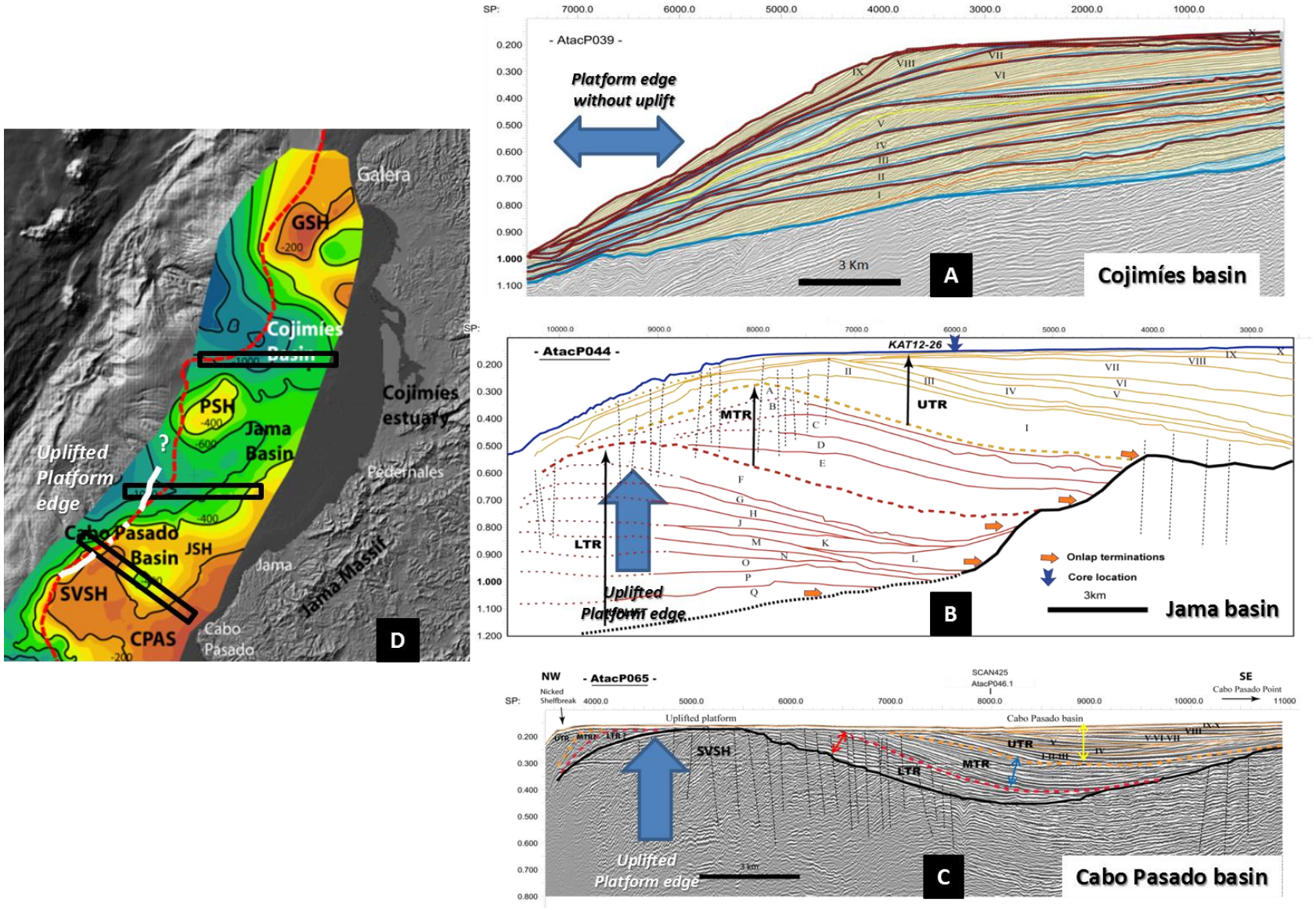

Figure 6.4: Differential behavior of the Platform edge displayed in the Northern basin, showing the uplift from the south side of the Jama basin.

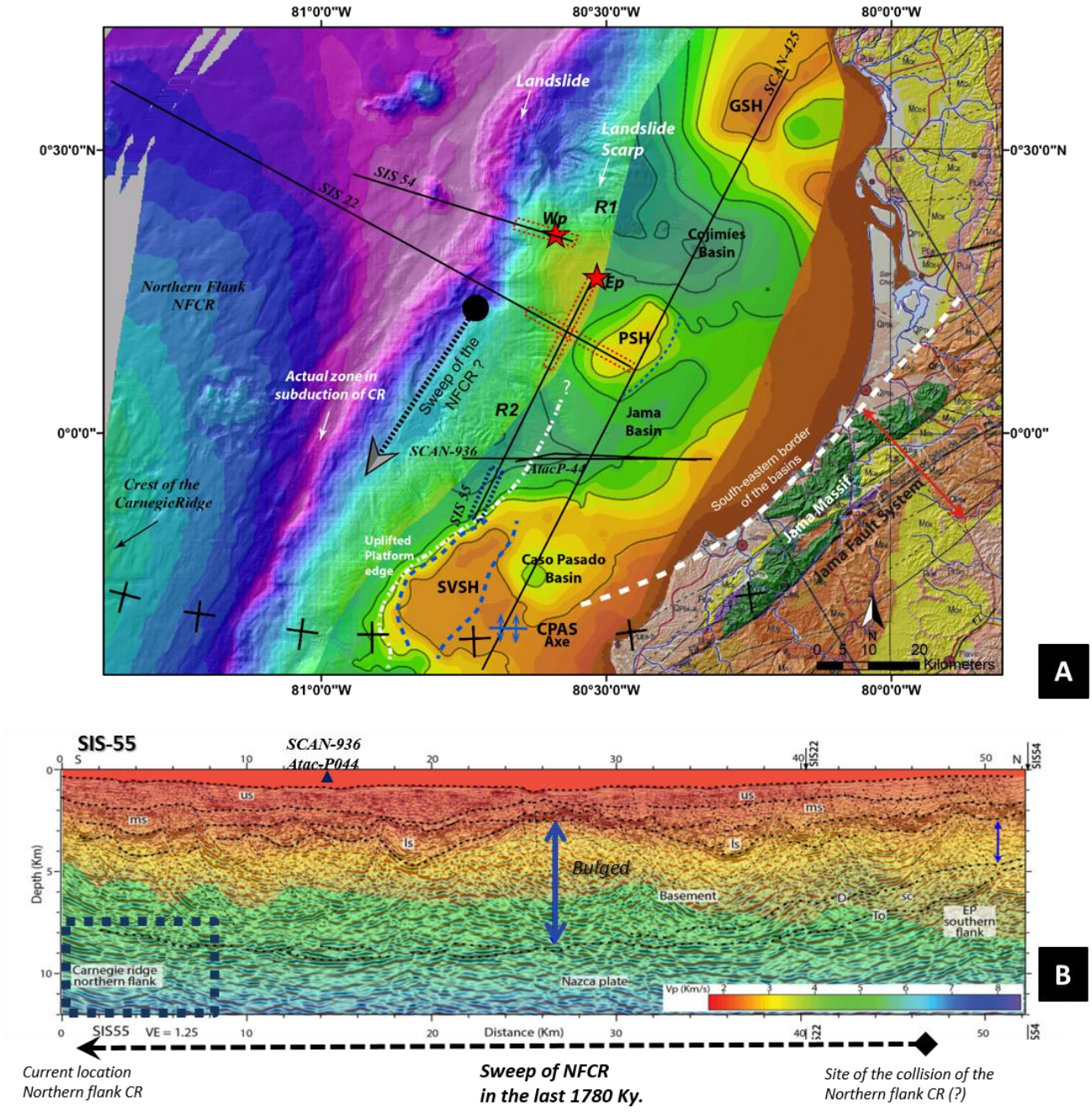

Figure 6.5: Structural elements of the Northern basins.

- Structural elements of the northern basins. ***A)*** *Composite map of: Grid of the acoustic basement, bathymetric grid and coastal geology (From Reyes, 2013). It shows: 1) the north basins at platform; 2) the South-eastern border of the basins which follow the direction of the Jama massif and the Jama Structural system; 3) The interpreted faults on the margin, and the CPAS axe; 4) The interpreted CR crest subducted (from Collot et. al., 2004); 5) The northern flank of the CR interpreted in the SIS-55 seismic line (blue dotted frame) from Marcaillou et al., (2016); 6) The uplifted platform edge zone (white dashed line), related to CR subduction; 7) The actual northern contact point of the CR subduction; 8) The proposed zone of sweep of the NFCR; 9) The eastern and western peaks (Ep, Wp) of the subducted Atacames seamount (red stars) and their influence zones in red dotted frame (from Marcaillou et al., 2016); 10) The location of the Seismic data from the different campaigns (Atacames, SCAN and SISTEUR).* ***B)*** *The interpreted SIS-55 seismic line from Marcaillou et al., (2016). In blue dotted frame the zone interpreted, by them, as the NFCR (represented also in the map above). The blue arrow shows the bulged basement from the location of the EP southern flank, which could evidence the sweep of the Northern Flank of the CR. The black dashed arrow, below the seismic line, shows the interpreted zone of sweep of the NFCR (the arrow is also shown in the map above).*

4.6. The slope basin of San Vicente

The San Vicente basin sits on the slope (Figure 5.4), unlike the Cojimíes, Jama and Cabo Pasado basins, which are located on the shelf. It is isolated from the northern basins by the SVSH and CPAS, and from the southern basins, by the Manta Horst.

- The San Vicente basin develops below a stepped slope area. This stepped slope is underlined by a positive flower structure (K2) (related to strike-slip compressional forces) at the origin of local knick points at the shelf break. These structures aligned with the Jama fault system on land. The positive structure separates the San Vicente basin in two parts: i.e. a thick and deep basin at and seaward of the stepped slope, and a thin and shallow depocenter on the platform.

- The basin fill is comprised of LTR, MTR and UTR sequences. A sharp acoustic basement high ("uplifted wall") bounds the basin to the West, when the reflectors onlap the acoustic basement rise to the East. The sequences show a divergent, concave and bag shape reflection configuration patterns in a landward direction (Figure 5.11B). On the platform, the acoustic basement is very shallow, only draped by a thin suite of the UTR sequences VI to X (Figure 5.11C).

- These observations suggest that the basin began to subside at about the same time as the northern basins (Figure 6.1). The western high was uplifted during the deposition of the sediments. However, the lack of the UTR at the top of the "uplifted wall" (west of bathymetric indent, Figure 5.11A) indicates that this side of the basin was isolated at the end of MTR. On the shelf, the accommodation space was created from the deposition of sequence VI onward. Before the sequence VI, either the sediments were not deposited or were eroded out. The "uplifted wall" seems to be an extension of SVSH (white dashed line in Figure 6.6A), when the platform is the southern continuation of CPAS.

Considering that:

The uplifted wall, which bounds the western side of the basin, seems to be a prolongation of the uplifted border of the margin observed from Jama basin to SVSH and that this uplift might relate to the subduction of the CR (white dashed line in figure 6.6A).

The concave and bag-shape reflection configuration patterns stepping westward into the deepest zone of San Vicente basin (Figure 5.11), suggest a compressional force in W-E direction (Figure 6.6). And, the positive flowers structures at the platform edge in line with the trans-compressional Jama fault system (Figure 6.6B).

We postulate that the relationship between the W-E compressional forces -caused by subduction of the CR- and the strike-slip forces -caused by the marine prolongation of the Jama fault system- creates the deepest zone of San Vicente basin (Figure 6.6). This deepest zone of the basin seems to be controlled by strike-slip forces (Collot et al., 2004; Hernández, 2014), which creates the sediment accommodation space on the slope when the limited accommodation space on the platform appeared later, during the deposition of sequence VI.

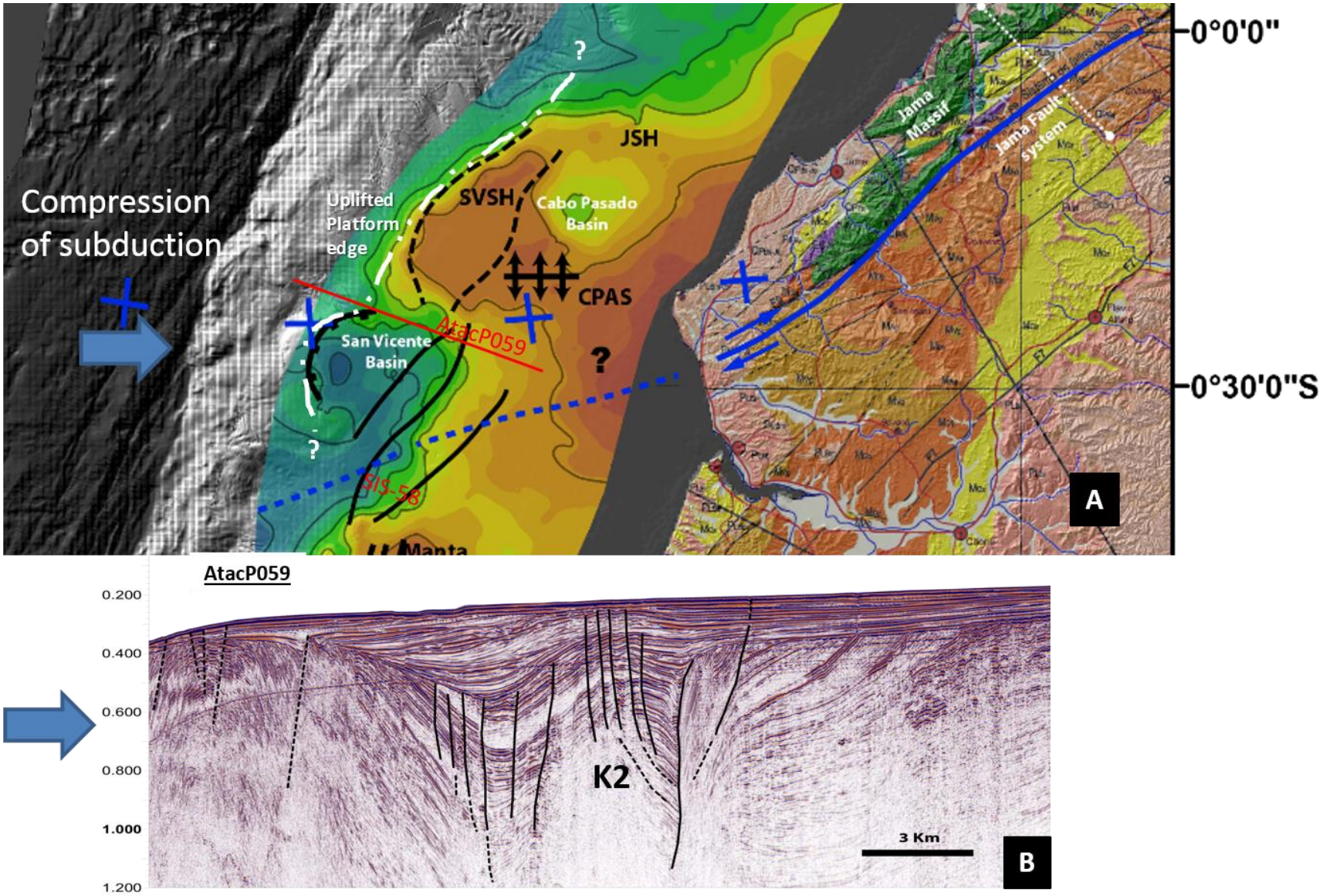

Figure 6.6: Structural elements around of San Vicente basin.

***Figure 6.6**- Structural elements around San Vicente basin. A) The San Vicente basin sector of the structural scheme, showing: Jama fault system prolongation to sea, proposed by Collot et al., 2004 and the structures interpreted on platform using the Atacames and SCAN seismic data. B) The AtacP059 seismic profile located just to the north of the San Vicente basin, displaying a flower structure (K2), which confirms the influences of the strike-slip forces in the basin evolution, proposed by Collot et al., 2004; Hernández, 2014.*

_____

5. Evolution of Central basins

5.1. Stratigraphic records of the subduction of a seafloor relief

Well-developed UTR sequences characterized the central basins (San Lorenzo and La Plata basins, see Chapter 4). Between these two basins the Isla de la Plata exhibits several marine terraces. On the slope, and controlled by faults, LTR and MTR are present locally.

The subsidence of the continental shelf acoustic basement, estimated by the stepwise backstripping of the sedimentary record, exhibits a complex deformation pattern with uplifting and subsiding regions (Proust et al., in press). Deep marine seismic data, evidences an anomalous plate boundary topography at the top of the Carnegie Ridge (seamount), beneath La Plata Island (Sanclemente, 2014). The pattern of the continental shelf deformation is consistent with the shape of this seamount. At sequence IV, the seamount collides the base of the continental slope and subducts beneath the continental shelf until it totally disappears from the surface at T-R VIII. At that time, the shelf shows a complex subsidence pattern with an uplift of La Plata Island and the subsidence of the surrounding areas, which mimics the gross shape of the subducting seamount. From T-R X to present day, subsidence tends to resume and relax, as the seamount can be too deep to influence the surface anymore (Proust et al., in press).

5.2. Manta Peninsula uplift

5.2.1. Comparison with the Nazca ridge subduction

The well-preservation of the UTR sequences just in front of the Manta Peninsula can be compared to the sequences observed in front of Pisco area where the Nazca ridge is subducted beneath the Peru margin (Hampel et al., 2004a) (Figure 1.7B). In both areas, Manta (Ecuador) and Pisco (Peru), the subsidence of the shelf break offshore is associated to uplift of marine terraces onshore. Along the Peruvian margin the subsidence of the shelf break and the coastal uplift were related to tectonic erosion enhanced by the subduction of the Nazca ridge (Hampel et al., 2004b). Meanwhile the Nazca ridge does not have the same shape/geometry than Carnegie ridge, this comparison supports in first order the idea that the origin of the Manta Peninsula uplift could be related to CR subduction.

5.2.2. Onshore/offshore tectonic timing and syntectonic sedimentation

Cantalamessa and Di Celma (2004) have proposed that the emersion of the Manta Peninsula starts during the Early Pleistocene (now Calabrian Pleistocene) and continues throughout 1800-

Ka to 781-Ka, by the inversion of "Canoa" basin. Pedoja et al., (2006) have proposed 1000 Ka (MIS27 to MIS 31), age for the oldest marine terrace (T5) in Manta Peninsula which correspond to the age of the boundary between MTR and LTR.

This chronology indicates that the vertical tectonic at Manta Peninsula, occurred during LTR and MTR, together with syntectonic sedimentation on the upper slope. Moreover, the uplift of Manta Peninsula began at the same time that the uplift of the platform edge reported in the north and that we assume to be related to CR subduction.

5.2.3. The Manta Peninsula uplift

In a palinspastic reconstruction of Manta Peninsula Cantalamessa and Di Celma (2004) report, during the Middle Pleistocene (Figure 6.8D), an earlier step corresponding to the emersion of an island, the San Lorenzo Island, surrounded at north and south by the Manta and Canoa basins respectively (Figure 6.8A). This "island step" seems similar to the current situation shown at La Plata Island, which is surrounded by two basins, San Lorenzo basin at north and by La Plata basin at south (Figure 6.8B).

Is the "island step" of Manta Peninsula (Pedoja et al. 2006), could be related to the subduction of an asperity as we have proposed to La Plata island uplift (Figure 6.8C) (Proust et al., in press). Many subducted asperities are inferred by Sanclemente, (2014) (Figure 6.7) in this area. The uplift of the four youngest marine terraces of La Plata Island are time correlative with the asperity subduction (Ocean Massif-OM in Figure 6.7), dated at around 563-Ka (Chapter 4). If we want to apply our model to the Manta Peninsula "Island step", we need to consider the subduction of an older asperity at around 1.000 Ka (age similar to the oldest T5 terrace described by Pedoja et al. (2006). However, the Manta Peninsula is more distant of the trench than the island of La Plata, which makes it difficult to make a simple transposition of our model proposed for La Plata Island, as the seamount can be too deep to influence the surface anymore. We suggest than E-W compressive deformation might explain the synchronous downwarp of the shelf edge and uplift of Manta Peninsula (Proust in press).

5.2.4. The Manta-Plata uplift: local effect of oceanic massif added to regional effect of the Carnegie ridge

The subduction of an oceanic asperity increment the subduction erosion, causing the subsidence at the slope and the uplift at platform (Figures 1.4 and 6.8F). The difference behavior, between the uplift of border of platform (shown from Jama basin to Manta horst, Figure 6.4) and the subsidence in front of Manta Peninsula (Figure 6.8E), could be explained by the significant roughness of the Carnegie ridge in front of and beneath the Manta-Plata uplifted area. This is consistent with the presence of many asperities in this area and with the alignment between the Mp6, SMt1 and a blade asperity of the CR (Figure 6.7).

These considerations allow us to suggest that the uplift of Manta-Plata zone could be partially due to the same regional cause than the uplift observed in the Jama basin to the North. But, the presence of additional asperities over the CR in front of Manta Peninsula, incremented erosion/bypassed process at platform, removing LTR and MTR deposits, and creating

subsidence on upper slope with accommodation space for the deposition of UTR. While at the same time, on the internal platform, the uplift was incremented forming the Manta Peninsula.

The smooth oceanic massif suggested by (Sanclemente, 2014) below La Plata Island is different of the other seamounts in size and by the fact that, in this area, the volcanic relief of the Carnegie ridge is crested by this oceanic massif. This could suggest that the local effect of this oceanic massif is added to the regional effect of the Carnegie ridge and explain the enhanced vertical deformation of this area. In a similar case off Chile (Laursen et al., 2002) show that the effect of the Juan Fernandez ridge is enhanced when it is crested by seamounts (Figure 1.10).

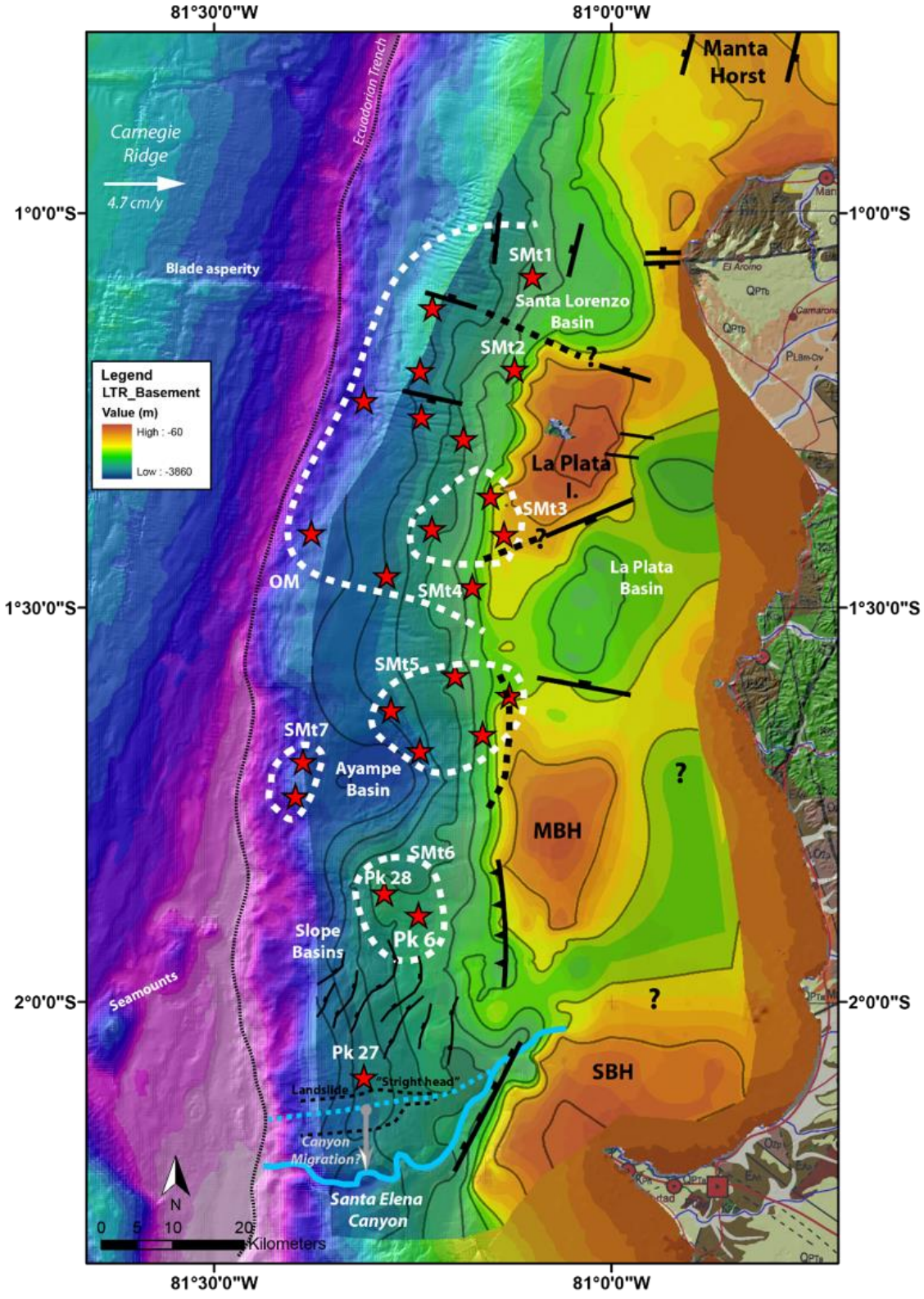

Figure 6.7: Map with the structural elements of the southern basins.
It shows the grid of the base of the LTR mega-sequence (grid of the acoustic-basement), the interpreted faults of the zone, and location of the peaks and seamounts interpreted by Sanclemente (2014). It shows, at south of the map, the interpretation of the southward migration of the Santa Elena canyon.

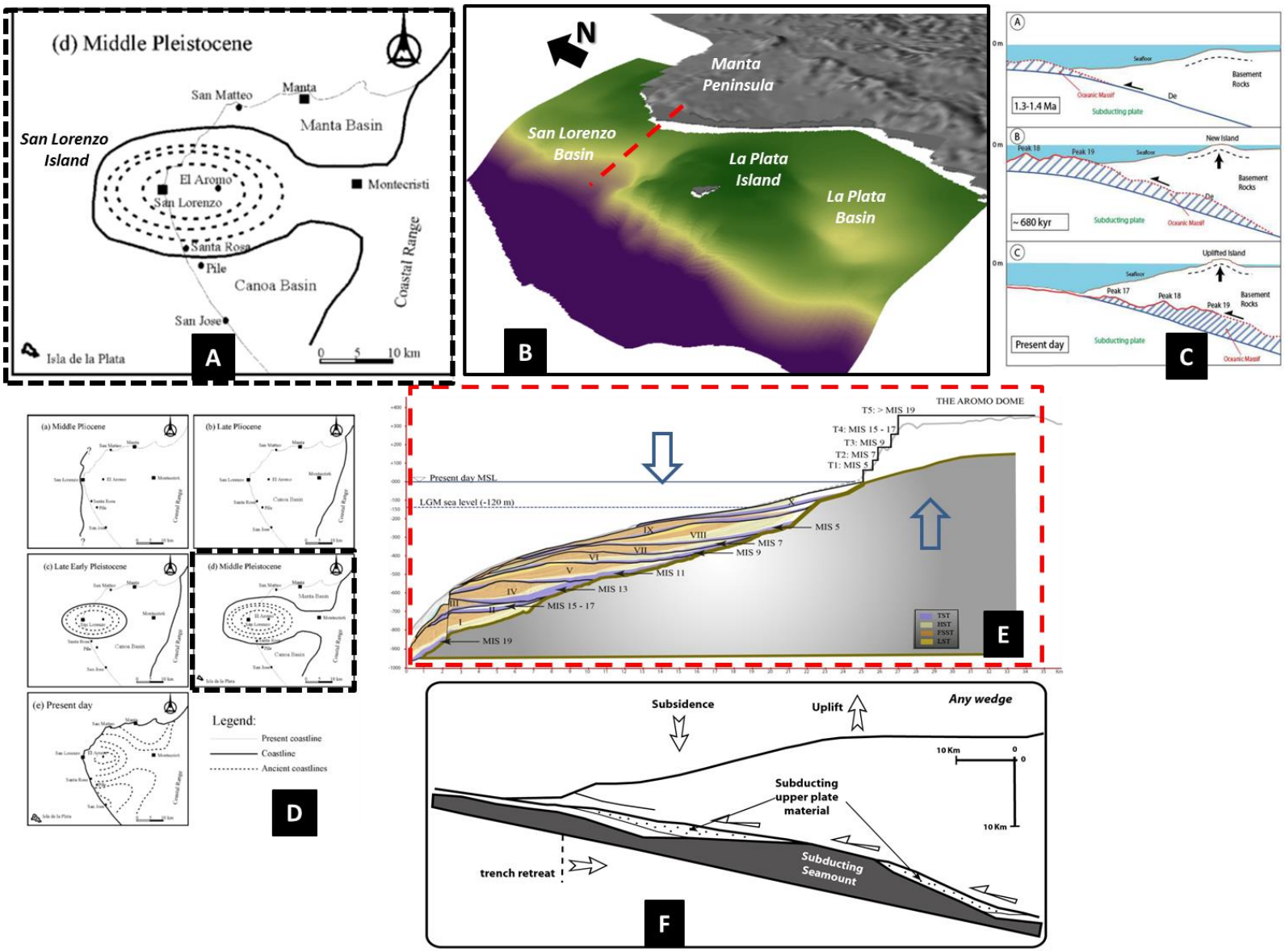

Figure 6.8: Analysis evolution of the Manta-Plata zone.

Figure 6.8- *A) Middle Pleistocene time of the Palinspastic reconstruccion, which show the Manta basin and Canoa basin surrounding the San Lorenzo island at this time. B) 3D model of the acoustic basement around La Plata Island surrounded by San Lorenzo and La Plata basins, this mimics the la figure A). C) Evolution model of La Plata Island suggested by Sanclemente (2014). D) Palinspastic reconstruction of the Cabo San Lorenzo proposed by Cantalamessa and Di Celma (2004). E) Interpretation of seismic profile (AtacP092) located in front of the marine terraces setting on Manta Peninsula (see location in 3D model figure). This figure shows the subsidence at platform and the uplift onshore caused by a seamount subducting, like the model proposed by Lallemand et. al (1994) in the Figure F). F) Sketch showing the subsidence and the uplift caused by a seamount subduction along any type of wedge, proposed by Lallemand et. al. (1994).*

_____

6. Evolution of the Southern basins

These basins are located mainly on the slope, between the south of La Plata basin and Salinas bathymetric high (SBH) (Figures 5.4 and 6.7). Only few deposits are reported on platform close to the Santa Elena canyon area.

6.1. The Ayampe basin

6.1.1. Origin and age of the Ayampe basin

The Ayampe basin is an isolated sub-circular-shaped bathymetric low located on the middle slope (Figures 5.3A and B). It is spatially related to a zone where is reported the subduction of several seamounts (Sage et al., 2006; Sanclemente, 2014; Villamar, 2001). The Ayampe basin is underlined by a large indentation of the inner trench wall, which affects not only the middle slope but also the platform edge. The presence of this reentrant indicates that the Ayampe basin is probably related to the prior subduction of an isolated asperity. Sanclemente (2014), have identified some multi-peak subducted seamounts around the Ayampe basin (Figure 6.7). But these subducted seamounts are located on the Ayampe basin sides. Consequently, this author suggests that the indentation, corresponding to the Ayampe basin, might be caused by the prior subduction of a very large conical shape seamount, located now at around 70 km landward from the trench. This assumption implies that this large conical seamount began to enter in subduction at more and less 1.5 Ma, which is coherent with a 70 km landward position taking into account the present-day subduction rate of 4.7 cm/yr (Nocquet et al., 2014; Vallée et al., 2013b) .

This proposed age for the formation of the Ayampe basin fit well with the age of the sedimentary infill that we have reported in this study, at the base the deposition of LTR. Moreover, using the sedimentation rate proposed in the North by Ratzov et al. (2010), Sanclemente (2014) suggests an age of 1450-Ky for the creation of the Ayampe re-entrant. Again, this age is time correlative with the age proposed for the base of LTR sequence, and supports the idea that this basin saves the same stratigraphy record than the north and central basins (Figure 6.1).

The LTR sequence, in the Ayampe basin, shows chaotic seismic reflection patterns in the N-S and W-E directions (Chapter 5), suggesting mass transfer deposits. The LTR seismic reflection

configuration patterns do not allow us to discriminate if LTR corresponds to several successive landslide events or only one huge landslide event.

6.1.2. Control of the uplift of the western Ayampe basin border

LTR, MTR and UTR, show a progressive migration of the depocenter location to the east (W-E SCAN-788 seismic profile, Figure 5.14A). Moreover the reflectors of the sedimentary infill are landward tilted; and the tilt increases, as the age of the deposits is older. These two observations document a progressive landward uplift of the western border of the Ayampe basin. The poor stratigraphic resolution of LTR does not allow us to know the timing of the beginning of the uplift. But the landward divergent reflection configuration at the base of MTR, in contact with LTR, suggests that the uplift was syn-sedimentary, at least from the beginning of MTR. Although this deformation of the western border of the Ayampe basin concerns the middle slope, this uplift formed at the same time than the uplift reported on the border of the platform in the Jama basin (Figure 5.8A). This supports the idea that these two contemporaneous uplifts correspond to the same tectonic event. However a seamount SMt7 (from Sanclemente, 2014 - Figure 6.7) is just located at the foot of the slope below the western border of the Ayampe basin. This recently subducted seamount, cannot be at the origin of all the uplift recorded during MTR and UTR deposits. But we cannot exclude that the subduction of this seamount enhances the uplift during upper UTR deposits (Figure 6.7).

6.1.3. Origin of mass-wasting deposits during MTR and lower UTR sequences

The chaotic to transparent seismic reflection configuration of the MTR sequences and at the base of the UTR sequences (N-S Atac-104 seismic profile, Figure 5.15A) indicates sliding sedimentary process during the deposition. Close and below the present southern boundary of the basin, we have identified chaotic to transparent seismic reflection configurations. These chaotic configuration patterns are in sub-vertical contact with subparallel reflection configuration group of sequences in MTR and into the base of UTR (sequences I and II). This indicates that “catastrophic” deposits (mass wasting deposits) “intrude” the normal sedimentary deposit of MTR and UTR. The location of the chaotic sequences close to the south border of basin, suggest that these mass wasting deposit came from the southern boundary of the basin and spread northward in the basin. After these intense mass wasting episodes, the sup-parallel seismic reflection configuration from III to X drapes the southern side of the basin. This suggests that these mass deposits may have occurred before the deposition of the sequence III, i.e. before around 600-Ky (Table 5.2).

The Ayampe basin is bounded to the south by a bathymetric crest which is related to the subduction of the SMt 6 seamount (Figure 6.7) (Sage et al., 2006; Villamar, 2001). Therefore, the chaotic mass wasting deposits that intruded the MTR sequences and the basal sequence of UTR could be related to the arrival in the subduction of this seamount. If we consider the present-day subduction rate of 4.7 cm/yr (Nocquet et al., 2014; Vallée et al., 2013b) during the last 600-Ky., we obtain a position of the seamount around 28 km from the trench. This position of the seamount coincides with the location of the eastern peak (Pk6) of the SMt6 (Figures 6.7, 2.6A and E). We assume that the subduction of this seamount have probably contributed to the

destabilization and deformation along the southern boundary of the Ayampe basin during part of MTR and the base of UTR deposition.

6.1.4. Origin of mass-wasting deposits during the UTR upper sequences

In the center of the basin the sequences V and VIII present chaotic seismic facies. On the contrary to the southern side of the basin, these same sequences reveal sub-parallel reflection configuration patterns. This suggests that the sources of the sediments related to the mass sliding deposition of sequences V and VIII, have probably an another source and are related to another process than during the MTR and lower UTR sequences. In fact the mass-wasting deposits of sequences V and VIII are thicker close to the foot of the eastern boundary of the Ayampe basin and thinner to the west. This geometry and thickness evolution suggest that the mass-wasting deposits of sequences V and VIII came from the eastern side (continental slope), spreading westward in the basin. This agrees with the facts that on the northern side of the basin all the sequences display sub-parallel reflection configuration patterns. The chaotic depositions of the sequences V and VIII, coming from the east, could have some causes, e.g. turbidites deposition triggered by climatic eustatic changes (Catuneanu, 2006). But the chaotic sequences, which came from the southern side of the basin, intruding into MTR and the base of UTR (sequences I and II), seems to be triggered by the subduction of the SMt6.

6.2. The slope basins

The slope basins corresponds to Montañita and Salinas slope basins, described in Chapter 5, and are located just beside of the relief created, on the slope, by the subduction of seamount SMt6.

6.2.1. The Montañita basin

Montañita basin is located between the bathymetric crest related to the subduction of the SMt 6 seamount below the slope, and the Montañita bathymetric high (MBH) on the platform (Figure 5.16). The Montañita basin sedimentary fill reveals two phases of deposits. The first phase corresponds to the sediments accumulated on the slope during LTR and MTR. These mega-sequences LTR and MTR are then deformed and faulted by the arrival of the seamount Smt6 during UTR. During the second phase UTR is deposited. The thicknesses of LTR and of MTR are greater than UTR (height of the arrows in Figure 5.16A). During the second one this evolution in thickness cannot correspond to a reduction of the accommodation space during UTR because the depth on the slope is more than 1000m at this place. More probably we need to consider a reduction of the sediment input along the slope from the continent trough the platform. Possibly the formation of the MBH on the platform has partly shut down the sediment supply from the continent to the slope.

6.2.2. The Montañita Bathymetric High (MBH)

The MBH (Figures 5.3), located at platform looks similar to the circular knoll caused by the landward thrust during the subduction of a seamount -note the Figures 5b) and 5c) of the sand-box model performed by Dominguez et al. (1998)- (Figure 2.5A in this work). The geometry and volume of this morphological shape caused by the backthrust, are controlled by the shape and

size of the asperity (Dominguez et al.,1998). The bending of the margin above of the subducted seamount produces a normal fault network. No clear seismic data evidence the details presented in the model, but the interpreted faults along the AtacP078 seismic line (Figure 5.16), as well as the morphological bathymetric data (Figure 6.7) suggest that the MBH could correspond to the backthrust related to a previous subducted seamount. If this speculation is correct, this implies the presence of a morphologic signature on the slope, just front of the current location of MBH. The indentation which corresponds to the Ayampe basin could be a possible candidate but it is not situated exactly in front of the MBH. May be the present subduction of the Smt6 erased the signature of the subduction of this speculative seamount.

6.2.3. The Salinas basin

The Salinas slope basin is located on the southern side of the scarp produced by the subduction of seamount SMt6. It is composed by several small basins which are developed along bathymetric landward curved scarps. These scarps are controlled by seaward dipping normal faults (Figure 5.17). The seaward dipping normal faults control little fan-shape basins since LTR deposit. We assume that the Salinas basins are controlled by the regional subduction-erosion process. The seaward dipping normal faults are associated to the subsidence of the upper slope as the consequence of the down drag of the tip of the upper plate. This implies that continuous subsidence occurred since the LTR deposit. Possibly the Carnegie ridge subduction or the collision of long-strike positive relief of the ridge is at the origin of an enhancement of the long-term erosive regime.

6.3. The Santa Elena basin (evolution of the Santa Elena Canyon)

The sedimentary deposits of the Santa Elena basin are present on the platform between the Montañita and Salinas bathymetric highs (MBS to SBH), and on the slope from the slope basins to SBH. The Santa Elena canyon (SEC) cuts this zone (Figure 6.7).

6.3.1. The age of the beginning of the deformation

The acoustic basement of this basin is wavy shaped (SCAN-417 seismic profile of Figure 5.19). This wavy shaped acoustic basement corresponds to a succession of synclines and anticlines with N-S trending axial planes. The sub-parallel to divergent reflection configuration patterns of the LTR sequences, which cover the wavy shaped acoustic basement, suggest that this deformation began during the deposition of LTR sequences. In the syncline, the sub-horizontal reflection configuration of MTR sequences displays concordant contact with the lower LTR sequences, suggesting that the deformation continues during the deposition of MTR.

6.3.2. Evidences of a possible paleo-course of the Santa Elena canyon

We have identified along the slope a filled channel (point 2 in the Figures 5.19). This filled channel is located in the prolongation of the E-W trending “straight head” of a landslide feature (Figures 5.3 A and B, 5.19B), and both are aligned with the present course of the Santa Elena canyon head (Figure 6.9). This suggests that, on the slope, the Santa Elena canyon was previously located further north. In this filled channel the upper sequences of LTR -above of the dotted light-blue line in Figure 5.19A- display seismic reflection patterns sub-parallel to the

upper “U” contact with the MTR. This looks similar to the reflection configuration patterns shown by the UTR sequences at top of the “V” channel of the present SEC. These points agree that the filled channel worked as a canyon and support the assumption of the existence, on the slope, of a paleo-course of Santa Elena canyon.

Additionally, the onlap terminations of the MTR against the “U” shape of the paleo-channel, as well as the absence of MTR in the actual position of the SEC, suggest that the SEC paleo-course was active until the end of the deposition of LTR. Then, the SEC migrates to south, to its current position, during the deposition of the MTR sequences. Consequently, during MTR the abandoned course is progressively filled meanwhile erosion or no-deposition is active in the current canyon.

This inferred migration is supported by the geometry of the current course of the Santa Elena canyon, which presents, on the slope, a southern deviation (Figure 6.9) just at the junction with the canyon paleo-course. This southern migration of the Santa Elena canyon at the middle slope, could be related to the vertical deformation as the regional uplift related to the subduction of the CR or related locally to the subduction of an asperitie like the Pk 27 reported by Sanclemente (2014). Other possibility is a fault control of the upper course of the canyon as suggested by Hernández, (2014) and Michaud et al., 2015). The fact that the Santa Elena canyon does not cut straight on the slope meanwhile the subsidence is significant at this zone, fits better with the hypothesis that the canyon course was triggered by the control of the normal SW-NE fault.

6.3.3. The evolution of the present head of the Santa Elena canyon

The head of the SEC (seismic line AtacP075 on Figures 5.18 A and B), is currently filled with sediments during the deposition of UTR. However, the sharp truncation of some seismic reflectors of this sedimentary fill at the top of the sequences VII, suggest a reactivation of the erosion process at this time.

The sedimentary filling geometry at the head of the course of the canyon exhibits several sequences belonging to UTR. This suggests that the canyon became inactive at around 790-Ka (base of Middle Pleistocene). But, the sharp truncation of the seismic reflectors at the top of the sequence VII, evidences a reactivation of erosion along the canyon. This reactivation is dated after the deposition of the sequence VII, and could be related to the Last Glacial Period (LGP that includes the ages of the sequences VIII and IX (Table 5.2)). The high amplitude of the sea-level changes related to the LGP could probably explain this reactivation.

_____

Figure 6.9- *Santa Elena canyon migration. A) Map showing the older interpreted location of the Santa Elena canyon, as well as the fault SE1, which seems to control the upper zone of the canyon (Hernández, 2014; Michaud et. al. 2015). It shows also the location of the Pk 27 at north of the landslide zone interpreted from the bathymetry. B) Seismic line SCAN-417 showing the syncline (1), the older location of the canyon, (2) and the current Santa Elena canyon (3).*

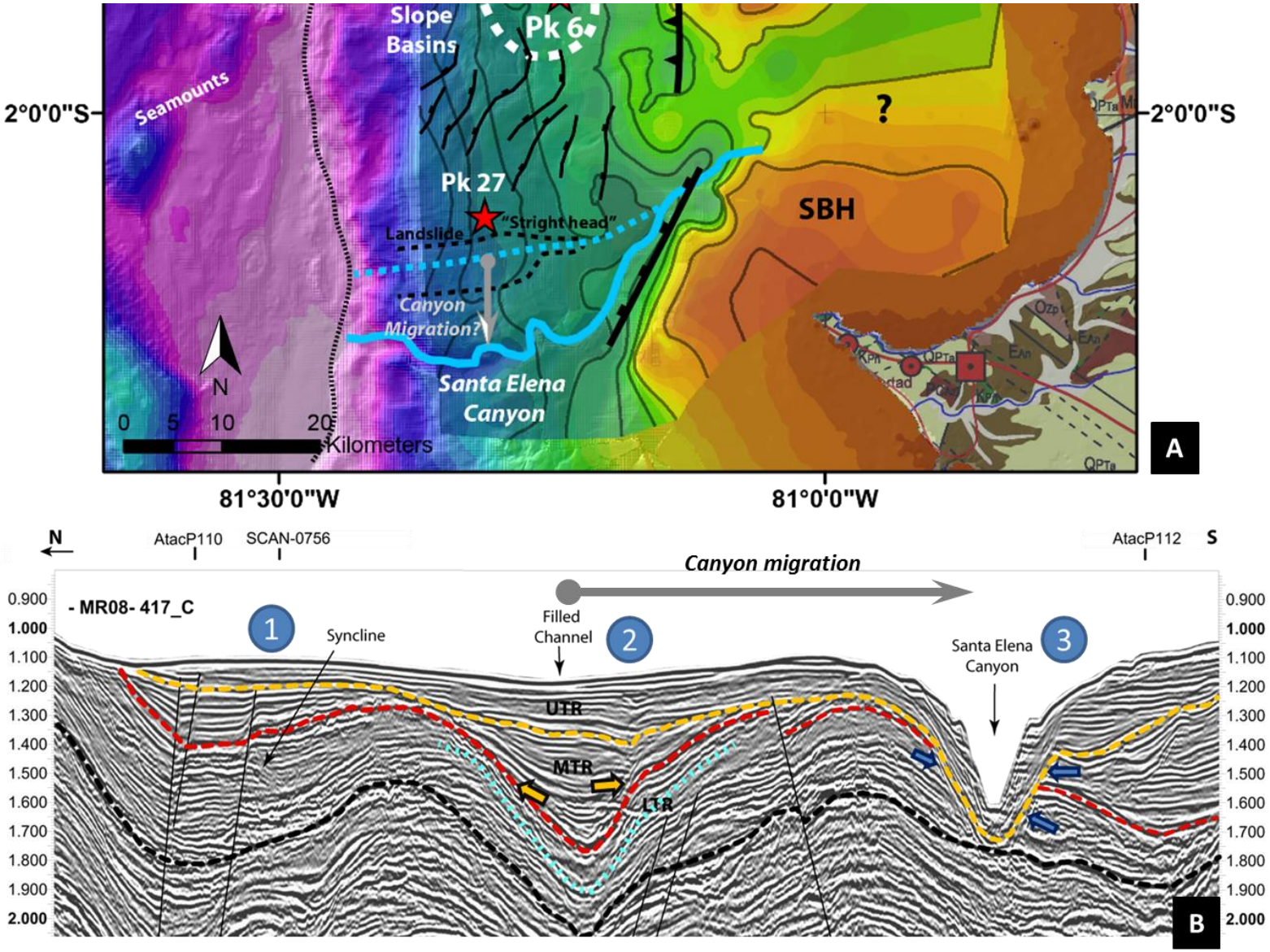

Figure 6.9: Analysis evolution of the Santa Elena canyon.

7. The signature, on the continental shelf, of the subduction of the Carnegie Ridge

The Atacames data set, allow us to report the repartition of the sedimentary deposits and the record of the deformation along of the margin during the Pleistocene. Taking into account our results we will discuss about the sedimentary and tectonic signatures along the margin of the Carnegie subduction. We try to establish a timing of the subduction of the ridge and where the effects of the Carnegie ridge subduction are significant through time and space. Finally, this allows us to discuss about the geometry of the inferred subducted continuation of the CR.

7.1. Segmentation of the margin versus Carnegie ridge location

The spatial distribution of the basins and the seafloor morphology suggest that the Central Ecuadorian margin is divided in two principal segments: 1) the northern segment from Galera Structural High to southern Jama basin, and 2) the southern segment from Cabo Pasado basin to Salinas Structural High (Figure 6.10).

Along of the northern segment the acoustic basement mapping shows subsidence at platform, the isopach map exhibits the thickest basins at platform and the bathymetry map expresses landward deviation of the shelf break. In contrary, in the southern segment the acoustic basement mapping displays uplift at platform; the isopach map presents some basins in the slope; and the bathymetric map shows a seaward trend of the shelf break (Figure 6.10). The boundary between these two segments of the margin is around 0º of latitude (white dashed line in Figures 6.10 and 6.11).

Considering the segmentation as propose above, we try to evaluate the possible links between these two margin segments and the Carnegie ridge location. The location of the boundary between the two segments is spatially related, in the trench, to the northern boundary of "current subduction of the Carnegie Ridge" as defined by Lonsdale (1978) (see profile L-L' in Figures 2.3A and 6.11A). However we need to take into account the geometry of the continuity of the Carnegie ridge below the margin. Considering that the north CR boundary keeps the same trend beneath the upper plate, Gutscher et al., (1999) and Collot et al., (2009) inferred a continuity of Carnegie ridge boundary subduction beneath of the Galera cape at around 0°50'N. Gailler et al., (2007) using another data set (travel time inversion of wide angle seismic data) proposed also that CR subducted continuation until beneath the Galera cape.

7.2. Repartition of the mega-sequences versus Carnegie ridge subduction

The spatial distribution of the mega-sequences along the margin allows us to define the evolution of the basins trough time. The spatial-time evolution scheme (Figure 6.12) displays the ages (at the X-axis each 100-Kyrs) vs. the spatial location of the structural features (at the Y-axis, e.g. basin, structural highs and subducted asperities). This figure replaces the deposits in each basin at platform (in dashed blue lines), and at slope (in dotted red line).

On the slope LTR, MTR and UTR are present along the margin, from GSH to SBH.

On platform LTR, MTR and UTR are present in north from GSH to Cabo Pasado basin; and at south around the Santa Elena canyon, as well as in Guayaquil Gulf (according Witt et al., 2006)

On platform, LTR and MTR are absent from south of Cabo Pasado basin to north of Santa Elena canyon (area limited by an orange curve). They have been eroded or bypassed.

On platform, UTR is present in San Lorenzo and La Plata basins since the deposition of sequence IV, and in San Vicente basin since the sequence VI.

From GSH to CPAS at north, and around the Santa Elena canyon at south, the basins present LTR, MTR and UTR both on the platform and on the slope. While between Cabo Pasado and Santa Elena canyon LTR, MTR and the base of UTR were not deposited or have been eroded on the platform.

The area without sequences at platform corresponds to the same area where we have evidenced an uplift of the platform edge. We have proposed that this uplift could be related to the CR subduction. Thus, following this assumption we suggest that the subduction of the CR affects, in this area, not only the border of the platform, but also the inner platform. As consequence the reduction of the space accumulation results in the erosion or bypass of the sediments, interrupting the lateral continuity of the sequences from the north basins to central and south basins.

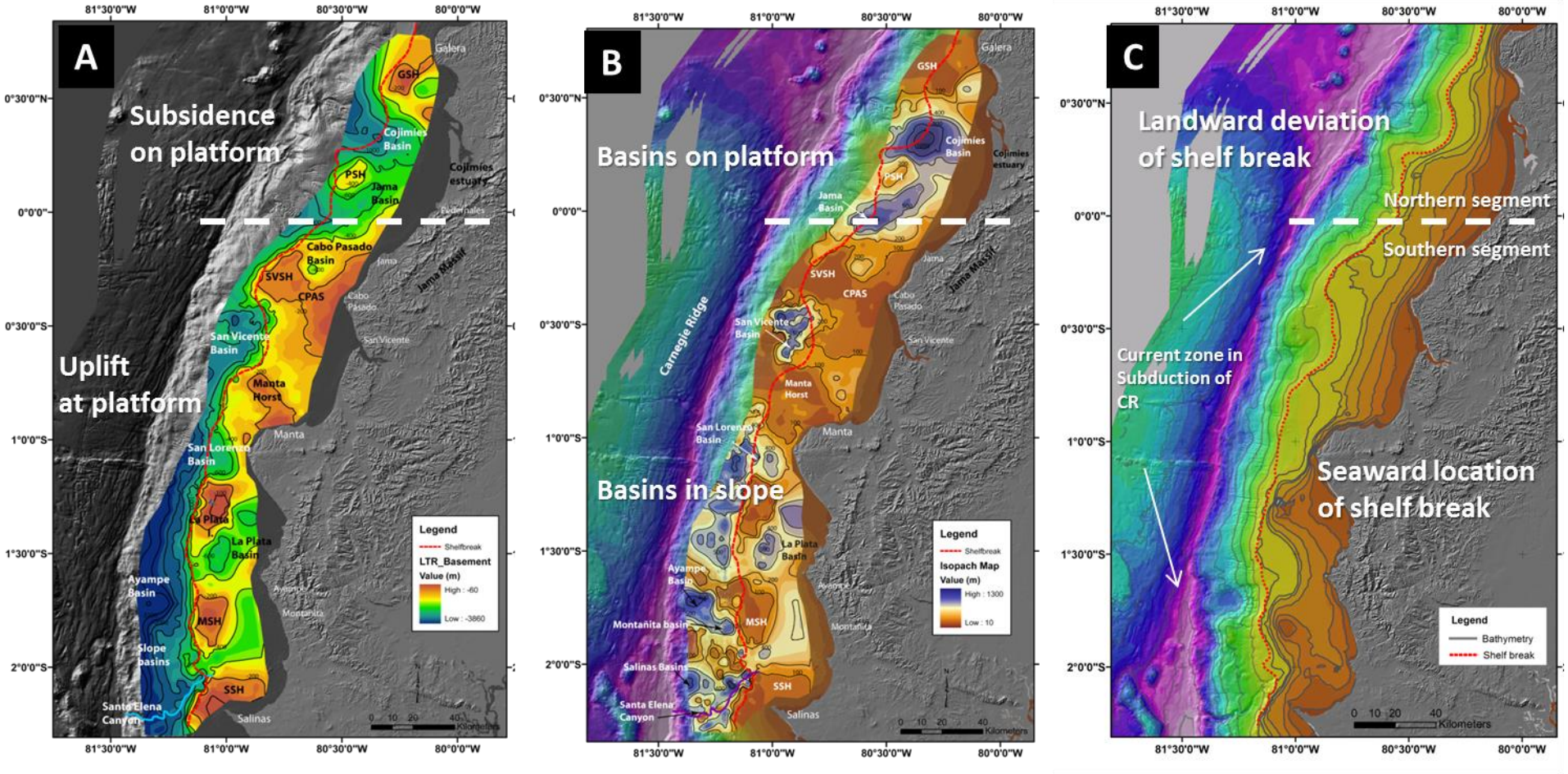

Figure 6.10: Different behaviors between the Northern and Southern segments displayed on the grids of the Acoustic Basement, the Isopach map and Seafloor Morphology. **A)** Grid of the acoustic basemen showing the subsidence at platform in the northern zone and the uplift at platform in the southern zone. **B)** The isopach map displaying the location of the basins along of the margin. **C)** The bathymetry grid presenting the different behavior of the shelf break between the northern and the southern zones.

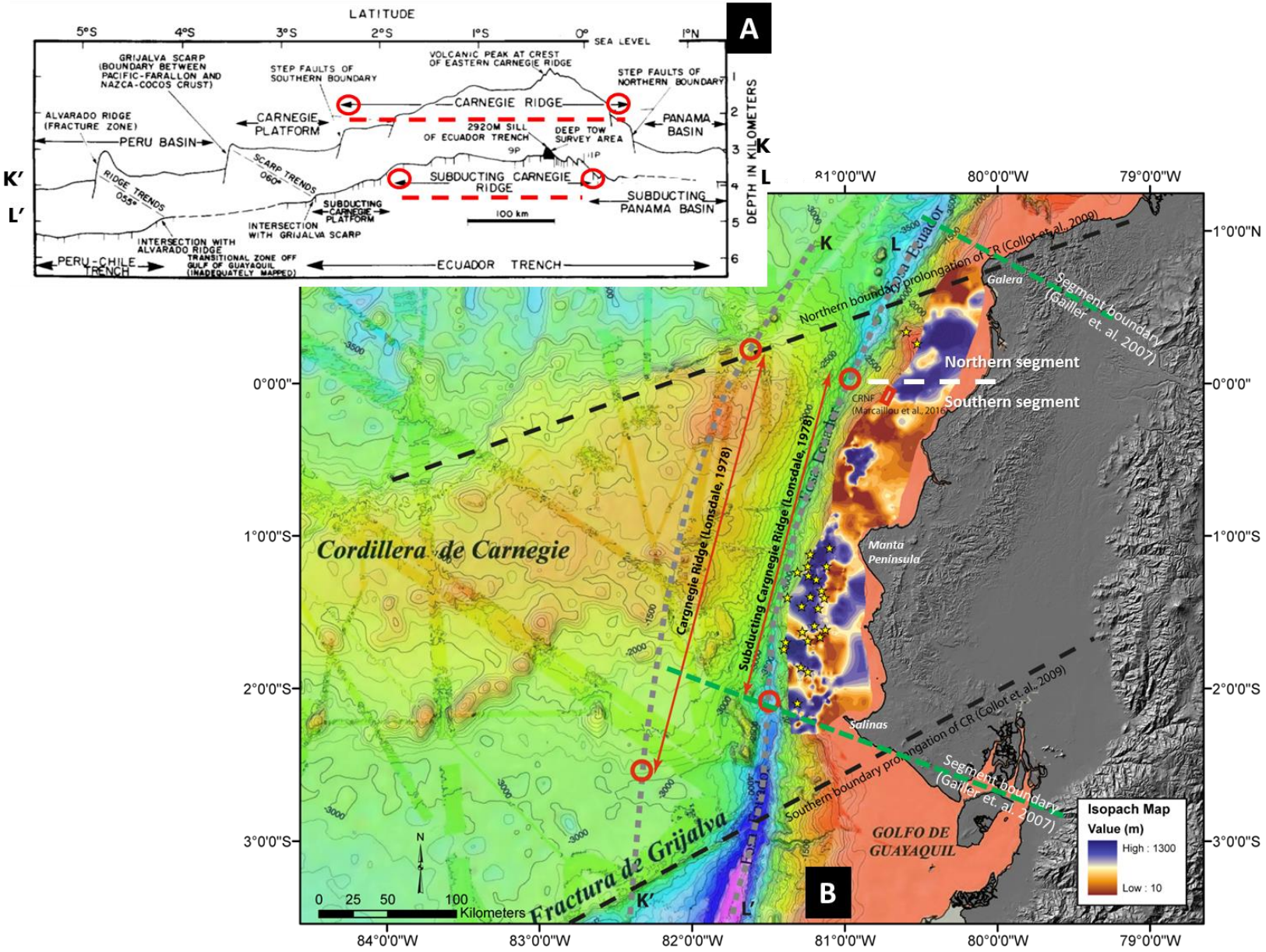

Figure 6.11: Models of the CR prolongation below the upper plate.

Figure 6.11- *Models of the CR prolongation below the upper plate. A) Bathymetric profiles crossing the CR (From Lonsdale, 1978). The profile L-L' is realized along of the trench, and it proposes de current zone in subduction of the CR. B) Map showing the models of the CR prolongation below the NAB: Collot et. al. (2009) and Gailler et al. (2007). It displays also the current zone of CR subduction proposed by Lonsdale (1978), which seems to be related to the spatial distribution of the forearc marine basins from the Calabrian Pleistocene (displayed in the isopach map).*

_____

7.3. Continuous stratigraphic record of the Carnegie ridge subduction

As it was discussed in the item of tectonic control (item 3.2 of this chapter), there is a periodicity record of the regional deformation, inferred in an average of 100-kyrs, which links to the periodicity of the eustatic-climatic changes from the base of the Middle Pleistocene. We suggest that this 100-kyrs continuous record of the deformation corresponds to the continuous ongoing subduction of the Carnegie ridge considered as a whole.

However, the stratigraphic scheme shows stronger record between some groups of sequences: acoustic basement-LTR, LTR-MTR, MTR-UTR, III-IV and VII-VIII (Figure 6.1). These stronger records between some groups of sequences indicate a differential changes in accommodation spaces than the "normal" shift registered each 100-Kyrs., related to a constant CR subduction and eustatic-climatic changes. The changes in the "normal "record may be triggered by changes in the shape or morphology of the CR, stronger changes in the eustatic-climatic changes, or combination of both.

7.4. Age of the collision of the Carnegie ridge

The age proposed for the collision of the Carnegie ridge (see the Chapter 2) vary between 1 to 3 Ma-old (Cantalamessa and Di Celma, 2004; Contreras-Reyes and Carrizo, 2011; Graindorge et al., 2004; Lonsdale, 1978; Witt et al., 2006) to 8 Ma-old (Collot et al., 2009; Gutscher et al., 1999) to up to 15 Ma-old (Pilger, 1984; Spikings et al., 2005, 2001).

The regional unconformity with the acoustic basement corresponds to the base of all the Pleistocene basins identified along the margin during this study. Above this regional unconformity the seismic configurations allow us to report a) uplift of the border of the platform along the margin; b) northward divergence trend of reflectors of the north basins; c) deformation around of the Santa Elena canyon. This regional unconformity and the deformation recording by the sediments above, allow us to propose a relationship with a regional tectonic event.

We suggest that this regional unconformity corresponds to the record of the Carnegie ridge collision (or at least, the arrival of along-strike positive relief of the Carnegie ridge). The oldest mega-sequence which lies immediately above the acoustic basement is the mega-sequence LTR. The age of the base of LTR is 1782-ka (base of Calabrian Pleistocene MIS 63). We propose 1782-Ka as minimum age for the collision of the Carnegie ridge. This age is coherent with: a) the proposed ages for the increment of subsidence in the Guayaquil Gulf, i.e. 1800-1600 ka (Witt et al., 2006), b) the age for the inversion of the "Canoa basin". Cantalamessa and Di Celma (2004).

However, as our study concerns only the Pleistocene time period, the 1.782-ka age that we propose for the arrival of the Carnegie ridge in the trench is a minimum age. We do not know when began the formation of this regional unconformity and its duration. So, maybe there is older regional unconformity that could record the arrival of previous asperities of the CR, it is not possible to identify it with our data set.

7.5. Significance of the LTR-MTR, MTR-UTR and intra-UTR boundaries

The LTR-MTR boundary is dated at around 1000-Ka (Figure 6.1). At this time, (Pedoja et al., 2006) have proposed the emersion of the oldest marine terrace of the Manta Peninsula (T5). We speculate that this local event (the uplift of T5 in Manta Peninsula) and the unconformity between LTR and MTR could be related to a regional variation of the CR morphology.

The MTR-UTR boundary, is dated in 790-Ka (Figure 6.1). This unconformity could be related to the eustatic-climatic changes occurred at the base of the Middle Pleistocene, (Brunhes-Matuyama reversal-Figure 4.8). In this case the MTR-UTR boundary could be related to eustatic-climatic change. This fit well with the fact that the MTR-UTR boundary is regional.

The III-VI boundary, is dated around 500-Ka (Figure 6.1). This unconformity is related to the subduction asperities that caused the emersion of La Plata Island, the record of the lowest marine terraces of the Manta Peninsula, as well as the formation of San Lorenzo and La Plata basins. So, this unconformity, like the LTR-MTR, seems caused by a local change in the morphology or shape of the CR.

The V-VI boundary was interpreted in the north basins (Figure 6.1), from Cojimíes to San Vicente basins. In these basins this unconformity could be correspond to the subduction of the western peak of the Atacames Seamount (item 4.3.1 of this chapter). The Cabo Pasado and San Vicente basins are far of the zone of the seamount subduction; so the record of this unconformity has probably another origin. In the San Vicente and Cabo Pasado basins, this boundary corresponds to the beginning of the opening of the accommodation space on the platform. We speculate that this opening is related to a variation of the relief of the CR around this area.

The VII-VIII boundary is dated about 130-Ka (Figure 6.1). It seems to be related to the high amplitude of the sea-level changes registered at the base of the Upper Pleistocene (MIS-5e) as the last major interglacial period before the Holocene. Thus, this contact between sequences VII and VIII is likely due to eustatic-climatic changes.

7.6. Interaction between upper plate transcurrent faults and Carnegie ridge subduction

The drastic increase of subsidence during the Pleistocene in Guayaquil gulf was attributed as a consequence of the entrance of the Carnegie ridge (or along-strike positive relief) into the subduction (Witt et al., 2006). This subsidence in the Gulf of Guayaquil is associated to an acceleration of the northward drift of the North Andean block along a regional transcurrent faults system. We have suggested that the northern basins (Cabo Pasado, Jama, Cojimíes and San Vicente basins) are partially controlled by transcurrent faulting belonging, at regional scale,

to the Jama faults system (see item 4.1.2 of this chapter), which is known as a transcurrent system.

As it was proposed for the subsidence of the Guayaquil gulf, we suggest that the Jama faults system could be activated (or reactivated) during the entrance of the Carnegie ridge into the subduction. Consequently local subsidence in Jama and San Vicente basins could be enhanced as it was proposed for the subsidence of the Guayaquil Gulf. Nevertheless meanwhile we suggest that the subsidence could be enhanced as the consequence of the same process, the effects are not of the same order. The Gulf of Guayaquil is located at the trailing edge of the northern Andean block. Consequently it is a considerable subsiding area and sedimentary infill in comparison with the Jama and san Vicente basins.

7.7. The evolution of the sediments transfer axis

Our bathymetry data set show some sectors with gullies along of the uplifted zone of the Central Ecuadorian margin, which probably worked as sediments transfer axis from the platform to the trench. The only canyon located in the Central Ecuadorian margin is the Santa Elena Canyon. According to Espurt et al. (2008) the uplift of the margin is sudden at the time of collision of a plateau asperity, but in long-term the uplift of the margin continues but slowly (Figure 1.8). Taking into account the location, the proposed age and the evolution of the Santa Elena Canyon (item 4.4 in this chapter), we propose that the SEC could have worked as sediments transfer axis from shelf to trench during the sudden uplift of the margin caused by the collision of CR. While the filling and inactivation of the SEC could be related with the long-term uplift of the zone, causing the transfer the sediments by other southern axis, possibly for example the canyon of Guayaquil (which began to worked at 800-Ka as proposed by Loayza, 2013).

7.8. Most significant sedimentary signatures of the Carnegie ridge subduction

The southern segment of central margin (see above items 7.1 and 7.2), is spatially related to the “current subduction zone of the CR”, defined by Lonsdale (1978) (Figure 6.11). Front of this “current subduction zone of the CR” the Carnegie ridge acts as a WE elongated asperity (as the consequence of the W-E convergence motion of the Nazca plate related to the NAB).

In this area the most significant imprints of the Carnegie ridge subduction are:

- Erosion/no deposition process starving the record of the LTR, MTR and UTR on platform from south of Cabo Pasado basin to Santa Elena canyon (Figure 6.12).
- Continuous uplift of the margin (Figure 6.10).

Additionally across the boundary area between the northern and southern segments, the subsidence and the thickness increase progressively to the north (Figure 6.10 and 6.12); and the three basins (Cabo Pasado, Jama and Cojimíes) show a continuous deepening of depocenters respectively and a divergence of reflection patterns toward north (Figure 6.3).

All these considerations show that, at regional scale, there is a good fit between this sedimentary signature with the Carnegie ridge present shape: the highest present day relief of the CR is just in front of the SVSH and CPAS highs, when the present day northern flank of the Carnegie ridge is in front of the platform area where basin subsidence increases sharply from south (Cabo Pasado basin) to north (Jama and Cojimíes basins). This complex subsidence pattern with uplift (SVSH and CPAS highs) area and progressive subsidence of the northern surrounding area (Cabo Pasado, Jama and Cojimíes basins) mimics the gross shape of the subducting Carnegie ridge northern flank. Additionally following a W-E convergence motion, the subduction of a large asperity at the beginning the Carnegie ridge arrival at the location of the Cojimíes basin could explain the stable location of this basin.

_____

Figure 6.12- *Scheme X-Y of the distribution of the stratigraphy sequences LTR, MTR and UTR along of the Central Ecuadorian Margin. The X axis shows the sequences, and the Y axis displays the Latitudes (the isopach map is the spatial reference). The blue dashed lines represent the deposition at platform, while the red dotted line expresses the deposition at the slope. The black dots represent the asperities subduction and ellipsoids the structural highs. The orange line mark the zone where is not present the LTR and MTR sequences at platform.*

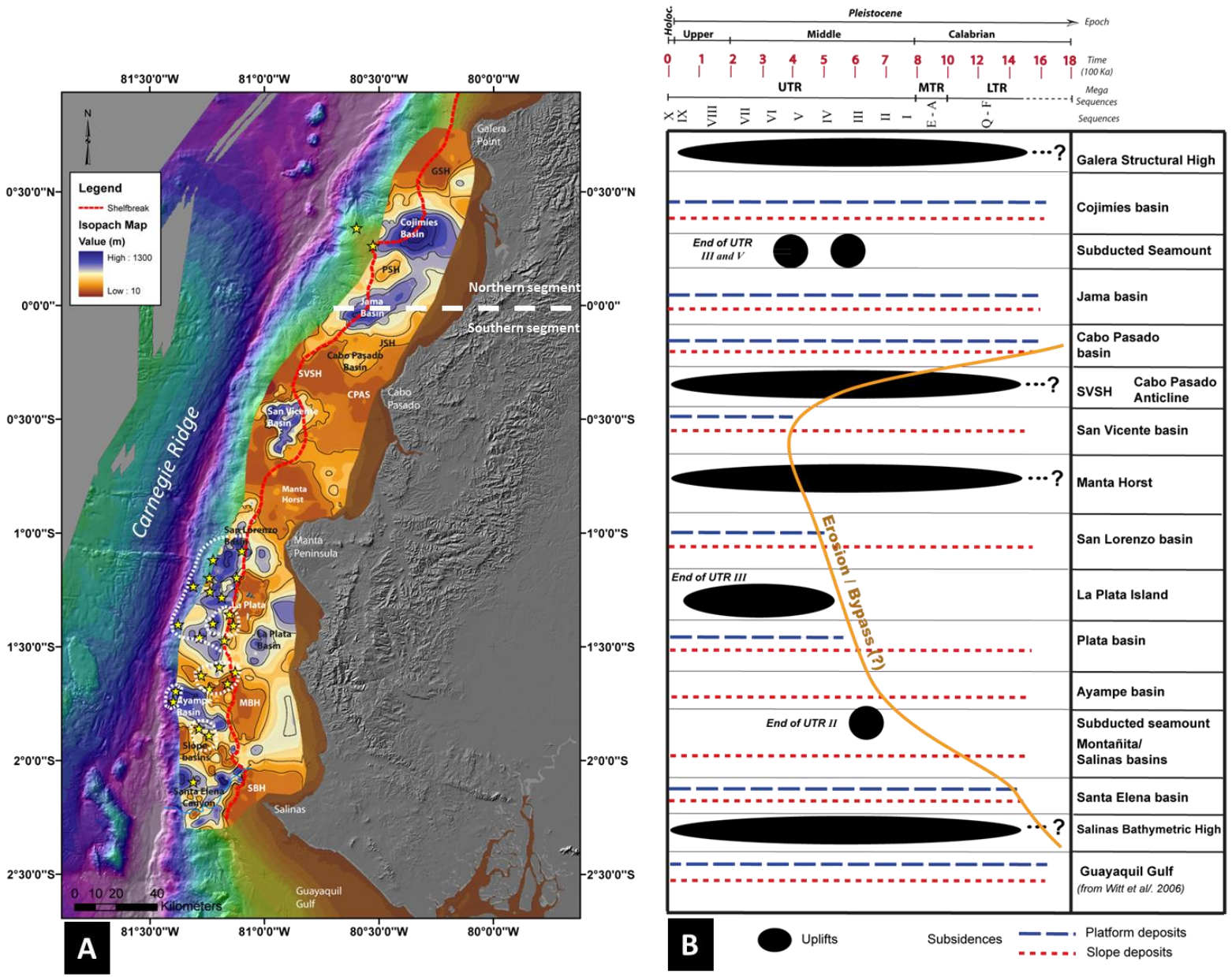

Figure 6.12: - Scheme X-Y of the distribution of the stratigraphy sequences LTR, MTR and UTR along of the Central Ecuadorian Margin.

7.9. Signature of the southward migration of the CR northern boundary

From the identification of perturbed slope areas along the margin, Collot et al. (2009) have suggested a southward migration of the CR northern boundary from the north of Galera cape to the actual position (Figure 2.2). Taking into account both the obliquity with the trench of the Carnegie ridge boundary and the kinematic models of Nocquet et al., (2009), Collot et al., (2009) assume a N180-N207 southward migration of the Carnegie ridge boundary with a velocity between 2.7 and 2.3 cm/yr. In this evolution it is proposed an age for the CR collision ranging between 4 to 5 Ma (see Chapter 2).

The sandbox models of an elongate asperity subduction, realized by Hampel, et al. (2004), predict continuous subsidence and slumping in the trailing flank. According to this model, the southward migration of the CR northern boundary (which corresponds to the trailing flank) would imply a continuous opening of basins from the north of Galera cape toward south, until the location of the present northern Carnegie ridge boundary (Figure 6.13). This involves a stratigraphic record with the deposition of older sequences from north to south and prograding configuration patterns in the direction of the creation of the space of accommodation.

Our results show that, on the platform, the basins are located southward of the Carnegie ridge northern boundary inferred by Collot et al., (2009) (Figure 6.13) and not northward where the sand box models predict subsidence and basins formation. On the contrary, at this place we have the Galera structural high.

The basins Cojimíes, Jama and Cabo Pasado were formed at the same time as a single basin that was divided later, and they show:

- the same stratigraphic record (presence of the LTR, MTR, and UTR)
- a permanent X-Y position of the depocenter of the Cojimies basin through time.
- deepening of depocenters from south to north,
- divergence and prograding seismic reflection configuration patterns in the same direction, suggesting the creation of accommodation space toward north.

This evolution of the basins is what it is expected, but north of the present location of the Carnegie ridge northern boundary, as a consequent of its southward migration. We report such basin evolution but south of the inferred Carnegie northern boundary. At least on the platform, the record of a southward migration of the northern boundary of the CR is not clearly supported by our results.

If we consider that 1782-Ka is the age of beginning of the collision of the CR (see item 7.5 of this Chapter) this imply that the southward migration of the CR boundary may have started further south. Assuming the same velocity proposed by Collot et al. (2009) (i.e. 2.7 and 2.3 cm/yr), we obtain a position of the northern boundary of the CR c.45 Km in the north to the current location (black dot at the beginning of NE-SW arrow in Figure 6.5A. This proposed site corresponds to the southern border of the PSH, and to a bathymetric reentrant R2 (Figures 5.1 and 6.5A). But this hypothesis does not explain why we have uplift at the GSH area.

To explain the uplift in GSH we can consider a more complicate geometry for the continuation of the subducted Carnegie ridge (both in relief and shape). We can imagine to the north a trench parallel subducted high which is still beneath the GSH as inferred by Collot et al. (2009) (Fig. 2.2B). Such geometry, could explain the vertical motion of the GSH area, the perturbated slope, the absence on the platform of important sedimentary basin and the thickening of the subducting crust at this location (Gaillier et al., 2007).

Figure 6.13- *Comparison between the location of the basins and the inferred prolongation of the subducted Carnegie ridge from Collot et al., (2009). This model suggests a southward migration of the oblique flanks of the Carnegie ridge. For the northern flank such southward migration implies an increasing subsidence from north to south along the margin. On the contrary we have observed a high at this place (north of the dashed line) and subsiding basins at the south.*

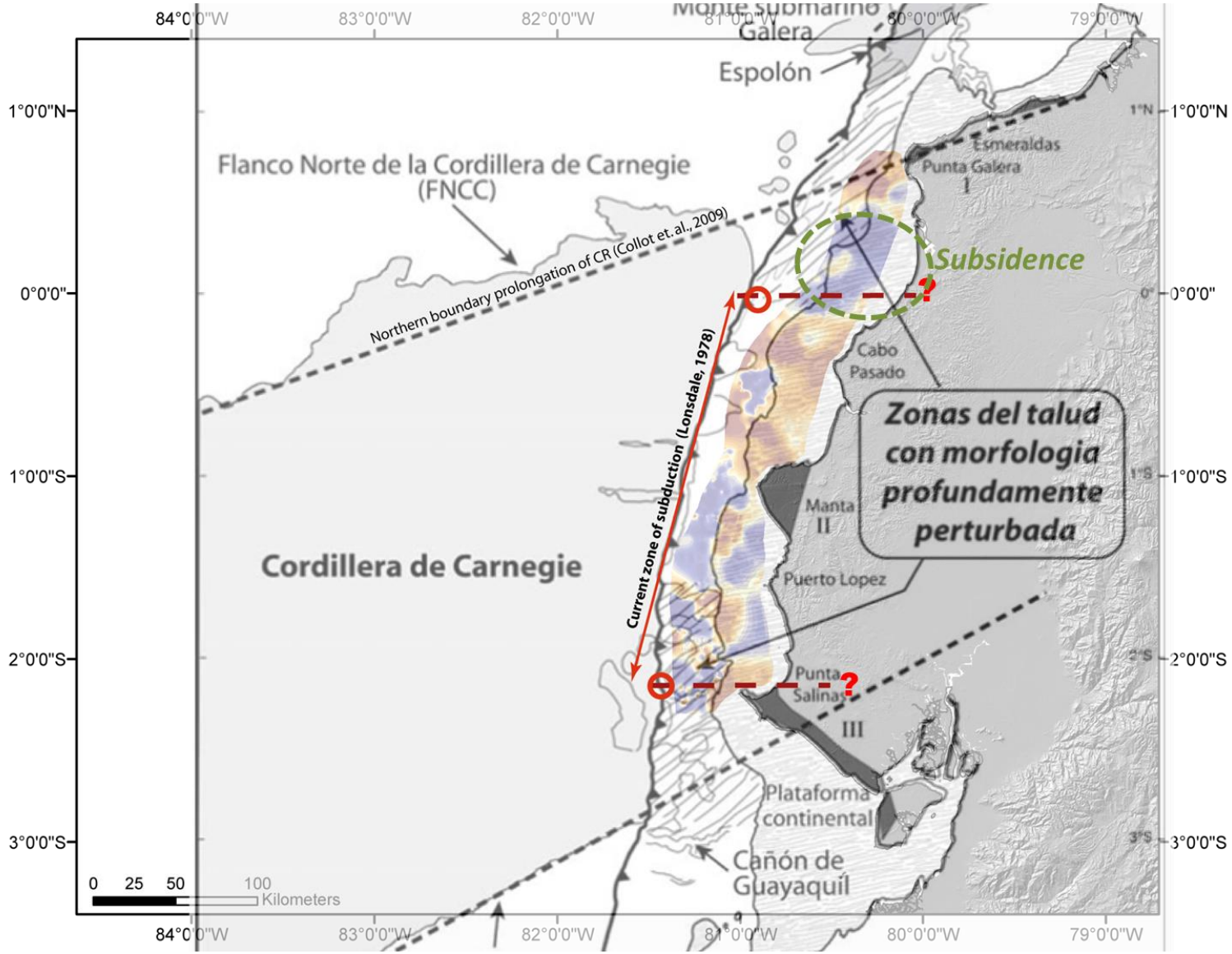

Figure 6.13: Comparison between the location of the basins and the inferred prolongation of the subducted Carnegie ridge from Collot et al.,

CONCLUSIONS:

This work is based on the sismo-stratigraphic analysis of Pleistocene sediment preserved on the margin shelf and upper slope. We have used high resolution seismic data collected during the Atacames scientific cruise (2012), complemented with some SCAN seismic data (2009) (propriety of the Secretaría de Hidrocarburos de Ecuador), as well as, piston core data, and high resolution and classical bathymetric data from different sources.
We propose a tectonic and stratigraphic evolution of the central Ecuadorian Margin during the Pleistocene, which illustrates a different scales, the link between the subduction of oceanic reliefs and the deformation of the continental shelf.

STRATIGRAPHY:

In the type area of Manta-Plata, we defined the basic stratigraphic motif (i.e. the T-R sequence) of the Quaternary sedimentation on the Ecuadorian shelf. The T-R sequences are stacked together and usually show a lateral shift in a landward direction with respect to each other. The main shifts underline angular unconformities of local to regional extend. The later ones bound three groups of T-R sequences (the mega-sequences): Low TR (LTR), Middle TR (MTR) and Upper TR (UTR), which constitute the margin shelf and slope basin fills. A total of 26 T-R sequences have been identified: 11 LTR, 5 MTR and 10 UTR.

The sedimentary record is dated by piston core analysis and C14 age dating and by correlation with coastal exposure and marine terraces. Moreover, the T-R sequences show excellent correlations with the global eustatic-climatic curve related to orbital forcing (i.e. Milankovitch cycles). This allows us to finely date the sequence deposition from the base of the Calabrian Pleistocene (1780-Ka) to Present (Figure 6.1), i.e. MIS 63 to MIS 1.

SEGMENTATION OF THE MARGIN:

The location, the geometry and the characteristics of the main Pleistocene depocenters were defined all along the central margin. This analysis includes the geometry of the pre-Pleistocene acoustic basement, the sediment thickness, the main structural elements and the onshore geology. The margin can be divided in a northern and southern segments with a boundary located at around 0° latitude. In the basins of the northern segment the LTR and MTR mega-sequences are well developed and preserved on the platform and the slope, while in the basins of the southern segment, they are eroded or bypassed on the platform and poorly preserved on the slope. On the contrary, the UTR sequences are well preserved on the platform and the slope in both areas (Figure 6.12).

In the northern segment:

The acoustic basement mapping shows the subsidence of the platform (Cojimíes, Jama and Cabo Pasado basins); the isopach map exhibits the thickest basins of the margin and the bathymetry map expresses a landward shift of the shelf break (Figure 6.10). The basins of the northern segments seem to be created as a single basin, which was separated later in the

current three basins by the subduction of seamounts and by the offshore prolongation of the Jama fault system.

In the southern segment:

The acoustic basement mapping displays an uplift of the platform with erosion and bypass (Figure 6.12). The isopach map exhibits few basins on the slope; and the bathymetric map shows a seaward shift of the shelf break (Figure 6.10). The basins located along the slope are controlled by seamounts subduction (e.g. San Lorenzo, La Plata, Ayampe basins in Figure 6.7). The uplift shown on the platform is located in front of the highest current reliefs of the CR, which links spatially with the southern segment (Figure 6.11).

SUBDUCTION OF OCEANIC RELIEFS:

This segmentation illustrates the link between the subduction of oceanic reliefs and the deformation of the Ecuadorian continental shelf and allows us to propose a tectonic evolution at different scales in time and space.

At the regional scale

We have shown a regional unconformity between the acoustic basement and LTR. We propose that this unconformity corresponds to the record of a tectonic regional event, which could correspond to the beginning of the Carnegie ridge collision, or at least, the arrival of along-strike positive relief of the Carnegie ridge. Following this assumption, the subduction of topographic reliefs of Carnegie ridge below the continental shelf could be related to (a) the uplift of the border of the platform from the south of Jama basin to the Santa Elena canyon area, (b) the divergence trend of reflectors and deepening toward the north of the basins of the northern segment; (c) the deformation and enhanced subduction erosion around of the Santa Elena canyon area. All these deformation observations began just above this regional unconformity. Consequently we suggest 1782-Ka as minimum age for the collision of the Carnegie ridge. This age is coherent with the proposed ages for the increment of subsidence in the Guayaquil Gulf (Witt et al., 2006), and the age for the inversion of the onshore “Canoa basin” Cantalamessa and Di Celma (2004).

Due to the obliquity of the northern boundary of the Carnegie ridge with the trench, Collot et al. (2009) postulate a southward migration of this boundary relatively to the upper plate. Consistent with this model, our results show that, south of the CR northern boundary (as located by Collot et al., 2009), the CR acts as a W-E elongated asperity during all the mid to late Pleistocene times. The highest present day relief of the CR is just in front of the SVSH and CPAS platform highs when the present day northern flank of the Carnegie ridge is in front of the platform area. In the latter area, basin subsidence increases sharply from south (Cabo Pasado basin) to north (Jama and Cojimies basins). Sand box models predicts such a subsidence to the north of the CR northern flank Collot et al., (2009) (Figure 6.13) and not on its southern part. The geometry of the CR northern boundary already subducted could be more complicated than inferred by Collot et al., (2009). A subducting oceanic relief still in subduction north of the CR current boundary is a possibility.

At the sub-regional scale

The unconformities between LTR-MTR, MTR-UTR, as well as the unconformities between III-IV and VII-VIII into the UTR mega-sequences (Figure 6.1), indicate changes in accommodation space different from the "normal" shift registered each 100-Kyrs, related to a steady subsidence and eustatic-climatic changes. These changes in the "normal "record may be triggered by changes in the shape or morphology of the CR, stronger changes in the eustatic-climatic changes, or a combination of both.

At the local scale

Careful backstripping and mapping of tectonic deformation shows that the deformation the continental shelf in the Manta-Plata area during the deposition of UTR. This deformation has been related to the subduction of topographic reliefs of Carnegie Ridge below the continental shelf. The pattern of the continental shelf deformation is consistent with the proposition of the oceanic relief subduction proposed by Sanclemente (2014). We tested the hypothesis of a link between the deformation and the subduction of the seamount, by comparing a stepwise subduction of the seamount to the palinspastic restoration of the deformation of the continental shelf for the last 1Ma. This comparison shows that the collision probably started c.500ka ago, together with the syntectonic sedimentation, and drastically slowed down by c.50ka, with the sealing of most of the deformation on the shelf (Proust et al., 2016).

CONCLUSIONS

Ce travail est basé sur l'analyse sismo-stratigraphique du Pléistocène de la plateforme et du haut de pente de la marge en subduction d'Equateur. Nous avons interprété des profils sismiques TR de la campagne ATACAMES (2012) complétés par des profils sismiques pétroliers de la campagne SCAN (propriété de Secretaria de Hidrocarburos de Ecuador). Nous avons aussi utilisé des données de bathymétrie multifaisceaux (campagne plus anciennes) et de bathymétrie classique (données INOCAR) ainsi que des carottes sédimentaires prélevées durant la campagne ATACAMES.

Cette étude nous permet de proposer une évolution, durant le Pléistocène, de la déformation et de la sédimentation le long de la marge et de l'associer à la subduction de reliefs océaniques portés par la plaque plongeante.

STRATIGRAPHIE

L'identification de la succession des séquences correspondant à l'enregistrement des cycles de variation du niveau de la mer a d'abord été réalisée dans le secteur de Manta Ile de La Plata et ensuite étendu à toute la marge. Au total 26 séquences T-R (Transgression-Régression) ont été identifiées qui peuvent être regroupées en trois mega-séquences séparées par des discontinuités d'échelle régionale. Il s'agit de UTR (« upper » TR séquences) qui est composé de 10 séquences, et de MTR (« middle » TR séquences) et LTR (« lower » TR séquences) composés de 16 séquences.

Les datations C14 des carottes sédimentaires ont permis de dater les séquences les plus récentes. Ces âges ont été complétés par la réalisation d'une corrélation directe entre les séquences sismiques et les séquences décrites et datées « onshore » et par corrélation avec les courbes climato-eustatiques globales (i.e cycles de Milankovich). Ceci nous a permis de dater les séquences avec à la base un âge minimum du Calabrien (1780-ka) jusqu'à l'actuel (stade MIS 63 au stade MIS 1).

SEGMENTATION DE LA MARGE

La localisation, la géométrie et les caractéristiques des principaux dépôts centres du Pléistocène ont été définis le long de la marge. La marge comporte un segment Nord et un segment Sud dont la limite est située vers 0° de latitude. Le long du segment Nord, les mega séquences MTR et LTR sont plutôt développées sur la plateforme et sur la pente ; alors que le long du segment Sud, ces deux mega-séquences sont absentes sur la plateforme (érodées ou « bypassed ») et peu développées sur la pente. Au contraire la mega-séquence UTR est bien développé le long des deux segments à la fois sur la plateforme et sur la pente.

Le long du segment nord, la géométrie du socle acoustique permet d'identifier trois basins sur la plateforme (Cojimies, Jama et Cabo Pasado). La carte isopaque du Pléistocène montre que la subsidence est de plus en plus importante du Sud vers le Nord ; comme la bathymétrie, elle montre une migration vers le continent de la rupture de pente. Ces trois basins ont probablement formé un basin unique avant d'être séparés par la subduction de

monts sous-marins (Cojimies et Jama) et, pour le bassin de Cabo Pasado, par le prolongement sur la plateforme du système de faille de Jama.

Le long du segment sud, le socle acoustique est proche du fond et souvent associé à l'absence de sédiments. Ceci suggère que la plateforme a été soulevée ou a été le lieu d'un « bypass » important. Ce secteur de la plateforme, sans sédiment, est situé juste en face du segment où entre en subduction actuellement la partie la plus élevée de la ride de Carnegie. Le long de la pente, la carte isopaque montre des bassins de petites tailles dont la géométrie et le remplissage sédimentaire sont localement contrôlés par l'arrivée en subduction de monts sous-marins

SUBDUCTION DE RELIEFS OCEANIQUES

A l'échelle régionale

La discordance entre le socle acoustique et la mega-séquence LTR peut être suivi régionalement. Cette discordance d'aspect régional pourrait marquer l'arrivée en subduction de la ride de Carnegie (ou d'un fort relief porté par cette dernière). Dans cette hypothèse l'arrivée de la ride de Carnegie serait associée 1) au soulèvement de la bordure de la plateforme observé depuis le sud du bassin de Jama jusqu'au Nord du canyon de Santa Elena ; 2) à la progradation vers le Nord observé au niveau du bassin de Cojimies ; 3) à la subsidence importante contrôlée par une subduction érosion accrue observée au niveau du secteur de Santa Elena.

Toutes ces déformations débutent juste après la discordance de base entre le socle acoustique et la mega-séquence LTR dont l'âge minimum d'après notre chrono-stratigraphie est de 1782 ka. Ceci suggère que l'âge minimum de l'arrivée en subduction de la ride de Carnegie pourrait être du Calabrien. Cet âge est en tout cas cohérent avec celui de l'inversion à terre du bassin de Canoa (Cantalamessa et Di Celma, 2004) et avec la brusque augmentation de la subsidence dans le golfe de Guayaquil (Witt et al., 2005).

Les modèles analogiques de subduction de reliefs océaniques montrent que, au droit du relief en subduction, la marge est en soulèvement alors que sur les bords du reliefs elle est plutôt en subsidence. Si nous appliquons ce modèle à la ride de Carnegie (en supposant que la géométrie actuelle de la ride de Carnegie se prolonge dans la subduction) cela implique que le prolongement du point le plus haut de la ride qui est entré en subduction est situé sous des secteurs soulevés de la marge ; ce qui semble être le cas (SVSH et le CPAS). Au nord de ce point, la subduction du flanc nord de la ride de Carnegie devrait se traduire par une subsidence de plus en plus marquée vers le Nord, au fur et à mesure que l'on s'éloigne de ce point. Cela n'est pas vraiment le cas, la subsidence étant bien marquée dans le bassin de Cojimies, mais pas plus au Nord, où la marge se soulève. Cela suggère que la géométrie du prolongement du flanc Nord de la ride de Carnegie en subduction est sans doute plus complexe.

A l’échelle locale

Dans le secteur de Manta Ile de La Plata, l’analyse sismo-stratigraphique des 10 séquences composant la mega-séquence UTR a permis d’établir une chrono-stratigraphie. L’établissement d’une chronologie de la déformation tectonique et des corps sédimentaires a permis de reconstituer l‘évolution morpho-structurale pléistocène de ce secteur de la marge et ses relations avec les structures profondes. Dans la région de Manta-La Plata, la reconstitution palinspatique de la déformation et de la sédimentation est cohérente avec la subduction depuis 500 ka, d’un relief porté par la ride de Carnegie (Proust et al., 2016).

CONCLUSIONES

El presente trabajo está basado en análisis sismo-estratigráfico de depósitos del Pleistoceno, peservados en la plataforma y en la pendiente del margen continental del Ecuador. Se ha utilizado datos de sísmica de reflexión de alta resolución colectados durante la campaña científica ATACAMES (2012), complementados con algunas líneas sísmicas de la campaña SCAN (2009) (propiedad de la Secretaría de Hidrocarburos del Ecuador); así como también datos de núcleos de sedimentos y batimetría monocanal y multicanal de diferentes fuentes.

A partir del análisis de los datos, se propone un modelo de evolución tectónica y estratigráfica para el margen central del Ecuador, durante el Pleistoceno, el mismo que ilustra a diferentes escalas la influencia de la subducción de relieves oceánicos en la deformación del margen continental.

ESTRATIGRAFÍA

En el área clave Manta-Plata, se definió la referencia estratigráfica básica (i.e. la secuencia T-R), de los depósitos Cuaternarios de la plataforma continental. Las secuencias T-R están apiladas

Las secuencias de T-R se encuentran apiladas unas sobre otras y por lo general muestran un desplazamiento lateral hacia tierra una con respecto a la otra. Los principales cambios registran discordancias angulares con extensión de local a regional. Las discordancias angulares regionales permitieron definir tres grupos de mega-secuencias T-R: Inferior (LowTR), Media (Middle T-R) y Superior (UpperT-R), que constituyen el relleno de las cuencas de la plataforma y de la pendiente del margen central del Ecuador. Se identificaron un total de 26 secuencias T-R, divididas en: 11 LTR, 5 MTR y 10 UTR.

El registro sedimentario está datado mediante el análisis de C14 con muestras tomadas de los núcleos de pistón, y mediante correlación con los afloramientos terrestres cuaternarios de la zona costera, tales como terrazas marinas. Por otra parte, las secuencias T-R muestran excelentes correlaciones con la curva climato-eustática global de los ciclos de Milankovitch. Esto ha permitido proponer que la edad de las secuencias T-R abarcan desde el Pleistoceno Calabriense (1780-Ka) hasta el presente (Figura 6.1), es decir, desde el MIS 63 hasta el MIS 1.

SEGMENTACIÓN DEL MARGEN

La localización, la geometría y las características estratigráficas de los depocentros Pleistocénicos fueron bien definidos a lo largo del margen. Este análisis incluye la geometría del basamento acústico pre-Pleistocénico, el análisis del espesor de sedimentos, los aspectos estructurales y la geología costera. El margen central del Ecuador puede ser dividido en segmento Norte y Sur, con un límite aproximado alrededor de la latitud 0. En las cuencas del segmento Norte, las mega-secuencias LTR y MTR están muy bien desarrolladas y preservadas en la plataforma y en la pendiente; mientras que en las cuencas localizadas en el segmento Sur, las mega-secuencias LTR y MTR han sido erosionadas o no-depositadas (bypass), en la

plataforma y en la pendiente. Por el contrario las secuencias UTR son bien preservadas en ambos segmentos, Norte y Sur, en la plataforma y en la pendiente (Figura 6.12).

Segmento Norte

La grilla del basamento acústico, de las líneas sísmicas de la campaña Atacames, muestran una subsidencia de la plataforma (cuencas Cojimíes, Jama y Cabo Pasado), el mapa isópaco muestra que las cuencas aumentan su grosor hacia el Norte, y el mapa batimétrico presenta un cambio de dirección, hacia tierra, del borde de plataforma (Figura 6.10). Las cuencas del Norte parecen haber sido creadas como una sola cuenca, y luego separadas por la influencia de la subducción de asperidades y la prolongación hacia el mar de la falla de Jama.

Segmento Sur

El mapa del basamento acústico del Cuaternario presenta un levantamiento general de la plataforma continental con la erosión o el bypass sedimentario (Figura 6.12), el mapa isópaco muestra pocas cuencas aisladas en la pendiente y el mapa batimétrico despliega un cambio hacia el mar en la dirección del borde de plataforma. El levantamiento general de la plataforma presentado en el segmento Sur se localiza frente a la actual zona de máximo relieve de la Cordillera de Carnegie, lo cual podría explicar la erosión sedimentaria en esta zona. La formación de las cuencas, en este segmento, es principalmente en la zona de pendiente y ha sido ligada al proceso de subducción de montes o asperidades submarinas (por ejemplo las cuencas San Lorenzo, la Plata, Ayampe en la Figura 6.7).

SUBDUCCIÓN DE RELIEVES OCEÁNICOS

La segmentación del margen sugiere una relación entre la subducción de relieves oceánicos y la deformación del margen central del Ecuador, y nos permite proponer una evolución tectónica a diferentes escalas en espacio y tiempo.

Escala regional

Los datos muestran una discordancia regional a la base de los depósitos pleistocénicos de la plataforma continental, a la base de LTR. Esta discordancia por lo tanto corresponde al registro de un evento tectónico regional, la misma que podría corresponder a la colisión de la Cordillera de Carnegie, o al menos, al arribo de una estructura elongada de relieve positivo de la cordillera de Carnegie. Siguiendo esta asunción, este relieve positivo de la cordillera de Carnegie sería el responsable de: a) el levantamiento general de la plataforma continental registrado desde el sur de la Cuenca de Jama hasta el cañón de Santa Elena; b) el sentido de divergencia de los reflectores y la profundización de los depocentros hacia el norte que muestran las líneas sísmicas de las cuencas del Norte (Figura 6.3); c) la deformación y la erosión de subducción mostrada alrededor del cañón de Santa Elena. Estas deformaciones se registran sobre la discordancia de LTR. Por lo cual se propone que la edad mínima de subducción de la Cordillera de Carnegie es de 1782-ka. Esta edad es coherente con la edad propuesta para el incremento de la subsidencia en el Golfo de Guayaquil (Witt, et al., 2006) y con la edad de la inversión de la cuenca “Canoa” propuesta por Cantalamessa y Di Celma (2004).

El relieve actual más alto de la Cordillera de Carnegie, coincide espacialmente con el alto estructural de San Vicente (SVSH) y el anticlinal de Cabo Pasado (CPAS) de la plataforma continental; mientras que flanco norte de la cordillera coincide espacialmente con la zona en subsidencia del segmento norte, que se incrementa en profundidad desde la cuenca Cabo Pasado hasta la cuenca Cojimíes. Esta relación se ve representada en los modelos analógicos de la subducción de una asperidad elongada, con levantamiento de la plataforma en la zona alta y subsidencia en la zona de los flancos. A partir de los resultados obtenidos, se sugiere que la Cordillera de Carnegie, ha subducido en sentido E-W, al menos desde el Pleistoceno. Sin embargo, debido al movimiento del bloque Nor-Andino hacia el Norte, este sentido de subducción de la cordillera de Carnegie, genera un barrido hacia el sur, planteado por Collot et al. (2009).

Escala Sub-Regional

Las discordancias entre LTR-MTR, MTR-UTR, así como las discordancia entre las secuencias T-R III-IV and VII-VIII dentro de la mega-secuencia UTR (Figura 6.1), sugieren un cambio en la Acomodación, diferente al cambio "normal" registrado cada 100-Kyrs., relacionados a los cambios glacio-eustáticos. Estos cambios en el registro "normal" podrían estar generados por cambios en la morfología de la subducción de la cordillera de Carnegie, o por cambios climato-eustáticos más fuertes que los regulares, o por una combinación de ambos procesos.

Escala local

El análisis de denudación de sedimentos (backstripping) y un detallado mapeo de la evolución tectónica muestran la deformación de la plataforma continental en el área de Manta-La Plata, durante la depositación de la mega-secuencia UTR. Esta deformación ha sido relacionada con la subducción de un relieve de la Cordillera de Carnegie. El patrón de deformación de la plataforma continental es consistente con la proposición de la subducción de un relieve submarino propuesto por Sanclemente (2014). Nosotros experimentamos la hipótesis de la relación entre la deformación y la subducción de este monte submarino, mediante la reconstrucción palinpástica de la deformación de la plataforma continental en este sector desde hace 1 Ma. Esta comparación muestra que esta colisión pudo haber comenzado hace unos 500ka., generando una deformación estratigráfica syn-tectónica, y que drásticamente finalizó hace aproximadamente 50ka. (Proust et al., 2016).

REFERENCES CITED

A

Aigner, T., 1985. Storm depositional systems, in : Friedman, G.M., Neugebauer, H.J., and Seilacher, A. (Eds.), Lecture Notes in Earth Sciences, Springer Verlag, Berlin v. 3, pp.1–174.

Allen, P.A., Allen, J.R., 2013. Basin analysis: Principles and application to petroleum play assessment. John Wiley & Sons.

Aubouin, J., Bourgois, J., Azéma, J., 1984. A new type of active margin: the convergent-extensional margin, as exemplified by the Middle America Trench off Guatemala. Earth Planet. Sci. Lett. 67, 211–218.

Aubouin, J., Von Huene, R., Baltuck, M., Arnott, R., Bourgois, J., Filewicz, M., Kvenvolden, K., Leinert, B., McDonald, T., McDougall, K., others, 1982. Leg 84 of the Deep Sea Drilling Project.

B

Ballance, P.F., Scholl, D.W., Vallier, T.L., Stevenson, A.J., Ryan, H., Herzer, R.H., 1989. Subduction of a Late Cretaceous Seamount of the Louisville Ridge at the Tonga Trench: A model of normal and accelerated tectonic erosion. Tectonics 8, 953. doi:10.1029/TC008i005p00953

Benitez, S., 1995. Évolution géodynamique de la province cotiere sud-équatorienne au Crétacé supérieur-Tertiare.

Bethoux, N., Segovia, M., Alvarez, V., Collot, J.-Y., Charvis, P., Gailler, A., Monfret, T., 2011. Seismological study of the central Ecuadorian margin: Evidence of upper plate deformation. J. South Am. Earth Sci. 31, 139–152. doi:10.1016/j.jsames.2010.08.001.

Bilderback, E.L., Pettinga, J.R., Lichtfield, N.J., Quigley, M., Marden, M., Roering, J.J., Palmer, A.S., 2015. Hillslope response to climate-modulated river incision in the Waipaoa catchment, East Coast North Island, New Zealand. Geological Society America Bulletin, 127, 131-148.

Blanco-Chao, R., Pedoja, K., Witt, C., Martinod, J., Husson, L., Regard, V., Audin, L., Nexer, M., Delcaillau, B., Saillard, M., Melnick, D., Dumont, J.F., Santana, E., Navarrete, E., Martillo, C., Pappalardo, M., Ayala, L., Araya, J.F., Feal-Pérez, A., Correa, D., Arozarena-Llopis, I., 2014. Author Query Form, in: Kennedy, D.M., Stephenson, W.J., Naylor, L.A. (Eds.), Memoir 40: Rock Coast Geomorphology: A Global Synthesis. The Geological Society, London, p. 304.

Boggs, S., 2010. Principles of sedimentology and stratigraphy, 4th edition, Pearson Prentice Hall, Upper Saddle River, New Jersey 07458, 655p.

Bonnet, S., 2009. Shrinking and splitting of drainage basins in orogeny landscapes from the migration of the main drainage divide. Nature Geoscience, 2, 766-771.

Braun, J., Simon-Labric ,Th., Murray, K.E., Reiners, P.W., 2014. Topographic relief driven by variations in surface rock density. Nature Geoscience, 7, 534-540.

Braaksma, H., Drijkoningen, G.G., Filippidou, N., Kenter, J.A.M., Proust, J.N., 2006. The origin and nature of seismic reflections of sharp-based shoreface deposits (Upper Jurassic siliciclastics, Northern France). Geophysical Prospecting, 54, 211–236.

Brown Jr, L.F., Fisher, W.L., 1977. Seismic-stratigraphic interpretation of depositional systems: examples from Brazilian rift and pull-apart basins, in: Seismic Stratigraphy-Applications to Hydrocarbon Exploration. American Association of Petroleum Geologists Memoir 26. Memoir, pp. 213–248.

C

Calahorrano, A., 2005. Structure de la marge du Golfe de Guayaquil (Equateur) et proprietes physiques du chenal de subduction, a partir de donnees de sismique marine reflexion et refraction. Pierre et Marie Curie. Paris VI.

Cande, S.C., others, 1985. Nazca--South America plate interactions since 60 my BP. Atlas Ocean Margin Program, Peru Cont. Margin Reg. 14.

Cantalamessa, G., Di Celma, C., 2004. Origin and chronology of Pleistocene marine terraces of Isla de la Plata and of flat, gently dipping. J. South Am. Earth Sci. 16, 633–648. doi:10.1016/j.jsames.2003.12.007

Cantalamessa, G., Di Celma, C., Ragaini, L., 2005. Sequence stratigraphy of the Punta Ballena Member of the Jama Formation (Early Pleistocene, Ecuador): insights from integrated sedimentologic, taphonomic and paleoecologic analysis of molluscan shell concentrations. Palaeogeogr. Palaeoclimatol. Palaeoecol. 216, 1–25. doi:10.1016/j.palaeo.2004.09.012

Cantalamessa, G., Di Celma, C., Ragaini, L., Valleri, G., Landini, W., 2007. Sedimentology and high-resolution sequence stratigraphy of the late middle to late Miocene Angostura Formation (western Borbon Basin, northwestern Ecuador). J Geol Soc 164, 653.

Carnevale, G., Landini, W., Ragaini, L., Di Celma, C., Cantalamessa, G., 2011. Taphonomic and paleoecological analyses (mollusks and fishes) of the Sua Member condensed shellbed, Upper Onzole Formation (Early Pliocene, Ecuador). Palaios, 26, 160-172.

Catuneanu, O., 2006. Principles of sequence stratigraphy. Elsevier.

Catuneanu, O., Abreu, V., Bhattacharya, J.P., Blum, M.D., Dalrymple, R.W., Eriksson, P.G., Fielding, C.R., Fisher, W.L., Galloway, W.E., Gibling, M.R., Giles, K. a., Holbrook, J.M., Jordan, R., Kendall, C.G.S.C., Macurda, B., Martinsen, O.J., Miall, A.D., Neal, J.E., Nummedal, D., Pomar, L., Posamentier, H.W., Pratt, B.R., Sarg, J.F., Shanley, K.W., Steel, R.J., Strasser, A., Tucker, M.E., Winker, C., 2009a. Towards the standardization of sequence stratigraphy. Earth-Science Rev. 92, 1–33. doi:10.1016/j.earscirev.2008.10.003

Catuneanu, O., Galloway, W.E., Kendall, C.G.S.C., Miall, A.D., Posamentier, H.W., Strasser, A., Tucker, M.E., 2011. Sequence Stratigraphy: Methodology and Nomenclature. Newsletters Stratigr. 44, 173–245. doi:10.1127/0078-0421/2011/0011

Catuneanu, O., Willis, A.J., Miall, A.D., 1998. Temporal significance of sequence boundaries. Sediment. Geol. 121, 157–178. doi:10.1016/S0037-0738(98)00084-0

Chlieh, M., Mothes, P. a., Nocquet, J.-M., Jarrin, P., Charvis, P., Cisneros, D., Font, Y., Collot, J.-Y., Villegas-Lanza, J.-C., Rolandone, F., Vallée, M., Regnier, M., Segovia, M., Martin, X., Yepes, H., 2014. Distribution of discrete seismic asperities and aseismic slip along the Ecuadorian megathrust. Earth Planet.

Sci. Lett. 400, 292–301. doi:10.1016/j.epsl.2014.05.027

Clift, P., Vannucchi, P., 2004. Controls on tectonic accretion versus erosion in subduction zones : implications for the origin and recycling of the continental crust. Rev. Geophys. 42, 1–31. doi:10.1029/2003RG000127.1

Clift, P.D., 2003. Tectonic erosion of the Peruvian forearc, Lima Basin, by subduction and Nazca Ridge collision. Tectonics 22. doi:10.1029/2002TC001386

Clift, P.D., MacLeod, C.J., 1999. Slow rates of subduction erosion estimated from subsidence and tilting of the Tonga forearc. Geology 27, 411–414.

Clift, P.D., Schouten, H., Vannucchi, P., 2009. Arc-continent collisions, sediment recycling and the maintenance of the continental crust. Geol. Soc. London, Spec. Publ. 318, 75–103.

Cloos, M., 1993. Lithospheric buoyancy and collisional orogenesis: Subduction of oceanic plateaus, continental margins, island arcs, spreading ridges, and seamounts. Geol. Soc. Am. Bull. 105, 715–737.

Collot, J., Charvis, P., Gutscher, M.–., S., O., 2002. Exploring the Ecuador-Colombia active margin and interplate seismogenic zone. EOS, Trans. … 83, 185–192. doi:10.1029/2002EO000120

Collot, J., Michaud, F., Alvarado, A., Marcaillou, B., Ratzov, G., Migeon, S., Calahorrano, A., Pazmino, A., Antipolis, U.D.N., Pierre, U., Od, G.H., Xu, W.H.G., Udqfh, V.P.H.U., 2009. Visión general de la morfología submarina del margen convergente de Ecuador-Sur de Colombia: implicaciones sobre la transferencia de masa y la edad de la subducción de la Cordillera de Carnegie. Geol. y Geofísica Mar. y Terr. del Ecuador 47–74.

Collot, J.-Y., Marcaillou, B., Sage, F., Michaud, F., Agudelo, W., Charvis, P., Graindorge, D., Gutscher, M.-A., Spence, G., 2004. Are rupture zone limits of great subduction earthquakes controlled by upper plate structures? Evidence from multichannel seismic reflection data acquired across the northern Ecuador-southwest Colombia margin. J. Geophys. Res. Solid Earth 109, n/a–n/a. doi:10.1029/2004JB003060

Contreras-Reyes, E., Carrizo, D., 2011. Control of high oceanic features and subduction channel on earthquake ruptures along the Chile–Peru subduction zone. Phys. Earth Planet. Inter. 186, 49–58. doi:10.1016/j.pepi.2011.03.002

Coronel, J., 2002. Les canyons de la marge Equatorienne: Approche morphostructurale et évolution. Univ. Nice Sophia Antip. — DEA Dyn. la Lithosphère, Nice.

D

Deniaud, Y., 2000. Enregistrements sedimentaire et structural de l'evolution geodynamique des andes equatoriennes au cours du Neogene : Etude des bassins d'Avant-arc et bilans de masse. Université Joseph Fourier - Grenoble I.

Deniaud, Y., Baby, P., Basile, C., Ordoñez, M., Montenegro, G., Mascle, G., 1999. Opening and tectonic and sedimentary evolution of the Gulf of Guayaquil Neogene and Quaternary fore-arc basin of the south Ecuadorian Andes 181–187.

Di Celma, C., Ragaini, L., Cantalamessa, G., Curzio, P., 2002. Shell concentrations as tools in characterizing sedimentary dynamics at sequence-bounding

unconformities : examples from the lower unit of the Canoa Formation (Late Pliocene , Ecuador). Geobios.

Di Celma, C., Ragaini, L., Cantalamessa, G., Landini, W., 2005. Basin physiography and tectonic influence on sequence architecture and stacking pattern: Pleistocene succession of the Canoa Basin (central Ecuador). Geol. Soc. Am. Bull. 117, 1226. doi:10.1130/B25684.1

Dominguez, S., Lallemand, S., Malavieille, J., Huene, R. von H., 1998a. Upper plate deformation associated with seamount subduction. Tectonophysics 293, 207–224.

Dominguez, S., Lallemand, S., Malavieille, J., Schnürle, P., 1998b. Oblique subduction of the Gagua Ridge beneath the Ryukyu accretionary wedge system: Insights from marine observations and sandbox experiments. Mar. Geophys. Res. 20, 383–402. doi:10.1023/A:1004614506345

Dumont, J.F., Santana, E., Bonnardot, M.-A., Pazmiño, N., Pedoja, K., Scalabrino, B., 2014. Geometry of the coastline and morphology of the convergent margin of Ecuador. Geol. Soc. Memoir 41.

Dumont, J.F., Santana, E., Vilema, W., Pedoja, K., Ordóñez, M., Cruz, M., Jiménez, N., Zambrano, I., 2005. Morphological and microtectonic analysis of Quaternary deformation from Puná and Santa Clara Islands, Gulf of Guayaquil, Ecuador (South America). Tectonophysics 399, 331–350. doi:10.1016/j.tecto.2004.12.029

Duan, B., 2012. Dynamic rupture of the 2011 Mw 9.0 Tohoku-Oki earthquake: role of a possible subducting seamount. J. Geophys. Res., 117, B5.

E

Ego, F., Sébrier, M., Lavenu, A., Yepes, H., Egues, A., 1996. Quaternary state of stress in the Northern Andes and the restraining bend model for the Ecuadorian Andes. Tectonophysics 259, 101–116. doi:10.1016/0040-1951(95)00075-5

Eguez, A., Alvarado, A., Yepes, H., Costa, C., Dart, R.L., Machette, M.N., Bradley, L., 2003. Database and Map of Quaternary faults and folds of Ecuador and its offshore regions Database and Map of Quaternary Faults and Folds of Ecuador and its offshore regions. USGS.

Embry, A.F., 1995. Sequence boundaries and sequence hierarchies: problems and proposals. Nor. Pet. Soc. Spec. Publ. 5, 1–11.

Embry, A.F., 1993. Transgressive-regressive (T-R) sequence analysis of the Jurassic succession of the Sverdrup Basin, Canadian Arctic Archipelago. Can. J. Earth Sci. 30, 301–320.

Emery, D., Myers, K.J., 1996. 1996, Sequence stratigraphy.

Espurt, N., Funiciello, F., Martinod, J., Guillaume, B., Regard, V., Faccenna, C., Brusset, S., 2008. Flat subduction dynamics and deformation of the South American plate: Insights from analog modeling. Tectonics 27, 1–19. doi:10.1029/2007TC002175

Etayo-Cadavid, M.F., Andrus, C.F.T., Jones, K.B., Hodgins, G.W.L., Sandweiss, D.H., Uceda-Castillo, S., Quilter, J., 2013. Marine radiocarbon reservoir age variation in Donax obesulus shells from northern Peru: Late Holocene evidence for extended El Ni{ñ}o. Geology 41, 599–602.

F

Feininger, T., 1977. Simple Bouguer anomaly

map of Ecuador. Contribution - Escuela Politénica Nacional, Department of Geology, n°2.

Font, Y., Segovia, M., Vaca, S., Theunissen, T., 2013. Seismicity patterns along the Ecuadorian subduction zone: new constraints from earthquake location in a 3-D a priori velocity model. Geophys. J. Int. 193, 263–286. doi:10.1093/gji/ggs083.

G

Gailler, A., Charvis, P., Flueh, E.R., 2007. Segmentation of the Nazca and South American plates along the Ecuador subduction zone from wide angle seismic profiles. Earth Planet. Sci. Lett. 260, 444–464. doi:10.1016/j.epsl.2007.05.045

Gales, J. a., Larter, R.D., Mitchell, N.C., Dowdeswell, J. a., 2013. Geomorphic signature of Antarctic submarine gullies: Implications for continental slope processes. Mar. Geol. 337, 112–124. doi:10.1016/j.margeo.2013.02.003

Galloway, W.E., 1989. Genetic stratigraphic sequences in basin analysis I: architecture and genesis of flooding-surface bounded depositional units. Am. Assoc. Pet. Geol. Bull. 73, 125–142.

Gardner, T.W., Verdonck, D., Pinter, N.M., Slingerland, R., Furlong, K.P., Bullard, T.F., Wells, S.G., 1992. Quaternary uplift astride the aseismic Cocos ridge, Pacific coast, Costa Rica. Geol. Soc. Am. Bull. 104, 219–232.

Gibbard, P., van Kolfschoten, T., 2004. The pleistocene and holocene epochs. na.

Gibbard, P.L., Head, M.J., Walker, M.J.C., Stratigraphy, T.S. on Q., 2010. Formal ratification of the Quaternary System/ Period and the Pleistocene Series/Epoch with a base at 2.58 Ma. J. Quat. Sci. 25(2), 96–102. doi:0.1002/jqs.1338

Graindorge, D., Calahorrano, A., Charvis, P., Collot, J., Bethoux, N., 2004. Deep structures of the Ecuador convergent margin and the Carnegie Ridge , possible consequence on great earthquakes recurrence interval 31, 1–5. doi:10.1029/2003GL018803

Gutscher, M.–., Malavieille, J., Lallemand, S., Collot, J.-Y., 1999. Tectonic segmentation of the North Andean margin: impact of the Carnegie Ridge collision. Earth Planet. Sci. Lett. 168, 255–270. doi:10.1016/S0012-821X(99)00060-6.

H

Hall, M.L., Wood, C.A., 1985. Volcano-tectonic segmentation of the northern Andes. Geology 13, 203–207.

Hampel, A., Adam, J., Kukowski, N., 2004a. Response of the tectonically erosive south Peruvian forearc to subduction of the Nazca Ridge: Analysis of three-dimensional analogue experiments. Tectonics 23. doi:10.1029/2003TC001585

Hampel, A., Kukowski, N., Bialas, J., Huebscher, C., Heinbockel, R., 2004b. Ridge subduction at an erosive margin: The collision zone of the Nazca Ridge in southern Peru. J. Geophys. Res. 109. doi:10.1029/2003JB002593

Hernández, M.J., 2014. Structures de la plateforme continentale de la marge d'Equateur à partir de l'interprétation de sismique pétrolière. Interaction plaque plongeante/plaque chevauchante et segmentation de la

marge. Université de Nice Sophia-Antipolis. Master Pro2 AGI Sciences de la Terre et Environnement.

Hicks, S.P., Rietbrock, A., Haberland, C. A., Ryder, I.M.A., Simons, M., Tassara, A. , 2012. The 2010 Mw8.8 Maule, Chile earthquake: nucleation and rupture propagation controlled by a subducted topographic high. Geophysical Research Letters, 39, 19

Hoffman, P.F., Grotzinger, J.P., 1993. Orographic precipitation, erosional unloading, and tectonic style. Geology, 21, 195-198.

Hunt, D., Tucker, M.E., 1992. Stranded parasequences and the forced regressive wedge systems tract: deposition during base-level'fall. Sediment. Geol. 81, 1–9.

Hunter, R.E., Clifton, H.E., 1982. Cyclic deposits and hummocky cross-stratification of probable storm origin in Upper Cretaceous rocks of the Cape Sebastian area, Southwestern Oregon. Journal of Sedimentary Petrology, 52, 127-144.

I

Izumi, N., 2004. The formation of submarine gullies by turbidity currents. J. Geophys. Res. 109, C03048. doi:10.1029/2003JC001898.

J

Jaillard, E., Ordóñez, M., Berrones, G., Bengtson, P., Bonhomme, M., Jiménez, N., Zambrano, I., 1996. Sedimentary and tectonic evolution of the arc zone of Southwestern Ecuador during Late Cretaceous and Early Tertiary times x L-3. South Am. Earth Sci. 9, 131–140.

Jervey, M.T., 1988. Quantitative geological modeling of siliciclastic rock sequences and their seismic expression. Sea-Level Chang. 42, 47–69. doi:10.2110/pec.88.01.0047

Jordá, J., 1995. El cuaternario: definición, límite inferior y divisiones. Zephyrvs XLVIII, 53–74.

Jordan, T.E., Flemings, P.B., Beer, J.A., 1988. Dating thrust-fault activity by use of foreland-basin strata, in: New Perspectives in Basin Analysis. Springer, pp. 307–330.

K

Kendall, C.G.S.C., Schlager, W., 1981. Carbonates and relative changes in sea level. Mar. Geol. 44, 181–212. doi:10.1016/0025-3227(81)90118-3

Kendrick, E., Bevis, M., Smalley, J.R., Brooks, B., Vargas, R.B., Lauria, E., Souto Fortes, L.P., 2003. The Nazca–South America Euler vector and its rate of change. Journal of South America Earth Science, 16, 2, 125–131.

Kidwell, S.M., 1991. Condensed deposits in siliciclastic sequences: expected and observed features. In: Einsele, G., Ricken, W., Seilacher, A. (Eds.), Cycles and Events in Stratigraphy. Springer-Verlag, Berlin Heidelberg, pp. 682– 695.

L

Lafont, F., 1994. Influences relatives de la subsidence et de l'eustatisme sur la localisation et la g{é}om{é}trie des

r{é}servoirs d'un syst{è}me delta{ï}que. Exemple de l'Eoc{è}ne du bassin de Jaca, Pyr{é}n{é}es espagnoles.

Lallemand, S., 1999. La subduction océanique. Pour Sci. 108.

Lallemand, S.E., Schnürie, P., Malavieille, J., 1994. Coulomb theory applied to accretionary and nonaccretionary wedges: Possible causes for tectonic erosion and/or frontal erosion. Geophys. Res. 99, 12,033–12,0055.

Laursen, J., Normark, W.R., 2002. Late Quaternary evolution of the San Antonio Submarine Canyon in the central Chile forearc. Mar. Geol. 188, 365–390. doi:10.1016/S0025-3227(02)00421-8

Laursen, J., Scholl, D.W., Huene, R. von, 2002. Neotectonic deformation of the central Chile margin: Deepwater forearc basin formation in response to hot spot ridge and seamount subduction. Tectonics 21, 1–27. doi:10.1029/2001TC901023

Lisiecki, L.E., Raymo, M.E., 2005. A Pliocene-Pleistocene stack of 57 globally distributed benthic δ 18 O records. Paleoceanography 20, n/a–n/a. doi:10.1029/2004PA001071

Loayza, G., 2013. Evolution du Système de canyons du Golfe de Guayaquil Contrôles paléo-climatiques et tectoniques. Sophia Antipolis, Nice.

Lobo, F.J., Ridente, D., 2013. Stratigraphic architecture and spatio-temporal variability of high-frequency (Milankovitch) depositional cycles on modern continental margins: An overview. Mar. Geol. doi:10.1016/j.margeo.2013.10.009

Lonsdale, P., 2005. Creation of the Cocos and Nazca plates by fission of the Farallon plate. Tectonophysics 404, 237–264. doi:10.1016/j.tecto.2005.05.011

Lonsdale, P., 1978. Ecuadorian Subduction System. Am. Assoc. Pet. Geol. Bull. 62, 2454–2477.

Lonsdale, P., Klitgord, K.D., 1978. Structure and tectonic hystory of the eastern Panama Basin. Geol. Soc. Am. Bull. 981–999.

M

Macharé, J., Ortlieb, L., 1992. Plio-Quaternary vertical motions and the subduction of the Nazca Ridge, central coast of Peru. Tectonophysics 205, 97–108. doi:10.1016/0040-1951(92)90420-B

Mahieux, G., Proust, J.N., Tessier, B., Debatist, M., 1998. High resolution seismic and sequence stratigraphy: relationships between the seismic record and the sequence stratigraphic picture. Marine Petrol. Geol., 3064, 15, 4, 329-342

Marcaillou, B., 2015. Hétérogénéités structurales et structure thermique des marges convergentes : deux approches complémentaires de la déformation tectonique et de la rupture sismique.

Marcaillou, B., Collot, J.-Y., Ribodetti, A., d'Acremont, E., Mahamat, A.A., Alvarado, A., 2016. Seamount subduction at the North-Ecuadorian convergent margin: effects on structures, inter-seismic coupling and seismogenesis. Earth Planet. Sci. Lett. 433, 146–158. doi:10.1016/j.epsl.2015.10.043

Marden, M., Betts, H., Palmer, A., Taylor, R., Bilderback, E., Lichtfield, N., 2014. Post-glacial maximum fluvial incision and sediment generation in the unglaciated Waipaoa catchment, North Island, New Zealand. Geomorphology, 214, 283-306.

Martillo, C., Proust, J.N., Michaud, F., Collot,

J.-Y., 2013. Pleistocene stratigraphic signature of active deformation along the central Ecuadorian subduction margin, in: 14ème Congrès Français de Sédimentologie. ASF. Paris.

Martinod, J., Husson, L., Roperch, P., Guillaume, B., Espurt, N., 2010. Horizontal subduction zones, convergence velocity and the building of the Andes. Earth Planet. Sci. Lett. 299, 299–309. doi:10.1016/j.epsl.2010.09.010

Mercier de Lépinay, B., Michaud, F., Calmus, T., Bourgois, J., Poupeau, G., Saint-Marc, P., 1997. Large Neogene subsidence event along the Middle America trench off Mexico (18-19°N): evidence from submersible observations. Geology 25, 387–390. doi:10.1130/0091-7613(1997)025<0387:lnseat>2.3.co;2

Miall, A., 2010. The geology of stratigraphic sequences. Springer Science & Business Media.

Michaud, F., Collot, J.Y., Alvarado, A., Lopez, E., INOCAR, 2006. República del Ecuador, Batimetria y Relieve Continental.

Michaud, F., Proust, J.N., Collot, J.Y., Lebrun, J.F., Witt, C., Ratzov, G., Pouderoux, H., Martillo, C., Hernández, M.J., Loayza, G., Penafiel, L., Schenini, L., Dano, A., Gonzalez, M., Barba, D., De Min, L., Ponce, G., Urresta, A., Calderon, M., 2015. Quaternary sedimentation and active faulting along the Ecuadorian shelf: preliminary results of the ATACAMES Cruise (2012). Mar. Geophys. Res. doi:10.1007/s11001-014-9231-y

Michaud, F., Proust, J.N., Collot, J.Y., Lebrun, J.F., Witt, C., Ratzov, G., Pouderoux, H., Martillo, C., Hernández, M.J., Loayza, G., Penafiel, L., Schenini, L., Dano, A., Gonzalez, M., Barba, D., De Min, L., Ponce, G., Urresta, A., Calderon, M., 2012. The ATACAMES Expedition.

Michaud, F., Witt, C., Royer, J.-Y., 2009. Influence of the subduction of the Carnegie volcanic ridge on Ecuadorian geology: Reality and fiction. Geol. Soc. Am. Mem. doi:10.1130/2009.1204(10)

Mitchum, R., Vail, R., Sangree, J.B., 1977. Seismic Stratigraphy and Global Changes of Sea level, Part 6: Stratigraphic Interpretation of Seismic Reflection Patterns in Depositional Sequences, in: AAPG Bulletin.

Mochizuki, K., Yamada, T., Shinohara, M., Yamanaka, Y., Kanazawa, T., 2008. Weak interplate coupling by seamounts and repeating Mw7 earthquakes. Science, 321, 1194-1197.

Montgomery, D.R., Balco, G., Willet, S.D., 2001. Climate, tectonics, and the morphology of the Andes. Geology, 29, 579-582.

N

Naish, T., Kamp, P.J.J., 1997. Sequence stratigraphy of sixth-order (41ky) Pliocene-Pleistocene cyclothems, Wanganui Basin, New Zealand: A case for the regressive systems tract. Geological Society of America Bulletin, 109, p. 978–999.

Nocquet, J.M., Mothes, P., Alvarado, A., 2009. Geodésia , geodinámica y ciclo sísmico en Ecuador. Geol. y Geofísica Mar. y Terr. del Ecuador Spec. Pub., 83–95.

Nocquet, J.-M., Villegas-Lanza, J.C., Chlieh, M., Mothes, P.A., Rolandone, F., Jarrin, P., Cisneros, D., Alvarado, A., Audin, L., Bondoux, F., Martin, X., Font, Y., Regnier, M., Vallee, M., Tran, T., Beauval, C., Maguina Mendoza, J.M., Martinez, W., Tavera, H., Yepes, H., 2014. Motion of continental slivers and

creeping subduction in the northern Andes. Nat. Geosci 7, 287–291.

P

Paquet, F., Proust, J.-N., Barnes, P.M., Pettinga, J.R., 2011. Controls on active forearc basin stratigraphy and sediment fluxes: The Pleistocene of Hawke Bay, New Zealand. Geol. Soc. Am. Bull. 123, 1074–1096. doi:10.1130/B30243.1

Paquet, F., Proust, J.-N., Barnes, P.M., Pettinga, J.R., 2009. Inner-Forearc Sequence Architecture in Response to Climatic and Tectonic Forcing Since 150 ka: Hawke's Bay, New Zealand. J. Sediment. Res. 79, 97–124. doi:10.2110/jsr.2009.019

Pedoja, K., Dumont, J.F., Lamothe, M., Ortlieb, L., Collot, J.-Y., Ghaleb, B., Auclair, M., Alvarez, V., Labrousse, B., 2006a. Plio-Quaternary uplift of the Manta Peninsula and La Plata Island and the subduction of the Carnegie Ridge, central coast of Ecuador. J. South Am. Earth Sci. 22, 1–21. doi:10.1016/j.jsames.2006.08.003

Pedoja, K., Husson, L., Johnson, M.E., Melnick, D., Witt, C., Pochat, S., 2014. Earth-Science Reviews Coastal staircase sequences re fl ecting sea-level oscillations and tectonic uplift during the Quaternary and Neogene. Earth-Science Rev. 132, 13–38.

Pedoja, K., Ortlieb, L., Dumont, J.F., Lamothe, M., Ghaleb, B., Auclair, M., Labrousse, B., 2006b. Quaternary coastal uplift along the Talara Arc (Ecuador, Northern Peru) from new marine terrace data. Mar. Geol. 228, 73–91. doi:10.1016/j.margeo.2006.01.004

Peñafiel, L., 2012. Calibration Géologique et Calage Chronostratigraphique des données sismiques de la Campagne ATACAMES dans le secteur de la Peninsule de Manta. Nice Sophia Antipolis.

Pilger, R.H., 1984. Cenozoic plate kinematics, subduction and magmatism: South American Andes. J. Geol. Soc. London. 141, 793–802.

Posamentier, H.W., 1988. Eustatic controls on clastic deposition II- sequence and systems tract models.

Pouderoux, H., Proust, J.N., Lamarche, G., Orpin, A., Neil, H., 2012. Postglacial (after 18 ka) deep-sea sedimentation along the Hikurangi subduction margin (New Zealand): characterisation, timing and origin of turbidites**.** Marine Geology, 295-298, 51-76

Proust, J.-N., Chanier, F., 2004. The Pleistocene Cape Kidnappers section in New Zealand: orbitally forced controls on active margin sedimentation? J. Quat. Sci. 19, 591–603.

Proust, J.-N., Lamarche, G., Nodder, S., Kamp, P.J.J., 2005. Sedimentary architecture of a Plio-Pleistocene proto-back-arc basin : Wanganui Basin , New Zealand. Sediment. Geol. 181. doi:10.1016/j.sedgeo.2005.06.010.

Proust, J.N., Mahieux, G., Tessier, B., 2001. Field and seismic images of sharp-based shoreface deposits: implications for sequence stratigraphic analysis. Journal of Sedimentary Research, 71, 6, 944-957.

R

Ranero, C.R., von Huene, R., 2000. Subduction erosion along the Middle America convergent margin. Nature 404, 748–52. doi:10.1038/35008046

Ranero, C.R., Von Huene, R., Flueh, E., Duarte, M., Baca, D., McIntosh, K., 2000. A cross section of the convergent Pacific margin of Nicaragua. Tectonics 19, 335–357. doi:10.1029/1999TC900045

Ratzov, G., Collot, J., Sosson, M., Migeon, S., 2008. Recent debris-flows and megaturbidite in a confined basin of the North Ecuador subduction trench 1906, 431–434.

Ratzov, G., Collot, J.-Y., Sosson, M., Migeon, S., 2010. Mass-transport deposits in the northern Ecuador subduction trench: Result of frontal erosion over multiple seismic cycles. Earth Planet. Sci. Lett. 296, 89–102. doi:10.1016/j.epsl.2010.04.048

Reyes, P., 2013. Thèse de doctorat de l'université de nice sophia antipolis. Thèse Dr. l'université nice sophia Antip.

Robin, C., 1997. Mesure stratigraphique de la déformation. Application a l'evolution Jurassique du bassin de Paris. Rennes 1. doi:ISBN 2-905532-76-3

S

Sage, F., Collot, J.-Y., Ranero, C.R., 2006. Interplate patchiness and subduction-erosion mechanisms: Evidence from depth-migrated seismic images at the central Ecuador convergent margin. Geology 34, 997. doi:10.1130/G22790A.1

Sallarès, V., Charvis, P., 2003. Crustal thickness constraints on the geodynamic evolution of the Galapagos Volcanic Province. Earth Planet. Sci. Lett. 214, 545–559. doi:10.1016/S0012-821X(03)00373-X

Sallarés, V., Charvis, P., Calahorrano, A., Tecnología, U. De, Cmima, M., 2009. Naturaleza y Formación de la Provincia Volcánica de Galápagos, in: Geología Y Geofísica Marina Y Terrestre Del Ecuador. pp. 203–219.

Sanclemente, E., 2014. Seismic Imaging of the Structure of the Central Ecuador Convergent Margin: Relationship With the Inter-Seismic Coupling Variations. Université de Nice-Sophia Antipolis.

Sangree, J.B., Widmier, J.M., 1977. Seismic Stratigraphy and Global Changes of Sea Level , Part 9 : Seismic Interpretation of Clastic Depositional Facies, in: AAPG Bulletin. pp. 752–771.

Scholz, C.H., Small, C., 1997. The effect of seamount subdcution on seismic coupling. Geology, 25, 487-490.

Siddall, M., Rohling, E. J., Almogi-Labin, A., Hemleben, C., Meischner, D., Schmelzer, I., Smeed, D. A., 2003. Sea-level fluctuations during the last glacial cycle. Nature, 423, 853–858.

Schwarzacher, W., 2000. Repetitions and cycles in stratigraphy. Earth-Science Rev. 51–75.

Siddall, M., Chappell, J., Potter, E.K., 2007. 7. Eustatic sea level during past interglacials. Dev. Quat. Sci. 7, 75–92. doi:10.1016/S1571-0866(07)80032-7

Shackleton, N.J., Sánchez-Goñi, M.F., Pailler, D., Lancelot, Y., 2003. Marine Isotope Substage 5e and the Eemian Interglacial. Glob. Planet. Change 36, 151–155. doi:10.1016/S0921-8181(02)00181-9

Sloss, L.L., 1962. Stratigraphic models in exploration. J. Sediment. Res. 32.

Sommerfield, C.K., Lee, H.J., Normark, W.R., 2009. Postglacial sedimentary record of the Southern California continental shelf and slope, Point Conception to Dana Point; Earth science in the urban ocean; the Southern California continental borderland. In: Lee, H.J., Normark, W.R.,

(Eds.), Earth Science in the Urban Ocean—The Southern California Continental Borderland: Geological Society of America Special Paper, 454, 89-115.

Steer, P., Simoes, M., Cattin, R., Shyu, J.B.H., 2014. Erosion influences the seismicity of active thrust faults, Nature Communications, 5:5564

Stuiver, M., Reimer, P.J., 1993. Extended C-14 data-base and revised calib 3.0 C-14 age calibration program. Radiocarbon 35, 215–230.

Sosson, M., Bourgois, J., Lpinay, M. De, 1994. MARINE SeaBeam and deep-sea submersible Nautile surveys in the Chiclayo canyon offPeru (7 ° S): subsidence and subduction-erosion of an Andean-type convergent margin since Pliocene times.

Spikings, R. a., Winkler, W., Hughes, R. a., Handler, R., 2005. Thermochronology of allochthonous terranes in Ecuador: Unravelling the accretionary and post-accretionary history of the Northern Andes. Tectonophysics 399, 195–220. doi:10.1016/j.tecto.2004.12.023

Spikings, R. a., Winkler, W., Seward, D., Handler, R., 2001. Along-strike variations in the thermal and tectonic response of the continental Ecuadorian Andes to the collision with heterogeneous oceanic crust. Earth Planet. Sci. Lett. 186, 57–73. doi:10.1016/S0012-821X(01)00225-4

Stuiver, M., Reimer, P.J., 1993. Extended 14C data base and revised CALIB 3.0 14C age calibration program. Radiocarbon 35, 215–230.

Susan M. Kidwell, 1988. Reciprocal sedimentation and noncorrelative hiatuse in marine-paralic siliciclastics: Miocene outcrop evidence. Geology 16, 609–612.

T

Trenkamp, R., Kellogg, J.N., Freymueller, J.T., Mora, H.P., 2002. Wide plate margin deformation, southern Central America and northwestern South America, CASA GPS observations. J. South Am. Earth Sci. 15, 157–171. doi:10.1016/S0895-9811(02)00018-4

V

Vail, P., Mitchum, R., Thompson, S., 1977. Seismic Stratigraphy and Global Changes of Sea Level, Part 3: Relative Changes of Sea Level from Coastal Onlap.

Vallée, M., Nocquet, J.-M., Battaglia, J., Font, Y., Segovia, M., Régnier, M., Mothes, P., Jarrin, P., Cisneros, D., Vaca, S., Yepes, H., Martin, X., Béthoux, N., Chlieh, M., 2013b. Intense interface seismicity triggered by a shallow slow slip event in the Central Ecuador subduction zone. J. Geophys. Res. Solid Earth 118, 2965–2981. doi:10.1002/jgrb.50216

Van Wagoner, J.C., 1988. An overview of the fundamentals of sequence stratigraphy and key definitions.

Vannucchi, P., Galeotti, S., Clift, P.D., Ranero, C.R., von Huene, R., 2004. Long-term subduction-erosion along the Guatemalan margin of the Middle America Trench. Geology 32, 617–620.

Vannucchi, P., Scholl, D.W., Meschede, M., McDougall-Reid, K., 2001. Tectonic erosion and consequent collapse of the Pacific margin of Costa Rica: Combined implications from ODP Leg 170, seismic offshore data, and regional geology of the Nicoya Peninsula. Tectonics 20, 649–668.

Villamar, R., 2001. Subduction de la ride de Carnegie sous la marge d ' Équateur :

structure et déformation à partir des données de sismique multitrace. Université Pierre et Marie Curie et Géosciences Azur.

Von Huene, R., E. Suess, 1988. Ocean Drilling Program Leg 112, Peru continental margin: Part 1, Tectonoci hystory. Geology 16, 934–938.

Von Huene, R., Lallemand, S., 1990. Tectonic erosion along the Japan and Peru convergent margins. Bull. Geol. Soc. Am. 102, 704–720. doi:10.1130/0016-7606(1990)102<0704:TEATJA>2.3.CO;2

Von Huene, R., Ranero, C.R., Vannucchi, P., 2004. Generic model of subduction erosion. Geology 32, 913–916. doi:10.1130/G20563.1

Von Huene, R., Ranero, C.R., Weinrebe, W., Hinz, K., 2000. Quaternary convergent margin tectonics of Costa Rica, segmentation of the Cocos Plate, and Central American volcanism. Tectonics 19, 314–334. doi:10.1029/1999TC001143

Von Huene, R., Scholl, D.W., 1991. Observations at convergent margins concerning sediment subduction, subduction erosion, and the growth of continental crust. Rev. Geophys. 29, 279. doi:10.1029/91RG00969

W

Waelbroeck, C., Labeyrie, L., Michel, E., Duplessy, J.C., McManus, J.F., Lambeck, K., Balbon, E., Labracherie, M., 2002. Sea-level and deep water temperature changes derived from benthic foraminifera isotopic records. Quat. Sci. Rev. 21, 295–305. doi:10.1016/S0277-3791(01)00101-9

Watts A.B., Koppers A.P., Robinson D.P., 2010. Seamount subduction and earthquakes. Oceanography, 23, 1, 166-173.

Whipple, K.X., 2009. The influence of climate on the tectonic evolution of mountain belts. Nature Geoscience, 2, 97-104.

Willet, S.D., 1999. Orogeny and orography: the effect of erosion on the structure of mountain belts. Journal of Geophysical Research, 104, 28957-28981.

Willet, S. D., Hovius, N., Brandon, M.T., Fisher, D.M., 2006. Tectonics, Climate and Landscape Evolution. Geological Society of America Special paper 398.

Witt, C., Bourgois, J., Michaud, F., Ordoñez, M., Jiménez, N., Sosson, M., 2006. Development of the Gulf of Guayaquil (Ecuador) during the Quaternary as an effect of the North Andean block tectonic escape. Tectonics 25, n/a–n/a. doi:10.1029/2004TC001723.

ANNEXES

Scientific Article 1

Quaternary sedimentation and active faulting along the Ecuadorian shelf: preliminary results of the ATACAMES Cruise (2012), Michaud et al., 2015. Marine Geophysical Research, March 2015, Volume 36, Issue 1, pp 81-98, First online: 01 August 2014.

Scientific Article 1

Flare-Shaped Acoustic Anomalies in the Water Column along the Ecuadorian Margin: Relationship with Active Tectonics and Gas Hydrates, Michaud et al., 2016. Pure and Applied Geophysics, pp 1-13, First online: 27 January 2016.

Abstract of Scientific Congress 1

Pleistocene stratigraphic signature of active deformation along the central Ecuadorian subduction margin. Martillo et al. 2013. 14eme Congrès Français de Sédimentologie, Paris-France.

Abstract of Scientific Congress 2

Margin sedimentary record of active deformation due to the subduction of topographic asperities (Carnegie Ridge, Manta Plata area, Central Ecuador. Proust et. al., 2015. 31st IAS Meeting of Sedimentology, Kraków-Poland.